INTERACTION OF THE GALAPAGOS PLUME

WITH THE SOUTHERN CENTRAL AMERICAN VOLCANIC FRONT

by

ESTEBAN GAZEL DONDI

A Dissertation submitted to the

Graduate School-New Brunswick

Rutgers, The State University of New Jersey

in partial fulfillment of the requirements

for the degree of

Doctor of Philosophy

Graduate Program in Geological Sciences

written under the direction of

Dr. Michael J. Carr

and approved by

____

____

____

____

New Brunswick, New Jersey

October, 2009

ABSTRACT OF THE DISSERTATION

Interaction of the Galapagos Plume with the Southern Central American Volcanic Front

By ESTEBAN GAZEL DONDI

Dissertation Director:

Dr. Michael J Carr

Form the accretion of Galapagos-related oceanic complexes to the recent recycling of Galapagos tracks and the possible influx of Galapagos-modified mantle, the volcanic front of southern Central America is an ideal natural laboratory to study the effects of different interactions between a convergent margin and a mantle plume. I produced a detailed characterization of the different accreted oceanic complexes in southern Central America. This characterization was then incorporated in a regional that allowed me to reconstruct the evolution of the Galapagos Plume since its initial peak in the Cretaceous and through different types of interaction between the plume and the arc in southern Central America. I also contributed to the first quantitative comparison between modern ocean-island basalt (OIB) and large igneous provinces (LIPS) that show petrological evidence that the mantle sources of LIPS were hotter and more magmatically productive than modern-day OIB. Here I also present the geochemical evolution of the volcanic arc in Costa Rica since the Oligocene, where I discover that the volcanic front lavas were "normal arc lavas" until c. 6 Ma, where the Galapagos-OIB signature is first evident in the arc. I interpreted the appearance of the OIB signature as the result of the recent (10-8 Ma) recycling of the subducting Galapagos Hotspot Tracks. Interaction

between partial melts of the Galapagos Tracks (Seamount Province and Cocos/Coiba Ridge) produced a metasomatic enrichment (re-fertilization) of the mantle in the wedge and the lithospere. I also present new petrologic and geochemical evidence that the Galapagos-modified asthenosphere may actually flow into the mantle wedge below southern Costa Rica and Panama, producing a broad thermal anomaly that triggered melting in the mantle wedge and in the previously re-fertilized lithosphere. From the accretion of exotic terranes to the recent recycling of the Galapagos hotspot tracks through the subduction system and the possible influx of Galapagos-modified asthenosphere, the geologic history of the convergent margin in Southern Central America has been characterized by long term interaction with the Galapagos Plume.

PREFACE

Planet earth is a dynamic system in constant evolution. The mass transfer between Earth's mantle, crust and atmosphere is controlled by the production of new oceanic crust in the spreading centers, the recycling of material into the mantle and the segregation of the continental crust at convergent margins. Additional mass transfer between deeper reservoirs and the crust are represented by isolated sources of magmatism and heat fed by deep mantle plumes.

Many volcanic front lavas in southern Central America have an OIB (ocean island basalt) geochemical signature, anomalous for a convergent margin. My dissertation work involves a comprehensive study about the interaction between a convergent margin and a mantle plume. I focused on the evolution of the Galapagos plume and the effects of the recent interactions of the Galapagos plume with the Central American arc. This study is divided into four main chapters described below. Each chapter provides an introduction, a geologic and tectonic background, previous work, data and analytical methods, results, discussions, conclusions and references.

Chapter 1

The first chapter is a synthesis of my work on the oceanic complexes of Costa Rica. The most important contributions to the geologic history of this active margin are the systematic characterizations of the different oceanic complexes accomplished through detailed field observations. Working with P. Denyer, I proposed the existence of an Upper Cretaceous autochthonous emerged-basement not related to the Galapagos Plume. Upon this basement lies a vast province of accreted oceanic complexes, so we suggested that accretionary processes have been important since the early evolution of this convergent margin.

For Chapter 1, I compiled a database from published sources that includes more than 600 major and trace elements, 50 Sr, Nd and Pb isotopic ratios, 36 K/Ar ages and 25 $^{40}Ar/^{39}Ar$ ages. I was part of field campaigns that involved the production of new geologic maps, stratigraphic sections and structural/tectonic relations between the different complexes. My field work in Santa Elena clarified the structural relations between the different units. The metamorphic facies of the Santa Elena Peninsula rocks is based on my detailed petrographic and mineral studies. My contribution to the paper includes the geochemical interpretation and modeling. I also contributed to my co-authors ideas and models during the writing process. The compilation I produced for this paper served as the basis for understanding the evolution of the Galapagos Plume (Chapter 2) and as the critical data for ruling out any significant role by these oceanic complexes in the magmatic processes of the modern arc (Chapter 3).

This work produced three published papers:

Denyer, P. and **Gazel, E.** Jurassic to Miocene Costa Rican oceanic complexes: Description, structures and relationships. ***Journal of South American Earth Science***, *in press.*

Gazel, E., Denyer, P. and Baumgartner, P.O., 2006. Magmatic and geotectonic significance of Santa Elena Peninsula, Costa Rica. ***Geologica Acta*** 4(1-2), 193-202.

Denyer, P., Baumgartner, P.O. and **Gazel, E**., 2006. Characterization and tectonic implications of Mesozoic-Cenozoic oceanic assemblages of Costa Rica and Western Panama. ***Geologica Acta*** 4(1-2), 219-235.

Chapter 2

In Chapter 2, working with C. Herzberg, I contributed to the geochemical and petrological reconstruction of the evolution of the Galapagos Plume since the Cretaceous. This chapter makes the first reconstruction of the thermal history of a mantle plume. For the first time, we show that Large Igneous Provinces (LIPS) were hotter and more magmatically productive than modern Ocean Island Basalts. My contribution was the geochemical synthesis and modeling and the synthesis of the regional geology and tectonics. C. Herzberg contributed the petrological modeling and the global implications. The publication of this paper in Nature produced a great impact in the scientific community and had important press coverage.

This chapter has resulted in one published paper:

Herzberg, C. and **Gazel. E.**, Petrological evidence for secular cooling in mantle plumes, ***Nature***, 485, 619-622

Chapter 3

Chapter 3 defines the effects of the interaction of the arc with the Galapagos hotspot. For this project, I obtained major and trace element data, radiogenic isotopes (Sr, Nd, Pb) and $^{40}Ar/^{39}Ar$ ages from samples I collected during my field campaigns in the

Tertiary volcanics of Costa Rica. I was in charge of petrographic studies and sample preparation. I produced 30 new radiogenic isotopes. The data collection and reduction was supervised by M. Feigenson and F. Hauff. The rest of the data were collected in collaboration with K. Hoernle, D. Symanzki and P. van den Bogaard, mostly on samples that I collected and prepared. In this chapter, I evaluated the geochemical evolution of the volcanic rocks in Nicaragua, Costa Rica and Panama. I proposed that the OIB-like signature in central Costa Rica and Panama has a relatively recent origin, ~6 Ma. I also showed that there was a temporal transition from typical arc magmas in the Oligocene-Mid Miocene (analogous to the modern Nicaraguan volcanic front) to OIB-like magmas in the Upper Miocene. I also produced quantitative geochemical models that suggest that the Galapagos hotspot contribution decreases systematically along the volcanic front from central Costa Rica to NW Nicaragua. Another paper related to this chapter about the geochemical evolution of the Nicaraguan arc is currently under revision by G-Cubed (Geochemistry, Geophysics, Geosystems).

This chapter has resulted in one published paper and one submitted:

Gazel, E., Carr, M.J., Hoernle, K., Feigenson, M.D., Hauff, F., Szymanski, D., and van den Bogaard, P, 2009. The Galapagos-OIB signature in southern Central America: Mantle re-fertilization by arc-hotspot interaction. ***Geochemistry, Geophysics, Geosystems (G^3)***, Q02S11, doi:10.1029/2008GC002246

Saginor, I., **Gazel, E.**, Carr, M.J., Swisher III, C., Turrin, B. Miocene to Recent volcanic history of Western Nicaragua: Insights from geochemistry and geochronology. ***Geochemistry, Geophysics, Geosystems (G^3),*** *in revision.*

Chapter 4

Chapter 4 involves petrologic and geochemical evidence for mantle upwelling and slab melting in southern Central America. For this project, I obtained major and trace element data, radiogenic isotopes (Sr, Nd, Pb) and $^{40}Ar/^{39}Ar$ ages from alkaline samples. The data were collected in collaboration with K. Hoernle, D. Symanzki, I. Saginor and P. van den Bogaard. I was in charge of field work and sample collection with M. Carr. The petrological modeling was supervised by C. Herzberg. I also collected petrographic and mineral data.

A paper on this chapter is in preparation and planned to be submitted to the Journal of Petrology:

Gazel, E., Hoernle, K., Carr, M. J., Herzberg C., Saginor I., Swisher III, C. ,Feigenson, M., Hauff, F., van den Bogaard, P. Petrological and Geochemical Evidence of Galapagos Asthenosphere Upwelling n Southern Central America. *To be submitted to the Journal of Petrology*.

ACKNOWLEDGMENTS

I was born in Costa Rica, a small land of freedom, peace and…active tectonics in the center of the Americas. I grew up in a country shaped by volcanoes and earthquakes. I was also very fortunate because I had the privilege to get a degree from the Central American School of Geology at the University of Costa Rica (UCR). Everyday at UCR was simply a dream come true. From climbing on lava flows to getting lost in the jungle, the geologist I am now is because of my experience at the UCR. Here I met P. Denyer, T. Aguilar, G. Alvarado and S. Kussmaul. I will forever be grateful for their input in my formation at the UCR as a field geologist. Also my first steps as a scientist were guided by R. Vindas at the Institute for Atomic and Molecular Research at UCR. During this time I was fortunate to explore among many spectacular places, including the Santa Elena Peninsula, where I fell in love with the Earth's mantle. The limitations of a developing country were never enough to end my motivation for science. Actually, this taught me to be more creative, to collaborate with people and expand my horizons. This is when L. Patino, M. Carr and K. Hoernle showed up in the equation of my life. Somehow I always found my way to get into their hotels when they were doing field work in Costa Rica to discuss petrology and geochemistry. Kaj motivated my enthusiasm for petrology and Lina was the first that encouraged me to get a graduate degree.

After a winter experience in Michigan, I ended up at Rutgers; in part because of the weather but mostly because of Mike. Coincidentally (but not accidentally) I meet C. Herzberg at Rutgers. Since my first chat with Claude (when I lost my mind looking at garnet lherzolites) we have been a good team. My years at Rutgers were highly productive. I was part of different research and academic initiatives, some worked out, others just taught me good lessons. I had the privilege to work with an excellent advisor M. Carr together with C. Herzberg, K. Hoernle, M. Feigenson and C. Swisher. They guided me but also gave me the freedom to work on my research driven by my own curiosity. I also had the opportunity to collaborate with IFM-GEOMAR and spent some good time in Kiel. V. Levin remained meme how all human activities, even science, are not independent of politics. The analytical support of my friend, D. Szymanski, was crucial for my research. I am also grateful for the time and scientific (and personal) discussions with L. Patino, T. Vogel, F. Hauff, S. Whattam, A. Borgia, T. Hansteen, A. Kerr, T. Plank, A. Hofmann, M. Hirshmann, B. Turrin, R. Rudnick, B. McDonough and everyone else that I annoyed with my e-mails, invited to Rutgers or who simply tolerated me at AGU. The support of my friends I. Saginor, P. Ruiz, F. Villalobos, S. Murillo, A. Kulpecz, A. Harris, A. Nikulin, P. Hidalgo, L. Neitzke and the rest of the Rutgers people has also been an important part of this experience. The universe would be more entropic without J. Reaves and J. Zabala. I will always be thankful to my family, especially my mother J. Dondi, my father A. Gazel and my grandma M. Protti. I am eternally grateful to my wife Naya, without her I would be lost floating in the air.

This dissertation work was sponsored by the Pre-Dissertation Award from the Graduate School, New Brunswick and Science Research Award from Rutgers University. I was also partially funded by the Geologic Society of America and NSF grants EAR0203388 and NSF OCE 0505924. The analytical data were collected at Rutgers or in collaboration with IFM-GEOMAR and Michigan State University

Table of Contents

Chapter 1

Characterization of the Accreted Oceanic Complexes in Southern Central America: Origin, Tectonics and Field Relations.

This chapter resulted in three published papers:

Denyer, P. and **Gazel, E.** Jurassic to Miocene Costa Rican oceanic complexes: Description, structures and relations. ***Journal of South American Earth Science****, in press.*

Gazel, E., Denyer, P., and Baumgartner, P.O., 2006. Magmatic and geotectonic significance of Santa Elena Peninsula, Costa Rica. ***Geologica Acta*** 4(1-2), 193-202.

Denyer, P., Baumgartner, P.O. and **Gazel, E**., 2006. Characterization and tectonic implications of Mesozoic-Cenozoic oceanic assemblages of Costa Rica and Western Panama. ***Geologica Acta*** 4(1-2), 219-235.

Abstract

The oceanic complexes on the Pacific coast of Costa Rica are the only available source of information to study the early evolution of the Central American convergent margin. Six regions of oceanic complexes are described in this chapter: 1) Santa Elena Peninsula (Santa Elena Nappe and Santa Rosa Accretionary Complex), 2) Nicoya Peninsula, 3) Tortugal Suite, 4) Herradura Block, 5) Quepos Block, 6) Osa-Burica Block, and 7) the Azuero and Sona Peninsulas (Panama). The oceanic complexes in

southern Central America are remnants of the Caribbean Large Igneous Province (CLIP), accreted seamounts/ocean islands and, in minor proportion, supra-subduction zone complexes. The Santa Rosa Accretionary Complex and the Tortugal Suite have a geochemical signature not consistent with a Galapagos Plume origin. The associated shallow submarine Caribbean Tethys fauna suggests that these complexes are part of a terrane emplaced during the Upper Cretaceous. We suggest that this terrane represents an "autochthonous" Cretaceous arc basement related to the accreted oceanic islands. The rest of the oceanic complexes in Costa Rica and Panama are part of the CLIP or are Galapagos tracks accreted from the end of Cretaceous in the northwest, to the Miocene in the southeast, forming the diverse province of oceanic complexes genetically connected to the Galapagos Hotspot activity.

1. Introduction

The oceanic complexes on the Pacific coast of Costa Rica are key pieces of the geotectonic puzzle of the Caribbean Plate. These oceanic complexes are part of several tectonic blocks, each one with a different geologic history. The tectonic blocks outcrop along a NW-SE trend, parallel to the present location of the Middle American Trench (Fig. 1A).

In this chapter, we use field observations, geologic maps, comparative stratigraphy, geochronology and geochemical signature to redefine the stratigraphic and structural relations of the oceanic complexes of the following areas: Santa Elena Peninsula, Nicoya Peninsula, Tortugal, Herradura, Quepos, Osa Peninsula and Burica

Peninsula. We describe the different complexes and integrate information generated through the last 30 years of research. Our main motivation is to understand the true significance of each complex in the geologic history of this active margin. We present a comprehensive updated geologic and geochemical synthesis of the different oceanic complexes in the region as the starting point for future studies.

1.1 Methodology

Geochronological and geochemical data is integrated with our field observations. The geochronological synthesis includes biostratigraphy as well as $^{40}Ar/^{39}Ar$ dates from Sinton et al. (1997), Hauff et al. (2000) and Hoernle et al. (2002). Some K/Ar ages are incorporated (Bellon and Tournon, 1978, Tournon, 1984 and Berrangé et al., 1988) for the areas that lack $^{40}Ar/^{39}Ar$ ages. The compiled geochronological database includes geochemical analyses from Sinton et al. (1997), Beccaluva (1999), Arias (2000), Hauff et al. (2000) and Hoernle et al. (2002). The geochronological and geochemical compilations are available upon request from the authors.

2. Geologic and tectonic setting

Costa Rica is located on the triple junction between the Cocos, Caribbean and Nazca plates (Fig. 1A). The Cocos Plate subducts beneath the Caribbean Plate at an average rate of 88 mm/yr (DeMets, 1995). The subduction of the Cocos Ridge below Costa Rica caused diversity in the subduction processes, varying from smooth subduction in front of Nicoya Peninsula to rough subduction where the Cocos Ridge collides with the

Middle American Trench (Gardner et al., 1992; Vannucchi et al., 2001). During the last 16 Ma the trench retreated 50 km offshore of the Nicoya Peninsula and 20 km offshore Osa Peninsula (Vannucchi et al., 2001; Vannucchi et al., 2006).

Tectonic erosion and seamount subduction is presently active for this margin (von Huene and Scholl, 1991; Ranero and von Huene, 2000; Clift and Vannucchi, 2004; Vannucchi et al., 2006; Ranero et al., 2003). However, the presence of large oceanic provinces along the Pacific coast of Costa Rica suggests that the accretionary processes have been more dominant than tectonic erosion (Denyer et al., 2006).

The interpretation of the origin and emplacement of the oceanic complexes in the Pacific coast of Costa Rica depends on the regional models of the Caribbean Plate evolution. The pioneer work of Malfait and Dinkelman (1972), Donnelly (1973, 1994), and Burke et al. (1978) suggested the present Caribbean Plate was formed in the Pacific and later displaced to the northeast between the Americas. Frisch et al. (1992) and Meschede and Frisch (1998), based on the paleomagnetic work by Sick (1989), proposed an *in situ* model for the origin of the CLIP (Caribbean Large Igneous Province) related to the separation of North and South America. Later, DiMarco (1994) and DiMarco et al. (1985) used the magnetostratigraphy of the oceanic complexes of Costa Rica to define an equatorial and southern-equatorial origin for these terranes.

Modern geochemical data, together with $^{40}Ar/^{39}Ar$ ages, have improved the understanding of origin of these oceanic complexes. Several authors (Sinton et al., 1997; Alvarado et al., 1997; Hauff et al., 1997; Beccaluva et al., 1999; Arias, 2000; Hauff et al., 2000; Hoernle et al., 2002; Hoernle et al., 2004; Ragazzi, 1996) confirmed that most of the oceanic complexes of Costa Rica have a Pacific origin genetically related to the

Galapagos Plume. This agrees with the Duncan and Hargraves (1984) model that a long-lived Galapagos mantle plume was responsible for the thickened Caribbean crust.

Although the ophiolite model has been applied to the Nicoya Complex and to the ultramafics of the Santa Elena Peninsula (e.g. DeBoer, 1979; Kuijpers, 1980; Berrangé and Thorpe, 1988; Frish et al., 1992; Beccaluva et al., 1999), we prefer to avoid the term ophiolite because the sequences are incomplete and the geochemistry does not show normal mid-ocean ridge basalt (NMORB) signature.

3. Oceanic complexes description and field relations

3.1. Santa Elena peninsula

The Santa Elena Peninsula is part of a major E-W trending nappe. The Santa Elena Nappe is composed of an ultramafic complex emplaced during the Upper Cretaceous (Azéma and Tournon, 1980; Tournon, 1984, 1994; Frisch et al., 1992). The footwall includes the Cretaceous igneous-sedimentary sequence of the Santa Rosa Accretionary Complex (Baumgartner and Denyer, 2006; Gazel et al., 2006). The tholeiitic Albian basalts of Murciélago Islands have a geochemical affinity to the Santa Elena Nappe (Hauff et al., 2000; Gazel et al., 2006). Nevertheless, the structural relations to the nappe are not clear. Santa Elena Peninsula ultramafics were originally considered part of an ophiolitic suite and/or related to the Nicoya Complex (Dengo, 1962b; Azéma and Tournon, 1980; Kuijpers, 1980; Azéma et al., 1982; Baumgartner et al., 1984; Bourgois et al., 1984). However, recent geochemical work (Beccaluva et al., 1999; Hauff et al., 2000; Geldmacher et al., 2008) suggests that the Santa Elena Nappe units are not related to the Nicoya Complex.

The nappe thrust has associated megabreccias, composed of decameter to meter-sized blocks, that formed during the emplacement of the nappe (Azéma and Tournon, 1980; Tournon, 1984, Azéma et al., 1982). The fragments includes dolerites, basalts and gabbros in a tectonically deformed serpentinite matrix (Tournon, 1984). A rudist reef limestone on top of the exhumed peridotites constrains the nappe overthrust to the pre-late Campanian (Schmidt-Effing 1980; Aguilar, in press), and the age of the youngest dated radiolarite in the underlying sediments (DeWever et al., 1985) suggests the nappe was emplaced after the Cenomanian. Previous authors (Azéma and Tournon, 1980; Tournon, 1984; Azéma et al., 1982) have considered the thrust fault plane roughly horizontal with steep undulations. However, our field observations provide evidence that the Santa Elena Nappe has tilted towards the north and the tectonic windows are related to east-west reverse-faults (Fig. 3).

3.1.1 Santa Elena Nappe

The Santa Elena Nappe is composed of an ultramafic-mafic association of serpentinized mantle peridotites, dunites, pegmatitic gabbros, layered gabbros, plagiogranites, doleritic and basaltic dikes. Ocean floor metamorphism/ metasomatism caused the serpentinization of the peridotites and the development of secondary amphibole phases in all mafic lithologies. The metamorphic assemblage is composed of albite + epidote + actinolite + chlorite, which indicates greenschist facies conditions

(Gazel et al., 2006). The peridotites and associated ultramafic rocks have low TiO_2 (0.01-0.14 wt. %), Zr (3-25 ppm), V (41-95 ppm), and high MgO (34-45 wt. %), Cr (1931-2471 ppm), and Ni (1993-2380 ppm). There are at least two generations of pegmatitic gabbros dikes (2 cm to 10 m in thickness). They do not show chilled margins at contacts with the peridotites. Therefore, it is likely that they emplaced when the peridotite was still hot (Gazel et al., 2006).

Dolerite dikes (1-10 m wide) (Fig. 4A) represent a later magmatic episode. They crosscut the peridotites and the pegmatitic gabbros and have chilled margins at the contacts with the host rocks. The dolerites mineralogy includes labradorite-bytownite plagioclase, light green uralite and clinopyroxene, showing in most cases mineral alignment (Fig. 4B). The abundance of doleritic dikes increases toward the west, where they constitute a very dense dike swarm. In those swarms, the peridotites become inclusions within the dolerites (Fig. 2C). One K/Ar date from one of these dolerites yield an age of 88 ± 4.5 Ma (Bellon and Tournon, 1978). The dolerites range from basalts to basaltic-andesites and trachy-basalts, with an arc-tholeiitic to transitional calc-alkaline composition. They are characterized by LREE (Light Rare Earth Elements) depletions (Fig. 5), and in LILE (Large Ion Lithophile Elements) enrichments (Hauf et al., 2000; Gazel et al., 2006).

Layered gabbros and plagiogranites are exposed in Bahia Nancite (locality C16, Fig. 1). Ultramafic cumulates (plagioclase bearing peridotites and pyroxenites) are also present (Tournon, 1994; Arias, 2002). The plagiogranites are composed of quartz, plagioclase (labradorite) and green hornblende (actinolite). Hauff et al. (2000) reported a $^{40}Ar/^{39}Ar$ date from the layered gabbros of 124.0 ± 4.0 Ma. The layered gabbros are strongly depleted in LREE and HFSE and relatively enriched in LILE. The plagiogranites are also depleted in LREE and HFSE. The trace element composition and field relations confirm a cumulate origin.

Basaltic dikes cut the layered gabbros at Bahía Nancite and the dolerite dike swarm. Field observations suggest that these rocks represent the latest magmatic phase of the Santa Elena Nappe (Tournon, 1994). These basalts are characterized by depletions in LREE, HFSE and enrichment in LILE (Gazel et al., 2006).

The structural relationship of the Murciélago Islands (localities 6 and 7, Fig. 1C) to the rest of the Santa Elena remains unclear. This archipelago includes seven islands made of a subvertical sequence of northward tilted of tholeiitic basalts to trachy-basalts (Figs. 4E, F). Their geochemistry is similar to the dolerites from the Santa Elena Nappe (Gazel et al., 2006). The Murciélago basalts are depleted in LREE and HFSE (Figs. 5 and 6) and enriched in LILE. A pillow basalt from Murciélago Islands yields a $^{40}Ar/^{39}Ar$ date of 109.0 ± 2.0 Ma (Hauff et al., 2000). The available Pb isotopes from the Santa Elena Nappe trend toward a depleted mantle (DM) component (Fig. 7).

3.1.2 Santa Rosa Accretionary Complex

Based on the diverse lithology, numerous sequence repetitions, and the variations in age, Baumgartner and Denyer (2006), Gazel et al. (2006) and Baumgartner et al. (2008) concluded that this sequence corresponds to an accretionary complex. This complex includes alkaline basaltic lavas, radiolarian cherts, tuffaceous mudstones, pelagic limestones, black shales, sandstones, volcanoclastic turbidites, breccias and conglomerates.

The radiolarites (Fig. 4H) are mostly of late Aptian to Cenomanian in age, with a minor population from Middle and Late Jurassic (Schmidt-Effing, 1980; DeWever et al., 1985; Baumgartner et al., 2008). East of Bahía Nancite (locality C16, Fig. 1), the sequence is composed of volcanic lithoclasts that suggest the proximity of felsic volcanism (Azéma and Tournon, 1980; Tournon, 1994). At Santa Rosa site (locality C5, Fig. 1) alkaline sills are interbedded in the radiolarian sequence (Fig. 4G). These sills are composed of phenocrysts of partially altered olivine, clinopyroxene (mostly titaniferous augite), plagioclase and magnetite. They are silica sub-saturated ranging from basanites to phonolites. They are characterized by high TiO_2 (1.25-3.66 wt. %), Ba (> 300 ppm), and Zr (> 200 ppm), variable MgO (1.99-8.49 wt. %), Cr (35-383) and Ni (20-166 ppm) (Gazel et al., 2006). In addition, they have the highest LREE and HFSE enrichments in all the oceanic complexes in southern Central America (Figs. 5 and 6). This unit originated in an intraplate setting and later accreted to the arc as part of an accretionary complex.

3.2. Nicoya Peninsula

The Nicoya Complex was defined by Dengo (1962a) and Kuijpers (1980) in the Nicoya Peninsula. The term Nicoya Complex was extended to other oceanic complexes along the Pacific coast of Costa Rica despite having different ages and origins (e.g. Schmidt-Effing, 1979; MIEM, 1982; Berrangé et al., 1989; Denyer and Arias, 1991). We suggest that the term Nicoya Complex should be restricted to the magmatic-radiolarian sequences older than Lower Campanian-Santonian originally described by Dengo (1962b). In addition, the sedimentary cover is excluded, as suggested by other authors (Kuijpers, 1980; Tournon, 1984; Baumgartner, 1984; Denyer and Baumgartner, 2006). Several authors use geochemical data, field relations, tectonic reconstructions and $^{40}Ar/^{39}Ar$ ages (e.g., Sinton et al., 1997; Hauff et al., 2000; Hoernle et al., 2004; Denyer et al., 2006) to conclude that the Nicoya Complex represents segments of the fragmented CLIP.

3.2.1 Igneous suite

Basalts, volcanic breccias, dolerites, gabbros, scarce plagiogranites and hyaloclastites are the igneous sequences of the Nicoya Complex. The basalts are generally aphyric, consisting of a few plagioclase, augite, and Fe-Ti oxide crystals in an aphanitic matrix generally altered to chlorite and zeolites (Fig. 8A). The basalts include different facies, from pillow to massive, and are tholeiitic in composition. Dolerites (centimeter to meter wide) have the same paragenesis as the basalts. They can be distinguished in the field because they crosscut the massive basalts (Fig. 8C) and generally have a holocrystalline texture. Some dolerites are characterized by rounded cm-long anorthite-rich (An_{88-83}) plagioclase megacrystals (Tournon, 1984). Gabbros and plagiogranites are restricted to the northwest part of the Nicoya Peninsula. Gabbros with the same mineralogical composition as the basalts cover more than 200 km^2 (Denyer and Arias, 1993). Plagiogranites have coarse textures with grain sizes up to 2 cm. They contain myrmekitic plagioclase, quartz, hedenbergite and Fe-Ti oxides (Denyer and Arias, 1993; Sinton et al., 1997). Plagiogranites from the Nicoya Complex have an oceanic crust affinity, in contrast to the plagiogranites within the layered gabbros from the Santa Elena Nappe that have an island-arc affinity (Gazel et al., 2006).

Fifteen $^{40}Ar/^{39}Ar$ dates (whole rock, matrix, glass and plagioclases) are published for the Nicoya complex. The intrusives range between 85-83 Ma (Santonian); the basalts yield dates between 95-88 Ma (Cenomanian-Turonian) (Sinton et al., 1997; Hauff et al., 2000), 119-111 Ma (Aptian-Albian) and 139-133 Ma (Berriasian-Hauterivian) (Hoernle et al., 2004).

The radiometric and geochemical data indicate that the Nicoya Complex represents disrupted fragments of the CLIP with at least four identifiable magmatic and/or accretionary pulses (Fig. 2). The most remarkable geochemical characteristics of the Nicoya Complex are their flat REE patterns (Fig. 5), moderate HFSE enrichments consistent with an EMORB-like source (Fig 6), $^{207}Pb/^{204}Pb$ ratios between 15.53-15.57 and $^{206}Pb/^{204}Pb$ of 18.54-19.00 (Fig. 7). These geochemical and isotopic signatures are also characteristic of other Cretaceous oceanic complexes included in the CLIP (Fig. 5). Alternatively, the 95-80 Ma rocks are part of the initial burst of the Galapagos Plume and the older sections are part of older accreted oceanic plateaus.

3.2.2 Radiolarites

Two facies of highly deformed (Fig. 8D) radiolarian cherts are distinguished in the Nicoya Complex, Mn-radiolarites and Fe-radiolarites (Kuijpers, 1980). They are up to

40 m thick and show cm thick beddings with varying colors (brown, red, green, white, gray or black). Their age is Jurassic to middle Cretaceous with a gap that extends from the middle Bathonian to Early Oxfordian (Baumgartner, 1984; Denyer and Baumgartner, 2006). Centimeter-wide sedimentary manganese nodules (Fig. 8E) are sometimes interbedded within the radiolarites (Kuijpers, 1980; Halbach et al., 1992). Hydrothermally remobilized Mn and Si from the Mn-nodules and chert produced meter-wide pockets of Mn-mineralizations and massive red-yellow jasper bodies (Kuijpers and Denyer, 1979; Denyer and Baumgartner, 2006). Coniacian-Santonian lenses of 3-10 m thick Fe-radiolarites are overlying and/or interbeded within the basalts. The Fe-radiolarites are characterized by whitish/brown or red cm-thick ribbon bedding. Locally, these radiolarites are impregnated with hematite and sometimes completely transformed into hematitic rock (Kuijpers, 1980).

3.2.3 Geologic History of the Nicoya Complex

The inconsistency between the igneous $^{40}Ar/^{39}Ar$ ages (Cretaceous) and the Mn-radiolarite fossil ages (Jurassic-Early Cretaceous) in the Nicoya Complex is explained by the model presented by Denyer and Baumgartner (2006). They proposed a Jurassic-Cretaceous chert deposit that was detached from its original basement by pervasive intrusions during the different CLIP pulses. In this way, the radiolarites of the Nicoya Complex were not only tectonically deformed and emplaced (Kuijpers, 1980; Gursky et al., 1982; Baumgarnter, 1984; Burgois et al., 1984; Beccaluva et al., 1999) but also magmatically disrupted and deformed because of intrusion of the CLIP magmas.

Fossil radiolarian ages suggest that the Mn-radiolarites were deposited on normal oceanic crust in Jurassic-Early Cretaceous. However, neither Jurassic ages nor NMORB geochemistry has been found in the Nicoya Peninsula (Sinton et al., 1997; Hauff, 2000; Hoernle, 2004; Denyer and Baumgartner, 2006). $^{40}Ar/^{39}Ar$ ages and biochronology suggest that the first CLIP pulses began during 139.1-132.9 Ma (Hoernle et al., 2004). During that time, CLIP-related magmas intruded the Mn-radiolarites . The geologic record suggests that the CLIP magmatism continued in a second and third pulse from 119.4-110.6 Ma and 95-88 Ma, respectively. The third pulse corresponds to the main CLIP event (Sinton et al., 1997; Hauff et al., 2000; Hoernle et al., 2004; Denyer and Baumgartner, 2006). Alternatively, as mentioned before, the older units of ~140-120 Ma could represent segments of older oceanic plateaus (Manihiki?) accreted to this margin.

The thermally driven circulation related with the magmatic processes, leached the Mn and Si from the radiolarites, and produced massive Mn-ore and jasper deposits (Kuijpers and Denyer, 1979; Denyer and Baumgartner, 2006). This process also bleached the radiolarites close to the igneous contacts (Figs. 8F, G). During the main CLIP event (95-88 Ma), the radiolarite package became buoyant with respect to the intrusive rocks, causing detachment and strong deformation of the Jurassic-Early Cretaceous sedimentary sequence (Fig. 8H). The result of this process is kilometer to meter-sized outcrops of bleached and strongly deformed radiolarites (Fig. 9A) inside a pervasive intrusive body (Fig. 9B) (Denyer and Baumgartner, 2006).

The magmatism finished with the last CLIP pulse between 87.5-83 Ma (Sinton et al., 1997; Hauff et al., 2000). During that time, pelagic sedimentation was accompanied by hydrothermal water, rich in Fe that produced the Fe-radiolarites deposits (Kuijpers, 1980).

3.3 Tortugal Suite

The Tortugal Suite is composed of picritic rocks intruded by alkaline basalts (Fig. 1C). The suite outcrops in a NW-trending, 14 km long and 1.5 km wide body surrounded by the Nicoya Complex (Alvarado and Denyer, 1998). The picrites are exposed in isolated and meter-size blocks at the top of small hills, generally less than 15 m high, easily recognized in the field because of their olivine phyric texture. The picrites have abundant euhedral olivine, orthopyroxene, clinopyroxene, ilmenite and chromium-rich spinel phenocrysts in a microlitic matrix with chlorite as a secondary phase (Fig. 9D). Microspinifex texture is visible in some of some of the piristic lavas (Fig. 9E). The picrites are enriched in compatible elements (MgO 26-29 wt.%, Ni 1385-1606 ppm and Cr 2189-2846 ppm) and depleted in incompatible elements (K_2O 0.02-0.37 wt.%, TiO_2 0.59-0.8 wt.%). A basalt from the Tortugal Suite yields a $^{40}Ar/^{39}Ar$ age of 89.7±1.4 Ma (Alvarado et al., 1997).

The Tortugal Suite lavas have an OIB signature enriched in LREE and HFSE (Figs. 5 and 6). The samples from Tortugal share the same $^{206}Pb/^{204}Pb$ ratios with the CLIP but have higher (> 15.57) $^{207}Pb/^{204}Pb$ ratios that trend toward an EMII (enriched mantle type II) reservoir (Fig. 7).

3.4 Herradura Block

The Herradura Block covers an area greater than 1000 km^2 with elevations up to 1500 m. Arias (2003) recognized the Nicoya Complex at the base, overthrusted by the Tulín Formation.

The Nicoya Complex outcrops in the southeast edge of the Herradura Block (Fig. 1) and its geochemical signature here is again consistent with the CLIP (Hauff et al., 2000) Fig. 5D. Two $^{40}Ar/^{39}Ar$ dates from Nicoya Complex basalts yield ages of 83.2 ± 1.8 Ma (Sinton et al., 1997) and 86.0 ± 2.0 Ma (Hauff et al., 2000). The samples from the Nicoya Complex at the Herradura Block have flat REE pattern and moderate HFSE enrichments (Figs. 5 and 6), typical of the CLIP.

The Tulín Formation (Fig. 1D) was originally defined by Malavassi (1967) and MIEM (1982), and was redefined by Arias (2003). It includes vesicular pillow basalts, microdolerites, scarce gabbros and olivine cumulates. Interbedded with the basalts are epiclastic sediments, breccias, sandstones and tuffs rich in juvenile volcanic fragments together with radiolarians and foraminifera (Arias, 2003). Based on the microfossil content, the Tulín Formation is Maastrichtian to Middle Eocene in age (Arias, 2003). The basalts have an OIB signature characterized by LREE enrichments (Fig. 5). The Tulin Formation is interpreted as an accreted oceanic island (Arias, 2003; Denyer et al., 2006).

3.5 Quepos Block

The Quepos Block (Fig. 1D) is composed of vesicular pillow basalts (Fig. 9F), dolerites, picrites (Fig. 9G) and gabbros. This block is correlated based on geochemistry, geochronology and field relations to the Tulín Formation (Arias, 2003; Denyer et al., 2006). It corresponds to a Late Cretaceous-Paleocene ocean island (Azéma et al., 1978; Bolz and Calvo, 2003). The volcanic stratigraphy provides evidence for submarine and subaerial conditions (Baumgartner et al., 1984). The volcano was active between 59.4 ± 1.8 Ma and 65.0 ± 0.4 Ma, according to the $^{40}Ar/^{39}Ar$ dates reported by Sinton et al. (1997), Hauff et al. (2000) and Hoernle et al. (2002). These dates are consistent with the paleontological ages of the interpillow sediments (Azéma et al., 1978; Baumgartner et al., 1984).

Basalts from the Quepos Block have REE patterns (Fig. 5) and HFSE enrichments (Fig. 6) similar to the Tulín Formation. Samples from the Quepos block have $^{207}Pb/^{204}Pb$ ratios, similar to the CLIP but have more radiogenic $^{206}Pb/^{204}Pb$ (> 19.00) (Fig. 7).

3.6 Osa-Burica Block

Originally, the Osa-Burica Block was considered part of the Nicoya Complex (e.g. Berrangé et al., 1989). Later, DiMarco (1994) restricted the igneous sequence to the northeast border of the Dulce gulf and suggested that most of the Osa peninsula is part of to the Osa-Caño Accretionary Complex. Finally, the block was divided based on tectonic units with different origins described below.

3.6.1 Golfito Terrane

The Golfito Terrane (Fig. 1E) was defined by DiMarco (1994) and includes basalts, dolerites and breccias with interbedded Upper Maastrichtian pelagic sediments. The presence of coarse sediments with olistostromes records the collision of this terrane with the arc during the Paleocene (DiMarco et al., 1995). The volcanic rocks are characterized by a flat REE-pattern (Fig. 5), moderate HFSE enrichments (Fig. 6) and $^{207}Pb/^{204}Pb$ ratios ranging from 15.53 to 15.57 and $^{206}Pb/^{204}Pb$ from 18.54 to 19.00 (Fig. 7). Based on geochemical data and field relations, the Golfito Terrane possibly corresponds to an accreted CLIP segment.

3.6.2 Burica Terrane

The Burica Terrane (Fig. 1E) includes basalts and dolerites with associated interflow radiolarites. It has been interpreted as an accreted seamount (Obando, 1986), but Frisch et al. (1992) argued for an island arc setting for this terrane. The available geochemical data (Hauff et al., 2000) show flat REE patterns, moderate HFSE enrichments (Figs. 5 and 6), and $^{207}Pb/^{204}Pb$ ratios between 15.53-15.57 and $^{206}Pb/^{204}Pb$ of 18.54-19.00 (Fig. 7). The Burica Terrane has been micropaleontologically dated as Campanian to Paleogene (DiMarco et al., 1995), which is consistent with the $^{40}Ar/^{39}Ar$ age of 64.2 ± 1.1 Ma (Hoernle et al., 2002). Based on the Galapagos geochemical signature and age younger than the CLIP, we consider that the Burica Terranes is possibly a segment of an older Galapagos track accreted to the margin.

3.6.3 Rincón Block

The Rincón Block (Fig. 1E) is an accreted seamount exposed in the innermost part of the Osa Peninsula. Microfossils ages range between Early Paleocene to Early Eocene (Buchs and Stucki, 2001). In addition, two $^{40}Ar/^{39}Ar$ ages obtained on basalts are consistent with a Paleocene age (54.5 ± 1.7 Ma and 62.1 ± 0.6 Ma) (Hauff et al., 2000; Hoernle et al., 2002). The accretion of this block was possibly 25 Ma (Vannucchi et al., 2006).

3.6.4 Osa-Caño Accretionary Complex

The Osa-Caño Accretionary Complex is also referred to as the Osa Mélange by Vannucchi et al. (2006) and Buchs and Baumgartner (2007). It is a chaotic unit, described as a block-in-matrix fabric *mélange*. Baumgartner (1986) documented a mélange in Caño Island. The Caño Accretionary Complex was defined by DiMarco (1994) and described by DiMarco et al. (1995), Buchs and Stucki (2001), Buchs and Baumgartner (2003) and Vannucchi et al. (2006). Originally, this *mélange* was considered an igneous complex and therefore associated with the Nicoya Complex (e.g. MIEM, 1982; Berrangé and Thorpe, 1988; Berrangé et al., 1989).

The *mélange*-reworked material includes igneous and sedimentary fragments. Areas with abundant sediments contrast with areas containing igneous mega blocks (>10 m in diameter). The igneous blocks include basalts, gabbros, dolerites and amphibolites (Tournon, 1984; DiMarco et al., 1995). The matrix of the *mélange* is a volcanic greywacke. Chemical analysis in the lava blocks from the *mélange* shows both CLIP and NMORB signatures. The CLIP affinity is characterized by a flat REE-pattern, moderate HFSE enrichments (Figs. 5 and 6) and $^{207}Pb/^{204}Pb$ ratios of 15.53-15.57 and $^{206}Pb/^{204}Pb$ of 18.54-19.00; The NMORB signature is characterized in LREE and HFSE depletions (Figs. 5 and 6) and $^{207}Pb/^{204}Pb$ - $^{206}Pb/^{204}Pb$ ratios with values between those of the Santa Elena Nappe and the CLIP. This geochemical and lithological diversity is consistent with what is expected from an accretionary prism. The sedimentary components are red radiolarian cherts (Fig. 9H), mudstones, shallow-water limestones, volcanic siltstones, sandstones and breccias (DiMarco et al., 1995; Buchs and Baumgartner, 2007).

The accretionary complex components are highly variable in age. The K/Ar ages of basalts and dolerites provide a range of 78-44 Ma (Tournon, 1984; Berrangé et al., 1989). The pelagic limestones and cherts are Late Cretaceous-Paleocene and the shallow water limestones are Eocene (Buchs and Baumgartner, 2003). The matrix of the accretionary complex is Late Paleocene to Middle Eocene (Ázema et al., 1985; Buchs and Baumgartner, 2003). The youngest pelagic sediments are Middle to Late Eocene. Therefore, based on this, the accretion possibly occurred during the Middle/Late Eocene to Middle Miocene (Buchs and Baumgartner, 2007).

Several hypotheses explain the origin of the Osa-Caño Accretionary Complex. Meschede et al. (1999) related its formation to subduction erosion. DiMarco et al. (1995)

and Buchs and Baumgartner (2003, 2007) considered it a combination of both sedimentary and accretionary mechanisms. Vannucchi et al. (2006) proposed that the accretion was caused by the subduction of seamounts and the exhumation was a result of active tectonic erosion.

3.6.5 Azuero and Sona Peninsulas, Panama

In western Panama are oceanic complexes are exposed in Azuero and Sona Peninsulas and various islands of the Chiriquí and Montijo gulfs, (e.g. Coiba, Cébaco, Montuosa, Ladrones, Parida, Boca Brava, Contreras), known as the Azuero-Sona Complex.

Pioneer mapping includes the work of DelGiudice and Recchi (1969), DGRM, (1991) and Kolarsky et al. (1995). This complex consists of massive, columnar and pillow basalts with some interbedded radiolarites. Schistose amphibolites (Tournon et al., 1989) are reported as slivers along the Azuero-Soná fault zone (Kolarsky et al., 1995). Metabasalts and metatuffs with a shear foliation and tectonic mélanges were found by Tournon et al. (1989). The metamorphic basement is covered by pillow basalts and cut by doleritic dikes. Tournon et al. (1995) considered that the metabasalts form Azuero and Sona are evidence for a regional metamorphism prior the intra-Senonian tectonic phase that affected the rest of Mesozoic formations to cropping out along the Pacific coast.

One Coniacian radiolarite is reported in the Azuero peninsula (Kolarsky et al., 1995). The $^{40}Ar/^{39}Ar$ ages from lava flows and pillow basalts from Panama range from 21

Ma to 71 Ma. The Azuero-Sona complex possibly represents accreted pieces of older Galapagos Hotspot tracks (Hoernle et al., 2004 and Denyer et al., 2006).

4. Discussions and concluding remarks

The oceanic complexes (Jurassic-Cretaceous to Miocene) outcropping on the Pacific shore of Costa Rica have been relatively well studied, especially on the Nicoya Peninsula. Micropaleontological, geochemical and petrological investigations were applied to these complexes during the last three decades (Ragazzi, 1996; Sinton et al., 1997; Alvarado et al., 1997; Hauff et al., 1997; Beccaluva et al., 1999; Arias, 2000; Hauff et al., 2000; Hoernle et al., 2002; Hoernle et al., 2004 and Denyer et al., 2006). These efforts helped to solve some specific problems, such as describing the tectonic structure of Santa Elena peninsula (Gazel et al., 2006) and the geotectonic origin of the Nicoya Complex (Denyer and Baumgartner, 2006). However, many other unknowns require significant additional study due to the complexity of the tectonic processes in this margin.

Although incomplete, the preserved sections of oceanic crust have made it possible to develop the geotectonic history of the region. Rocks of the Santa Elena Nappe, with a geochemical signature of island arc affinity, were emplaced between the Aptian and Cenomanian (e.g., Gazel et al., 2006) (Fig. 2). In this scenario, the ultramafic complex corresponds to the upper-most mantle, the layered gabbros to the magmatic chambers, and sheeted dike complexes representing transport. The relationship of the Murciélago Islands to rest of the Santa Elena Nappe is not clear. However, both have similar geochemical signatures. This suggests that the basalts of the Murciélago islands may represent the upper level of the arc.

The serpentinized mantle peridotites of the Santa Elena Nappe have been correlated to serpentinized peridotites outcropping at both sides of the Costa Rican-Nicaraguan border (locality B1, Fig. 1) and also with the base of the Tonjibe 1 drill hole (locality B2, Fig. 1) (Astorga, 1992; Vargas and Alfaro, 1992; Pizarro, 1993; Tournon et al., 1995). All of these ultramafic suites have been interpreted as part of an east-west suture zone between the southern oceanic-type crust of the Chorotega Block and the northern continental-type crust of the Chortis Block (Dengo, 1985; Tournon et al., 1995). This suture zone represents a major tectonic structure in alignment with the Hess Escarpment (Holcombe et al., 1990). Similar serpentinized mantle peridotites and mafic associations are exposed in Siuna, Nicaragua (Venable, 1994; Rogers, 2003; Baumgartner et al., 2008) and in the DSDP (Deep Sea Drilling Project) sites 494 and 567 in the fore-arc of Central America (Geldmacher et al., 2008). The complexes north of this east-west structure are part of the Mesquito Terrane (Baumgartner et al., 2008) and represent a supra-subduction complex related to the subduction of the Pacific-Farallon plate (Geldmacher et al., 2008). The northern boundary between this terrane and the Chortis Block is somewhere between Siuna and northern continental crust in Nicaragua (Fig. 10).

The arc-like geochemical signatures of rocks at Santa Elena and DSDP sites 494 and 567 (Hauff et al., 2000; Hoernle, 2004; Geldmacher et al., 2008), are convincing evidence that these rocks are not genetically related to the CLIP or the Galapagos Plume (Geldmacher et al., 2008). For example, the rocks of the Santa Elena Nappe show depletions in HFSE (Fig. 6) and enrichments in LILES, suggesting a subduction modified NMORB source. In addition, OIB lavas with similar geochemical characteristics to the ones at the Santa Rosa Accretionary Complex have been found in DSDP sites 494 and 567 and are possibly related to another Pacific hotspot (Geldmacher et al., 2008).

The geochemical and isotopic correlation between the Tortugal Suite and the alkaline basalts of the Santa Rosa Accretionary Complex (Hauff et al., 2000) and the fact that both localities are overlain by Upper Cretaceous Caribbean rudists (Fischer and Aguilar, 2007) suggests they were formed as part of the autochthonous Tethys ocean. This evidence suggests that Santa Elena and Tortugal (and the Mesquito Terrane) were already in place by the Upper Cretaceous. This was basement where other exotic terranes, such as fragments of the CLIP and Galapagos oceanic islands accreted from the end of Cretaceous through Miocene.

The Nicoya Complex and the rest of the Cretaceous oceanic complexes that are part of the CLIP are characterized by a distinctive flat REE-pattern (Fig. 5) and HFSE ratios between EMORB and NMORB values (Sun and McDonough, 1989). Their Zr/Nb ratios are within the range of oceanic plateau basalts (Condie, 2005). The $^{207}Pb/^{204}Pb$ ratios range from 15.53-15.57 and $^{206}Pb/^{204}Pb$ from 18.54-19.00 (Fig. 7). These isotopic ratios are more enriched than typical oceanic crust, indicating a FOZO (Focal Zone) to HIMU (high U/Pb ratio mantle) mantle reservoir (Zindler and Hart, 1986; Strake et al., 2005). This suggests the participation of a plume component, possibly related to the Galapagos Hotspot, interacting with a mid-ocean ridge system.

There are two geochemical populations of accreted oceanic islands/seamounts on Pacific coast of Costa Rica. First, the Cretaceous oceanic islands that include the Tortugal

Suite and the OIB's within the Santa Rosa Accretionary Complex. They have LREE enrichments, HFSE values between EMORB and OIB. Their Pb isotope ratios suggest an EMII component. Second, the post-Paleocene oceanic islands like the Tulín Formation, Quepos Block and Rincon Block. Samples from these units are also enriched in LREE (but with less steep patterns) and have HFSE ratios close to EMORB (Fig. 6). They have Pb-isotopic ratios more radiogenic than the CLIP and trending towards a HIMU reservoir. All evidence suggests that the post-Paleocene complexes represent Galapagos tracks accreted to this convergent margin.

After this comprehensive analysis, we recognized that the oceanic complexes consist mainly of obducted-accreted slabs of oceanic crust. The presence of this large province of accreted oceanic complexes suggests that accretionary processes have been more relevant than tectonic evolution in the early history of this margin.

5. References

Alvarado, G., Denyer, P., 1998. Implications for the Caribbean region of the high-Mg volcanic rocks in the Costa Rican ophiolitic complexes: The case of the Tortugal komatiitic-like suite. Zentralblatt für Geologie und Paläontologie 1977(3-6) 409-429.

Alvarado, G., Denyer, P., Sinton, C., 1997. The 89 Ma Tortugal komatiitic suite, Costa Rica: Implications for a common geological origin of the Caribbean and Eastern Pacific region from a mantle plume. Geology 25(5) 439-442.

Arias, M., 2002. Petrografía y geoquímica de las rocas del Complejo Ígneo Estratificado de Bahía Nancite y su relación con los filones basálticos, península de Santa Elena, Costa Rica. Lic. Thesis. Universidad de Costa Rica. 94 pp.

Arias, O., 2000. Geología y petrología magmática del bloque Herradura (Cretácico Superior-Eoceno), Costa Rica. PhD Thesis. Université de Lausanne. 186 pp.

Arias, O., 2003. Redefinición de la Formación Tulín (Mastrichtiano-Eoceno Inferior) del pacífico central de Costa Rica. Revista Geológica de América Central 28, 47-68.

Astorga, A., 1992. Descubrimiento de corteza oceánica mesozoica en el norte de Costa Rica y el sur de Nicaragua. Revista Geológica de América Central 14, 109-112.

Azéma, J.; Tournon, J., 1980. La péninsule de Santa Elena, Costa Rica: Un massif ultrabasique charrié en marge pacifique de l'Amérique Centrale, Costa Rica: Comptes Rendus de L'Academie des Sciences des Paris 290, 9-12.

Azéma, J., Glaçon, G., Tournon, J., Vila, J.-M., 1978. Precisiones acerca del Paleoceno de puerto Quepos y sus alrededores, provincia de Puntarenas, Costa Rica. Informe Semestral Instituto Geográfico Nacional 1978(2) 77-88.

Azéma, J., Origlia, I., Tournon, J., DeWever, P., 1982. Nouvelles données sur la présence de Crétacé Moyen au sein des formations volcano-sedimentaires de l'autochtone relatif de la péninsule de Santa Elena (Costa Rica, Amérique Centrale). 9[a] Réunion annuelle des Sciences de la Terre, Paris 1982. Société Géologique de France 1(2) 173-179.

Azéma, J., Bourgois, J., Tournon, J., Baumgartner, P.O., Desmet, A., 1985. L'Orogène pré-sénnonien supérieur de la marge pacifique du Costa Rica (Amérique Centrale). Bulletin Sociètè Géologique de France 1(2) 173-179.

Baumgartner, P.O, 1984. El complejo ofiolítico de Nicoya (Costa Rica): Modelos estructurales analizados en función de las edades de los Radiolarios (Calloviense a Santoniense). In: Spechmann, P. (Ed.), Manual de Geología de Costa Rica. San Josè- Costa Rica, Editorial Universidad de Costa Rica, pp. 115-123.

Baumgartner, P.O., 1986: Discovery of subduction-related mélange on Caño Island and Osa Peninsula (Pacific, Costa Rica, Central America): Réunion annuelle des Sciences de la Terre, 1 lème, Clermond-Ferrand, France. Abstract, p. 12.

Baumgartner, P.O, 1987. Tectónica y sedimentación del Cretácico superior en la zona pacífica de Costa Rica (América Central). In: Barbarin, J.M., Gursky, H.-J., Meiburg, P. (Eds.), El Cretácico de México y América Central: Actas Facultad de Ciencias de la Tierra, Universidad Autónoma de Nuevo León, Linares (México) 2, pp. 251-260.

Baumgartner, P.O., Denyer, P. 2006. Evidence for Middle Cretaceous accretion at Santa Elena Peninsula (Santa Rosa Accretionary Complex), Costa Rica. Geologica Acta 4(1/2) 179-19.

Baumgartner, P.O., Flores, K., Bandini, A.N., Girault, F. Cruz, D.. 2008. Upper Triassic to Cretaceous radiolaria from Nicaragua and northen Costa Rica - the Mesquito Composite Oceanic Terrane. Ofioliti 33(1) 1-19.

Baumgartner, P.O., Mora, C.R., Butterlin, J., Sigal, J., Glacon, G., Azéma, J. Burgois, J., 1984. Sedimentación y paleogeografía del Cretácico y Cenozoico del litoral pacífico de Costa Rica. Revista Geológica de América Central 1, 57-136.

Beccaluva, L., Chinchilla-Chaves, A.L., Coltorti, M., Giunta, G., Siena, F. Vaccaro, C., 1999. Petrological and structural significance of the Santa Elena-Nicoya Ophiolitic Complex in Costa Rica and geodynamic implications. European Journal of Mineralogy 11, 1091-1107.

Bellon, H., Tournon, J., 1978. Contribution de la geochronometrie K-Ar á l'etudie du magmatism de Costa Rica, Amerique Central. Bulletin Socièté Géologique de France 6(7), 955-959.

Berrangé, J.P., Thorpe, R.S., 1988. The geology, geochemistry and emplacement of the Cretaceous-Tertiary ophiolitic Nicoya Complex of the Osa peninsula, southern Costa Rica. Tectonophysics 147, 193-220.

Berrangé, J.P., Bradley D.R., Snelling N.J., 1989. K/Ar dating of the ophiolitic Nicoya Complex of the Osa Peninsula, southern Costa Rica. Journal of South America Earth Sciences 2(1), 49-59.

Bolz, A., Calvo, C., 2003. Nuevos datos bioestratigráficos y sedimentológicos sobre el origen del Complejo Básico de Quepos, Costa Rica. Revista Geológica de América Central 28, 31-45.

Buchs, D.M., Baumgartner, P.O., 2003. The Osa-Caño Accretionary Complex (Southern Costa Rica): Sedimentary processes in the Middle American Trench recorded in an emerged Eocene-Miocene accretionnary prism. Programe and Abstracts. 11th Swiss Meeting of Sedimentologist, Fribourg, p. 35.

Buchs, D.M., Baumgartner, P.O., 2007. Comment “From seamount accreation to tectonic erosion: Formation of Osa Mélange and the effects of Cocos Ridge subduction in southern Costa Rica” by P. Vannucchi et al. Tectonics 26, TC3009, doi:10.1029/2006TC002032.

Buchs, D.M., Stucki, 2001. Etude géologique, éochmique et structurale du complexe d'accrétion de la péninsule d'Osa, Costa Rica. Diplome Thesis. Université de Lausanne. 103 pp.

Burgois, J., Azéma, J., Baumgartner, P.O., Tournon, J., Desmet, A., Aubouin, J., 1984. The geologic history of the Caribbean-Cocos plate boundary with special reference to the Nicoya Ophiolite Complex (Costa Rica) and Deep Sea Drilling Project results (legs 67 and 84 off Guatemala): A synthesis. Tectonophysics 108, 1-32.

Burke, K., Fox, P.J., Sengor, A.M.C., 1978. Buoyant ocean floor and the evolution of the Caribbean. Journal of Geophysical Research 83, 1255-1258.

Clift, P., Vannucchi, P., 2004. Controls on tectonic accretion versus erosion in subduction zones: Implications for the origin and recycling of the continental crust. Reviews of Geophysics 42, RG2001, doi 10.1029/2003RG000127.

Condie, K.C., 2005. High field strength element ratios in Archean Basalts: A window to evolving sources. Lithos 79, 491-504.

DeBoer, J., 1979. The outer arc of the Costa Rican orogen (oceanic basement complexes of the Nicoya and Santa Elena peninsulas. Tectonophysics 56(3/4) 221-259.

DelGiudice, D., Recchi, G., 1969. Geología del área del proyecto minero de Azuero. Map 5. Scale 1:250,000. Administración de Recursos Minerales. República de Panamá.

DeMets, C., 1995. Plate motions and crustal deformation, Reviews of Geophysics 33, 365-369.

DeMets, C., Gordon, R.G., Argus, D.F., Stein, S., 1990. Current plate motions. Geophysical Journal International 101, 425-478.

Dengo, G., 1962a. Tectonic-igneous sequence in Costa Rica. In: Engel, A. E. J., James, H. J., Leonard, B. F. (Eds.), A volume to honor A. F. Budington. Geological Society of America Special Volume, pp. 133-161.

Dengo, G., 1962b. Estudio Geológico de la Región de Guanacaste, Costa Rica. Instituto Geográfico Nacional, San José-Costa Rica, 112 pp.

Dengo, G., 1985. Mid America: Tectonic setting for the Pacific margin from southern Mexico to northwestern Columbia. In: Nairn, A.E.M., Stechli, F.G. (Eds.), The ocean basins and margins. Plenum Press, New York, pp. 123-180.

Denyer, P., Arias, O., 1991. Estratigrafía de la Región Central de Costa Rica. Revista Geológica de América Central 12, 1-59.

Denyer, P., Baumgartner, P.O., 2006. Emplacement of Jurassic-Lower Cretaceous radiolarites of the Nicoya Complex (Costa Rica). Geologica Acta 4(1/2), 203-218.

Denyer, P., Arias, O., 1993. Geología del norte de la península de Nicoya, Costa Rica. Revista Geológica de América Central 16, 69-84.

Denyer, P., Baumgartner, P.O., Gazel, E., 2006. Characterization and tectonic implications of Mesozoic-Cenozoic oceanic assemblages of Costa Rica and Western Panama. Geologica Acta 4(1/2), 219-235.

DeWever, P., Azéma, J, Tournon, J., Desmet, A., 1985. Découverte de matériel océanique du Lias-Dogger inférieur dans la péninsule de Santa Elena (Costa Rica, Amérique Centrale). Comptes Rendus de L'Académie des Sciences des Paris 300(15), 759-764.

DGRM (Dirección General de Recursos Minerales), 1997. Mapa geológico de Panamá. Scale 1:500 000. Panamá. Instituto Geográfico Nacional Tomy Guardia.

DiMarco, G., 1994. Les terrains accrétés du sud du Costa Rica: Evolution tectonostratigraphique de la marge occidentale de la plaque Caraïbe. Mémoires de Géologie 20, 1-185.

DiMarco, G., Baumgartner, P. O., Channell, J.E.T., 1995. Late Cretaceous-early Tertiary paleomagnetic data and a revised tectonostratigraphic subdivision of Costa Rica and western Panama. In: Mann, P. (Ed.), Geological and tectonic development of the Caribbean Plate Boundary in Southern Central America. Geological Society of America Bulletin Special Paper 295, pp. 1-27.

Donnelly, T.H., 1973. Late Cretaceous basalts from the Caribbean, a possible flood basalt province of vast size. Eos Transactions American Geophysical Union 54, 1004.

Donnelly, T.H., 1994. The Caribbean Cretaceous basalt association : A vast igneous province that includes the Nicoya Complex of Costa Rica. Profil 7, 17-45.

Duncan, R. A., Hargraves, R.B., 1984. Plate tectonic evolution of the Caribbean region in the mantle reference frame. Geological Society of America Bulletin Memoir 162, 81-93.

Fischer, R., Aguilar, T., 2007. Chapter 17: Invertebrate paleontology. In: Bundschuh, J., Alvarado, G.E., Taylor & Francis, London, pp. 453-466.

Frisch, W., Meschede, M., Sick, M., 1992. Origin of the Central America ophiolites: Evidence from paleomagnetic results. Geological Society of America Bulletin 104, 1301-1314.

Galli-Olivier, C., 1979. Ophiolite and island-arc volcanism in Costa Rica: Geological Society of America Bulletin 90(1), 444-452.

Gardner, T.W., Verdonck, N., Pinter, N., Slingerland, R., Furlong, K., Bullard, T.F., Wells, S.G., 1992. Quaternary uplift astride the aseimic Cocos Ridge, Pacific coast of Costa Rica. Geological Society of America Bulletin 104, 219-232.

Gazel, E., Denyer, P., Baumgartner, P.O., 2006. Magmatic and geotectonic significance of Santa Elena Peninsula, Costa Rica. Geologica Acta 4(1/2), 193-202.

Gradstein, F.M., Ogg, J.G., Smith, A.G., Bleeker, W., Lourens, L.J., 2004. A New Geologic Time Scale, with special reference to Precambrian and Neogene. Episodes 27(2) 83-100.

Gursky, H.J., 1984. Verbreitung, fazies und geologische geschichtre der sedimentgesteine, insbesondere der radiolarite, im opiolithisschen Nicoya

Komplex (Ober- Jura bis Alt- Tertiär von Costa Rica). PhD Thesis. University of Marburg. 394 pp.

Gursky, H.-J., Gursky, M., 1988. Thermal alteration of chert in the ophiolite basement of southern Central America. In: Hein, J.R., Obradovic, J. (eds.). Siliceous deposits of the Pacific and Tethys Regions. Springer-Verlag, New York, pp. 217-233.

Gursky, H.-J., Schmidt-Effing, R., Strebin, M., Wildberg, H., 1982. The ophiolite sequence in northwestern Costa Rica (Nicoya Complex): Outlines of stratigraphical, geochemical, sedimentological, and tectonical data. Actas V Congreso Latinoamericano de Geología, Buenos Aires 3, 607-619.

Gursky, H.-J., Gursky, M., Schmidt-Effing, R., Wildberg, H., 1984. Karten zur Geologie von Nordwest-Costa Rica (Mittelamerika) mit Erläuterungen. Geologica et Palaeontologica 18, 173-182.

Gursky, M.M., 1988. Estructuras tectónicas de edad cretácica y terciaria en la Peninsula de Nicoya (Costa Rica) y su significado geotectónico. In: Barbarin, J.M., Gursky, H.-J., Meiburg, P. (Eds.), El Cretácico de México y América Central: Actas Facultad de Ciencias de la Tierra. Universidad Autónoma de Nuevo León. Linares (México) 2, pp. 261-265.

Halbach, P., Gursky, H.J., Gursky, M.M., Schmidt-Effing, R., Maresch, W.V., 1992. Composition and formation of fossil manganese nodules in Jurassic to Cretaceous radiolarites from the Nicoya Ophiolite Complex. Mineralium Deposita 27, 153-160.

Hanan, B.B., Pyle, D.G., Sinton, C.W., Denyer, P., Alvarado, G.E., 1998. The Tortugal komatiitic lavas of Costa Rica: Early Galápagos hotspot volcanism in the Caribbean Plateau? Penrose Conference Series: Evolution of ocean island volcanoes, Islas Galápagos, p. 35.

Hauff, F., Hoernle, K., Bogaard, P., 2000. Age and geochemistry of basaltic complexes in western Costa Rica: Contributions to the geotectonic evolution of Central America. Geochemistry, Geophysics, Geosystems 1(5), doi 10.1029/1999GC000020.

Hauff, F., Hoernle, K., Schmincke, H.-U., Werner, R., 1997. A mid Cretaceous origin for the Galapagos hotspot: Volcanological, petrological and geochemical evidence from Costa Rica oceanic crustal fragments. Geologische Rundschau 86, 141-155.

Hoernle, K., van den Bogaard, P., Werner, R., Lissinna, B., Hauff, F., Alvarado, Garbe-Schönberg, D., 2002. Missing history (16-71 Ma) of the Galápagos hotspot: Implications for the tectonic and biological evolution of the Americas. Geologic Society of America Bulletin 30(9), 795-798.

Hoernle, K., Hauff, F., van den Bogaard, P., 2004. 70 m.y. history (139-69 Ma) for the Caribbean large igneous province. Geology 32(8), 697-700.

Holcombe, T.L., Ladd, J.W., Westbrook, G., Edgar, T.N., Bowland, C.L., 1990. Caribbean marine geology: Ridges and basins of the plate interior. In: Dengo, G., Case, J.E. The Caribbean Region: The Geology of North America. Geological Society of America H, pp. 231-260.

Kolarsky, R.A., Mann, P., Monechi, S., 1995. Stratigraphic development of southwestern Panama as determined from integration of marine seismic data and onshore geology. In: Mann, P. (ed.). Geological and tectonic development of the Caribbean Plate Boundary in Southern Central America. Geologic Society of America Bulletin, Special Paper, 195, 159-200.

Kuijpers, E., 1980. The geologic history of the Nicoya Ophiolite Complex, Costa Rica, and its geotectonic significance, Tectonophysics 68, 233-255.

Kuijpers, E.P., Denyer, C.P., 1979. Volcanic exhalative manganese deposits of the Nicoya Ophiolite Complex, Costa Rica. Economic Geology and the Bulletin of the Society of Economic Geologists 74(3), 672-678.

Malavassi, E., 1967. Informe geológico de la hoja Candelaria. Informes Ministerio Economía, Industria y Comercio 1967, 1-16.

Malfait, B.T., Dinkelman, M.G., 1972. Circum-Caribbean tectonic and igneous activity and the evolution of the Caribbean plate. Geological Society of America Bulletin 83, 2512-2272.

Meschede, M., Frisch, W., 1994. Geochemical characteristics of basaltic rocks from the Central American ophiolites. Profil 7, 71-85.

Meschede, M., Frisch, W., 1998. A plate tectonic model for the Mesozoic and Early Cenozoic history of the Caribbean plate. Tectonophysics 296, 269-291.

MIEM (Ministerio de Industria, Economía y Comercio), 1982. Mapa Geológico de Costa Rica. 9 maps. Scale 1:200 000. Instituto Geográfico Nacional. San José, Costa Rica.

Obando, J.A., 1986. Sedimentología y tectónica del Cretácico y Paleógeno de la región de Golfito, península de Burica y península de Osa, provincia de Puntarenas, Costa Rica. Licenciature Thesis. Universidad de Costa Rica, 211 pp.

Pizarro, D., 1993. Los pozos profundos perforados en Costa Rica: Aspectos litológicos y bioestratigráficos. Revista Geológica de América Central, 14, 81-85.

Ragazzi, C., 1996. Petrologia e geologia del Complesso Ofiolitico di Nicoya-St. Elena (Costa Rica). PhD Thesis. Università degli Studi di Ferrara, 115 pp.

Ranero, C.R, vonHuene, R., 2000. Subduction erosion along the Middle America convergent margin. Nature 404(6779), 748-52.

Ranero, C.R., Phipps Morgan, J., McIntosh, K., Reichert, C., 2003. Bending-related faulting and mantle serpentinization at the Middle America trench. Nature 425, 367-373.

Rogers, R. S., 2003. Jurassic-Recent tectonic and stratigraphic history of the Chortis block of Honduras and Nicaragua (northern Central America). PhD Thesis. University of Texas, 264 pp.

Schmidt-Effing, R., 1979. Alter und Genese des Nicoya-Komplexes, einer ozeanischen Palaokruste (Objura bis Eozan) im sudlichen Zentral-Amerika. Geologische Rundschau 68(2), 457-494.

Schmidt-Effing, R., 1980a. Radiolarien der Mittel-Kreide aus dem Santa Elena-Massiv von Costa Rica. Neves Jahrbuch Geologie und Pläontologie 160(2), 241-257.

Schmidt-Effing, R., 1980b. Rasgos fundamentales en la historia del Complejo de Nicoya (América Central Meridional). Brenesia 18, 231-252.

Sick, M., 1989. Paleomagnetism of the Ophiolite Complex from the southern Middle American Landbridge (Costa Rica and Western Panamá). Geowissenschaftliche Abhandlungen 4, 1-108.

Sinton, C. W., Duncan, R. A., Denyer, P., 1997. Nicoya península: A single suite of Caribbean oceanic plateau magmas. Journal of Geophysical Research 102(B7), 15507-15520.

Strake, A., Hofmann, A.W., Hart. 2005: FOZO, HIMU and the rest of the mantle zoo, Geochemistry, Geophysics, Geosystems (G^3), 1(5), doi 10.1029/ 2004GC000824.

Sun, S-S., McDonough, W.F., 1989. Chemical and isotopic systematics of oceanic basalts: Implications for mantle compositions and processes. In: Saunders, A.D., Norry, M.J. (Eds.). Magmatism in the Ocean Basins. Geological Society, Special Paper 42, pp. 313-345.

Tournon, J. 1984, Magmatismes du Mesozoique á l' actuel en Amerique Centrale: L' exemple de Costa Rica, des ophiolites aux andesites. PhD Thesis. University Pierre and Marie Curie, 335 pp.

Tournon, J., Triboulet, C., Azéma, J., 1989. Amphibolites from Panama: Anticlockwise P-T paths from a pre-Upper Cretaceous metamorphic basement in Isthmian Central America. Journal of Metamorphic Geology 7, 539-546.

Tournon, J., 1994. The Santa Elena Peninsula: An ophiolitic nappe and a sedimentary volcanic relative autochthonous. Profil 7, 87-96.

Tournon, J., Seyler, M., Astorga, A., 1995. Les peridotites du Rio San Juan (Nicaragua et

Costa Rica); jalons possibles d'une suture ultrabasique E-W en Amerique Centrale meridionale. Comptes Rendus de L' Academie Des Sciences Serie II, 757-764.

Vannucchi, P. Fisher, D.M., Gardner, T.W., 2007. Reply to comment by David M. Buchs and Peter O. Baumgartner on "From seamount accreation to tectonic erosion: Formation of Osa Mélange and the effects of Cocos Ridge subduction in southern Costa Rica." Tectonics 26, TC3010, doi:10.1029/2007TC002129.

Vannucchi, P. Fisher, D.M. Bier, S., Gardner, T.W., 2006. From seamount accretion to tectonic erosion: Formation of Osa Mélange and the effects of Cocos Ridge subduction in southern Costa Rica. Tectonics 25, TC2004. doi: 10.1029/2005TC001855.

Vannucchi, P.,D. W. Scholl, M. Meschede, McDougall-Reid, K., 2001. Tectonic erosion and consequent collapse of the Pacific margin of Costa Rica: Combined implications from ODP Leg 170, seismic offshore data and regional geology of the Nicoya Peninsula. Tectonics 20, 649-668.

Vargas, F., Alfaro, A., 1992. Presencia de serpentinitas, basaltos alcalinos y rocas volcánicas ácidas en la zona norte-Atlántica de Costa Rica. Revista Geológica de América Central 14, 105-107.

Venable, M.E., 1994. A geologic, tectonic, an metallogenic evaluation of Siuna Terrane. PhD Thesis. University of Arizona, 154 pp.

Von Huene, R., Scholl, D.W., 1991. Observations at convergent margins concerning sediment subduction, subduction erosion, and the growth of continental crust. Reviews of Geophysics 29, 279-316.

Widberg, H.G.H., 1984. Der Nicoya Komplex, Costa Rica, Zentralamerika: Magmatismus und genese eines polymagmatischen Ophiolith-Komplexes. Münster Forschungsschwerpunkte Geologisch Paläontologisches 62, 1-123.

Zindler, A., Hart, S.R., 1986. Chemical geodynamics. Annual Review of Earth and Planetary Sciences 14, 493-571.

Figure captions

Figure 1

A) Present day tectonic setting of the Caribbean region, showing the occurrences of oceanic complexes in the region based on Dengo (1985), DeMets et al. (1990) Donnelly (1994), Meschede and Frisch (1994), Tournon et al. (1995), Ranero and von Huene (2000), Ranero et al. (2003) B) Location of the oceanic complexes of Costa Rica mentioned in this paper. Geologic sketched maps of the oceanic complexes of Santa Elena - Nicoya peninsulas (C) Herradura-Quepos (D) and Osa-Burica (E) The numbers in circles correspond to localities mentioned in the text.

Figure 2

Generalized chrono-stratigraphic column of the oceanic complexes of Costa Rica showing the main tectonic and magmatic events. Triangles indicate accretion and nappe tectonic events. Ages based on Gradstein et al. (2004).

Figure 3

North-south cross section of Santa Elena Peninsula. Santa Elena Nappe and Santa Rosa Acretionary Complex have been tilted toward the north. The Santa Rosa Accretionay Complex outcrops in east-west trending reverse fault controlled tectonic windows.

Figure 4

A) Doleritic dike swarm crossing the peridotite of Santa Elena in Potrero Grande Bay (locality C1, Fig. 1). B) Microphotograph of an amphibolitic dolerite of the Santa Elena Nappe collected in the Seco River, Santa Elena Peninsula (locality C2, Fig. 1). Note the hornblende alignment. C) The dolerite swarm becomes so dense in Punta Santa Elena (locality C3, Fig. 1) that only isolated peridotite (π) relicts can be recognized. Punta Santa Elena. D) Tectonically isolated meter-size-block of dolerite rounded by serpentinized dunite (locality C4, Fig. 1). E) Vertical-northward tilted pillow lavas of the Murciélago Islands (locality C6, Fig. 1). F) 90 degrees tilted columnar basalts of the Murciélago Islands (locality C7, Fig. 1). G) Part of the Santa Rosa Accretionary Complex vertical section, showing meter-thick alkaline-basaltic sills (locality C5, Fig.1) between radiolarites. H) Folded green ribboned cherts of the Santa Rosa Accretionary Complex (locality C5, Fig.1).

Figure 5

Average REE patterns from lavas of the different oceanic complex Costa Rica. Data from Sinton et al. (1997), Beccaluva (1999), Arias (2000), Hauff (2000) and Hoernle (2002). Santa Elena Nappe and Murciélago Islands n=2, Nicoya Complex at Nicoya Peninsula n=34, Nicoya Complex at Herradura Block n=7, Tulín Formation n=8, Quepos Block n=9, Osa-Rincón Block n=7 for the flat REE and 2 for the LREE depleted. There is only one REE analysis from the Santa Rosa Accretionary Complex OIB’s. Normalization values after Sun and McDonough (1989).

Figure 6

HFSE ratios from lavas of the different Costa Rican oceanic complexes. NMORB, EMORB and OIB after Sun and McDonough (1989) reference values.

Figure 7

Age corrected Pb isotope ratios of the different Costa Rican oceanic complexes. Data from Hauff et al. (2000) and Hoernle et al. (2002). These complexes trend to mantle reservoirs defined by Zindler and Hart (1986); DMMa (Depleted MORB mantle a), EMII (Enriched Mantle II) and HIMU (High U/Pb mantle).

Figure 8

A) Microphotograph of typical basalt of the Nicoya Complex (locality C9, Fig. 1). B) Microphotograph of a gabbro from the Potrero Intrusive, Nicoya Complex (locality C10, Fig. 1). C) Two magmatic events recognized based on the secondary veins density (locality C11, Fig. 1). D) Chevron folded Upper Jurassic radiolarites of Sardinal (locality C8, Fig. 1). E) Centimeter-size manganese nodules interbedded in the radiolarites of El Encanto (locality C13, Fig. 1), the nodules were digitally enhanced to better distinguished in the photograph. F) Gabbro-radiolarite contact showing bleached meter-wide zone of radiolarites, north of Flamingo beach (locality C12, Fig. 1). G) Detail of the gabbro-radiolarite contact of photograph E, note the dolerite sill close to the contact (locality C12, Fig. 1). H) Plastically deformed radiolarite as a result of the intrusion of the leucocratic dolerite, El Encanto (locality C13, Fig. 1).

Figure 9

A) Meter-size-xenolith of radiolarite included within a leucocratic dolerite, El Encanto (locality C13, Fig. 13). B) Fold in radiolarites showing pervasive intrusion of dolerites in the hinge zone, El Encanto (locality C13, Fig. 1). C) Typical outcrop of the Tortugal Suite, blocks on top of small hills in flat areas (locality C14, Fig. 1). D) Microphotograph of a picrite of the Tortugal Suite showing a clear porphyritic texture, defined by euhedral olivine phenocrysts (locality C15, Fig. 1). E) Micro-spinifex texture in the komatiite-like lava of the Tortugal Suite (locality C14, Fig. 1). F) Sub-horizontal pillow lavas of the Tulín Formation (locality D1, Fig. 1), photographed by O. Arias. G) Microphotograph of a Quepos picrite (locality D2, Fig. 1). H) Blocks of radiolarites included into a basaltic sheared matrix are common in the Osa-Caño Accretionary Complex (locality E1, Fig. 1).

Figure 10

Main tectonic structures and units of Central America and Caribbean region, modified from Dengo (1985).

Figure 1

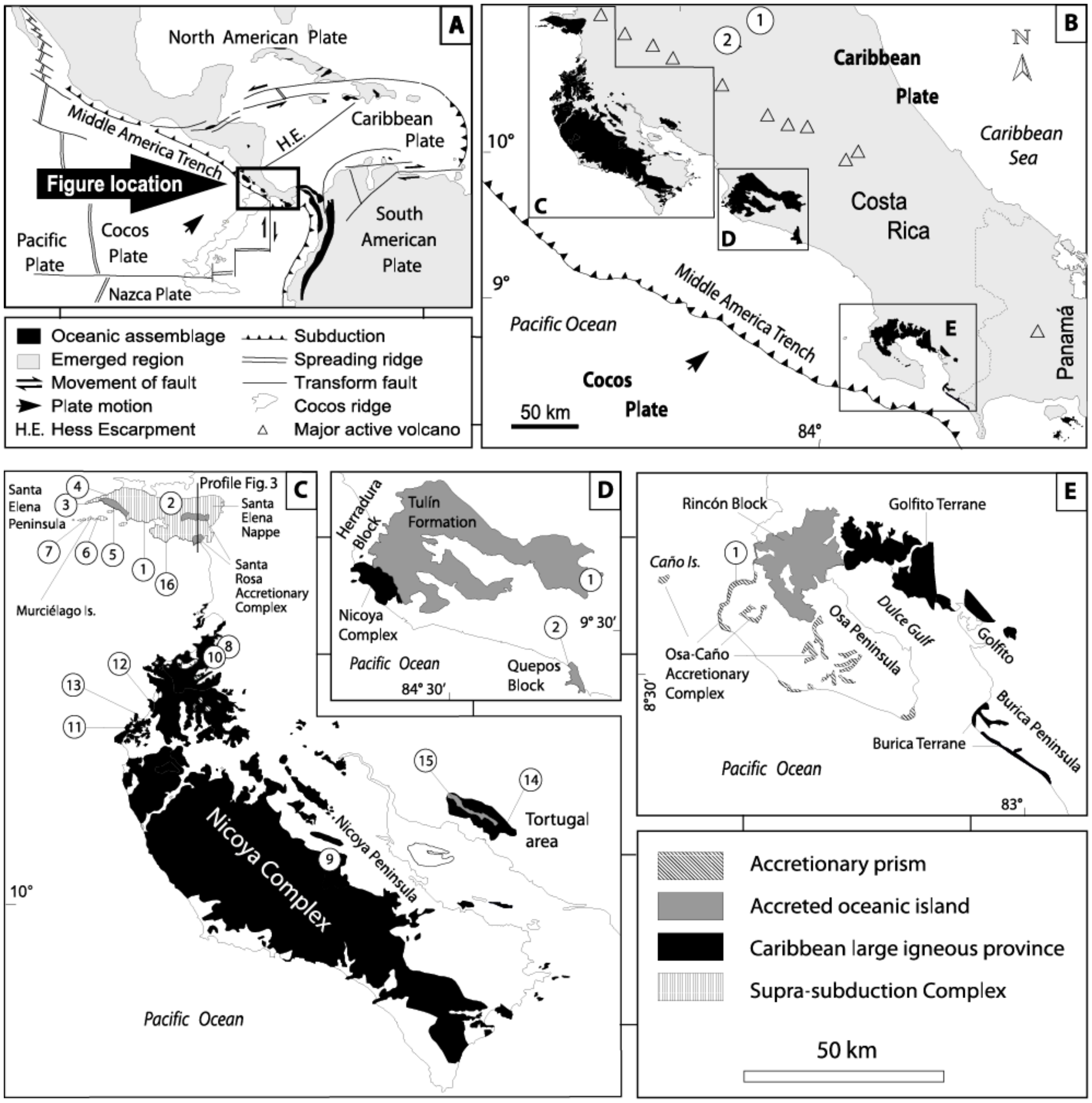
A
North American Plate
Middle America Trench
Caribbean Plate
H.E.
Figure location
Pacific Plate
Cocos Plate
South American Plate
Nazca Plate
Oceanic assemblage
Emerged region
Movement of fault
Plate motion
H.E. Hess Escarpment
Subduction
Spreading ridge
Transform fault
Cocos ridge
Major active volcano
B
Caribbean Plate
Caribbean Sea
Costa Rica
10°
9°
Pacific Ocean
Middle America Trench
Cocos Plate
50 km
84°
Panamá
C
Santa Elena Peninsula
Profile Fig. 3
Santa Elena Nappe
Santa Rosa Accretionary Complex
Murciélago Is.
Nicoya Complex
Nicoya Peninsula
Tortugal area
10°
Pacific Ocean
D
Herradura Block
Tulín Formation
Nicoya Complex
9° 30′
Pacific Ocean
84° 30′
Quepos Block
E
Rincón Block
Golfito Terrane
Caño Is.
Dulce Gulf
Osa Peninsula
Golfito
Osa-Caño Accretionary Complex
8°30′
Burica Terrane
Burica Peninsula
Pacific Ocean
83°
Accretionary prism
Accreted oceanic island
Caribbean large igneous province
Supra-subduction Complex
50 km

Figure 2

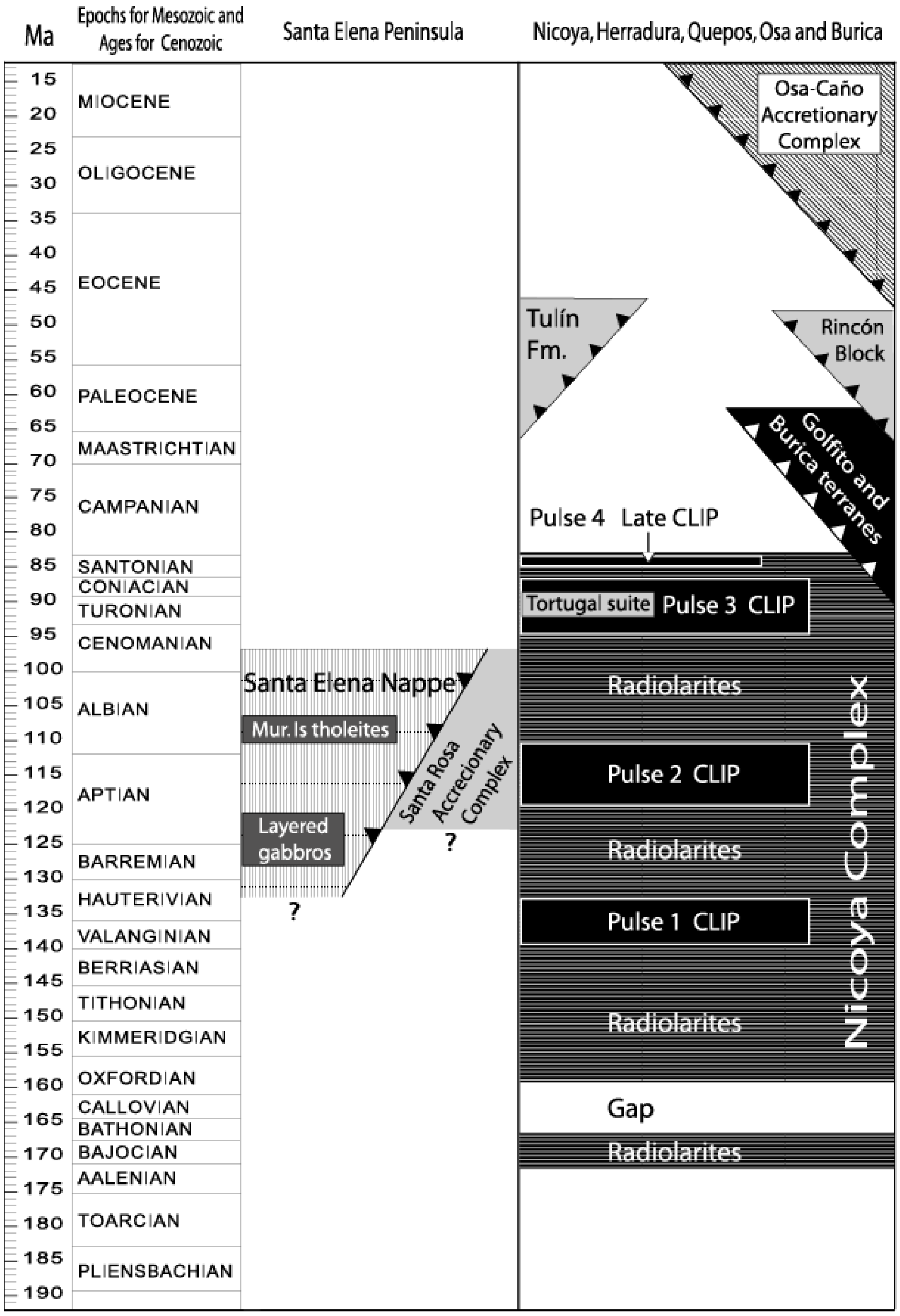
Ma
Epochs for Mesozoic and Ages for Cenozoic
Santa Elena Peninsula
Nicoya, Herradura, Quepos, Osa and Burica
15
20
25
30
35
40
45
50
55
60
65
70
75
80
85
90
95
100
105
110
115
120
125
130
135
140
145
150
155
160
165
170
175
180
185
190
MIOCENE
OLIGOCENE
EOCENE
PALEOCENE
MAASTRICHTIAN
CAMPANIAN
SANTONIAN
CONIACIAN
TURONIAN
CENOMANIAN
ALBIAN
APTIAN
BARREMIAN
HAUTERIVIAN
VALANGINIAN
BERRIASIAN
TITHONIAN
KIMMERIDGIAN
OXFORDIAN
CALLOVIAN
BATHONIAN
BAJOCIAN
AALENIAN
TOARCIAN
PLIENSBACHIAN
Santa Elena Nappe
Mur. Is tholeites
Layered gabbros
Santa Rosa Accrecionary Complex
?
?
Osa-Caño Accretionary Complex
Tulín Fm.
Rincón Block
Golfito and Burica terranes
Pulse 4 Late CLIP
Tortugal suite
Pulse 3 CLIP
Radiolarites
Pulse 2 CLIP
Radiolarites
Pulse 1 CLIP
Radiolarites
Nicoya Complex
Gap
Radiolarites

Figure 3

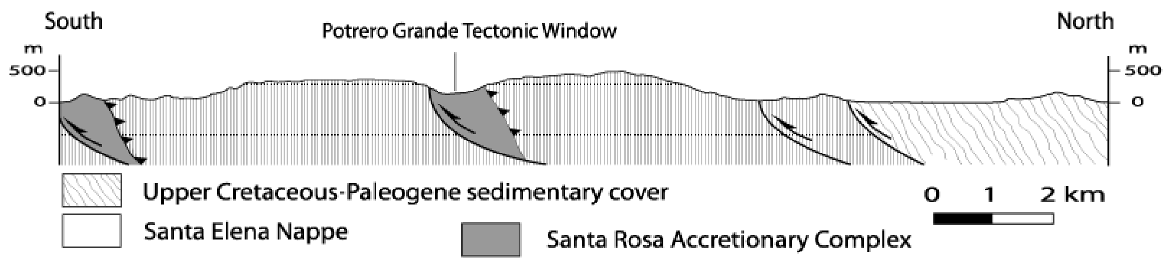
South
Potrero Grande Tectonic Window
North
m
500
0
m
500
0
Upper Cretaceous-Paleogene sedimentary cover
Santa Elena Nappe
Santa Rosa Accretionary Complex
0 1 2 km

Figure 4

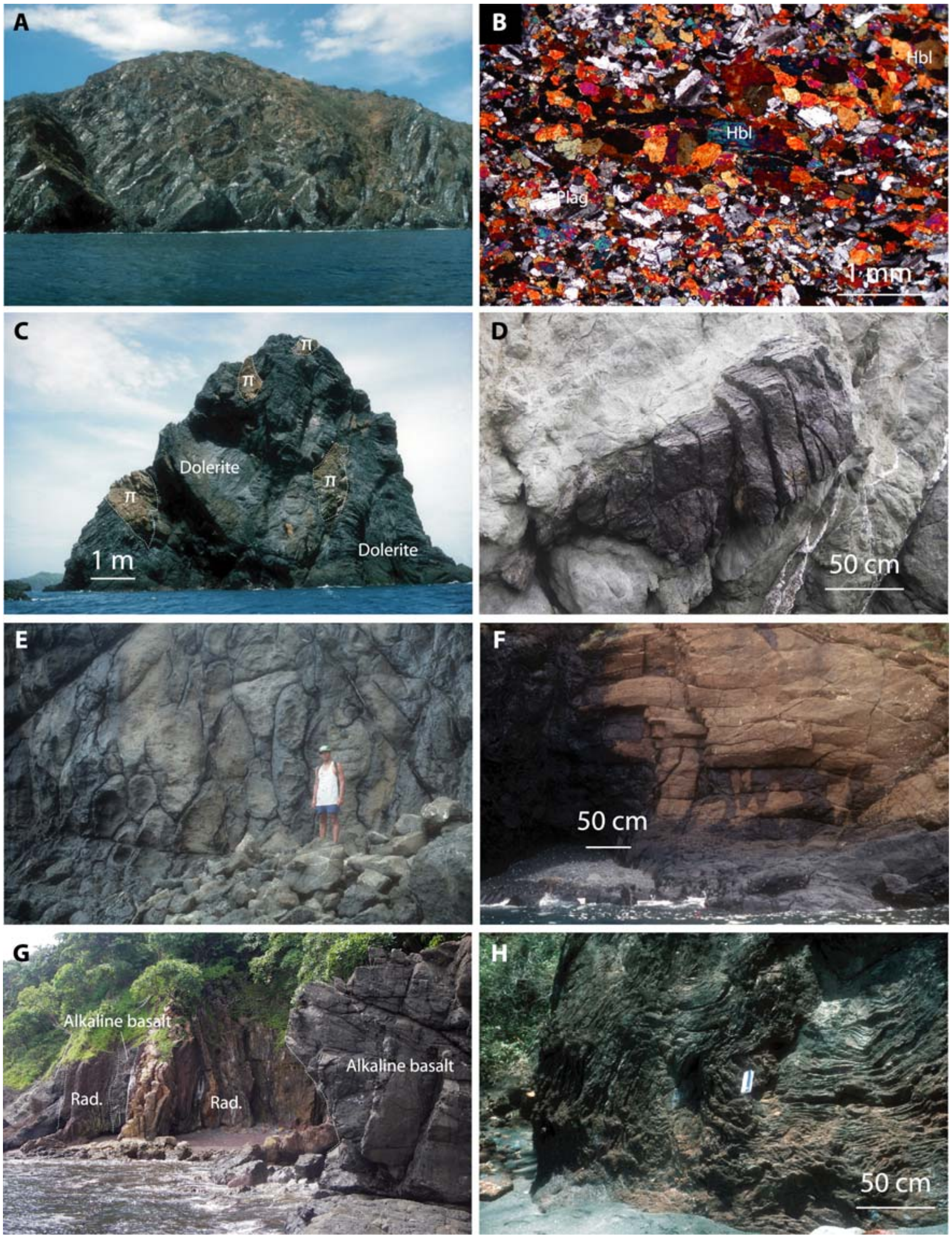
A
B
Hbl
Hbl
Plag
1 mm
C
π
π
Dolerite
π
π
1 m
Dolerite
D
50 cm
E
F
50 cm
G
Alkaline basalt
Alkaline basalt
Rad.
Rad.
H
50 cm

Figure 5

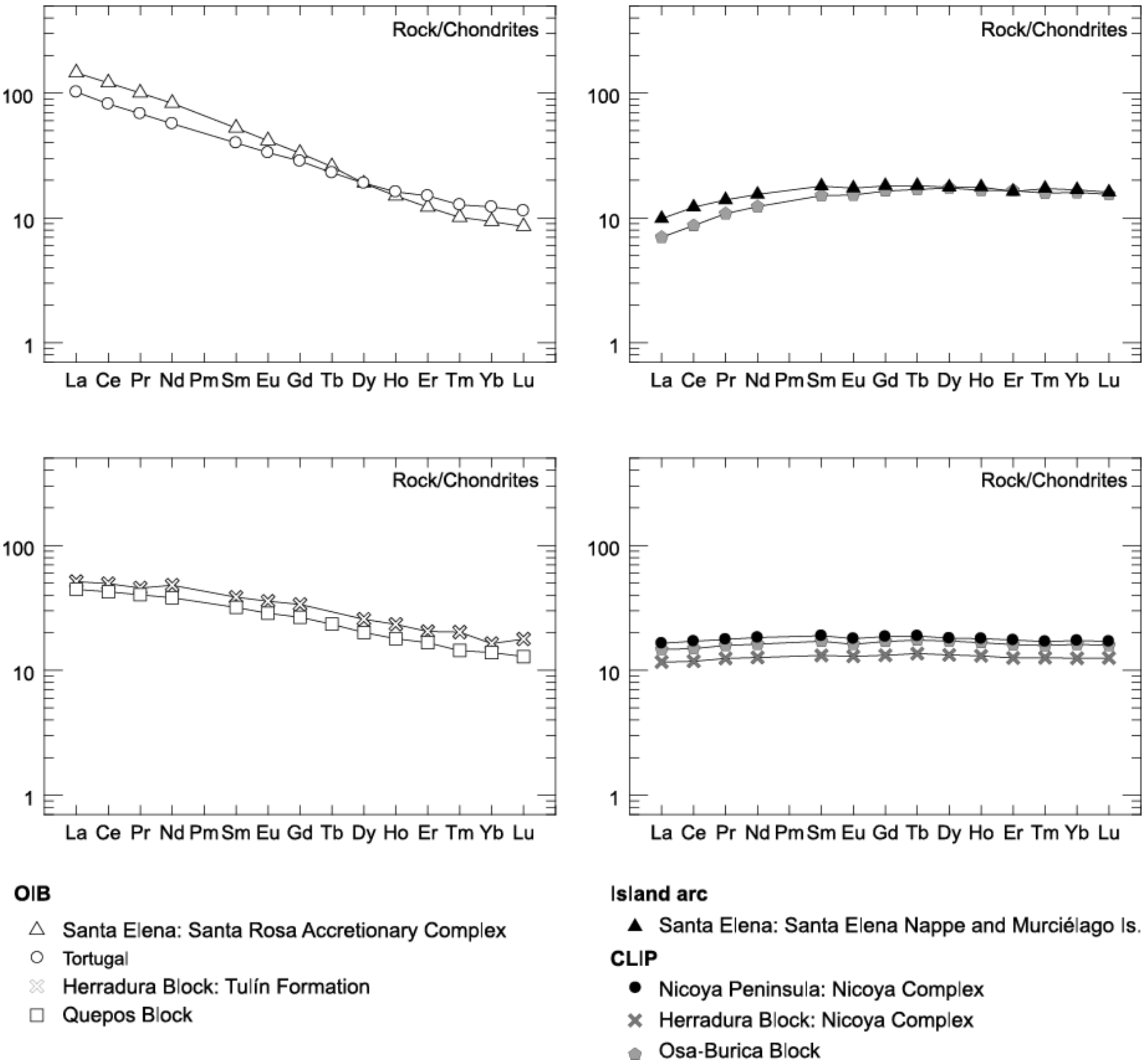
Rock/Chondrites
100
10
1
La Ce Pr Nd Pm Sm Eu Gd Tb Dy Ho Er Tm Yb Lu
OIB
Santa Elena: Santa Rosa Accretionary Complex
Tortugal
Herradura Block: Tulín Formation
Quepos Block
Island arc
Santa Elena: Santa Elena Nappe and Murciélago Is.
CLIP
Nicoya Peninsula: Nicoya Complex
Herradura Block: Nicoya Complex
Osa-Burica Block

Figure 6

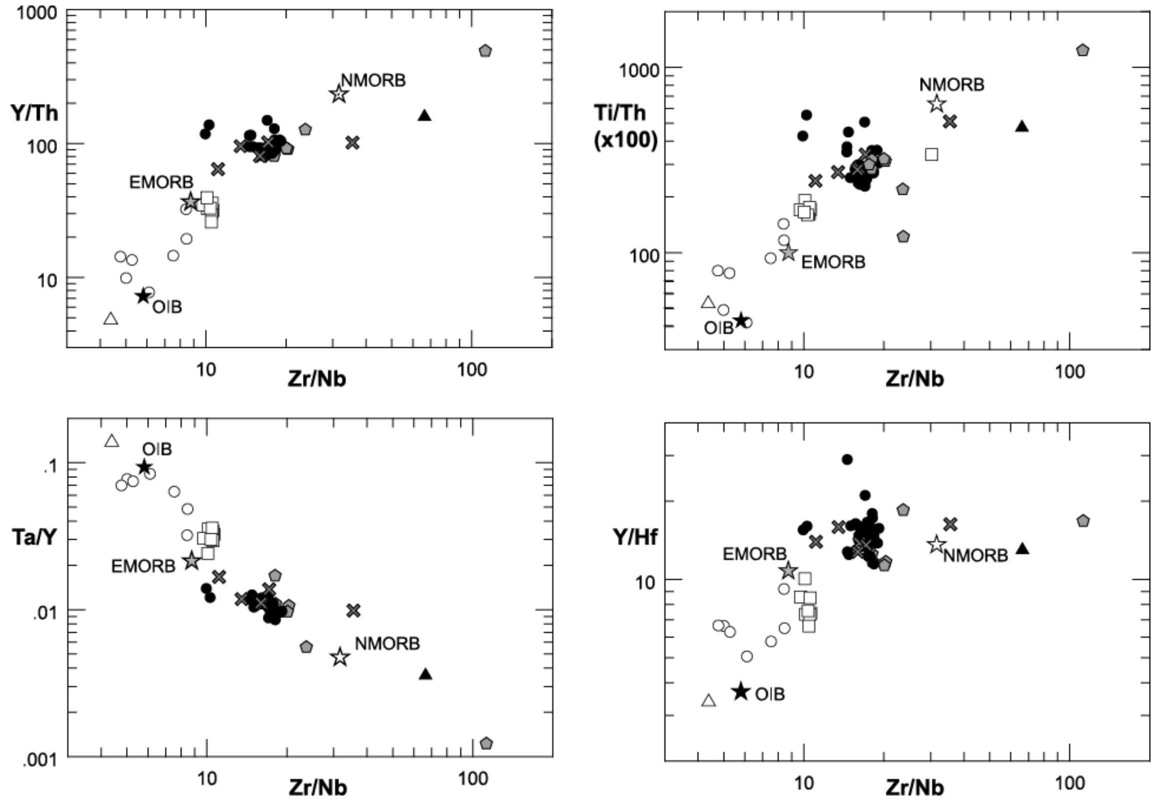

OIB

- △ Santa Elena: Santa Rosa Accretionary Complex
- ○ Tortugal
- ✖ Herradura Block: Tulín Formation
- □ Quepos Block

Island arc

- ▲ Santa Elena: Santa Elena Nappe and Murciélago Islands

CLIP

- ● Nicoya Peninsula: Nicoya Complex
- ✖ Herradura Block: Nicoya Complex
- ⬟ Osa-Burica Block

Figure 7

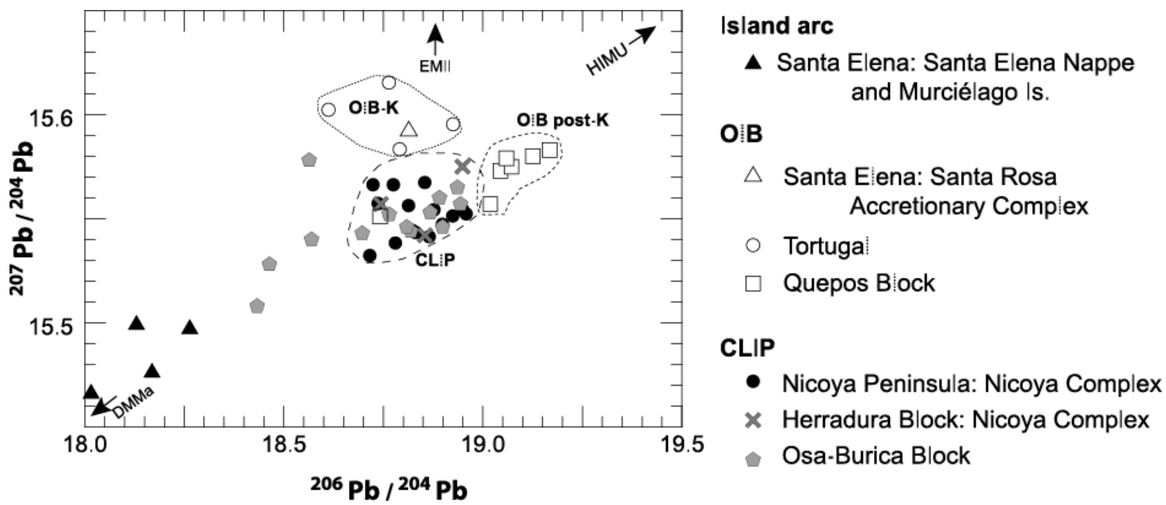
Island arc
Santa Elena: Santa Elena Nappe and Murciélago Is.
OIB
Santa Elena: Santa Rosa Accretionary Complex
Tortugal
Quepos Block
CLIP
Nicoya Peninsula: Nicoya Complex
Herradura Block: Nicoya Complex
Osa-Burica Block
OIB-K
OIB post-K
CLIP
EMII
HIMU
DMMa
15.6
15.5
18.0
18.5
19.0
19.5
^{206}Pb / ^{204}Pb
^{207}Pb / ^{204}Pb

Figure 8

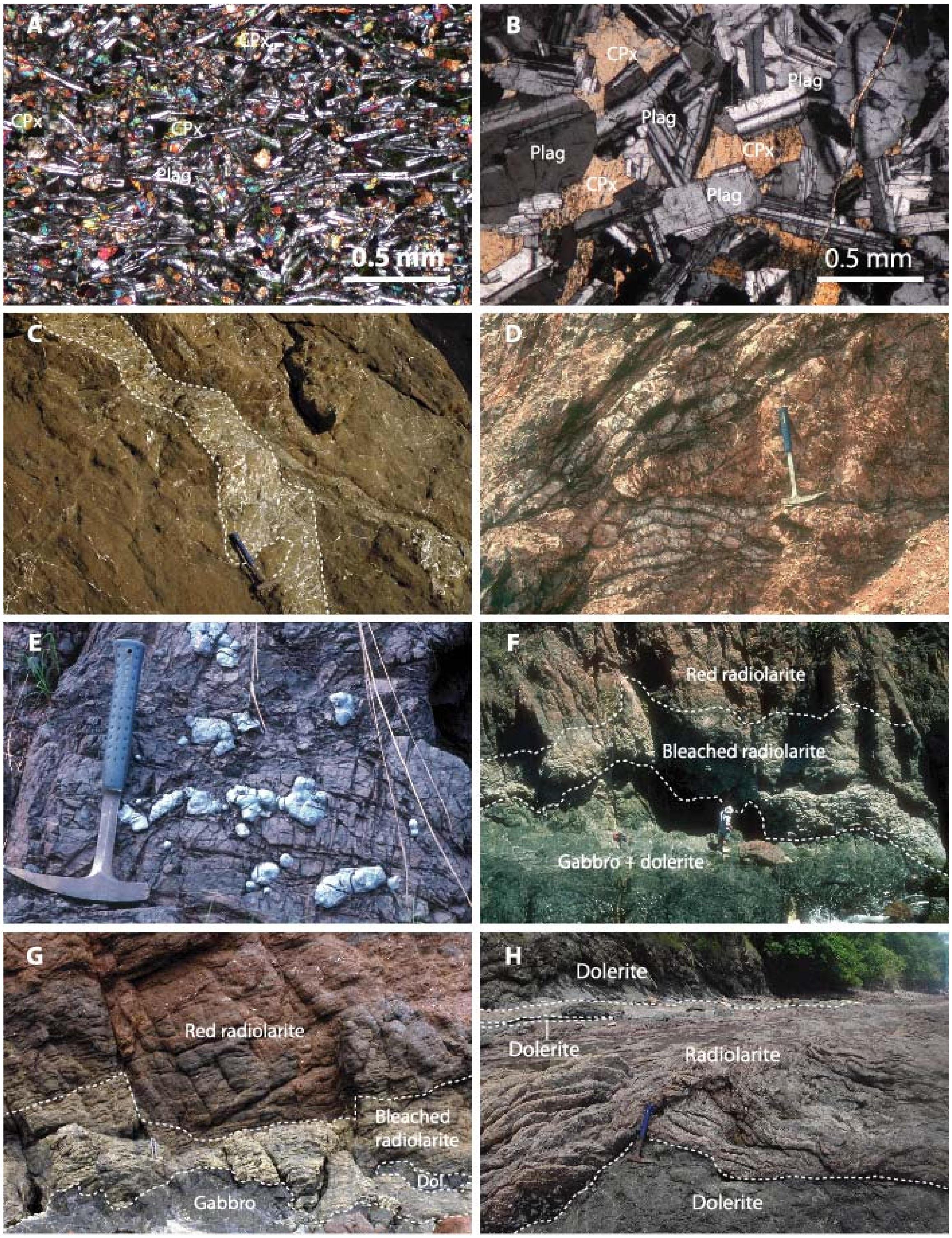
A
CPx
CPx
CPx
Plag
0.5 mm
B
CPx
Plag
Plag
Plag
CPx
CPx
Plag
0.5 mm
C
D
E
F
Red radiolarite
Bleached radiolarite
Gabbro + dolerite
G
Red radiolarite
Bleached radiolarite
Dol.
Gabbro
H
Dolerite
Dolerite
Radiolarite
Dolerite

Figure 9

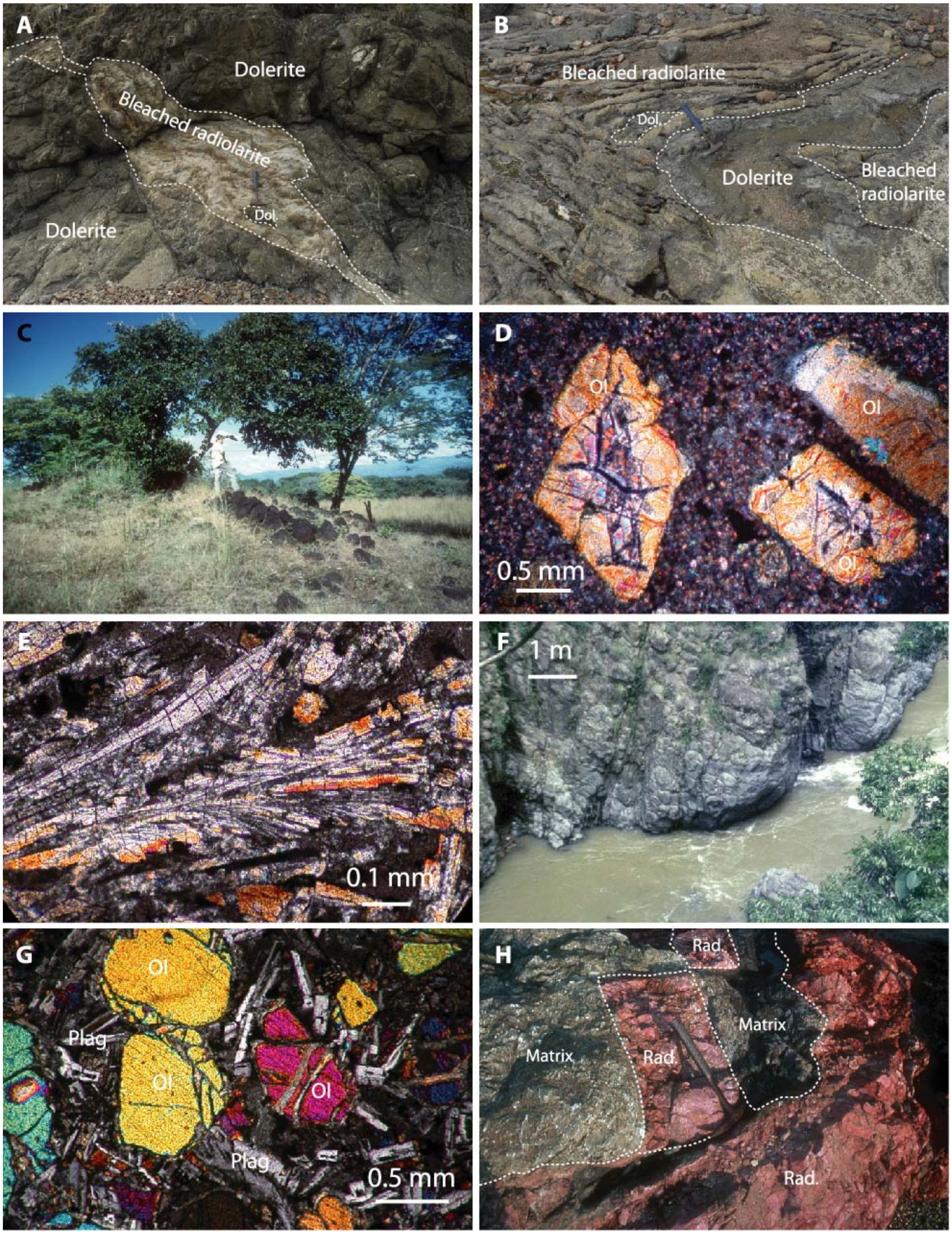
A
Dolerite
Bleached radiolarite
Dol.
Dolerite
B
Bleached radiolarite
Dol.
Dolerite
Bleached
radiolarite
C
D
Ol
Ol
Ol
0.5 mm
E
0.1 mm
F
1 m
G
Ol
Plag
Ol
Ol
Plag
0.5 mm
H
Rad.
Matrix
Matrix
Rad.
Rad.

Figure 10

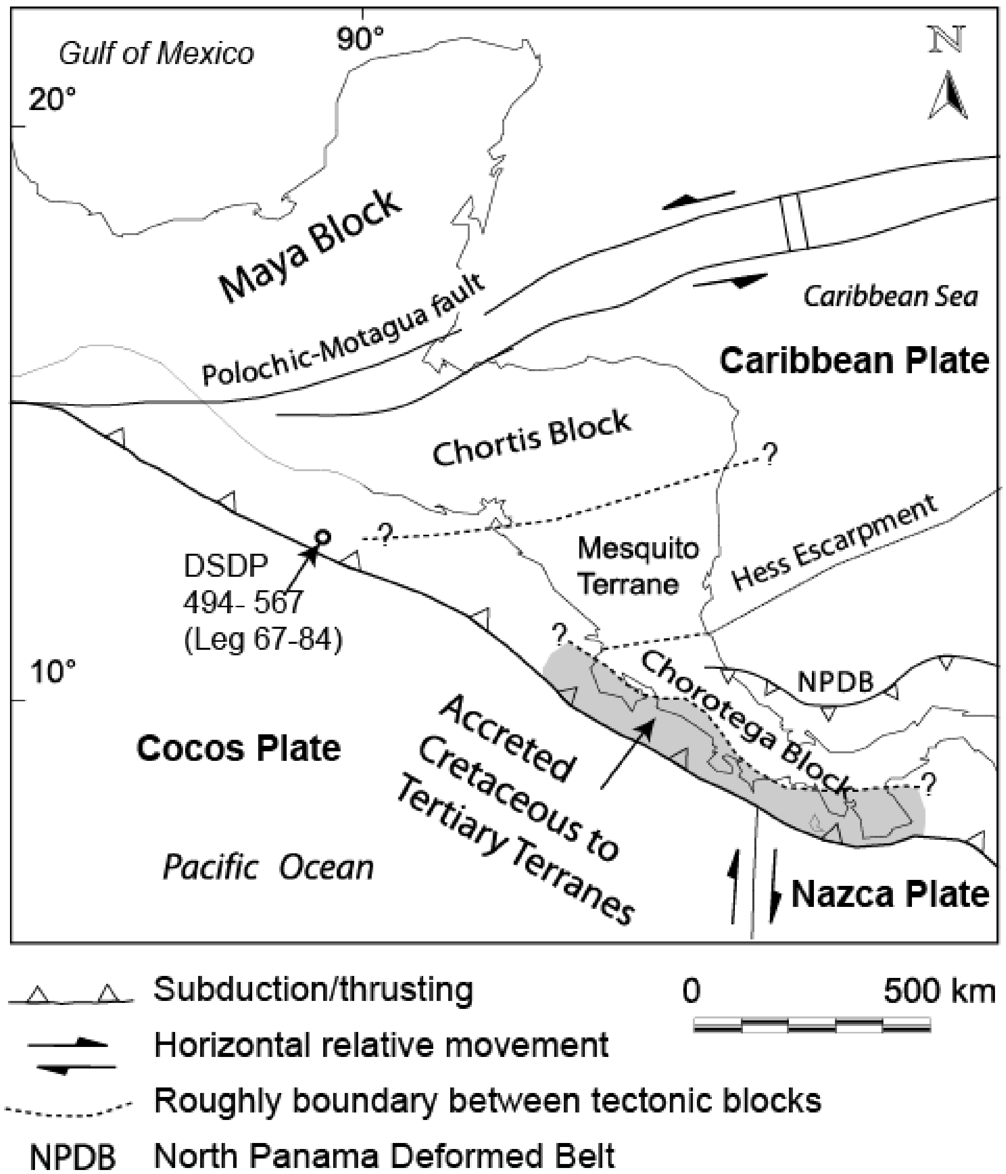
Gulf of Mexico
90°
20°
N
Maya Block
Polochic-Motagua fault
Caribbean Sea
Caribbean Plate
Chortis Block
?
Hess Escarpment
Mesquito
Terrane
DSDP
494- 567
(Leg 67-84)
10°
NPDB
Chorotega Block
Cocos Plate
Accreted
Cretaceous to
Tertiary Terranes
Pacific Ocean
Nazca Plate
Subduction/thrusting
0
500 km
Horizontal relative movement
Roughly boundary between tectonic blocks
NPDB
North Panama Deformed Belt

Chapter 2

Life cycles of Mantle Plumes: Perspective from the Galapagos Plume

This chapter resulted in one published paper and a National Science Foundation initiative in process.

Herzberg, C. and **Gazel. E.**, Petrological evidence for secular cooling in mantle plumes, ***Nature***, 485, 619-622.

Abstract

Geological mapping and geochronological studies show much lower eruption rates for oceanic island basalts (OIB) compared to lavas from Large Igneous Provinces (LIPS) such as oceanic plateaus and continental flood provinces. However, a quantitative petrological comparison has never been made of mantle source temperature and extent of melting for OIB and LIP sources. Here, we show that the MgO and FeO contents of lavas from the Galápagos Islands and their primary magmas have decreased since the Cretaceous. From petrological modeling, we infer that these changes reflect a cooling of the Galápagos mantle plume from a potential temperature of 1560 - 1620°C in the Cretaceous to 1500°C at the present time. Iceland also exhibits secular cooling, in agreement with previous studies. Our work provides the first quantitative petrological evidence that, in general, mantle plumes for LIPS with Paleocene-Permian ages were hotter and melted more extensively than plumes of more modern oceanic islands. This is

interpreted to reflect episodic flow from lower mantle domains that are lithologically and geochemically heterogeneous.

1. Introduction

Extensive outcrops of oceanic complexes, remnants of the Caribbean Large Igneous Province (CLIP) and accreted Galapagos hotspot tracks are exposed along the Pacific coast of southern Central America and northern South America (Fig. 1A). Donnelly et al. (1973) suggested that the present Caribbean Plate was formed in the Pacific as anomalously thick-buoyant crust that subsequently moved into its present position between the Americas. Duncan and Hargraves (1984) proposed that the Galapagos mantle plume was responsible for a thickened Caribbean crust. More recent work by Sinton et al. (1997), Alvarado et al. (1997), Hauff et al. (1997), Hauff et al. (2000) and Hoernle et al. (2004) concluded that the majority of the complexes of the Pacific coast of southern Central America are part of the CLIP with a clear geochemical affinity with the Galapagos hotspot.

The affinity of the CLIP fragments to the Galapagos hotspot is more controversial in South America. The island of Gorgona, famous for its outcrops of Phanerozoic (~90 Ma) komatiites (Echeverría, 1980; Kerr, 2005) is perhaps the most controversial of all. Originally this island was considered as part of the CLIP (Storey et al., 1991; Kerr et al., 1996a). Results from unpublished paleomagnetic studies and the geochemical heterogeneity of the Gorgona lavas led Révillon et al. (2000) and Kerr and Tarney (2005) to suggest that the island of Gorgona and other South American complexes belong to a second ~90 Ma oceanic plateau related to the Salas y Gomez hotspot. Recently, geochemical correlation with Leg 165 site 1001 basalts in the Hess Escarpment again opens the possibility that Gorgona Island is part of the CLIP (Kerr et al., in press). The depleted geochemical end-member typical of Gorgona samples is also present in the Rincon Block (Osa, Costa Rica), Patallanga Unit (Ecuador), and Leg 165 site 10001 (Hess Escarpment, Caribbean Plate) (Fig. 1B). Te connection between Gorgona Island and the Galapagos hotspot requires further evaluation.

2. The Geologic record of the Galapagos Plume

The most voluminous pulse of magmatism related to Galapagos Plume extended from ~95-85 Ma (eg., Lapierre et al., 2000; Kerr et al., 2002; Denyer and Gazel, *in press*) (Fig. 2). Tectonic reconstructions from the Late Cretaceous through Oligocene suggest that there were no spreading centers located close to the Galapagos hotspot. Therefore, only one hotspot track was formed after the formation of the CLIP. Geochemical data from accreted igneous complexes (66.0-16.6 Ma) along the Pacific margin of Costa Rica and Panama are consistent with these complexes being part of older Galapagos tracks (Hoernle et al., 2002).

During the last 20 Ma, the geometry between the Galapagos hotspot and Galapagos or Cocos-Nazca spreading center has been in constant change, leading to the formation of geochemically zoned Galapagos hotspot tracks on the Cocos and Nazca Plates (Werner et al., 2003). Four main portions of the Galapagos hotspot tracks are exposed on the seafloor, Cocos Ridge and NW seamount province, Carnegie Ridge, Malpelo Ridge and Coiba Ridge (Fig. 1A). The oldest preserved part of the Cocos track adjacent to the Costa Rican trench preserved a drowned 14.5-13.0 Ma paleo-Galapagos Archipelago (Werner et al., 1999; Hoernle et al., 2000). The Coiba Ridge is presently located south of the Azuero Peninsula (Panama) and its age is between 16.7-5.2 Ma (O'Connor et al., 2007). The Malpelo Ridge, situated on the Nazca Plate, ranges between 17.3-10.7Ma (O'Connor et al., 2007).

The modern Galapagos Archipelago (Fig. 1A) was built up on a platform that range in age between ~10-3 Ma (Sinton et al., 1996). The archipelago itself is younger than 3 Ma and has been active since then (White et al., 1993).

3. Geochemical zonation of the Galapagos Plume

Radiogenic Sr, Nd, Hf, Pb, and He isotope data from present-day Galapagos islands and submarine volcanic platform lavas are defined by four distinct isotopic end-members, spatially distributed in four Galapagos Domains (Fig. 3) (White and Hofmann, 1978; Geist et al., 1988; White et al., 1993; Harpp and White, 2001). Fernandina, the most active volcano in the archipelago, is located in the Central domain and likely overlies the plume, based on elevated $^{3}He/^{4}He$ (Kurz and Geist, 1999). Mixing between enriched and relatively depleted components defines four spatially distinct geographical domains for the Galapagos archipelago, the Cocos and Carnegie Ridges and associated seamount provinces. The southern domain is presently located at Floreana, the central domain at Fernandina and most of Isabela Island, and the northern domain at Pinta, Wolf and Darwin islands (Fig. 3) (Hoernle et al., 2000; Blichert-Toft and White, 2001; Harpp and White, 2001; Geldmacher et al., 2003; Werner et al., 2003).

The internal consistency between the different Galapagos Plume isotopic domains can be used to fingerprint the Galapagos signature. This internal consistency will allow us to discriminate between the Galapagos Plume and other plumes as the source of lavas collected from accreted oceanic complexes in the pacific of Central and South America and in the Caribbean. For example, we compared the isotopic compositions of the four Galapagos Domains to the isotopic compositions of unrelated OIB from the Azores, Cook-Austral, Easter/Sala y Gomez, Hawaii (Mauna Kea and Maui) and Samoa (from the Georoc database). While there is overlap in some cases, the internal consistency is poor. For example, Mauna Kea lavas have $^{206}Pb/^{204}Pb$ and $^{208}Pb/^{204}Pb$ isotopic ratios similar to the Eastern Galapagos Domain, but much lower $^{143}Nd/^{144}Nd$ and higher $^{87}Sr/^{86}Sr$ (Fig. 4)

4. Methods

Primary magma compositions, mantle potential temperatures and source melt fractions were calculated from primitive whole rock compositions using PRIMELT2.XLS software (Herzberg and Asimow, 2008). A detailed discussion of method is given elsewhere (Herzberg and Asimow, 2008; Herzberg et al., 2007; Herzberg and O'Hara, 2002). The algorithm calculates primary magma composition for a primitive lava that differs by it owing to variable amounts of olivine that was added or subtracted. Lavas that had experienced plagioclase and/or clinopyroxene fraction are excluded from this analysis.

PRIMELT2.XLS software was calibrated from experiments on fertile peridotite with 8% FeO, and all calculated primary magma compositions are assumed to have been derived by fractional melting. It provides for each primary magma the olivine liquidus temperature T_{OL} at one atmosphere and the mantle potential temperature T_P. Adiabatic melting paths of Iwamori et al. (1995) were used to obtain: $T_P(^oC) = 1463 + 12.74MgO - 2924/MgO$ (Herzberg and Asimow, 2008; Herzberg et al., 2007). As both T_{OL} and T_P are dependent on the MgO content of the primary magma (Herzberg and Asimow, 2008; Herzberg et al., 2007), the accuracy of the former is a guide to the precision of the latter. For any specific peridotite composition, accuracy of T_{OL} is ± 31°C at the 2σ level of confidence (Herzberg at al., 2007). Uncertainties of the FeO content of peridotite can propagate to an uncertainty of ± 50-70°C in T_P. Uncertainties in all other major elements for fertile peridotite do not propagate to significant variations in melt fraction and mantle potential temperature. Melting of depleted peridotite propagates to calculated melt fractions that are too high, but with a negligible error in mantle potential temperature (Herzberg and Asimow, 2008; Herzberg et al., 2007; Herzberg and O'Hara, 2002). Melt fraction is more difficult to quantify than mantle potential temperature because it is strongly dependent on the composition of the source (Herzberg and Asimow, 2008; Herzberg et al., 2007; Herzberg and O'Hara, 2002).

PRIMELT2.XLS software identifies magmas generated from pyroxenite sources and excludes them. Magmas that have been degassed from CO_2-rich sources are identified and similarly excluded. Fe_2O_3 is calculated with $Fe_2O_3/TiO_2 = 0.5$, a reduced mode, based on MORB-like FeO_T enrichment for most LIPS (Herzberg and Asimow, 2008).

We have assumed that primary magmas are formed by accumulated fractional melting. The initial melting pressure, P_i, and final melting pressure, P_f, are indicated in the FeO-MgO diagram of Fig. 5A by the red and blue lines, respectively. These have been calculated by forward simulations of fractional melting of fertile peridotite (Herzberg and O'Hara, 2002; Forte and Mitrovica, 2001). Final melting pressure is useful because it permits the construction of a synthetic T-P adiabatic melting path. Final melting pressure can be inferred by simply plotting FeO and MgO for a PRIMELT2 primary magma in Fig. 5A and interpolation using the blue lines. Alternatively, final melting pressure P_f can be calculated with the following equations:

$$P1_f = a + b\mathrm{FeO} + c\mathrm{FeO}^2 \qquad (1)$$

for primary magmas with < 15wt % MgO. FeO is the weight % iron in the primary magma and a, b, and c are variables that depend on the MgO content of the primary magma:

$$a = -196.4 + 2.942\mathrm{MgO} + 430/\mathrm{MgO} \qquad (2)$$

$$b = 17.7 - 0.444\mathrm{MgO} + 228/\mathrm{MgO} \qquad (3)$$

$$c = 2.2 - 0.047\mathrm{MgO} - 42.78/\mathrm{MgO} \qquad (4)$$

For primary magmas having 15% > MgO < 20%, the appropriate pressure to use is:

$$P2_f = P1_f + (-10.96 + 0.67\mathrm{MgO}) \qquad (5)$$

The difference between calculated P_f and those shown in Fig. 1a by the blue lines is ± 0.28 GPa (2σ) . Complex changes in phase equilibria will likely restrict pressure inferences for other OIB and LIP primary magmas to MgO < 20% and P_f < 3.5 GPa, similar to those for Galápagos and CLIP primary magmas.

Initial melting for garnet peridotite in the 2.7 < P_i < 7 GPa range can be inferred by simply plotting FeO and MgO for a PRIMELT2 primary magma in Fig. 5A and interpolation using the red lines. Alternatively, they can be calculated from PRIMELT2 solutions for primary magma MgO contents using the equation:

$$P_i = 11.248\text{MgO} - 13700(1/\text{MgO})^3 - 8.13\ (\ln(\text{MgO}))^3 \qquad (6)$$

Where, the difference between calculated P_i and those shown in Fig. 5A by the red lines is ± 0.20 GPa (2σ).

With the purpose to fingerprint the Galapagos signature in older samples thought to be related to the Galapagos Plume, we projected the modern Galapagos Plume isotopic domains into the past following Hauff et al. (2000). However, in this case, instead of assuming a source composition, the source Rb, Sr, Sm, Nd, Pb, Th and U required for each projection were estimated by inverting a primitive basalt/primary magma composition representative of each domain (Figure 3 D). The melting model used these regressions was aggregated fractional melting (Shaw, 1970) described by the following equation:

$$C_L/C_0=1/F\times[1-(1-F)^{1/Do}] \quad (7)$$

Where C_L is the average concentration of the element in the liquid, C_0 is the initial concentration of the element in the source, F is the melt fraction, and D_0 is the initial bulk partition coefficient. Equation 1 is derived from the mass balance equation:

$$C_0=F\times C_L+(1-F)C_S \quad (8)$$

and the bulk partition coefficient

$$D = C_S/C_L \quad (9)$$

Where C_S is the concentration of the element in the solid phase. The partition coefficients used in our modeling are from the compilation of Kelemen et al. (2003).

Once we inverted the source composition of each domain, we used the isotopic ratios of the samples from each domain and the source Rb, Sr, Sm, Nd, Pb, Th and U to project the Galapagos isotopic domains to different hypothetical stages (e.g. initial ratios at 90 Ma, 60 Ma, etc) of the plume activity using the following equations (Faure, 1986):

$$^{87}Sr/^{86}Sr=(^{187}Sr/^{86}Sr)_{initial}+^{87}Rb/^{86}Sr(e^{\lambda 1t}-1) \quad (10)$$

$$^{143}Nd/^{144}Nd=(^{143}Nd/^{144}Nd)_{initial}+^{147}Sm/^{144}Nd(e^{\lambda 2t}-1) \quad (11)$$

$$^{206}Pb/^{204}Pb=(^{206}Pb/^{204}Pb)_{initial}+^{238}U/^{204}Pb(e^{\lambda 3t}-1) \quad (12)$$

$$^{207}Pb/^{204}Pb=(^{207}Pb/^{204}Pb)_{initial}+^{235}U/^{204}Pb(e^{\lambda 4t}-1) \quad (13)$$

$$^{208}Pb/^{204}Pb=(^{208}Pb/^{204}Pb)_{initial}+^{232}Th/^{204}Pb(e^{\lambda 5t}-1) \quad (14)$$

Once we had these diagrams we plotted the initial ratios (age corrected) of samples of the CLIP, accreted and modern Galapagos tracks, to compare the collected data to the projected modern Galapagos domains into the past and test for internal consistency.

5. Petrological evidence for secular cooling in the Galapagos Plume

The temporal progression between the modern day Galapagos hotspot and the associated tracks, the accreted ridges and oceanic islands/seamounts and the CLIP, gives us a unique opportunity to study the petrological evolution of a mantle plume over the last 90 Ma. The lowest FeO contents are mostly found in lavas with 0 to 13 Ma from the present-day Galápagos Archipelago and the Carnegie and Cocos hotspot tracks (Fig.5 A). FeO contents are highest for Gorgona komatiites and intermediate for all other lavas. When olivine is the sole crystallizing phase, lavas with higher FeO contents can be differentiated from peridotite-source primary magmas having higher FeO and MgO contents (Herzberg and Asimow, 2008; Herzberg et al., 2007; Putirka, 2005; Herzberg and O'Hara, 2002). A primary magma is a partial melt of the mantle formed in most cases by the mixing of small melt droplets that are separated from the remainder of the solid residue. Addition and subtraction of olivine from a primary magma will produce lavas having higher or lower MgO, respectively, with minor change in FeO (Fig. 5A).

This has been simulated and the primary magma compositions have been reconstructed using PRIMELT2 Herzberg and Asimow (2008). Results are given in Tables 1-3 and in Fig. 5A.

The MgO content of a volatile-deficient primary magma is positively correlated with the temperature of the mantle (Herzberg and Asimow, 2008; Herzberg et al., 2007; Putirka, 2005; Herzberg and O'Hara, 2002). It provides a petrological record of mantle potential temperature T_P, which is the temperature that the solid adiabatically convecting mantle would attain if it could reach the surface without melting (McKenzie and Bickle, 1988). Using the relationship $T_P(^oC) = 1463 + 12.74MgO – 2924/MgO$ (Herzberg and Asimow, 2008; Herzberg et al., 2007) , we can now readily calculate how hot the mantle was to yield the primary magma compositions given in Fig. 1a. Results are shown in Figs. 5B.

For the present-day Galápagos Plume, T_P ranges from 1400 to 1500°C, similar to 1440 to 1500°C T_P recorded by lavas from the Cocos and Carnegie ridges. Older lavas were hotter. Those from the CLIP and accreted tracks with 65-95 Ma record T_P in the 1500 to 1560°C range, and up to 1620°C if Gorgona lavas were part of the CLIP. This is petrological evidence for secular cooling of the Galápagos Plume (Fig. 5B)

The MgO content of an accumulated fractional melt does not change substantially as melt fraction increases during decompression (Herzberg and Asimow, 2008; Herzberg et al., 2007; Putirka, 2005). The adiabatic T-P melting path is approximately coincident with olivine liquidus temperatures, and the latter can be calculated using T_{OL} (^oC) = 935 + 33MgO – 0.37MgO^2 + 54P – 2P^2, where MgO is in weight % and the pressure (GPa) (Herzberg and Asimow, 2008; Herzberg and O'Hara, 2002). Using final melting pressures and the MgO contents of primary magmas in this equation (Fig. 5A), a synthetic adiabatic melting path can be obtained (Fig. 6). The majority of lavas from the present-day Galápagos Plume formed in a column where melting ended at > 2 GPa, and this pressure is highly variable. Melting ended at much lower pressures for lavas from the Cocos and Carnegie ridges, consistent with the channeling of the Galápagos Plume to locations of thinner lithosphere. Low pressures of final melting are also inferred for older CLIP lavas, but the tectonic interpretation is not clear.

Note the wide range of primary magma compositions and inferred mantle potential temperatures for each LIP and ocean island occurrence (Fig. 7). These ranges have been interpreted as originating from a hotspot, a spatially localized source of heat and magmatism restricted in time (Herzberg and Asimow, 2008). Primary magmas are tapped from both the hot axis and the cool periphery of the plume as illustrated in Fig.8. The 1500°C T_P maximum for Galápagos is characteristic of the plume axis. The low end of the Galápagos range approaches 1350±50°C, a T_P range for ambient mantle (Herzberg et al., 2007; Coutier et al., 2007; McKenzie et al., 2005; Langmuir et al., 1992) necessary for the production of MORB with 10-13% MgO. What is particularly relevant for the present purpose is that there is a decrease in T_P maxima from 1560-1620°C for rocks with 65-95 Ma to 1500°C at the present time (Fig 5B). The exact form of the secular cooling curve depends on whether the Gorgona komatiites were produced by the Galápagos or another plume (see background discussion).

6. Global implications for the life cycles of mantle plumes.

We now provide petrological evidence for secular cooling in other areas. Results are given in Tables 2 and 3 and are shown in Fig. 2. Fig. 7 illustrates that Large Igneous Provinces with ages Paleocene and older were formed by mantle sources that were generally hotter than present-day ocean islands. But there are several important exceptions. First, Hawaii is the OIB Island that is most similar to LIPS because it has a T_P maximum of 1600°C. It is only surpassed by rocks from the North Atlantic Igneous Province, the Deccan Traps, and the CLIP if we include Gorgona. Second, T_P for the Central Atlantic Magmatic Province (CAMP) is notably different from all other LIPS in being cooled (Fig. 7). The ~ 100°C excess T_P for CAMP is consistent with model temperatures (Coltice et al., 2007) that can arise from an internally heated mantle capped by Pangea (Coltice et al., 2007; Anderson, 1982). This is evidence indicating that continental insulation is not capable of producing LIPS with the much higher T_P (Fig. 7).

Melt fractions computed from PRIMELT2 are generally higher for LIPS than for oceanic islands (Fig. 9), consistent with suggestions of higher eruption rates (Richards et al., 1989). The high melt fractions, high mantle potential temperatures, and vast areas of magmatism associated with the largest LIPS are all consistent with formation in mantle plume heads (Richards et al., 1989) (but note the CAMP exception). In contrast to LIPS, many ocean islands display melt fractions that must be lower than ~ 0.05 (Fig. 9B). These are often readily characterized by very low SiO_2, high CaO and high lithophile trace element abundances in OIB owing to low degree melting of carbonated peridotite (Dasgupta et al., 2007). Low melt fraction CO_2-rich OIB are abundant in Azores, Canaries, Cape Verde, Cook-Austral, Marquesas, Pitcairn-Gambier, St. Helena, Samoa, and the Society Islands, and many other OIB (http://georoc.mpch-mainz.gwdg.de/georoc/; Table 4). Even more of this OIB-type melt is likely to metasomatize the mantle rather than erupt. The melt fraction frequency spectrum for OIB in Fig. 9B is therefore likely to be exponential in form. Results for these OIB occurrences are interpreted as the transport of low melt fraction magmas from the cool plume peripheries and high melt fraction magmas from the hotter plume axes (Fig.8). However, it has been proposed that low melt fraction OIB can also form without a plume by volatile-induced melting of ambient mantle and transport through lithospheric fractures (Hirano et al., 2006). This suggestion is fully consistent with experiments from Dasgupta et al. (2007). Both plume and non-plume origins are indicated for oceanic islands (Dasgupta et al., 2007; Hirano et al., 2006).

A very high cooling rate is inferred for the Icelandic plume. Most Paleocene lavas with pre-breakup ~ 60 Ma (Storey et al., 2007) from east and west Greenland reveal T_P maxima of ~ 1550-1570°C, similar to the CLIP, and crystallized from primary magmas with 18-20% MgO. Our model primary magmas are in excellent agreement with many previous estimates (Herzberg and Asimow, 2008; Herzberg et al., 2007; Herzberg and O'Hara, 2002; Holm, 1993) although we obtained T_P as high as 1650°C (Fig. 2). A ~200°C spread in T_P and melt fractions in the 0.05–0.37 range are recorded in east Greenland lavas (Table 2) from a restricted area close to the Tertiary Icelandic hotspot track (Saunders et al., 1997). These ranges are an expected consequence of the tapping of primary magmas from a mantle plume (Fig. 8). T_P as low as 1460°C is obtained from ~55 Ma syn-breakup lavas from the seaward-dipping reflector sequence, similar to present-day Iceland (Slater et al., 2001) (Fig. 7). Our work indicates T_P dropped from the 1550-1650°C range to 1460°C in about 5 Ma, in agreement with estimates of Armitage et al. (2008). T_P for the Icelandic Plume appears unchanged at about 1460°C from 55 Ma to the present, and is now in a comparatively steady state. The early rapid secular cooling of the Icelandic Plume is much greater than that seen for the Galápagos, although more work is needed to fill the gap in the Galápagos data (Table 1). We also acknowledge an Icelandic Plume cooling curve is compromised by an absence of data from the Greenland-Iceland and the Iceland-Faeroes ridges with ~ 50-15 Ma.

7. Discussions and Conclusions

Our work provides petrological evidence that mantle plumes for LIPS with Paleocene-Permian ages were hotter and melted more extensively than plumes of more modern oceanic islands. In the case of the Galapagos Plume, the lithological characteristics of the sources of Galapagos-related magma may correlate changes in plume temperature over the entire ~0-95 Ma eruption history.

It is commonly assumed that mantle peridotite is the dominant source lithology for magmatic processes (e.g., O'Hara et al., 1968). However, exposed pieces of the upper mantle also show the importance of pyroxenite or eclogite components (Schulze, 1989; Hirschmann and Stolper, 1996; Kogiso et al., 2004). Isotopic studies of oceanic islands suggested the presence of recycled crust (Chase, 1981; Hofmann and White, 1982; Hauri, 1996; Chauvel et al., 2008). Nevertheless, it is not always clear how the melting of recycled crust can be distinguished from the melting of metasomatized peridotite (Niu and O'Hara, 2003; Pilet et al., 2008), especially if the metasomatizing agent originates from recycled carbonate (e.g., Dasgupta et al., 2006, 2007; Jackson and Dasgupta, 2008). Furthermore, the panorama gets more complicated if an oceanic island is melted from a source that had recycled crust that was completely mixed back into peridotite during convective stirring (Jackson et al., 2008; Gurenko et al., 2008).

CaO has been suggested to represent an indicator of source lithology and its application has been discussed in detail (Herzberg, 2006; Herzber and Asimow, 2008). The green line in Fig. 10 separates lavas that melted from peridotite and pyroxenite sources (Herzberg and Asimow, 2008). At this point we have to rely on the considerable circumstantial evidence from currently available data for many oceanic islands, which indicate that high CaO in lavas and their olivine phenocrysts are negatively correlated with NiO, indicating a peridotite source (Sobolev et al., 2005; Gurenko et al., 2008; Herzberg, work in progress). In contrast, many examples of lavas for which a pyroxenite source has been inferred have low CaO and high NiO (Sobolev et al., 2005).

Numerical and laboratory simulations show that mantle flow can be episodic where there are thermal and compositional components to buoyancy (Kumagi et al., 2008; Faertani et al., 2005; Lin and Van Keken, 2005). Mantle plumes with these characteristics might originate in lower mantle domains where shear wave velocities are low and bulk density is intrinsically high (Garnero et al., 2008). Silica may be elevated, iron may be high (Burke et al., 2008) and low in these domains and mixing will yield heterogeneities on a range of length scales. Plumes may randomly sample this complexity, or lighter components might preferentially separate from more dense lithologies that stay behind. While progress is being made on identifying peridotite and pyroxenite source lithologies from the compositions of lavas, inferring iron content is a much more difficult problem (see Methods).

In the case of the Galapagos Plume, the initial stage represented by the CLIP is totally dominated by peridotite source melts. It is up to 65 Ma when a recycled component first recorded in the lavas from Galapagos accreted seamount at Quepos, Costa Rica (Fig. 10). This new source lithology composition correlates with the first appearance of the Northern Galapagos Domain (Fig. 11 and also see Fig. 3), with an EMII (enriched mantle-II) recycled signature (Geldmacher et al., 2003). About 44% of the high MgO lavas indicated by yellow squares for the Galapagos Archipelago from the Central and Northern Domains are candidates for pyroxenite-source melting (Fig. 10) (Herzberg and Gazel, work in progress). Therefore, the secular cooling in the Galapagos Plume and in other mantle plume could be related to the presence of a pyroxenitic source that limits the plume buoyancy (Herzberg, work in progress). This limitation may allow more time of contact with the surrounding ambient mantle that translates in a more efficient heat transfer and cooling of the plume. The effect of a recycled component in the evolution of a mantle plume will be the goal for future research initiatives.

8. References

Alvarado, G. E., P. Denyer, and C. W. Sinton (1997), The 89 Ma Tortugal komatiitic suite, Costa Rica: Implications for a common geological origin of the Caribbean and Eastern Pacific region from a mantle plume. *Geology 25*(5), 439-442.

Anderson, D.L. (1982), Hotspots, polar wander, Mesozoic convection and the geoid. *Nature* 297, 391-393.

Armitage, J.J., Henstock, T.J., Minshull, T.A. and Hopper, J.R. (2008), Modeling the composition of melts formed during continental breakup of the Southeast Greenland margin. *Earth Planet. Sci. Lett.* 269, 248-258.

Beck, C. M., D. Girard, and P. DeWeber (1984), Volcanosédimentaire du Rio Guare: Un e´le´ment de la nappe ophiolitique de Lomo de Hierro, chaone Caraôbe Vénézuélienne: *Comptes Rendus de Seances* (D) 299, 337–34.

Beets, D.J., W.V. Maresch, G. Th. Klaver, A. Mottana, R. Bocchio, F. F. Beunk and H. P. Monen (1984), Magmatic rock series and high-pressure metamorphism as constraints on the tectonic history of the southern Caribbean In: Bonini, W. E. et al. (Eds.) The Carribean-South American plate Boundary and Regional Tectonics, *GSA Memoir* 162, 95-130.

Blichert-Toft, J., and W. M. White (2001), Hf isotope geochemistry of the Galapagos Islands. *Geochemistry Geophysics Geosystems*, *2*.

Burke, K., B. Steinberger, T. H. Torsvik, and M. A. Smethurst (2008), Plume generation zones at the margins of large low shear velocity provinces on the core-mantle boundary. *Earth Planet. Sci. Lett.* 265(1-2), 49-60.

Chase, C.G. (1981), Ocean island Pb: Two-stage histories and mantle evolution. *Earth Planet. Sci. Lett. 52*, 277-284.

Chauvel, C., E. Lewin, M. Carpentier, N. T. Arndt, and J. C. Marini (2008), Role of recycled oceanic basalt and sediment in generating the Hf-Nd mantle array. *Nature Geoscience* ll(1), 64-67.

Coltice, N., Phillips, B.R., Bertrand, H., Richard, Y. and Rey, P. (2007), Global warming of the mantle at the origin of flood basalts over supercontinents. *Geolog*y 35, 391-394.

Courtier, A.M., *et al*. (2007), Correlation of seismic and petrological thermometers suggests deep thermal anomalies beneath hotspots. *Earth Planet. Sci. Lett.* 264, 308-316.

Dasgupta, R., M. M. Hirschmann, and K. Stalker (2006), Immiscible transition from carbonate-rich to silicate-rich melts in the 3 GPa melting interval of eclogite plus CO2 and genesis of silica-undersaturated ocean island lavas. *Journal of Petrology 47*(4), 647-671.

Dasgupta, R., M. M. Hirschmann, and N. D. Smith (2007), Partial melting experiments of peridotite CO2 at 3 GPa and genesis of alkalic ocean island basalts. *Journal of Petrology 48*(11), 2093-2124.

Denyer P. and E. Gazel (2009), The Costa Rican Jurassic to Miocene oceanic complexes: Origin, tectonics and relationship. Jour. South Ameri. Earth Sci. *in press*

Denyer, P., P. O. Baumgartner, and E. Gazel (2006), Characterization and tectonic implications of Mesozoic-Cenozoic oceanic assemblages of Costa Rica and Western Panama. *Geologica Acta* 4, 1-2, 203-218.

DiMarco, G. (1994), Les terrains accrétés du sud du Costa Rica: Evolution tectonostratigraphique de la marge occidentale de la plaque Caraïbe. *Mémoires de Géologie* 20, 1-185.

Donnelly, T.H. (1994), The Caribbean Cretaceous basalt association: A vast igneous province that includes the Nicoya Complex of Costa Rica. *Profil 7*, 17-45.

Donnelly, T.W., Melson, W.G., Kay, R., Rogers, J.J.W. (1973), Basalts and diabases of Late Cretaceous age from the Caribbean. Initial Reports Deep Sea Drilling Project, 15, 989-1011.

Duncan, R. A. and R.B. Hargraves, (1984), Plate tectonic evolution of the Caribbean region in the mantle reference frame. *Geol. Soc. Amer. Bull.* 162, 81-93.

Dupré, B. and L.M Echeverria (1984), Pb isotopes of Gorgona Island (Colombia): Isotopic varations correlated with magma type, *Earth Planet. Sci. Lett.* 67 (2), 186-190.

Echeverría, L.M. (1980), Tertiary or Mesozoic komatiites from Gorgona Island, Colombia. *Contr. Mineral. Petrol.* 73, 253-266.

Farnetani, C. G., and H. Samuel (2005), Beyond the thermal plume paradigm, *Geophysical Research Letters*, 32(7).

Faure, G. (1986), *Principles of Isotope Geology*, 2nd ed., 589 pp., John Wiley & Sons, New York.

Forte, A.M. and Mitrovica, J.X. (2001), Deep-mantle high-viscosity flow and thermochemical structure inferred from seismic and geodynamic data. *Nature* 410, 1049-1056.

Garnero, E. J., and A. K. McNamara (2008), Structure and dynamics of Earth's lower mantle. *Science* 320(5876), 626-628.

Geist, D., T. Naumann, and P. Larson (1998), Evolution of Galapagos magmas: Mantle and crustal fractionation without assimilation. *Journal of Petrology* 39(5), 953-971.

Geldmacher, J., B. B. Hanan, J. Blichert-Toft, K. Harpp, K. Hoernle, F. Hauff, R. Werner, and A. C. Kerr (2003), Hafnium isotopic variations in volcanic rocks from the Caribbean Large Igneous Province and Galapagos hot spot tracks. *Geochemistry Geophysics Geosystems*, 4.

Gurenko, A. A., A. V. Sobolev, K. A. Hoernle, F. Hauff, and H. U. Schmincke (2009), Enriched, HIMU-type peridotite and depleted recycled pyroxenite in the Canary plume: A mixed-up mantle. *Earth Planet. Sci. Lett.* 277(3-4), 514-524.

Harpp, K. S., and W. M. White (2001), Tracing a mantle plume: Isotopic and trace element variations of Galapagos seamounts. *Geochemistry Geophysics Geosystems* 2.

Hauff, F., K. Hoernle, H. U. Schmincke, and R. Werner (1997), A Mid Cretaceous origin for the Galapagos hotspot: Volcanological, petrological and geochemical evidence from Costa Rican oceanic crustal segments. *Geologische Rundschau* 86(1), 141-155.

Hauff, F., K. Hoernle, G. Tilton, D. W. Graham, and A. C. Kerr (2000), Large volume recycling of oceanic lithosphere over short time scales: Geochemical constraints from the Caribbean Large Igneous Province. *Earth Planet. Sci. Lett.*, 174(3-4), 247-263.

Hauri, E. H. (1996), Major-element variability in the Hawaiian mantle plume. *Nature* 382(6590), 415-419.

Herzberg, C. (2006), Petrology and thermal structure of the Hawaiian plume from Mauna Kea volcano. *Nature 444*(7119), 605-609.

Herzberg, C., and M. J. O'Hara (2002), Plume-associated ultramafic magmas of Phanerozoic age. *Journal of Petrology* 43(10), 1857-1883.

Herzberg, C., and P. D. Asimow (2008), Petrology of some oceanic island basalts: PRIMELT2.XLS software for primary magma calculation. *Geochemistry Geophysics Geosystems*, *9*.

Herzberg, C., and E. Gazel (2009), Petrological evidence for secular cooling in mantle plumes. *Nature* 458(7238), 619-U683.

Herzberg, C., P. D. Asimow, N. Arndt, Y. L. Niu, C. M. Lesher, J. G. Fitton, M. J. Cheadle, and A. D. Saunders (2007), Temperatures in ambient mantle and plumes: Constraints from basalts, picrites, and komatiites. *Geochemistry Geophysics Geosystems*, 8.

Hirano, N. *et al*. (2006), Volcanism in response to plate flexure. *Science* 313, 1426-1428.

Hirschmann, M. M., and E. M. Stolper (1996), A possible role for garnet pyroxenite in the origin of the "garnet signature" in MORB. *Contributions to Mineralogy and Petrology* 124(2), 185-208.

Hoernle, K., F. Hauff, and P. van den Bogaard (2004), 70 m.y. history (139-69 Ma) for the Caribbean large igneous province. *Geology* 32(8), 697-700.

Hoernle, K., P. van den Bogaard, R. Werner, B. Lissinna, F. Hauff, G. Alvarado, and D. Garbe-Schonberg (2002), Missing history (16-71 Ma) of the Galpapagos hotspot: Implications for the tectonic and biological evolution of the Americas. *Geology* 30(9), 795-798.

Hoernle, K., R. Werner, J. P. Morgan, D. Garbe-Schonberg, J. Bryce, and J. Mrazek (2000), Existence of complex spatial zonation in the Galapagos plume for at least 14 m.y. *Geology 28*(5), 435-438.

Hofmann, A.W. and W.M. White (1982), Mantle plumes from ancient oceanic crust. *Earth Planet. Sci. Lett. 57*, 421-436.

Holm, P.M. et al. (1993), The Tertiary picrites of West Greenland: Contributions from 'Icelandic' and other sources. *Earth Planet. Sci. Lett.* 115, 227-244.

Iwamori, H., McKenzie, D. and Takahashi, E. (1995), Melt generation by isentropic mantle upwelling. *Earth Planet. Sci. Lett.* 134, 253-266.

Jackson, M. G., and R. Dasgupta (2008), Compositions of HIMU, EM1, and EM2 from global trends between radiogenic isotopes and major elements in ocean island basalts. *Earth Planet. Sci. Lett*. 276(1-2), 175-186.

Jackson, M. G., S. R. Hart, A. E. Saal, N. Shimizu, M. D. Kurz, J. S. Blusztajn, and A. C. Skovgaard (2008), Globally elevated titanium, tantalum, and niobium (TITAN) in ocean island basalts with high He-3/He-4. *Geochemistry Geophysics Geosystems*, 9.

Jaillard, E., M. Ordonez, S. Benitez, G. Berrones, N. Jimenez, G. Montenegro, and I. Zambrano (1995), Basin development in an accretionary, oceanic-floored fore-arc setting: Southern coastal Ecuador during late Cretaceous time. In: A.J. Tankard, Suarez, S. and H.J. Welsink, Petroleum Basins of South America. *AAPG Memoir* 62, 615-631.

Kerr, A.C., Pearson D.G., Nowell, G.M., Magma source evolution beneath the Caribbean oceanic plateau: New insights from elemental and Sr-Nd-Pb-Hf isotopic studies of ODP Leg 165 Site 1001 basalts in *Caribbean Evolution* (eds. Pindel, J. and James, K.) (Geol. Soc. Sp. Pub., The Geologic Society, London, *in press.*

Kerr, A.C., (2005), La isla de Gorgona, Colombia: A petrological enigma?, *Lithos* 84, 77-101.

Kerr, A. C., and J. Tarney (2005), Tectonic evolution of the Caribbean and northwestern South America: The case for accretion of two Late Cretaceous oceanic plateaus. *Geology* 33(4), 269-272.

Kerr, A. C., R. V. White, P. M. E. Thompson, J. Tarney, and A. D. Saunders, (2003), No oceanic plateau— no Caribbean plate? The seminal role of an oceanic plateau in Caribbean plate evolution, in C. Bartolini, R. T. Buffler, and J. Blickwede, eds., The Circum-Gulf of Mexico and the Caribbean: Hydrocarbon habitats, basin formation, and plate tectonics: *AAPG Memoir* 79, 126– 168.

Kerr, A. C., J. Tarney, P. D. Kempton, P. Spadea, A. Nivia, G. F. Marriner, and R. A. Duncan (2002), Pervasive mantle plume head heterogeneity: Evidence from the late Cretaceous Caribbean-Colombian oceanic plateau. *Journal of Geophysical Research-Solid Earth* 107(B7).

Kerr, A.C., Marriner, G.F., Tarney, J., Nivia, A., Saunders, A.D., Thirlwall, M.F., and Sinton, C.W. (1997), Cretaceous basaltic terranes in western Colombia: Elemental, geochronogical and Sr-Nd constraints on petrogenesis. *Journ. Petrol.* 38, 667-702.

Kerr, A.C., Marriner, G.F., Arndt, N.T., Tarney, J., Nivia, A., Saunders, A.D., Duncan, R.A. (1996a), The petrogenesis of Gorgona komatiites, picrites and basalts: New field, petrographic and geochemical constrains. *Lithos* 37, 245-260.

Kerr, A. C., J. Tarney, G. F. Marriner, A. Nivia, G. T. Klaver, and A. D. Saunders (1996b), The geochemistry and tectonic setting of late Cretaceous Caribbean and Colombian volcanism. *Journal of South American Earth Sciences 9*(1-2), 111-120.

Kogiso, T., M. M. Hirschmann, and P. W. Reiners (2004), Length scales of mantle heterogeneities and their relationship to ocean island basalt geochemistry. *Geochimica Et Cosmochimica Acta* 68(2), 345-360.

Kumagai, I., A. Davaille, K. Kurita, and E. Stutzmann (2008), Mantle plumes: Thin, fat, successful, or failing? Constraints to explain hotspot volcanism through time and space. *Geophysical Research Letters* 35(16).

Kurz, M. D., and D. Geist (1999), Dynamics of the Galapagos hotspot from helium isotope geochemistry. *Geochim. Cosmochim. Acta* 63 (23-24), 4139-4156 Langmuir, C.H., Klein, E.M. and Plank, T. (1992) in Mantle Flow and Melt Generation at Mid-Ocean Ridges (eds Morgan, J.P., Blackman, D.K. and Sinton J.M.) Vol. 71, 183-280 *Geophys. Monogr. Ser., AGU*, Washington DC.

Lapierre, H., et al. (2000), Multiple plume events in the genesis of the peri-Caribbean Cretaceous oceanic plateau province. *Journal of Geophysical Research-Solid Earth* 105(B4), 8403-8421.

Lapierre, H., V. Dupuis, B. Mercier de Le´pinay, D. Bosch, P. Monie, M. Tardy, R. C. Maury, J. Hernandez, M. Polvé, D.Yeghicheyan and J. Cotten (1999), Late Jurassic Oceanic Crust and Upper Cretaceous Caribbean Plateau Picritic Basalts Exposed in the Duarte Igneous Complex, Hispaniola. *Journal of Geology* 107, 193-207.

Lin, S. C., and P. E. van Keken (2005), Multiple volcanic episodes of flood basalts caused by thermochemical mantle plumes *Nature* 436(7048), 250-252.

Mamberti, M. *et al*. (2003), Accreted fragments of the Late Cretaceous Caribbean-Colombian Plateau in Ecuador. *Lithos* 66 (3-4), 173-199.

McKenzie, D. and M.J. Bickle (1988), The volume and composition of melt generated by extension of the lithosphere. *J. Petrol.* 29, 625-679.

McKenzie, D., Jackson, J. and Priestley K. (2005), Thermal structure of oceanic and continental lithosphere. *Earth Plant. Sci. Lett.* 233, 337-349.

Niu, Y., and M.J. O'Hara (2003), Origin of ocean island basalts: A new perspective from petrology, geochemistry, and mineral physics considerations. *J. Geophys. Res. 108*, B4, 2209.

O'Connor, J.M., P. Stoffers, J.R. Wijbrans, and T.J. Worthington (2007), Migration of widespread long-lived volcanism across the Galapagos Volcanic Province: Evidence for a broad hotspot melting anomaly? *Earth Planet. Sci. Lett.* 263 (3-4), 339-354.

O'Hara, M.J. (1968), Are ocean floor basalts primary magmas? *Nature* 220, 683-686.

Pilet, S., M. B. Baker, E.M. Stolper (2008), Metasomatized lithosphere and the origin of alkaline lavas. *Science* 320, 916-919.

Putirka, K. D. (2005), Mantle potential temperatures at Hawaii, Iceland, and the mid-ocean ridge system, as inferred from olivine phenocrysts: Evidence for thermally driven mantle plumes. *Geochemistry Geophysics Geosystems*, *6*.

Revillon, S., C. Chauvel, N. T. Arndt, R. Pik, F. Martineau, S. Fourcade, and B. Marty (2002), Heterogeneity of the Caribbean plateau mantle source: Sr, O and He isotopic compositions of olivine and clinopyroxene from Gorgona Island, *Earth Planet. Sci. Lett*. 205(1-2), 91-106.

Reynaud, C., E. Jaillard, H. Lapierre, M. Mamberti, M., and G. Mascle, (1999), Oceanic Plateau and island arcs of southwestern Ecuador: Their place in the geodynamic evolution of northwestern South America. *Tectonophysics* 307, 235-254.

Richards, M.A., R.A Duncan and V.E Courtillot (1989), Flood basalts and hot-spot tracks: Plume heads and tails. *Science 246*, 103-107.

Saunders, A.D., Fitton, J.G., Kerr, A.C., Norry, M.J., and Kent, R.W. (1997), in Large Igneous Provinces: Continental, Oceanic, and Planetary Flood Volcanism (eds Mahoney, J.J. and Coffin, M.J.) Vol. 100, 45-93 *Geophys. Monogr. Ser.* AGU, Washington, DC.

Schulze, D. J. (1989), Constrains of abundance of eclogite in the upper mantle. *Journal of Geophysical Research-Solid Earth and Planets* 94(B4), 4205-4212.

Sinton, C. W., D. M. Christie, and R. A. Duncan (1996), Geochronology of Galapagos seamounts. *Journal of Geophysical Research-Solid Earth* 101(B6), 13689-13700.

Sinton, C. W., R. A. Duncan, and P. Denyer (1997), Nicoya Peninsula, Costa Rica: A single suite of Caribbean oceanic plateau magmas. *Journal of Geophysical Research-Solid Earth* 102(B7), 15507-15520.

Sinton, C.W., R.A. Duncan, M. Storey, J. Lewis, and J.J. Estrada (1998), An oceanic flood basalt province within the Caribbean plate. *Earth Planet. Sci. Lett.* 155 (3-4), 221-235.

Sinton, C.W., H. Sigurdsson, and R.A. Duncan (2000), in Proceedings of the Ocean Drilling Program, Scientific Results Leg 165 (eds, Leickie, R.M, Sigurdsson, H., Acton, G.D., & Draper G.) 233-236 *Ocean Drilling Program, A&M University, Texas*.

Sobolev, A. V., A. W. Hofmann, S. V. Sobolev, and I. K. Nikogosian (2005), An olivine-free mantle source of Hawaiian shield basalts. *Nature 434*(7033), 590-597.

Storey, M., J. J. Mahoney, L. W. Kroenke, and A. D. Saunders (1991), Are oceanic plateaus sites of komatiite formation. *Geology 19*(4), 376-379.

Sleep, N. (2008), Channeling at the base of the lithosphere during the lateral flow of plume material beneath flow line hot spots. *Geochem. Geophys. Geosys. 9*

Storey, M, R.A. Ducan, and C. Tegner (2007), Timing and duration of volcanism in the North Atlantic Igneous Province: Implications for geodynamics and links to the Iceland hotspot. *Chemical Geology* 241, 264-281.

Storey, M., J.J Mahoney, L.W. Kroenke and A.D Saunders (1991), Are oceanic plateaus sites for komatiite formation? *Geology* 19, 376-379.

Thompson, P. M. E., P. D. Kempton, R. V. White, A. D. Saunders, A. C. Kerr, and J. Tarney (2002), Hf-Nd isotope systematics of the Gorgona komatiites, and their relationship with the Caribbean Plateau. *Geochimica et Cosmochimica Acta* 66(15A), A773-A773.

Wadge, G., T.A. Jackson, M.V., Isaacs and T.E., Smith (1982), The ophiolitic Bath-Dunrobin Formation, Jamaica: Significance for Cretaceous plate margin evolution in the north-western Caribbean. *Journal of the Geologic Society London* 139, 321-333.

Walker, R.J., M., Storey, A. Kerr, J. Tarney, and N. T. Arnt (1999), Implications of ^{187}Os isotopic heterogeneities in a mantle plume: Evidence from Gorgona Island and Curaçao. *Geochimica et Chomoschimica Acta* 63 (5), 713-728.

Walker, R.J., L.M Echeverria, S.B. Shirey, and M.F Horan (1991), Re-Os Isotopic constraints on the origin of volcanic-rocks, Gorgona Island, Colombia: Os isotopic evidence for ancient heterogeneities in the mantle. *Contrib. Min. Petrol.* 107 (2), 150-162.

Werner, R., K. Hoernle, U. Barckhausen, and F. Hauff (2003), Geodynamic evolution of the Galapagos hot spot system (Central East Pacific) over the past 20 m.y.: Constraints from morphology, geochemistry, and magnetic anomalies. *Geochemistry Geophysics Geosystems*, 4.

White, W. M., A. R. McBirney, and R. A. Duncan (1993), Petrology and geochemistry of the Galapagos-Islands - Portrait of a pathological mantle plume. *Journal of Geophysical Research-Solid Earth* 98(B11), 19533-19563.

White, W. M., and A. W. Hofmann (1978), Geochemistry of the Galapagos Islands: Implications for mantle dynamics and evolution. *Yearbook Carnegie Inst*. 77, 596–606.

Wignall, P. (2005), The link between large igneous province eruptions and mass extinctions. *Elements 1*(5), 293-297.

Wilkinson, I. P., (1998), Foraminifera from a suite of Late Cretaceous to Palaeogene samples of the Cordillera Occidental, Ecuador: Biostratigraphy and Sedimentology Research Group. *British Geological Survey*, Nottingham, U.K.

Figure Captions

Figure 1

A) Tectonic setting of the CLIP and Galapagos hotspot and tracks, showing the location of successful petrological solutions for this study. Geologic synthesis after Denyer et al., (2006), Kerr et al. (2003) and references therein. Galapagos hotspot tracks and other bathymetric structures after Werner et al. (2003). **B)** Age-corrected Pb isotope diagram that illustrates the geochemical diversity of the CLIP-related suites compared to samples from Gorgona Island. The regression line with r=0.95 suggests that most of the samples require binary mixing between the DMM and HIMU reservoirs. Data (n=117) from Dupré & Echeverría (1984), Walker et al. (1991), Hauff et al. (2000a, b), Kerr et al. (2002a), Mamberti et al. (2003) and (Kerr et al. *in press*).

Figure 2

Geochronological correlation of the different oceanic complexes of the Caribbean and Central and South America. Note that the main CLIP event ranges between 95-85 Ma. Biochronological and $^{40}Ar/^{39}Ar$ age data from Wadge et al. (1982), Beets at al. (1984), Beck et al. (1984), Walker et al. (1991, 1999), DiMarco (1994), Donelly (1994 and references therein), Jaillaid et al. (1995), Alvarado et al. (1997), Kerr et al. (1996 a and b, 1997, 2002), Sinton et al. (1997, 1998, 2000), Wilkinson (1998), White (1999), Reynaud et al. (1999), Lapierre et al. (1999, 2000), Revilon (2000), Thomson et al. (2004), Hauff et al. (2001, 2004), Hoernle et al. (2002), Denyer et al. (2006 and references therein).

Figure 3

Galapagos source mantle domains. Mantle domains in $^{206}Pb/^{204}$ Pb and $^{208}Pb/^{204}Pb$ isotopic space **(A)** and$^{206}Pb/^{204}$ Pb and $^{143}Nd/^{144}Nd$ isotopic space. Data from GEOROC database. Note how the different domains represent different mantle heterogeneities (end-members) and scatter between the different end-members is explained by mixing. Panel **C)** shows the present distribution of the isotopic domains in the Galapagos archipelago. Panel **D)** shows inferred trace element composition of the mantle sources of the different Galapagos plume domains (modified from Hoernle et al., 2000). The source trace-element composition was calculated by inverting a primitive basalt/primary magma composition representative of each domain. For the Central and Southern Galapagos domains, primary magma compositions Table 1 were inverted using the modal composition of a fertile peridotite and melt fraction inferred in Table 1. For the Eastern Domain we were not able to use a primary magma because of lack of trace element data; therefore, we used the average melt fraction from the primary magmas of Table 1 and the trace element composition of a primitive basalt. In the case of the Northern Galapagos Domain there is no available complete trace element data. Therefore, we used the average Costa Rican seamount province composition (Werner et al., 2003) as a best approximation. This composition was inverted using melt fraction for alkaline basalt (~0.02F) and using a fertile peridotite composition.

Figure 4

Galapagos isotopic domains compared with other modem OIB. Note that event though there is overlap in some of the isotopic systems, internal consistency is very poor. The internal consistency among the different Galapagos isotopic domains could be a key to fingerprint the Galapagos plume signature in accreted oceanic complexes in Central and South America and the Caribbean. The different Galapagos plume domains modified from Hoernle et al. (2000), data from GEOROC database.

Figure 5

Compositions and inferred T conditions of melting for Galápagos – related magmatism.

a) FeO and MgO contents lavas and calculated primary magmas from the present-day Galápagos hotpot, the Cocos and Carnegie ridges, old accreted Galápagos tracks, and the Caribbean Large Igneous Province (CLIP). Lavas from the island of Gorgona are plotted separately because it is not clear whether they were part of the CLIP or some other oceanic complex. Arrays of small circles identify liquid compositions that result from olivine addition and subtraction from specific lava compositions. These are used to compute primary magma compositions, indicated as colored crosses, using PRIMELT2.XLS software of Herzberg and Asimow (2008). All primary magmas of fertile peridotite KR-4003 plot within the gray-colored area (Herzberg and Asimow, 2008). The intersection of the red and blue lines identify the composition of an accumulated fractional melt at the pressure of initial and final melting, respectively. Individual lavas and their sources from which primary magmas are calculated are identified in Table 1.

Figure 6

Inferred temperatures and pressures in the mantle where accumulated fractional melts are assumed to have resided prior to eruption. The olivine liquidus crystallization temperature at the surface is similar to the eruption temperature, and can be extended along the adiabat using the equation in the text for T_{OL}. This equation is solved using the MgO contents of the primary magmas and the pressure at which melting terminates, inferred from the blue lines in Fig. 4a. Gorgona komatiites probably formed from a more depleted peridotite source, and solutions are not provided.

Figure 7

Mantle potential temperatures inferred for lavas from some Large Igneous Provinces (LIPS) and Oceanic Islands. Data sources and calculated T_P for oceanic islands and LIPS are given in Tables 2 and 3. CLIP results are for rocks with ages ≥ 65 Ma and include old accreted Galápagos tracks. Gorgona is shown separately as the grey crosses. Galápagos results are from lavas within the archipelago. OJP = primary magmas for lavas from the Ontong Java Plateau. Results for the Society Islands, Pitcairn-Gambier, St. Helena, and Tristan da Cunhan are not shown for clarity purposes and can be obtained in Table 3. North Atlantic = primary magmas for Paleocene lavas from the North Atlantic Igneous province found at east and west Greenland. CAMP = primary magmas for the Central Atlantic Magmatic Province.

Figure 8

A generic model for interpreting the spatial localization of primary magmas with highly variable compositions, inferred mantle potential temperatures, and melt fractions. This is the mantle plume model wherein hot primary magmas originate from the axis and cooler primary magmas originate from the periphery.

Figure 9

Melt fractions inferred for lavas for some Large Igneous Provinces (LIPS) and Oceanic Islands. Melt fractions refer to the total melt fraction with respect to source mass for accumulated fractional melting of fertile peridotite. **A)** LIPS. Data sources for model primary magmas for LIPS are given in Tables 1 and 2. **B)** Oceanic Island basalts (OIB). Solid blue bars = primary magma solutions from oceanic islands (Tables 1-3). The hatched region designates an abundance of OIB melted from volatile-enriched sources at very low melt fractions; these are generally more abundant than lavas that can be modeled by PRIMELT2.XLS (Herzberg and Asimow, 2008) calibrated from volatile-free experimental results.

Figure 10

CaO - MgO contents of partial melts of peridotite and pyroxenite sources from Herzberg (2006) and Herzberg and Asimow (2008). Small black circles are differentiated lavas that had experienced variable clinopyroxene fractionation in the crust and mantle (e.g., Geist et al., 1998). About 44% of the high MgO lavas indicated as yellow squares for the Galapagos Archipelago are candidates for pyroxenite-source melting. In contrast, all hot

CLIP lavas with ~ 90 Ma ages were melted from a peridotite source. Pyroxenite source lavas appear for the first time at ~ 65 Ma in the accreted Galapagos oceanic island at Quepos Block (Costa Rica). Lava compositions from GEOROC database.

Figure 11

Isotopic evolution of the Galapagos plume in different stages of plume activity. The isotopic source composition of each domain was projected into the past at 90 Ma (for the 95-85 diagram) and to 60 Ma (for the 65-50 Ma diagram). The initial ratios (age corrected) of samples of the CLIP, accreted and modern track are plotted and compared to the projected modern Galapagos domains into the past. For the Central and Southern Galapagos domains, primary magma compositions from Herzberg and Gazel, (2009) were inverted using the modal composition of a fertile peridotite and melt fraction published by them. For the Eastern Domain we were not able to use a primary magma because of lack of trace element data; therefore, we used the average melt fraction from the primary magmas of Herzberg and Gazel (2009) (Table 1) and the trace element composition of primitive basalt. In the case of the Northern Galapagos Domain there is no available complete trace element data. Therefore, we used the average Costa Rican seamount province composition (Werner et al., 2003) as a best approximation. This composition was inverted using melt fraction for alkaline basalt (~0.02F) and using a fertile peridotite composition.

Tables Captions

Table 1

PRIMELT2 Model Primary Magma Compositions (wt%) for lavas from the CLIP, Gorgona, Galapagos Islands and Ridges. See Herzberg and Gazel (2009) for the original source of the lavas.

Table 2

RIMELT2 Model Primary Magma Compositions (wt%) for lavas from some Large Igneous Provinces, excluding CLIP. See Herzberg and Gazel (2009) for the original source of the lavas.

Table 3

RIMELT2 Model Primary Magma Compositions (wt%) for lavas from some Ocean island basalts, excluding Galapagos. See Herzberg and Gazel (2009) for the original source of the lavas.

Figure 1

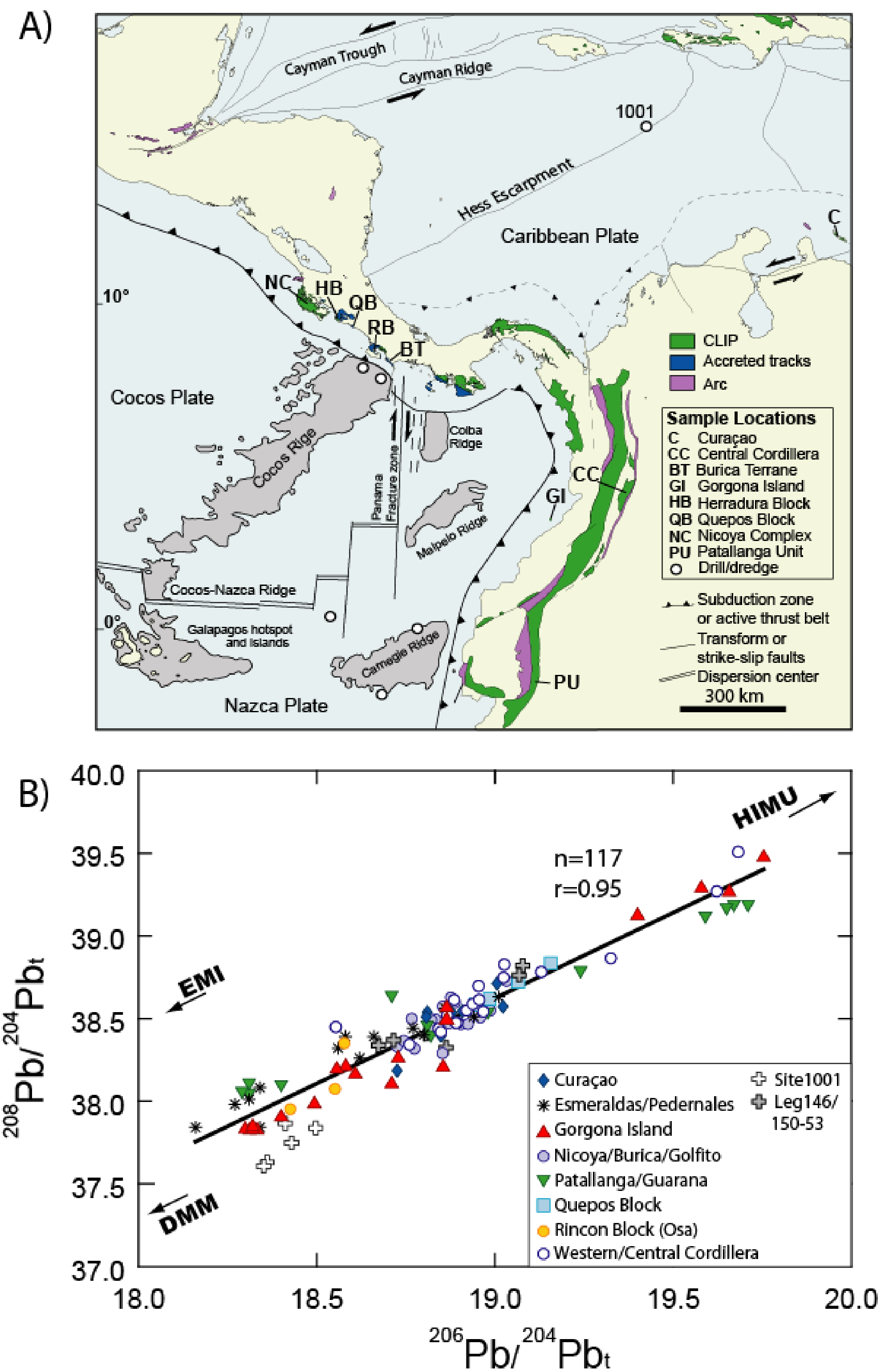
A)
Cayman Trough
Cayman Ridge
1001
Hess Escarpment
Caribbean Plate
C
NC
HB
QB
RB
BT
10°
Cocos Plate
Cocos Ridge
Panama Fracture zone
Coiba Ridge
Malpelo Ridge
CC
GI
Cocos-Nazca Ridge
0°
Galapagos hotspot and islands
Carnegie Ridge
Nazca Plate
PU
CLIP
Accreted tracks
Arc
Sample Locations
C Curaçao
CC Central Cordillera
BT Burica Terrane
GI Gorgona Island
HB Herradura Block
QB Quepos Block
NC Nicoya Complex
PU Patallanga Unit
Drill/dredge
Subduction zone or active thrust belt
Transform or strike-slip faults
Dispersion center
300 km
B)
HIMU
n=117
r=0.95
EMI
DMM
Curaçao
Esmeraldas/Pedernales
Gorgona Island
Nicoya/Burica/Golfito
Patallanga/Guarana
Quepos Block
Rincon Block (Osa)
Western/Central Cordillera
Site1001
Leg146/ 150-53
208Pb/204Pbt
206Pb/204Pbt
40.0
39.5
39.0
38.5
38.0
37.5
37.0
18.0
18.5
19.0
19.5
20.0

Figure 2

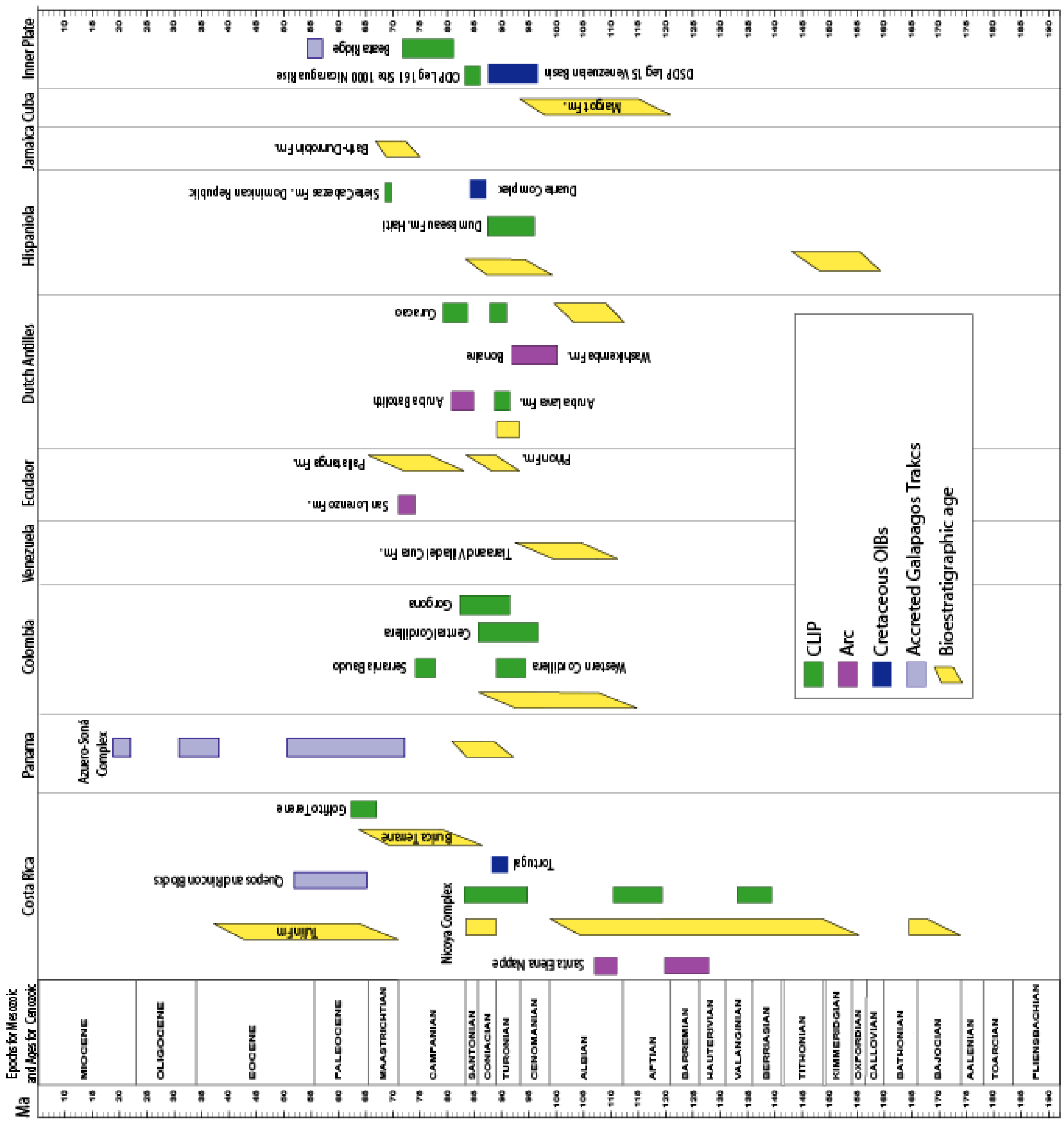
CLIP
Arc
Cretaceous OIBs
Accreted Galapagos Trakcs
Bioestratigraphic age

Figure 3

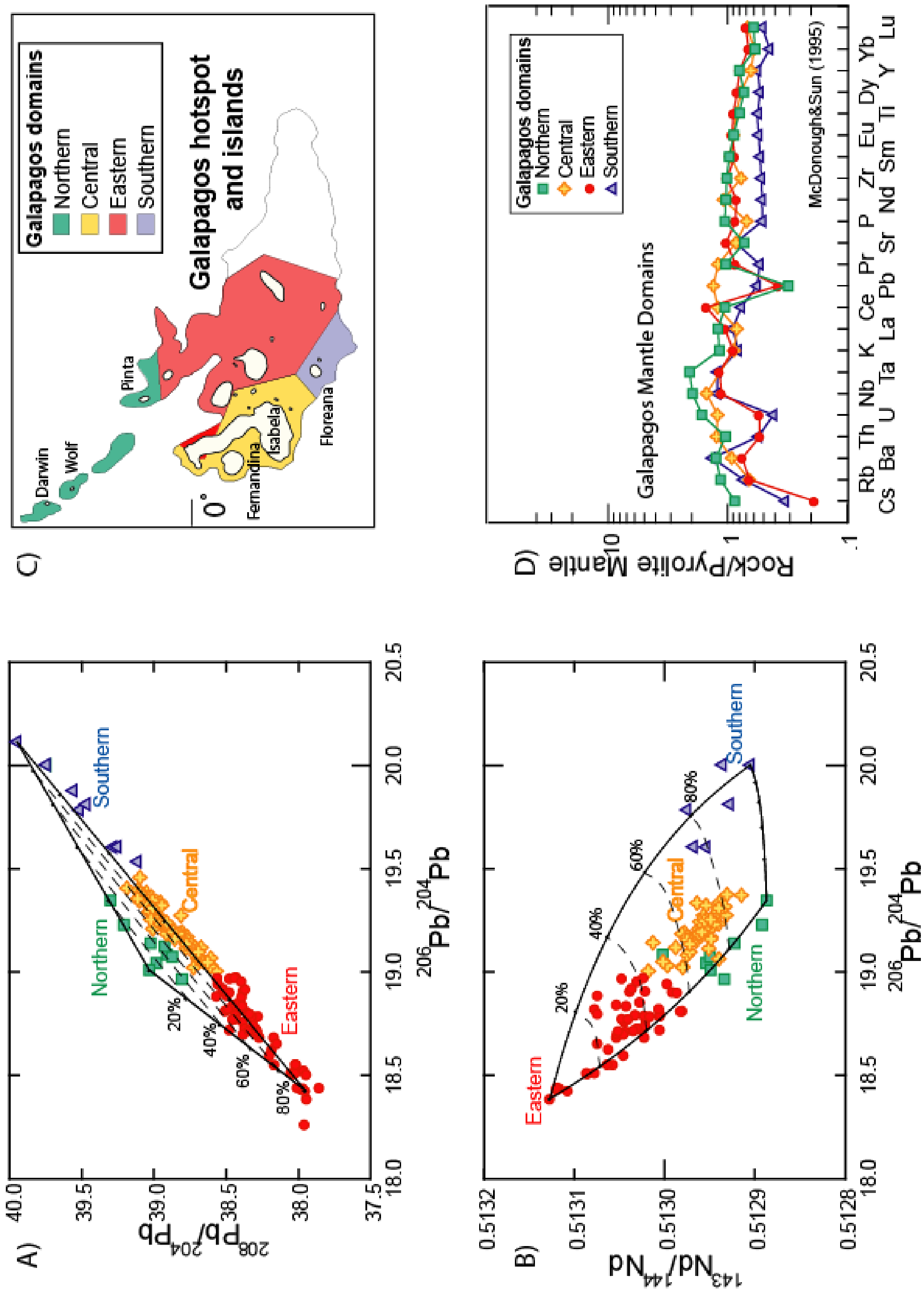
A)
$^{208}Pb/^{204}Pb$
$^{206}Pb/^{204}Pb$
Northern
Southern
Central
Eastern
20%
40%
60%
80%
B)
$^{143}Nd/^{144}Nd$
$^{206}Pb/^{204}Pb$
Eastern
Northern
Southern
Central
C)
Galapagos domains
Northern
Central
Eastern
Southern
Galapagos hotspot and islands
0°
Darwin
Wolf
Pinta
Fernandina
Isabela
Floreana
D)
Rock/Pyrolite Mantle
Galapagos Mantle Domains
McDonough&Sun (1995)

Figure 4

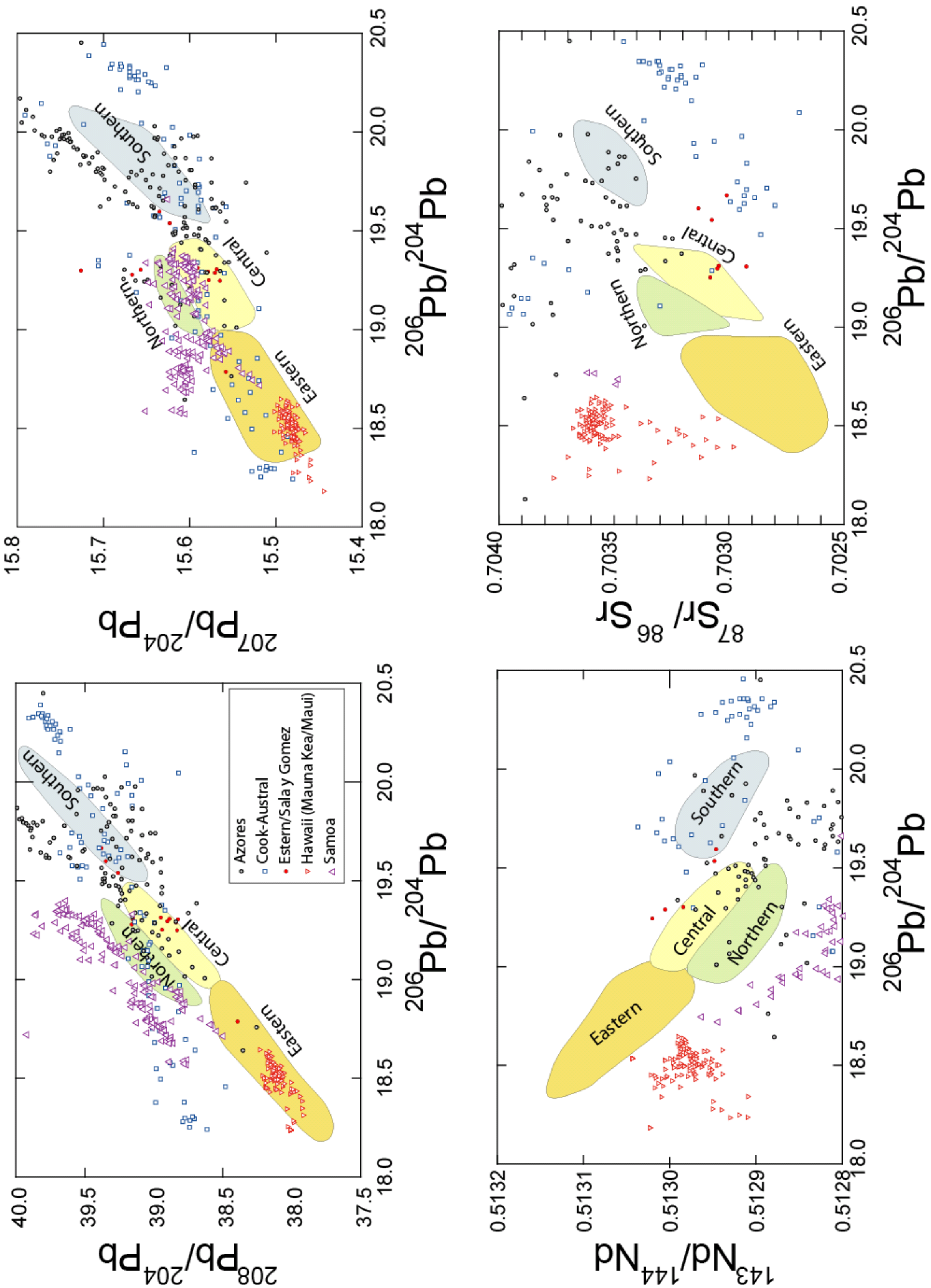

Azores
Cook-Austral
Estern/Sala y Gomez
Hawaii (Mauna Kea/Maui)
Samoa
Southern
Central
Northern
Eastern
$^{206}Pb/^{204}Pb$
$^{208}Pb/^{204}Pb$
$^{207}Pb/^{204}Pb$
$^{87}Sr/^{86}Sr$
$^{143}Nd/^{144}Nd$

Figure 5

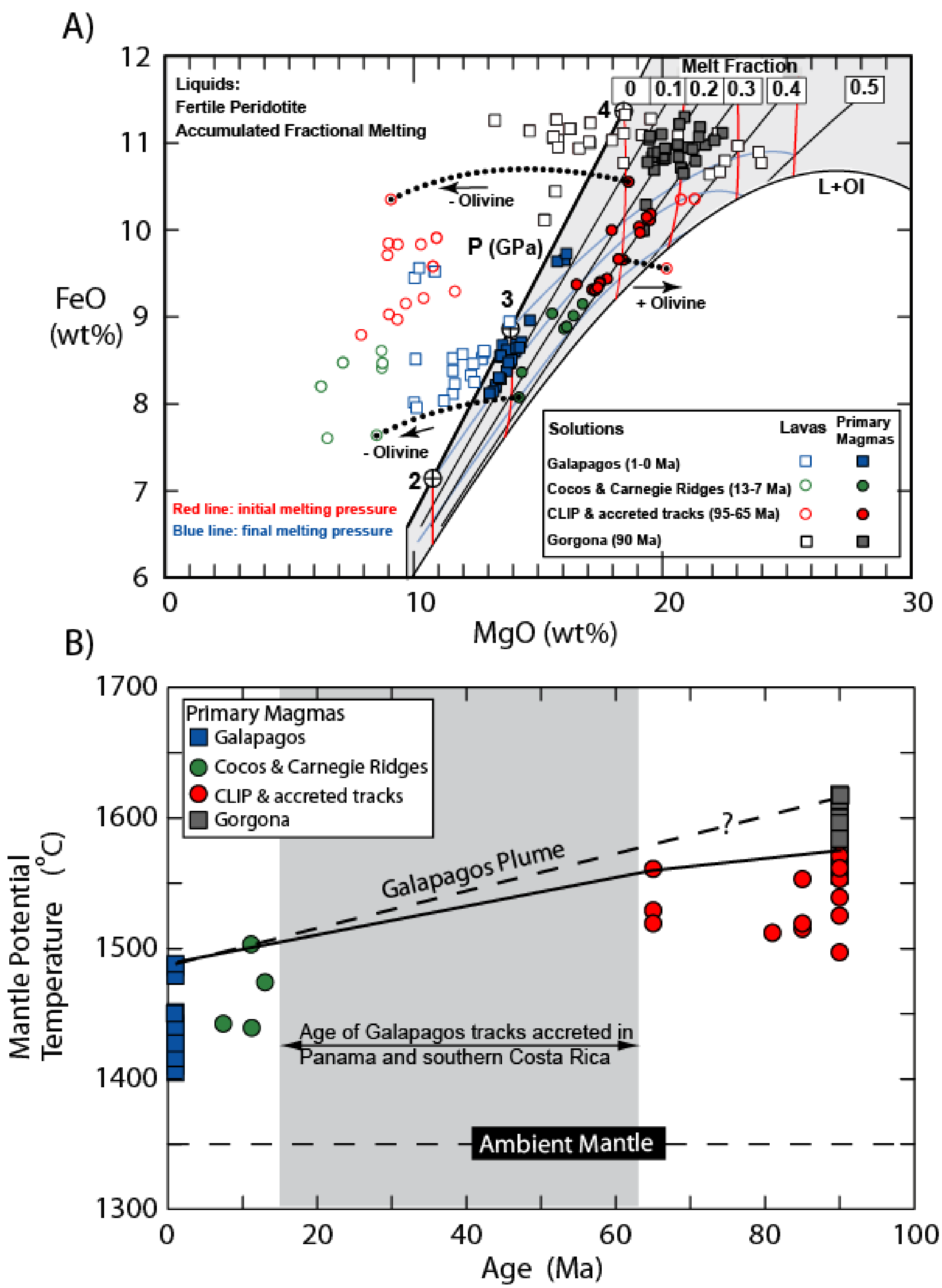
A)
Liquids:
Fertile Peridotite
Accumulated Fractional Melting
Melt Fraction
0 0.1 0.2 0.3 0.4 0.5
L+Ol
- Olivine
P (GPa)
+ Olivine
FeO (wt%)
MgO (wt%)
Red line: initial melting pressure
Blue line: final melting pressure
Solutions
Lavas
Primary Magmas
Galapagos (1-0 Ma)
Cocos & Carnegie Ridges (13-7 Ma)
CLIP & accreted tracks (95-65 Ma)
Gorgona (90 Ma)
B)
Primary Magmas
Galapagos
Cocos & Carnegie Ridges
CLIP & accreted tracks
Gorgona
Galapagos Plume
?
Age of Galapagos tracks accreted in Panama and southern Costa Rica
Ambient Mantle
Mantle Potential Temperature (°C)
Age (Ma)

Figure 6

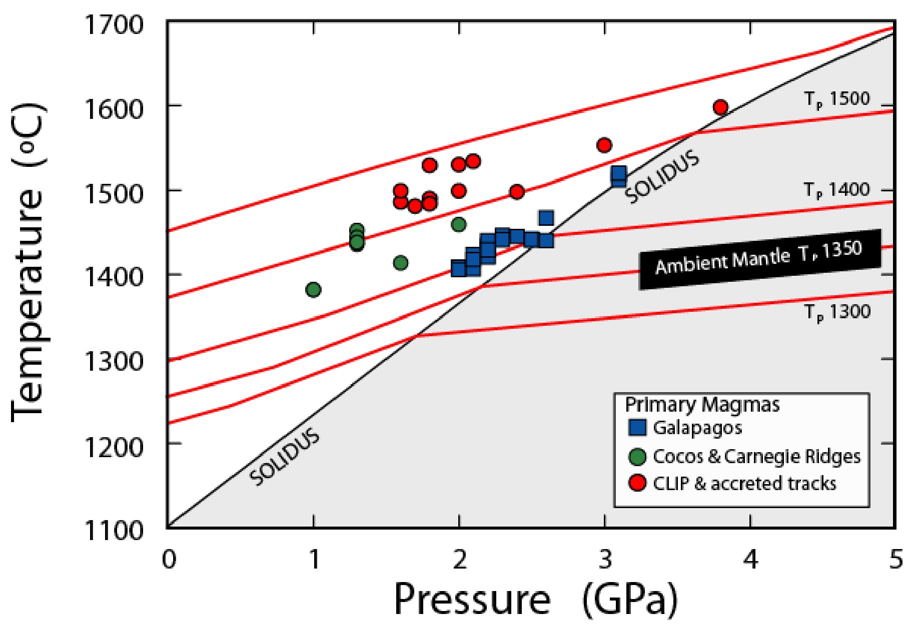
1700
1600
1500
1400
1300
1200
1100
0
1
2
3
4
5
Temperature (oC)
Pressure (GPa)
Tp 1500
Tp 1400
Ambient Mantle Tp 1350
Tp 1300
SOLIDUS
SOLIDUS
Primary Magmas
Galapagos
Cocos & Carnegie Ridges
CLIP & accreted tracks

Figure 7

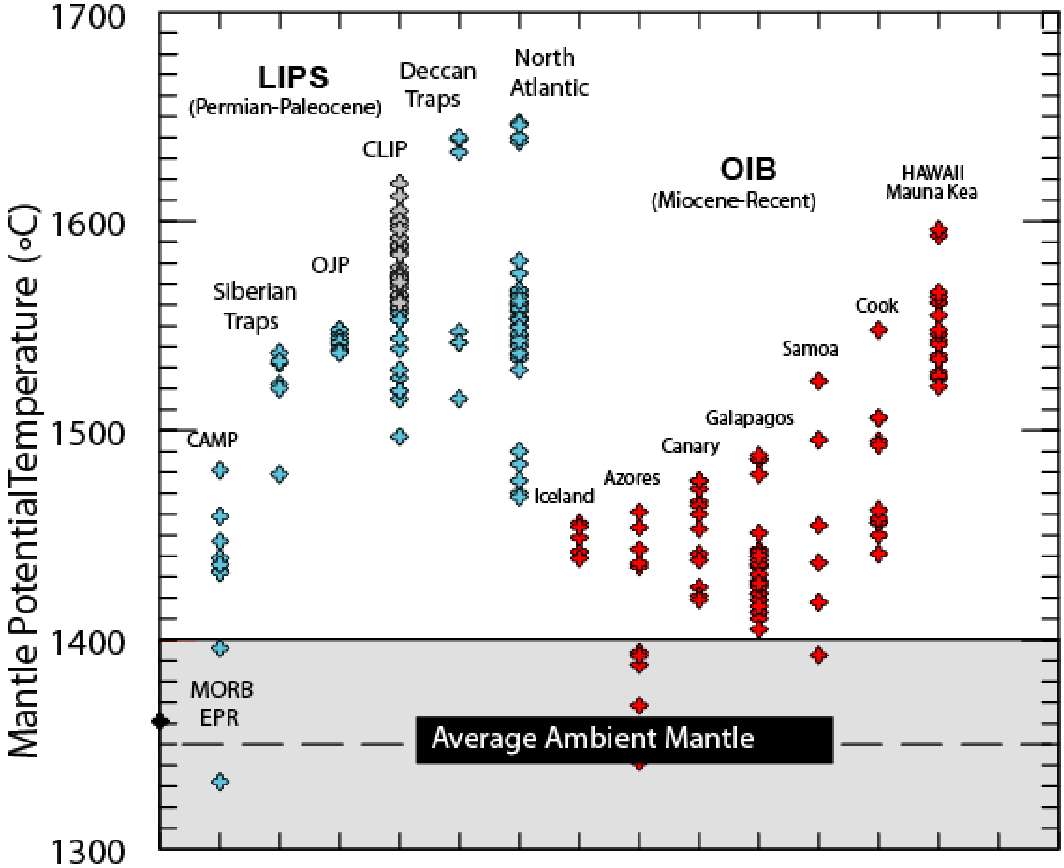
1700
1600
1500
1400
1300
Mantle PotentialTemperature (oC)
LIPS
(Permian-Paleocene)
Deccan
Traps
North
Atlantic
CLIP
OJP
Siberian
Traps
CAMP
Iceland
OIB
(Miocene-Recent)
HAWAII
Mauna Kea
Cook
Samoa
Galapagos
Canary
Azores
MORB
EPR
Average Ambient Mantle

Figure 8

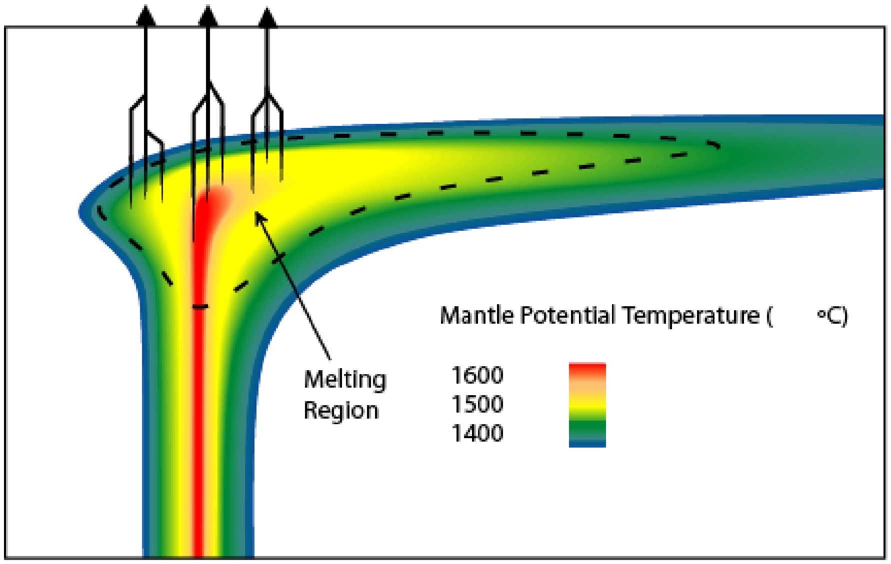
Mantle Potential Temperature (°C)
1600
1500
1400
Melting
Region

Figure 9

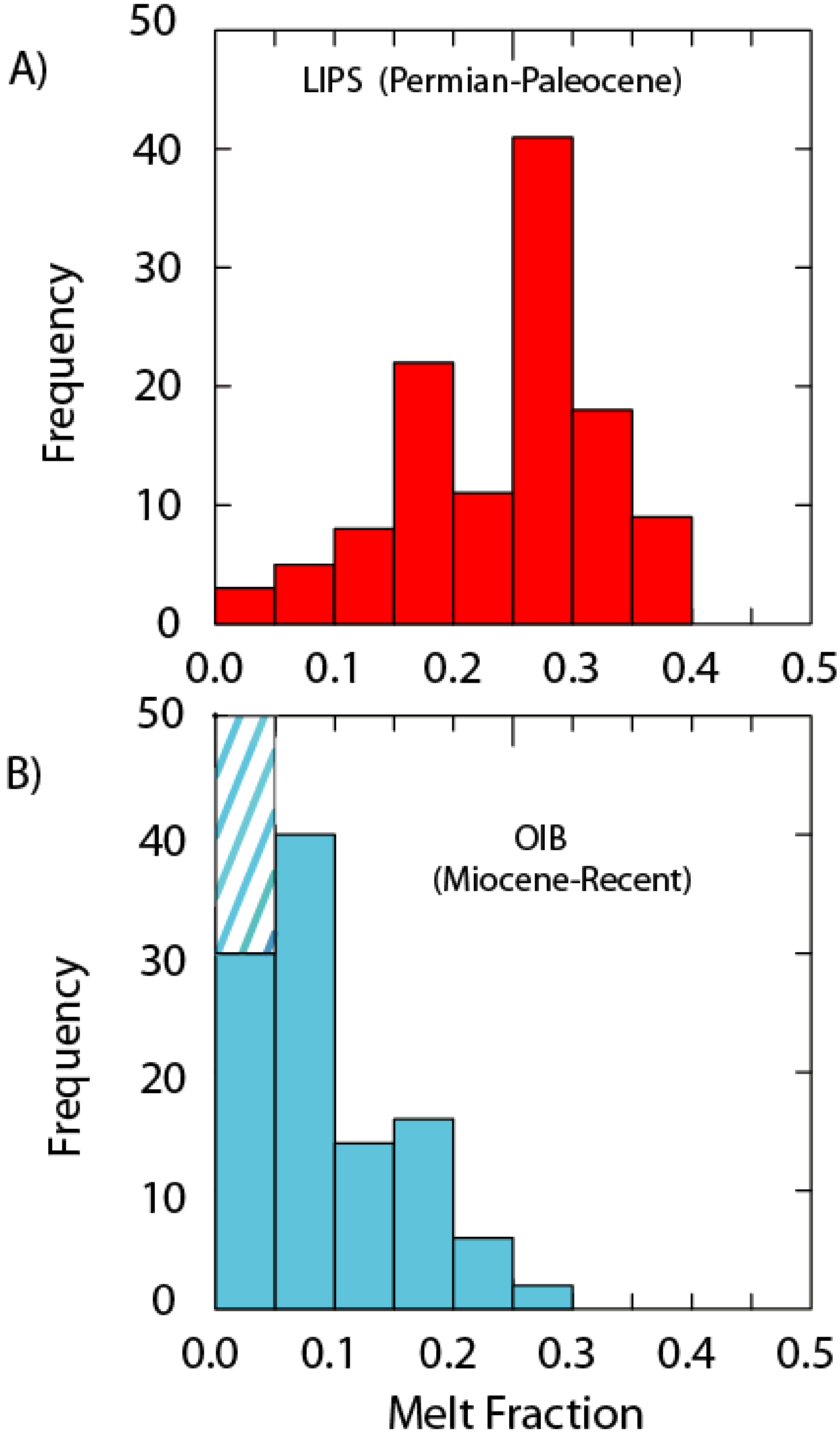
A)
LIPS (Permian-Paleocene)
Frequency
50
40
30
20
10
0
0.0
0.1
0.2
0.3
0.4
0.5
B)
OIB
(Miocene-Recent)
Frequency
50
40
30
20
10
0
0.0
0.1
0.2
0.3
0.4
0.5
Melt Fraction

Figure 10

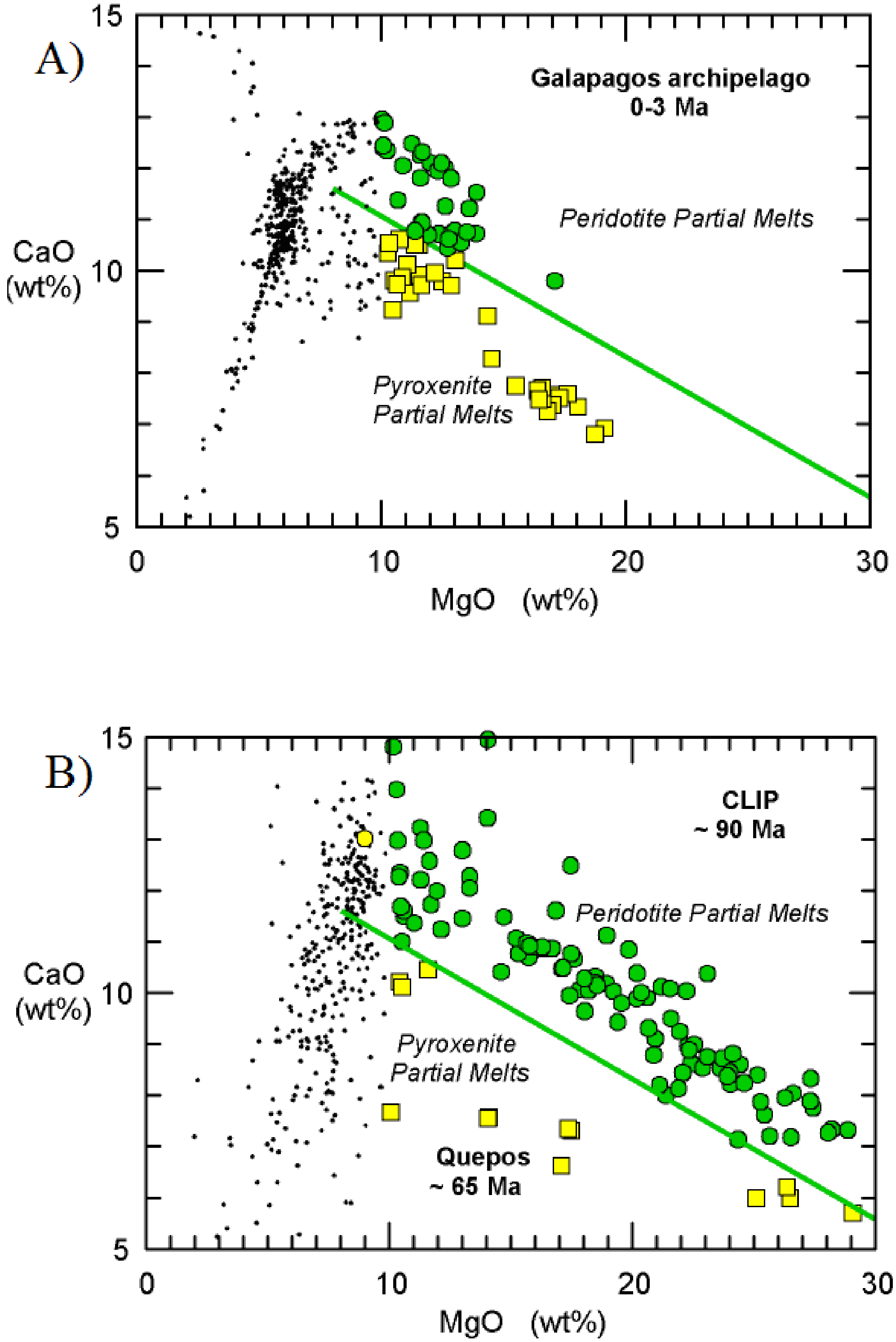
A)
Galapagos archipelago
0-3 Ma
Peridotite Partial Melts
Pyroxenite
Partial Melts
CaO
(wt%)
MgO (wt%)
15
10
5
0
10
20
30
B)
CLIP
~ 90 Ma
Peridotite Partial Melts
Pyroxenite
Partial Melts
Quepos
~ 65 Ma
CaO
(wt%)
MgO (wt%)
15
10
5
0
10
20
30

Figure 11

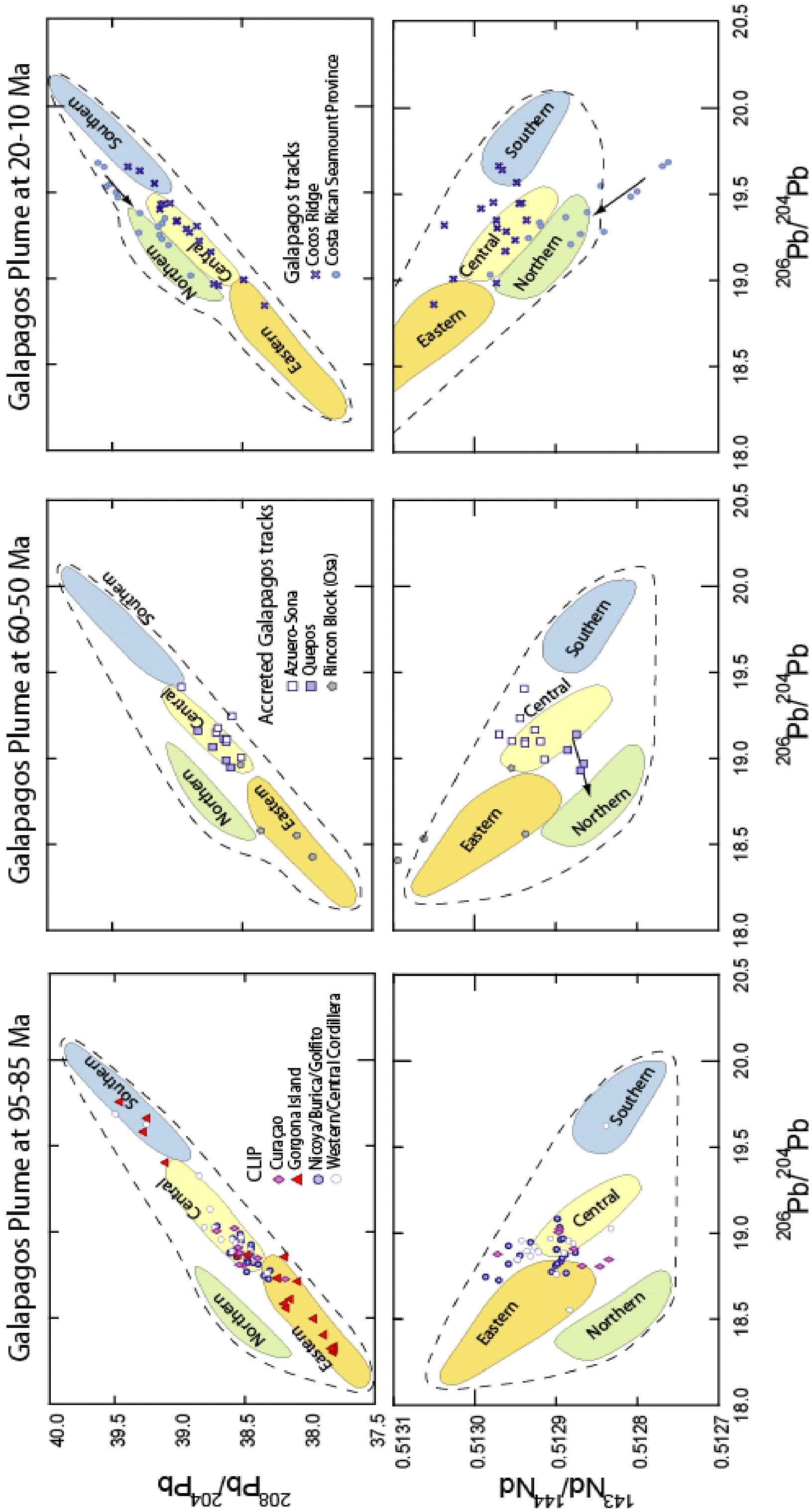
Galapagos Plume at 95-85 Ma
Galapagos Plume at 60-50 Ma
Galapagos Plume at 20-10 Ma
CLIP
Curaçao
Gorgona Island
Nicoya/Burica/Golfito
Western/Central Cordillera
Accreted Galapagos tracks
Azuero-Sona
Quepos
Rincon Block (Osa)
Galapagos tracks
Cocos Ridge
Costa Rican Seamount Province
Southern
Central
Northern
Eastern
$^{208}Pb/^{204}Pb$
$^{143}Nd/^{144}Nd$
$^{206}Pb/^{204}Pb$

Table 1

Sample[a]	Age (Ma)	Lat.	Lon.	SiO_2	TiO_2	Al_2O_3	Cr_2O_3	Fe_2O_3	FeO	MnO	MgO	CaO	Na_2O	K_2O	NiO	P_2O_5	T_{α}[b]	T_P[c]	Ol Mg[d]	Melt Fraction[e]
Central Cordillera, Colombia																				
AMA3	90	2.5	-75.4	48.8	0.72	11.24	0.079	0.36	9.44	0.18	17.8	10.0	1.18	0.06	0.108	0.064	1405	1525	91.5	0.30
COL472	90	2	-77.04	48.2	0.79	11.31	0.190	0.39	9.37	0.17	16.6	10.2	2.55	0.07	0.080	0.079	1380	1497	91.2	0.18
Western Cordillera, Pallatanga Unit, Ecuador																				
PND1508	85	-2	-78	47.7	0.77	10.37	0.063	0.38	9.97	0.17	19.1	10.1	1.23	0.05	0.080	0.062	1430	1553	91.8	0.30
Gorgona, Colombia																				
GOR-94-7	90	3	-78.32	47.7	0.43	11.48	0.108	0.21	9.99	0.17	19.2	9.6	0.94	0.04	0.099	0.035	1433	1556	91.8	0.31
6	90	3	-78.32	46.1	0.62	10.91	0.000	0.31	10.71	0.19	20.8	9.4	0.97	0.04	0.000	0.000	1460	1587	92.0	0.28
38	90	3	-78.32	45.8	0.57	11.77	0.000	0.28	10.84	0.20	19.6	9.6	1.27	0.02	0.000	0.000	1440	1564	91.6	0.16
71	90	3	-78.32	46.0	0.61	11.23	0.000	0.31	10.81	0.18	20.0	9.6	1.21	0.02	0.000	0.000	1447	1572	91.7	0.20
72	90	3	-78.32	45.7	0.64	11.27	0.000	0.32	10.93	0.20	20.1	9.7	1.06	0.02	0.000	0.000	1449	1574	91.7	0.19
73	90	3	-78.32	45.9	0.62	11.39	0.000	0.31	10.82	0.20	20.1	9.6	1.10	0.03	0.000	0.000	1449	1573	91.8	0.21
3P	90	3	-78.32	45.7	0.65	11.46	0.000	0.32	10.89	0.19	19.6	10.0	1.13	0.02	0.000	0.000	1440	1564	91.6	0.15
5P	90	3	-78.32	46.0	0.57	11.60	0.000	0.28	10.69	0.16	19.7	10.0	1.07	0.02	0.000	0.000	1441	1565	91.7	0.20
GOR 501	90	3	-78.32	45.2	0.64	10.69	0.261	0.32	11.30	0.19	20.9	9.4	0.86	0.02	0.123	0.031	1463	1589	91.8	0.18
GOR 502	90	3	-78.32	45.7	0.64	11.24	0.143	0.32	10.89	0.19	19.8	9.8	1.08	0.03	0.131	0.034	1444	1568	91.6	0.17
GOR 519	90	3	-78.32	46.6	0.43	11.37	0.156	0.21	10.29	0.18	19.3	9.6	1.13	0.53	0.111	0.027	1435	1558	91.8	0.25
GOR-94-32	90	3	-78.32	45.7	0.63	11.51	0.171	0.31	10.78	0.19	19.4	10.0	1.14	0.03	0.120	0.049	1436	1559	91.5	0.15
GOR-94-7	90	3	-78.32	47.7	0.43	11.47	0.108	0.21	10.00	0.17	19.3	9.6	0.94	0.04	0.099	0.036	1433	1556	91.8	0.31
G-160	90	3	-78.32	45.5	0.63	11.55	0.000	0.32	11.04	0.18	19.5	9.9	1.27	0.06	0.000	0.048	1437	1561	91.4	0.11
G-159	90	3	-78.32	45.4	0.63	11.63	0.000	0.32	11.08	0.18	19.5	10.0	1.22	0.03	0.000	0.040	1438	1562	91.4	0.11
G-142	90	3	-78.32	45.4	0.63	11.45	0.000	0.32	11.10	0.19	20.0	9.8	1.04	0.02	0.000	0.044	1446	1571	91.6	0.15
G-156	90	3	-78.32	45.5	0.61	11.03	0.000	0.30	11.22	0.19	20.7	9.5	0.97	0.01	0.000	0.045	1459	1585	91.8	0.18
GOR-156	90	3	-78.32	46.0	0.46	10.32	0.000	0.23	11.11	0.00	22.4	8.8	0.63	0.01	0.000	0.000	1489	1618	92.4	0.33
GOR-139	90	3	-78.32	45.7	0.49	10.84	0.000	0.24	11.18	0.00	21.5	9.2	0.77	0.02	0.000	0.000	1474	1601	92.1	0.25
GOR-142	90	3	-78.32	46.2	0.54	10.87	0.000	0.27	10.79	0.00	21.3	9.2	0.74	0.02	0.000	0.000	1471	1598	92.2	0.31
GOR-145	90	3	-78.32	45.9	0.51	10.74	0.000	0.26	10.98	0.00	21.7	9.0	0.81	0.03	0.000	0.000	1477	1605	92.2	0.31
GOR-166	90	3	-78.32	46.0	0.49	10.41	0.000	0.24	11.03	0.00	22.1	9.0	0.74	0.00	0.000	0.000	1483	1612	92.3	0.32
GOR-141	90	3	-78.32	45.8	0.50	10.81	0.000	0.25	11.07	0.00	21.5	9.2	0.82	0.00	0.000	0.000	1473	1600	92.1	0.27
GOR-149	90	3	-78.32	46.1	0.53	11.12	0.000	0.27	10.84	0.00	20.7	9.5	0.98	0.07	0.000	0.000	1459	1585	91.9	0.25
GOR-146	90	3	-78.32	46.0	0.54	10.95	0.000	0.27	10.95	0.00	21.0	9.3	0.93	0.06	0.000	0.000	1466	1592	92.0	0.26
GOR-157	90	3	-78.32	46.1	0.50	10.81	0.000	0.25	10.93	0.00	21.2	9.2	0.92	0.08	0.000	0.000	1469	1596	92.1	0.28
GOR-167	90	3	-78.32	45.8	0.54	11.14	0.000	0.27	10.98	0.00	20.6	9.6	0.93	0.02	0.000	0.000	1458	1584	91.9	0.22
Curacao																			0.0	
CUR-7	90	12	-68.75	48.4	0.77	11.37	0.285	0.38	9.66	0.18	18.4	9.5	0.64	0.15	0.089	0.071	1417	1539	91.6	0.31
Nicoya Complex, Nicoya Peninsula, Costa Rica																			0.0	
NI003V	90	10.087	-85.387	46.7	0.72	11.83	0.000	0.36	10.03	0.19	19.1	9.5	1.44	0.09	0.000	0.069	1430	1553	91.8	0.28
CR366T86	85	9.65	-84.66	48.5	0.65	12.18	0.000	0.32	9.30	0.17	17.3	9.8	1.64	0.05	0.000	0.064	1395	1515	91.5	0.28
BH11	85	9.591	-84.622	48.1	0.73	11.85	0.058	0.36	9.40	0.18	17.5	9.7	1.88	0.07	0.096	0.057	1399	1519	91.5	0.28
Leg 165, Site 1001, Hess E		16.550	-80.130																0.0	
55R-1,72-75	81			47.9	1.06	12.11	0.035	0.53	9.31	0.20	17.2	9.7	1.75	0.06	0.088	0.069	1393	1512	91.5	0.27
Quepos Block, Costa Rica																			0.0	
CR372T92	65	9.425	-84.173	46.4	1.99	10.57	0.000	0.99	10.00	0.21	18.0	10.1	1.44	0.21	0.000	0.130	1408	1529	91.4	0.18
Burica Terrane, Costa Rica																			0.0	
BUR5	65	8.395	-83.14	48.2	0.69	11.69	0.051	0.34	9.39	0.16	17.5	10.2	1.55	0.09	0.079	0.048	1399	1519	91.5	0.28
Rincon Block, Osa Peninsula, Costa Rica																			0.0	
C17	65	8.38	-83.289	45.6	0.85	12.08	0.043	0.42	10.55	0.18	18.6	10.2	1.20	0.10	0.059	0.069	1421	1544	91.4	0.13
MS319	65	8.551	-83.32	47.5	0.64	10.82	0.039	0.32	10.11	0.16	19.5	9.5	1.25	0.05	0.107	0.045	1438	1561	91.8	0.30

Table 1 continued

Sample[a]	Age (Ma)	Lat.	Lon.	SiO_2	TiO_2	Al_2O_3	Cr_2O_3	Fe_2O_3	FeO	MnO	MgO	CaO	Na_2O	K_2O	NiO	P_2O_5	T_{OL}[b]	T_P[c]	Ol Mg[d]	Melt Fraction[e]
Carnegie Ridge																			0.0	
11a DR-1	11.1	0.056	-82.12	48.0	1.00	12.03	0.060	0.50	9.15	0.15	16.8	10.4	1.53	0.12	0.147	0.100	1385	1503	91.4	0.27
18 DR-1	11.2	-2.23	-83.68	49.8	0.72	13.77	0.061	0.36	8.07	0.14	14.2	10.9	1.57	0.19	0.059	0.078	1330	1439	90.9	0.26
26 TVG-1	7.4	0.3	-84.98	48.6	1.35	13.18	0.028	0.67	8.36	0.15	14.3	10.9	1.97	0.13	0.066	0.172	1332	1442	90.9	0.18
SE Cocos Ridge																			0.0	
25/96 Co	13	8.2	-83.49	47.3	0.91	13.90	0.034	0.45	9.04	0.17	15.6	10.5	1.83	0.11	0.124	0.087	1359	1474	91.0	0.15
22/96 Co	13	8.35	-83.72	48.1	0.91	12.77		0.45	9.02	0.16	16.4	10.2	1.74	0.12		0.137	1377	1494	91.4	0.26
22/96 Co	13	8.35	-83.72	48.3	0.87	12.91		0.43	8.86	0.21	16.0	10.3	1.79	0.12		0.123	1369	1485	91.3	0.26
22/96 Co	13	8.35	-83.72	48.2	0.92	12.87		0.46	8.90	0.16	16.1	10.3	1.75	0.14		0.122	1371	1487	91.3	0.26
Galapagos Islands																			0.0	
G86-3	1	-1.37	-89.76	46.8	1.18	14.14	0.047	0.59	8.56	0.18	13.6	10.5	2.54	1.09	0.029	0.792	1316	1422	90.7	0.03
FL-3	1	-1.24	-90.4	46.6	1.18	14.09	0.000	0.59	8.54	0.18	13.6	10.4	2.53	1.07	0.057	1.088	1316	1422	90.7	0.03
JH-86	1	-0.76	-90.57	46.0	1.10	13.91	0.000	0.55	9.65	0.18	16.1	10.4	1.98	0.05	0.000	0.087	1370	1486	90.9	0.06
SC-75	1	-0.75	-89.4	47.0	1.03	16.08	0.074	0.52	8.19	0.17	13.3	11.3	1.97	0.17	0.043	0.096	1308	1413	90.7	0.07
SC-23	1	-0.75	-89.4	46.8	1.38	14.77	0.061	0.69	8.60	0.19	14.1	10.2	2.48	0.50	0.051	0.216	1326	1435	90.8	0.07
JH-86	1	-0.25	-91.7	46.0	1.10	13.91	0.000	0.55	9.65	0.18	16.1	10.4	1.98	0.05	0.000	0.087	1370	1486	90.9	0.06
FL-3	1	-1.24	-90.4	47.0	1.18	14.20	0.039	0.60	8.62	0.18	13.8	10.5	2.56	1.08	0.057	0.209	1319	1426	90.7	0.03
FL-25	1	-1.24	-90.4	45.9	1.31	13.34	0.049	0.65	9.64	0.19	15.8	10.6	2.11	0.22	0.084	0.128	1363	1479	90.8	0.03
FL-26	1	-1.24	-90.4	45.9	1.25	13.41	0.000	0.62	9.73	0.18	16.1	10.5	1.96	0.15	0.075	0.111	1371	1488	90.9	0.05
FL-78	1	-1.24	-90.4	46.4	1.50	13.99	0.000	0.75	8.96	0.19	14.7	10.5	2.22	0.52	0.062	0.177	1340	1451	90.8	0.06
SG93-19	1	-0.23	-90.42	46.5	1.72	13.92	0.120	0.86	8.69	0.17	14.1	11.1	2.13	0.47	0.047	0.186	1327	1436	90.8	0.05
SG93-23	1	-0.28	-90.49	47.0	1.27	14.00	0.150	0.64	8.55	0.16	13.5	10.8	2.78	0.89	0.044	0.222	1313	1419	90.6	0.02
PL 13-12	1	0.1	-89.05	47.5	0.76	15.77	0.000	0.38	8.22	0.11	13.3	11.9	2.00	0.00	0.000	0.037	1309	1413	90.6	0.07
PL 13-21	1	0.1	-89.05	47.5	0.75	15.98	0.000	0.38	8.14	0.12	13.2	11.9	1.94	0.01	0.000	0.055	1306	1410	90.6	0.07
14	1	-0.85	-91	46.9	1.64	13.55	0.086	0.82	8.71	0.16	14.3	11.1	2.04	0.39	0.074	0.186	1332	1442	90.8	0.07
50	1	-0.85	-91	47.0	1.53	14.12	0.110	0.76	8.47	0.15	13.8	11.6	1.89	0.35	0.061	0.168	1320	1428	90.7	0.07
16	1	-0.85	-91	46.8	1.51	13.97	0.109	0.76	8.64	0.15	14.1	11.4	1.91	0.34	0.062	0.168	1327	1436	90.7	0.07
42	1	-0.85	-91	47.3	1.58	14.32	0.130	0.79	8.12	0.15	13.1	11.9	2.09	0.36	0.052	0.169	1303	1405	90.6	0.06
46	1	-0.85	-91	47.1	1.52	13.92	0.115	0.76	8.51	0.15	13.9	11.5	1.91	0.35	0.059	0.162	1323	1431	90.7	0.08
47	1	-0.85	-91	47.2	1.54	14.08	0.114	0.77	8.38	0.16	13.7	11.5	1.93	0.35	0.058	0.163	1318	1425	90.7	0.08
53	1	-0.85	-91	47.2	1.57	14.22	0.124	0.79	8.29	0.15	13.5	11.8	1.86	0.34	0.055	0.165	1313	1419	90.7	0.08
54	1	-0.85	-91	47.0	1.54	13.72	0.130	0.77	8.65	0.16	14.3	11.4	1.85	0.34	0.060	0.163	1330	1440	90.8	0.08
45A	1	-0.85	-91	47.1	1.56	14.33	0.115	0.78	8.30	0.15	13.4	11.8	1.90	0.34	0.056	0.173	1311	1416	90.6	0.06
racaldera sco	1	-0.85	-91	47.0	1.60	13.88	0.151	0.80	8.48	0.16	13.8	11.6	2.02	0.35	0.048	0.168	1320	1427	90.7	0.06

[a] Lava sample in original source reference for which PRIMELT2.XLS has been applied
[b] Olivine liquidus temperature at 1 atmosphere (^oC)
[c] Mantle potential temperature (^oC)
[d] Mg number of olivine to crytallize from primary magma at 1 atmosphere
[e] Melt fraction for peridotite KR-4003 for the case of accumulated fractional melting. This cannot be resolved for F in the 0 to 0.02 range, and is indicated as ~ 0

Table 2

Sample ID[a]	Lat.	Lon.	SiO_2	TiO_2	Al_2O_3	Cr_2O_3	Fe_2O_3	FeO	MnO	MgO	CaO	Na_2O	K_2O	NiO	P_2O_5	T_{Ol}[b]	T_P[c]	Ol Mg[d]	Melt Fraction[e]
East Greenland																			
2242	66	-30	48.5	0.88	8.27	0.00	0.44	10.13	0.17	20.2	9.5	1.11	0.66	0.098	0.083	1450	1575	92.0	0.35
75-755	66	-24	46.1	2.06	5.86	0.00	1.02	11.35	0.18	24.0	8.0	0.92	0.26	0.000	0.229	1514	1647	92.7	0.38
75-301	66	-24	45.7	2.14	6.97	0.00	1.06	11.36	0.18	23.5	7.7	0.82	0.35	0.000	0.229	1506	1638	92.6	0.35
228139	73.5	-21.66	46.6	1.47	13.35	0.16	0.74	9.08	0.17	15.4	9.9	1.76	1.06	0.066	0.198	1356	1470	91.1	0.12
227982	73	-26	48.2	1.54	8.66	0.26	0.77	9.97	0.18	19.3	10.0	0.71	0.23	0.064	0.167	1434	1557	91.7	0.32
227984	73	-26	47.4	1.40	10.12	0.10	0.70	9.64	0.17	18.2	10.0	1.14	0.90	0.078	0.157	1413	1534	91.7	0.29
227958	73	-26	48.4	1.32	11.71	0.07	0.66	8.83	0.15	16.0	10.7	1.51	0.46	0.052	0.144	1368	1484	91.3	0.26
227993	73	-26	47.9	1.35	12.74	0.07	0.67	8.92	0.16	16.2	9.8	1.41	0.50	0.068	0.157	1373	1490	91.4	0.26
228050	73	-26	47.1	1.60	8.81	0.17	0.80	10.08	0.17	19.4	9.6	1.12	0.89	0.067	0.179	1437	1560	91.9	0.31
917A-57R-2/56-59/3B	65.7043	-34.871	45.9	1.41	13.82	0.17	0.71	9.50	0.19	15.7	9.9	2.27	0.27	0.082	0.146	1361	1476	90.9	0.05
917A-72R-6/31-34/2	65.7043	-34.871	47.6	1.24	12.90	0.09	0.62	8.93	0.18	15.4	10.9	1.75	0.30	0.105	0.097	1354	1468	91.0	0.15
83820	68.5	-27.83	46.5	0.76	11.81	0.10	0.38	10.16	0.17	19.4	9.4	1.11	0.02	0.103	0.058	1437	1560	91.9	0.29
404232	68.5	-27.83	46.2	0.76	11.63	0.13	0.38	10.29	0.17	19.8	9.4	1.15	0.03	0.122	0.059	1442	1567	92.0	0.29
404263	68.5	-27.83	46.9	0.74	11.81	0.13	0.37	9.82	0.18	18.5	10.1	1.22	0.04	0.111	0.062	1419	1541	91.7	0.28
GGU 416401	66.6	-35	45.7	2.45	5.75	0.24	1.22	11.35	0.18	23.6	8.6	0.38	0.13	0.163	0.206	1508	1640	92.7	0.36
GGU 426547	66.6	-35	45.9	1.68	6.55	0.38	0.84	11.37	0.17	23.9	7.7	1.00	0.25	0.145	0.184	1513	1646	92.7	0.37
GGU 426553	66.6	-35	47.4	1.24	10.48	0.12	0.62	9.72	0.17	18.3	9.6	1.81	0.34	0.126	0.139	1415	1536	91.7	0.28
83820	68.5	-27.83	46.6	0.77	11.92	0.09	0.38	10.05	0.17	19.1	9.6	1.12	0.01	0.105	0.059	1431	1554	91.8	0.29
83839	68.5	-27.83	46.8	0.72	11.36	0.06	0.36	10.03	0.18	19.1	9.9	1.22	0.03	0.127	0.069	1430	1553	91.8	0.29
West Greenland																			
136943	70.1911	-53.405	45.8	1.18	11.34	0.00	0.59	10.53	0.17	19.1	9.7	1.31	0.18	0.000	0.091	1430	1553	91.6	0.18
138228	70.2331	-53.6858	45.4	1.19	10.36	0.00	0.59	11.14	0.19	19.5	10.1	1.38	0.08	0.000	0.107	1437	1561	91.4	0.09
113236	70.2114	-53.5558	46.1	1.23	11.24	0.08	0.61	10.32	0.17	19.0	9.5	1.40	0.07	0.131	0.126	1427	1550	91.6	0.21
7757	69	-52	45.8	0.92	11.37	0.20	0.46	10.62	0.20	19.1	9.6	1.44	0.07	0.099	0.082	1430	1553	91.5	0.16
264217	70.3833	-53.6889	45.7	0.98	11.21	0.25	0.49	10.69	0.18	19.4	9.6	1.34	0.01	0.101	0.076	1436	1560	91.6	0.17
138228	70.2331	-53.6858	45.3	1.19	10.35	0.19	0.60	11.10	0.19	19.3	10.1	1.38	0.08	0.139	0.107	1434	1558	91.3	0.09
136943	70.1911	-53.405	45.7	1.19	11.34	0.21	0.59	10.50	0.17	18.9	9.7	1.32	0.18	0.104	0.091	1427	1549	91.5	0.16
137000	70.0908	-53.6119	45.9	1.24	10.97	0.19	0.62	10.48	0.18	18.7	10.0	1.45	0.07	0.110	0.137	1423	1545	91.5	0.15
156741	70.0908	-53.6119	46.0	1.17	10.61	0.11	0.58	10.55	0.19	19.7	9.7	1.21	0.03	0.123	0.092	1440	1565	91.8	0.22
400450	70.5194	-54.1742	45.9	1.05	11.00	0.00	0.52	10.64	0.19	19.8	9.7	1.17	0.02	0.000	0.062	1443	1567	91.8	0.22
264217	70.3833	-53.6889	45.8	0.98	11.19	0.00	0.49	10.72	0.18	19.6	9.5	1.34	0.01	0.000	0.077	1440	1564	91.7	0.19
362148	70.3694	-53.3008	46.6	1.02	10.69	0.00	0.51	10.19	0.16	19.5	10.0	1.15	0.11	0.000	0.083	1438	1562	91.9	0.29
136943	70.1911	-53.405	45.8	1.18	11.34	0.00	0.59	10.53	0.17	19.1	9.7	1.31	0.18	0.000	0.091	1430	1553	91.6	0.18
156737	70.0931	-53.6119	45.6	1.34	10.73	0.00	0.67	10.78	0.22	18.8	10.2	1.50	0.07	0.000	0.114	1424	1546	91.3	0.10
264099	70.0744	-53.5344	45.6	1.19	10.29	0.00	0.59	10.93	0.18	20.5	9.4	1.12	0.06	0.000	0.140	1456	1581	91.9	0.22
264113	70	-53	45.5	1.81	10.58	0.18	0.90	10.44	0.18	18.0	10.1	1.31	0.74	0.063	0.269	1408	1529	91.2	0.09
136915	70	-53	45.1	1.91	10.80	0.09	0.95	10.59	0.18	18.5	9.6	1.00	0.96	0.076	0.276	1418	1540	91.4	0.11
264114	70	-53	45.5	1.92	10.32	0.10	0.95	10.40	0.17	18.3	10.1	1.05	0.75	0.071	0.264	1416	1537	91.4	0.13
113253	70	-53	45.4	1.98	10.63	0.09	0.99	10.38	0.17	18.6	9.6	1.02	0.79	0.087	0.320	1420	1543	91.5	0.16
136943	70	-53	45.7	1.19	11.35	0.20	0.59	10.50	0.17	18.9	9.7	1.32	0.18	0.105	0.091	1426	1549	91.5	0.16

Table 2 continued

Sample ID[a]	Latitude	Longitude	SiO_2	TiO_2	Al_2O_3	Cr_2O_3	Fe_2O_3	FeO	MnO	MgO	CaO	Na_2O	K_2O	NiO	P_2O_5	T_{OL}[b]	T_P[c]	Ol Mg[d]	Melt Fraction[e]
Deccan Traps																			
SA82-21B	23.41	80.19	46.8	1.08	7.32	0.00	0.53	11.14	0.00	23.2	8.1	1.41	0.07	0.194	0.125	1502	1633	92.5	0.37
D81	20	68	45.6	1.69	10.48	0.13	0.84	10.52	0.14	18.8	9.8	1.13	0.55	0.093	0.238	1425	1547	91.5	0.15
D44	21.5	70.5	45.5	1.93	11.25	0.07	0.96	10.18	0.16	17.3	10.1	1.61	0.55	0.057	0.384	1395	1515	91.1	0.08
331/A	21.92	74.08	47.2	0.74	10.47	0.00	0.37	10.08	0.20	18.6	10.0	1.44	0.76	0.096	0.157	1420	1542	91.6	0.23
IG-15	19.68	73.63	47.0	1.08	7.50	0.01	0.53	11.08	0.16	23.6	7.5	1.15	0.35	0.038	0.080	1507	1639	92.6	0.40
AB04-22	16	74.2	45.8	1.23	8.26	0.05	0.60	11.38	0.15	23.6	7.2	1.18	0.09	0.347	0.096	1508	1640	92.6	0.35
Siberian Traps																			
1F(25)	69.4	90	47.7	0.70	12.20	0.04	0.35	9.63	0.15	18.1	9.6	1.39	0.10	0.071	0.061	1411	1532	91.6	0.29
1F-25	69.4	90	47.4	0.71	11.94	0.04	0.35	9.73	0.16	18.4	9.7	1.36	0.08	0.107	0.076	1416	1537	91.7	0.29
MCH-3	69	90	47.9	0.67	11.73	0.00	0.33	9.62	0.19	18.1	9.9	1.31	0.17	0.000	0.072	1412	1533	91.6	0.29
MCH-6	70	88	48.6	0.66	11.45	0.00	0.33	9.41	0.21	17.7	10.2	1.28	0.14	0.000	0.064	1402	1522	91.5	0.29
MCH-9ZH-1	69	88	51.2	0.49	10.82	0.00	0.24	8.54	0.17	15.8	10.5	1.07	1.18	0.000	0.000	1364	1479	91.2	0.32
1FG-34	72	101	45.3	3.23	7.98	0.04	1.60	10.70	0.18	17.5	9.7	1.93	1.39	0.099	0.411	1400	1520	90.9	0.02
Ontong Java Plateau																			
1185-1	-0.3	-161.8	47.7	0.56	11.48	0.06	0.28	9.87	0.17	18.8	9.6	1.28	0.04	0.133	0.046	1425	1548	91.7	0.30
1185-2	-0.3	-161.8	47.5	0.57	11.64	0.06	0.28	9.85	0.17	18.7	9.7	1.25	0.12	0.122	0.046	1423	1546	91.7	0.30
1185-4	-0.3	-161.8	47.6	0.56	11.57	0.06	0.28	9.87	0.17	18.8	9.7	1.12	0.09	0.123	0.048	1425	1548	91.7	0.30
1185-5	-0.3	-161.8	47.9	0.57	11.55	0.06	0.28	9.79	0.17	18.6	9.6	1.25	0.06	0.145	0.047	1421	1544	91.7	0.30
1185-6	-0.3	-161.8	47.8	0.57	11.74	0.06	0.29	9.77	0.17	18.6	9.6	1.25	0.06	0.106	0.046	1420	1542	91.7	0.29
1185-10	-0.3	-161.8	47.7	0.57	11.71	0.06	0.28	9.76	0.17	18.5	9.8	1.25	0.02	0.122	0.046	1419	1541	91.7	0.29
1187-5	1	-161.5	47.6	0.57	11.62	0.06	0.28	9.82	0.16	18.7	9.7	1.30	0.04	0.126	0.048	1422	1544	91.7	0.29
1187-6	1	-161.5	47.6	0.57	11.63	0.06	0.28	9.78	0.20	18.6	9.7	1.30	0.04	0.190	0.049	1420	1542	91.7	0.29
1187-7	1	-161.5	47.6	0.58	11.81	0.06	0.29	9.72	0.17	18.4	9.9	1.29	0.04	0.107	0.049	1416	1538	91.7	0.29
1187-8	1	-161.5	47.7	0.59	11.73	0.07	0.29	9.73	0.17	18.4	9.8	1.29	0.07	0.112	0.048	1417	1539	91.7	0.29
1187-9	1	-161.5	47.6	0.58	11.62	0.06	0.29	9.79	0.17	18.6	9.9	1.30	0.05	0.123	0.048	1420	1542	91.7	0.29
1187-11	1	-161.5	47.6	0.58	11.84	0.06	0.29	9.71	0.17	18.4	9.9	1.31	0.04	0.102	0.048	1416	1538	91.7	0.29
1187-14	1	-161.5	47.6	0.58	11.90	0.06	0.29	9.70	0.17	18.3	9.9	1.30	0.04	0.109	0.050	1415	1537	91.7	0.29
Central Atlantic Magmatic Province																			
W-241422	38.6625	-77.6958	48.1	0.25	15.55	0.08	0.12	8.28	0.14	14.0	11.3	1.49	0.53	0.091	0.042	1325	1433	90.8	0.15
W-241803	36.1156	-78.7722	48.9	0.30	17.71	0.12	0.15	6.91	0.13	10.9	12.8	1.79	0.20	0.035	0.049	1249	1332	90.2	0.08
W-241805	36.1156	-78.7722	48.4	0.31	16.40	0.11	0.16	7.76	0.14	12.7	11.9	1.70	0.19	0.045	0.058	1295	1396	90.6	0.12
W-241807	36.1156	-78.7722	48.7	0.36	14.61	0.12	0.18	8.30	0.15	14.3	11.4	1.62	0.22	0.057	0.055	1330	1439	90.9	0.18
W-241808	36.1156	-78.7722	48.5	0.39	15.61	0.07	0.20	8.20	0.15	14.0	10.7	1.75	0.27	0.064	0.063	1324	1432	90.8	0.18
W-241809	36.1156	-78.7722	48.2	0.39	14.71	0.09	0.19	8.62	0.15	15.0	10.5	1.73	0.25	0.079	0.070	1346	1459	91.0	0.19
W-241810	36.1156	-78.7722	48.2	0.41	13.71	0.10	0.20	8.79	0.16	15.9	10.5	1.61	0.24	0.076	0.069	1366	1481	91.3	0.26
W-243838	39.0667	-77.4597	48.4	0.38	14.86	0.09	0.19	8.45	0.15	14.5	10.9	1.70	0.23	0.050	0.071	1336	1447	90.9	0.18
W-243888	36.1125	-78.6903	48.4	0.37	15.34	0.08	0.19	8.29	0.15	14.1	10.9	1.74	0.24	0.047	0.081	1327	1436	90.8	0.17

[a] Lava sample in original source reference for which PRIMELT2.XLS has been applied
[b] Olivine liquidus temperature at 1 atmosphere (^oC)
[c] Mantle potential temperature (^oC)
[d] Mg number of olivine to crytallize from primary magma at 1 atmosphere
[e] Melt fraction for peridotite KR-4003 for the case of accumulated fractional melting.

Table 3

Sample ID[a]	Lat.	Long.	SiO_2	TiO_2	Al_2O_3	Cr_2O_3	Fe_2O_3	FeO	MnO	MgO	CaO	Na_2O	K_2O	NiO	P_2O_5	T_{Ol}[b]	T_P[c]	Ol Mg[d]	Melt Fraction[e]
Azores																			
ASM36	37.8	-25.5	47.7	2.45	12.6	0.107	2.45	7.32	0.17	11.4	11.8	2.40	1.13	0.031	0.384	1264	1353	90.5	0.04
SMB-6	37.8	-25.5	46.8	3.20	12.6	0.113	3.20	7.22	0.17	11.1	11.6	2.23	1.23	0.028	0.501	1256	1342	90.4	0.03
SMB-7	37.8	-25.5	45.6	3.52	12.0	0.005	3.52	7.73	0.18	11.9	11.6	2.18	1.33	0.041	0.427	1275	1368	90.6	~0
P26	38.47	-28.3	46.5	2.53	13.0	0.087	2.53	7.95	0.16	12.5	10.5	2.88	0.97	0.036	0.392	1289	1388	90.7	0.03
G-4	39.05	-28.05	45.8	2.45	14.2	0.068	2.45	8.04	0.17	12.7	10.5	2.38	0.82	0.043	0.45	1294	1394	90.7	0.03
F-2	38.58	-28.7	46.9	1.97	12.0	0.127	1.98	8.58	0.17	14.1	10.6	2.45	0.84	0.042	0.301	1326	1435	90.9	0.07
2	38.58	-28.7	46.1	2.24	13.0		2.24	8.16	0.14	12.6	11.7	2.68	0.84		0.305	1293	1392	90.6	~0
1	27.22	-38.72	46.1	2.31	11.5		2.31	9.21	0.20	15.1	10.0	2.48	0.79			1348	1461	90.9	0.05
10	27.22	-38.72	46.4	2.06	13.2		2.06	8.59	0.20	14.2	10.7	1.87	0.84			1328	1437	90.9	0.08
SC4	37.83	-25.78	45.5	3.08	11.6		3.08	8.75	0.19	14.4	10.1	1.99	0.97		0.29	1333	1443	90.9	0.07
Canaries																			
A6_LEACHED	28	-15.6	46.0	3.32	9.9		3.32	8.73	0.18	14.3	10.7	2.22	0.86	0.058	0.385	1331	1441	90.9	0.06
T1	28	-15.6	46.7	2.68	9.9		2.68	9.06	0.18	15.6	10.1	1.94	0.68	0.089	0.31	1361	1476	91.2	0.15
T4	28	-15.6	46.2	3.14	9.6		3.14	9.00	0.19	15.3	10.0	2.05	0.84	0.093	0.379	1352	1466	91.1	0.12
G1379	28	-15.6	45.7	3.36	9.8		3.36	9.10	0.18	15.5	10.0	1.68	0.89	0.074	0.393	1358	1472	91.2	0.12
G1378	28	-15.6	45.8	3.32	9.6		3.31	9.04	0.19	15.2	10.7	1.64	0.86	0.074	0.378	1351	1464	91.0	0.10
LP 134	28.75	-19	44.9	3.19	11.3		3.19	8.77	0.18	13.7	10.4	2.53	1.22	0.059	0.494	1318	1425	90.7	~0
13.632 ILM	29.1	-13.42	46.4	2.09	12.4		2.09	8.46	0.16	13.6	10.5	2.54	1.01	0.000	0.773	1315	1421	90.8	0.04
12.861 ILM	29.12	-13.53	45.5	2.15	12.0		2.15	9.34	0.19	15.0	10.0	2.37	0.89	0.000	0.397	1347	1460	90.8	0.02
16	28.4	-14	44.8	2.25	12.1		2.25	9.18	0.15	14.7	10.1	2.83	1.12	0.000	0.554	1341	1453	91.0	0.02
21	28.4	-14	45.8	2.15	12.3		2.15	8.96	0.14	14.2	10.1	2.67	1.01	0.000	0.486	1328	1438	90.7	~0
LPF96-46	28.6	-17.9	44.7	2.76	10.7		2.76	9.79	0.18	15.7	9.9	2.33	0.76	0.000	0.461	1361	1476	90.8	~0
LPF96-63	28.6	-17.9	45.1	3.43	11.0		3.44	8.66	0.17	13.5	10.3	2.58	1.36	0.000	0.43	1314	1419	90.7	~0
Cook-Austral Islands																			
68D-2	-29	-140.25	45.2	2.62	11.6	0.072	2.61	9.24	0.18	14.9	10.3	2.20	0.70	0.060	0.305	1344	1456	90.8	0.02
68DS-2	-29	-140.25	45.4	2.61	12.0	0.068	2.62	8.94	0.18	14.3	10.3	2.38	0.75	0.063	0.317	1332	1441	90.8	0.02
RPA-031 7263	-27.58	-144.33	45.0	2.96	11.3	0.086	2.96	9.05	0.15	14.7	10.5	1.90	0.90	0.035	0.493	1339	1450	90.9	0.03
64-2	-29	-140.25	45.2	2.62	11.6	0.079	2.63	9.23	0.18	14.9	10.3	2.20	0.70	0.040	0.305	1344	1456	90.8	0.02
68-2	-29	-140.25	45.2	2.62	11.6	0.079	2.63	9.23	0.18	14.9	10.3	2.20	0.70	0.040	0.305	1344	1456	90.8	0.02
ATU114	-19.98	-158.1	45.2	2.35	9.3		2.35	10.28	0.20	16.9	10.1	2.03	0.81	0.000	0.435	1387	1506	91.0	0.03
ATU123	-19.98	-158.1	46.0	2.17	9.9		2.17	9.71	0.18	16.4	10.2	1.96	0.84	0.000	0.356	1377	1495	91.1	0.08
RVV-139	-23.869	-147.702	45.2	2.10	10.1	0.110	2.10	10.26	0.16	16.9	9.8	2.16	0.64	0.066	0.363	1388	1506	91.0	0.03
RRT-B-21	-22.42	-151.33	44.7	1.96	9.5	0.072	1.96	10.89	0.18	18.8	9.9	1.37	0.25	0.087	0.24	1425	1548	91.4	0.08
TBA-B-15	-23.38	-149.45	44.9	2.17	10.5	0.077	2.17	10.15	0.21	16.4	10.4	2.05	0.63	0.067	0.324	1376	1493	90.8	~0
2	-19.98	-158.1	46.0	2.20	11.7	0.060	2.20	9.15	0.20	15.0	10.1	2.40	0.88	0.067	0.166	1346	1458	90.9	0.05
RPA-488	-27.3806	-144.2053	45.1	2.91	11.4	0.082	2.90	9.06	0.16	15.1	10.2	1.66	0.91	0.056	0.416	1349	1462	91.0	0.08

Table 3 continued

Sample ID[a]	Latitude	Longitude	SiO_2	TiO_2	Al_2O_3	Cr_2O_3	Fe_2O_3	FeO	MnO	MgO	CaO	Na_2O	K_2O	NiO	P_2O_5	T_{Ol}[b]	T_P[c]	Ol Mg[d]	Melt Fraction[e]
Iceland																			
408706	64.7958	-17.1811	48.0	0.85	15.5		0.43	8.54	0.15	14.8	9.9	1.66	0.08		0.066	1343	1455	91.0	0.19
408707	64.7958	-17.1811	48.0	0.87	15.5		0.43	8.50	0.16	14.7	10.0	1.66	0.07		0.067	1340	1452	91.0	0.19
408709	64.7939	-17.1819	47.9	0.84	15.3		0.42	8.63	0.16	15.4	9.6	1.63	0.07		0.075	1355	1469	91.2	0.24
408710	64.7939	-17.1819	47.7	0.83	15.1		0.42	8.61	0.16	15.3	9.8	1.61	0.07	0.110	0.26	1354	1468	91.2	0.24
408712	64.8033	-17.2153	47.7	0.96	14.9		0.48	8.78	0.16	15.3	9.8	1.67	0.07		0.066	1354	1468	91.1	0.19
Marquesas																			
6465	-7.93	-140.55	47.2	2.55	9.6	0.187	2.56	8.83	0.18	15.3	10.4	1.90	0.90	0.058	0.361	1353	1466	91.1	0.17
6457	-7.93	-140.55	46.4	2.86	11.3	0.081	2.87	8.46	0.17	13.8	10.2	2.32	0.98	0.067	0.396	1321	1428	90.9	0.07
HTT-12	-7.93	-140.55	47.4	2.63	10.0	0.191	2.64	8.51	0.17	14.6	10.8	1.71	0.91	0.051	0.386	1337	1448	91.0	0.16
HTT-19	-7.93	-140.55	47.2	2.55	9.6	0.187	2.56	8.83	0.18	15.3	10.4	1.90	0.90	0.058	0.361	1353	1466	91.1	0.17
HTT-04	-7.93	-140.55	46.4	2.86	11.3	0.081	2.87	8.46	0.17	13.8	10.2	2.32	0.98	0.067	0.396	1321	1428	90.9	0.07
70C	-10.5	-138.8	45.7	2.53	10.6		2.53	9.58	0.19	16.5	10.3	1.59	0.41			1379	1497	91.2	0.12
Mauna Kea																			
115-12	19.6	-155.7	46.7	1.78	9.9	0.164	0.89	9.97	0.16	17.9	10.2	1.65	0.43	0.089	0.205	1408	1528	91.4	0.18
H-1	19.5	-155.7	44.3	2.35	9.3	0.165	1.18	11.36	0.19	19.5	9.7	1.17	0.46	0.099	0.292	1437	1561	91.3	0.06
MU-9	20	-155.25	45.6	1.77	8.3	0.186	0.89	11.03	0.18	21.1	9.3	1.09	0.19	0.097	0.19	1466	1593	92.0	0.25
KI-8	19.83	-155.42	46.4	1.75	8.5	0.257	0.88	10.61	0.16	19.5	9.9	1.70	0.12	0.083	0.183	1437	1561	91.6	0.20
C-209	20	-155.25	45.8	1.81	9.8		0.90	10.60	0.19	18.6	10.0	1.51	0.42	0.087	0.281	1421	1543	91.4	0.12
C-71	20	-155.25	45.5	1.91	11.7		0.96	10.17	0.17	17.8	9.9	1.40	0.41	0.000	0.207	1404	1525	91.3	0.12
90/66110	19.6	-155.7	45.7	2.07	9.4	0.168	1.04	10.68	0.17	19.2	9.6	1.43	0.41	0.000	0.22	1431	1555	91.5	0.15
HQ-3	19.63	-155.62	44.4	2.34	9.3		1.16	11.40	0.19	19.6	9.6	1.16	0.46	0.000	0.291	1440	1564	91.4	0.07
HU-7	19.63	-155.13	46.1	1.98	9.6		0.99	10.40	0.17	18.3	10.3	1.58	0.44	0.000	0.246	1415	1536	91.3	0.13
IQ-15	19.75	-155.62	45.7	2.07	10.6		1.03	10.29	0.17	17.8	10.3	1.58	0.25	0.000	0.209	1405	1526	91.3	0.10
JQ-13	19.88	-155.62	46.1	1.91	9.9		0.95	10.40	0.17	18.5	9.8	1.61	0.48	0.000	0.231	1419	1541	91.4	0.15
JQ-17	19.88	-155.62	45.3	2.22	9.9		1.11	10.72	0.17	18.8	9.6	1.55	0.39	0.000	0.261	1424	1546	91.4	0.11
JQ-25	19.88	-155.62	46.0	1.99	10.3		0.99	10.31	0.17	18.2	9.7	1.69	0.45	0.000	0.227	1412	1534	91.4	0.13
JS-9	19.88	-155.37	46.5	1.94	9.2		0.97	10.27	0.17	18.8	10.0	1.52	0.38	0.000	0.227	1425	1548	91.6	0.21
KI-8	19.83	-155.42	46.5	1.74	8.4		0.87	10.64	0.16	19.7	9.9	1.69	0.11	0.000	0.182	1442	1566	91.7	0.21
MU-9	20	-155.25	45.8	1.77	8.3		0.89	11.06	0.18	21.3	9.3	1.09	0.19	0.000	0.189	1469	1596	92.1	0.26
SR0684-8.95	19.74	-155.05	46.3	1.98	9.8		1.00	10.25	0.18	18.2	9.9	1.70	0.55	0.001	0.231	1413	1534	91.4	0.15
SR0684-9.00	19.74	-155.05	46.5	2.14	10.1		1.08	9.97	0.00	17.6	10.2	1.72	0.53	0.001	0.206	1401	1521	91.3	0.15
Pitcairn																			
80DS-2	-25.28	-129.54	49.0	0.96	12.1	0.033	0.96	8.76	0.18	16.0	10.0	1.82	0.13	0.054	0.071	1367	1483	91.3	0.28
FA682.7	-22.29	-138.54	47.8	1.96	11.4		1.96	8.70	0.14	15.5	10.2	1.80	0.27	0.000	0.258	1358	1473	91.3	0.24
MG5H	-23.17	-135	47.3	2.20	12.2		2.19	8.52	0.14	14.6	10.3	1.84	0.34	0.001	0.353	1337	1448	91.0	0.16
709.1	-22.29	-138.54	47.1	2.06	11.7	0.066	2.06	8.92	0.15	15.5	10.2	1.85	0.25	0.082		1356	1471	91.1	0.16
G-AK-39	-23.14	-135	47.5	1.74	12.5	0.041	1.73	8.66	0.15	15.0	10.1	1.81	0.45	0.110	0.25	1347	1459	91.1	0.18
Samoa																			
131	-14.22	-169.44	45.5	2.52	9.4		2.53	9.98	0.18	17.7	9.9	1.50	0.45	0.000	0.292	1403.3	1523.6	91.5	0.16
63-3	-14.218	-169.059	47.7	2.40	11.3	0.126	2.39	7.82	0.17	12.6	12.2	2.02	0.92	0.053	0.275	1292.7	1392.5	90.6	0.08
68-3	-14.217	-169.064	47.1	2.35	10.9	0.115	2.36	8.30	0.17	13.5	11.8	2.17	0.92	0.066	0.267	1312.5	1417.9	90.8	0.07
T16	-14.337	-169.98	46.2	3.21	10.7	0.104	3.20	8.59	0.18	14.2	10.3	2.11	0.82	0.065	0.369	1327.9	1436.8	90.9	0.08
T33	-14.2163	-169.4421	46.6	2.87	9.8	0.137	2.87	8.83	0.17	14.8	10.7	2.03	0.70	0.058	0.306	1342.8	1454.7	91.0	0.11
76-9	-14.569	-169.718	45.6	2.67	9.5	0.127	2.67	9.67	0.17	16.5	9.9	1.83	0.98	0.064	0.312	1378.2	1495.5	91.2	0.10

Table 3 continued

Sample ID[a]	Latitude	Longitude	SiO_2	TiO_2	Al_2O_3	Cr_2O_3	Fe_2O_3	FeO	MnO	MgO	CaO	Na_2O	K_2O	NiO	P_2O_5	T_{Ol}[b]	T_P[c]	Ol Mg[d]	Melt Fraction[e]
Society																			
TH-6	-17.7	-149.45	46.3	2.41	10.4		2.41	9.27	0.00	15.9	10.5	1.70	0.80	0.000	0.364	1366	1481.7	91.1	0.13
TH-8	-17.7	-149.45	45.1	2.73	11.1		2.73	9.40	0.00	15.3	10.3	1.96	0.95	0.000	0.383	1352.8	1466.4	90.9	0.03
TC-77	-17.7	-149.45	45.1	2.64	11.2		2.64	9.38	0.18	14.9	10.3	2.21	0.99	0.000	0.42	1344.8	1457	90.8	~0
7-Feb	-17.33	-148.5	47.2	0.70	17.5		0.71	7.86	0.04	12.5	11.2	2.39	0.01	0.000		1289.1	1387.7	90.5	0.05
8B	-16.5	-151.5	45.6	2.98	10.8	0.122	2.98	8.67	0.15	13.8	11.1	1.95	1.42	0.054	0.394	1319.2	1426.3	90.7	0.02
81W1	-17.7	-149.45	46.3	2.60	11.2		2.60	8.80	0.17	14.7	10.2	2.04	1.11	0.000	0.353	1339.1	1450.3	91.0	0.09
56Q	-17.7	-149.45	45.5	3.08	10.5		3.09	9.05	0.19	15.1	10.2	1.73	1.12	0.000	0.439	1349.3	1462.3	91.1	0.09
81W	-17.7	-149.45	45.4	2.39	10.8		2.39	9.71	0.17	16.2	9.9	1.96	0.86	0.000	0.306	1372.5	1489.1	91.0	0.06
56C	-17.7	-149.45	45.4	2.74	9.8		2.75	9.53	0.18	15.6	10.4	2.03	1.04	0.000	0.458	1360.2	1475	90.9	0.04
St. Helena																			
SH-7	-15.95	-5.7	45.9	1.92	10.3		1.92	9.95	0.18	17.7	10.0	1.54	0.58	0.000		1402	1522	91.4	0.16
Tristan																			
64768	-37.05	-12.3	46.0	2.36	12.7	0.051	2.36	8.59	0.18	14.2	10.1	1.97	0.95	0.058	0.518	1328	1437	90.9	0.08

[a] Lava sample in original source reference for which PRIMELT2.XLS has been applied
[b] Olivine liquidus temperature at 1 atmosphere (^oC)
[c] Mantle potential temperature (^oC)
[d] Mg number of olivine to crytallize from primary magma at 1 atmosphere
[e] Melt fraction for peridotite KR-4003 for the case of accumulated fractional melting. This cannot be resolved for F in the 0 to 0.02 range, and is indicated as ~ 0

Chapter 3

The Galapagos-OIB Signature in Southern Central America:

Mantle Re-Fertilization by Arc-Hotspot Interaction

This chapter resulted in one published paper:

Gazel, E., Carr, M.J., Hoernle, K., Feigenson, M.D., Hauff, F., Szymanski, D., and van den Bogaard, P, 2009. The Galapagos-OIB signature in southern Central America: Mantle re-fertilization by arc-hotspot interaction. ***Geochemistry, Geophysics, Geosystems (G^3^)***, Q02S11, doi:10.1029/2008GC002246

Abstract

Although most Central American magmas have a typical arc geochemical signature, magmas in southern Central America (central Costa Rica and Panama) have isotopic and trace element compositions with an OIB affinity, similar to the Galapagos-OIB lavas (e.g., Ba/La<40, La/Yb>10, $^{206}Pb/^{204}Pb>18.8$). Our new data for Costa Rica suggest that this signature, unusual for a convergent margin, has a relatively recent origin (Late Miocene ~6 Ma). We also show that there was a transition from typical arc magmas (analogous to the modern Nicaraguan volcanic front) to OIB-like magmas similar to the Galapagos Hotspot. The geographic distribution of the Galapagos signature in recent lavas from southern Central America is present landward from the subduction of the

Galapagos Hotspot tracks (the Seamount Province and the Cocos/Coiba Ridge) at the Middle American Trench. The higher Pb isotopic ratios, relatively lower Sr and Nd isotopic ratios and enriched incompatible-element signature of central Costa Rican magmas can be explained by arc-hotspot interaction. The isotopic ratios of central Costa Rican lavas require the subducting Seamount Province (Northern Galapagos Domain) component, whereas the isotopic ratios of the adakites and alkaline basalts from southern Costa Rica and Panama are in the geochemical range of the subducting Cocos/Coiba Ridge (Central Galapagos Domain). Geological and geochemical evidence collectively indicate that the relatively recent Galapagos-OIB signature in southern Central America represents a geochemical signal from subducting Galapagos Hotspot tracks, which started to collide with the margin ~8 Ma ago. The Galapagos Hotspot contribution decreases systematically along the volcanic front from central Costa Rica to NW Nicaragua.

1. Introduction

1.1 Geotectonic setting

The Central American Volcanic Front extends parallel to the Middle American Trench from the Mexico-Guatemala border to central Costa Rica (Fig. 1). The convergence rate between the Cocos and Caribbean plates increases to the southeast from ~60 mm/year off southern Guatemala to ~90 mm/year off southern Costa Rica (DeMets, 2001). Smooth crust, produced at the East Pacific Rise spreading center, characterized by extensive trench-parallel structures (Ranero et al., 2003) subducts to the north of the Nicoya Peninsula (Fig. 1). The crust subducting to the south of the Nicoya Peninsula was produced at the relatively slow spreading Cocos-Nazca ridge (Fig. 1). Much of this segment of subducting crust has been overprinted by Galapagos Hotspot tracks. The Galapagos Hotspot tracks in front of Costa Rica (Fig. 1) range in age between 13.0-14.5 Ma (Werner et al., 1999). Active tectonic erosion has been reported in the Middle American Trench off Costa Rica (Ranero and von Huene, 2000; Ranero et al., 2003). The presence of a large province of accreted oceanic complexes along the Pacific coast of southern Central America suggest, however, that accretionary processes have also been important in the earlier evolution of this margin (Denyer et al., 2006).

The sediment cover of the Cocos Plate appears to be entirely subducted along most of the margin. The geochemical signature of the subducted sediment can be traced into the Central American volcanoes by Ba/La (Fig. 2a). This ratio is particularly useful for Central America because it does not change significantly within the Cocos Plate sediment stratigraphy (Patino et al., 2000). Furthermore, since Ba/La correlates with $^{10}Be/^{9}Be$, the most definitive tracer of subducted sediment (Leeman et al., 1994), it is a robust proxy to evaluate the sediment component. Along the volcanic front, the geochemical indicators of subducting sediments (e.g. Ba/La, U/Th and $^{10}Be/^{9}Be$), define a slightly asymmetrical chevron pattern with a maximum in northwest Nicaragua (Carr et al., 2003). Higher La/Yb (steeper REE patterns) implies a lower degree of partial melting or derivation from a more enriched source. The overall correlation between La/Yb and Pb isotope ratios (Fig. 2b and 2c) indicates that more enriched sources are present where

La/Yb is higher (e.g. beneath Costa Rica and Guatemala). The mirror image in the along strike variations of La/Yb, Ba/La and $^{206}Pb/^{204}Pb$ (Figs. 2a-c) suggests that the subducted sediment component, characterized by high Ba/La but low La/Yb and $^{206}Pb/^{204}Pb$ (probably in the form of a fluid) is dominant beneath Nicaragua and that an enriched OIB-type component, with low Ba/La but high La/Yb and $^{206}Pb/^{204}Pb$ (probably in the form of a melt), is dominant beneath Guatemala and central Costa Rica (Eiler et al., 2005, Hoernle et al., 2008, Sadofsky et al., 2008).

Feigenson and Carr (1993) proposed two mantle reservoirs for Central America. The most common reservoir is analogous to depleted mantle (DM) similar to the source of mid-ocean ridge basalt (MORB). The second reservoir has a more enriched composition and was visualized as veins within the DM reservoir. Melting of this veined mantle source and its interaction with the subduction component produced magmas with a typical arc signature (Carr et al., 2003; Feigenson et al., 2004). This signature is dominant along most of the volcanic front; however, in central Costa Rica the lavas have an anomalous Galapagos-OIB signature (Regan and Gill, 1989; Herrstrom et al., 1995; Gazel, 2003; Feigenson et al., 2004) (Fig. 2).

An array of often contradictory models exist to explain this anomalous OIB signature. Herrstrom et al. (1995) suggested that trench parallel flow above the subducting Nazca Plate proposed by Russo and Silver (1994), brings this enriched component from the mantle wedge beneath South America to the mantle wedge beneath southern Central America. Abratis and Wörner (2001) suggested that a "slab window" in the subducting Cocos Plate, proposed by Johnston and Thorkelson (1997), allowed

Galapagos asthenosphere to rise through the window into the mantle wedge below southern Costa Rica and Panama. Feigenson et al. (2004) suggested that the OIB signature is the result of melting a Galapagos-modified mantle below central Costa Rica and Panama. Goss and Kay (2006) explained the OIB signature by incorporation of fore-arc oceanic complexes into the mantle wedge via tectonic erosion. Hoernle et al. (2008 and this study) consider that this signature is derived from the Galapagos Hotspot tracks subducting beneath Costa Rica and Panama.

1.2 Previous work: Temporal Evolution of Arc Volcanism in Central America

In contrast to the substantial international efforts to understand the active volcanic front, the temporal evolution of arc volcanism in Central America has been the focus of few studies. Miocene volcanic stratigraphy in Central America was compiled in El Salvador by Wiesemann (1975) and in Nicaragua by Ehrenborg (1996) and Plank et al. (2002). In Costa Rica, there is evidence of arc volcanism in the sedimentary record since the Albian (Calvo and Bolz, 1994). Nevertheless, the oldest in situ remnants of arc activity are the Sarapiquí Arc (22.2-11.4 Ma) (Gazel et al., 2005), located behind the modern volcanic front of central Costa Rica (Fig. 3). Older portions of the arc are also exposed in the Dominical area and the Talamanca Range (17.5-10.5 Ma) (MacMillan et al., 2004) and the Aguacate Arc (11.35-4.04 Ma) (Kussmaul et al., 1994; MacMillan et al., 2004) (Fig. 3). Normal arc volcanism ceased in the Talamanca area circa 14-11 Ma according to MacMillan et al. (2004), possibly as a result of the collision of older

Galapagos Hotspot tracks (e.g. Coiba Ridge) at this time with the Caribbean Plate (Hoernle et al., 2008). Subsequent volcanic activity in southern Costa Rica is represented by volumetrically minor adakitic-like suites. Although the term "adakite" is controversial (Kelemen et al., 2003), we use it to refer to magmas interpreted to be derived through the melting of subducting oceanic crust within the garnet stability field, and the subsequent reaction of these melts with the mantle wedge, following the model of Kay (1978). In the Talamanca Range, adakitic lavas <5 Ma are exposed as individual domes or minor lava flows in the central part of the range and near the Panamanian-Costa Rican border (Abratis and Wörner, 2001; MacMillan et al., 2004). Their upper-mantle-like oxygen isotope ratios require mixing of slab melts from the upper low-temperature and lower high-temperature altered parts of the subducting crust (Bindeman et al., 2005). Slab melts in this part of the arc can be explained by melting of relatively young subducting Galapagos Hotspot tracks (13.0-14.5 Ma) (Werner et al., 1999) or by hot mantle upwelling (Abratis and Wörner, 2001).

The data presented here on the geochemical evolution of the Costa Rican arc allow us to test the different models that attempt to explain the origin of the Galapagos-OIB signature. We report major and trace element, isotopic and geochronological data that allow us to trace the geochemical evolution of magmas from Oligocene to Pliocene, and to explain the anomalous OIB signature as a result of the interaction of the arc with the subducting Galapagos Hotspot tracks.

2. Samples and analytical methods

Outcrops of Tertiary lavas and shallow intrusions were sampled from quarries, river beds, and road cuts following geologic maps of Tournon and Alvarado (1997) and Gazel et al. (2005). We also sampled outcrops dated by MacMillan et al. (2005) (locations in Table 1). The objective was to elucidate the temporal geochemical evolution in Costa Rica in order to explain the anomalous OIB signature of the southern Central America magmas.

Samples with no visible weathering, as verified by petrographic studies, were crushed in an alumina jaw crusher and washed with de-ionized water in an ultrasonic bath. Alteration-free rock chips (e.g. those free of oxides, veins, and zeolites) were selected under stereoscopic microscope and powdered in an alumina mill. Homogenous glass disks were produced at Michigan State University by fusing each powdered sample with lithium tetraborate ($Li_2B_4O_7$). Glass disks were then analyzed for major elements and selected trace elements (e.g. Cr, Cu, Ni, Sr, Rb, Zr, and Zn) by X-ray fluorescence (XRF) in a Bruker S4 Pioneer. Trace elements were obtained in the same glass disks by laser ablation inductively-coupled plasma mass spectrometry (LA-ICP-MS) in a Micromass Platform ICP-MS with a Cetac LSX 200+ Nd:YAG laser (266 nm). The methods and precision are reported by Hannah et al. (2002).

Sr-Nd-Pb isotope analyses were carried out on whole rock powders at the Department of Earth and Planetary Sciences, Rutgers University. About 100 mg of samples were weighed into a Teflon beaker and dissolved for 6 hours (open beaker) in a 5:1 mixture of

HF and HNO_3 at 150°C until the acids were volatilized. The sample were then re-dissolved in 3 ml of 0.5 N HNO_3 and centrifuged for 5 minutes. Sample digestion and element chromatography were performed in a Class 1000 clean room, equipped with Class 100 laminar flow hoods with downdraft exhaust. HCl, HF and HNO_3 are Fisher Chemical trace metal grade acids, and ultrapure HBr is obtained from SEASTAR©. A Barnstead Nanopure II© purifying system provided 18.2 MΩ water.

The ion-exchange chromatography followed established standard procedures (e.g., Hart and Brooks, 1974). These include Pb separation using 30 µl Teflon micro-columns filled with BIORAD© AG 1x8 (100-200 mesh) resin that is equilibrated with 0.5 N HBr for highest Pb retention and from which Pb is released with 1 ml of 0.5 N HNO_3. The sample matrix collected during Pb chromatography (before the Pb is released) was then loaded in 1.5 N HCl onto 20 ml borosilicate glass columns filled with BIORAD© AG50W-X8 (100-200 mesh). Then the column loaded with 2.3 N HCl and 7.3 N HCl to separate Sr. The rare earth elements (REE) were obtained by loading 20 ml of 7.3 N HCl after Sr collection. The solution containing REE was then loaded in 0.23 N HCl onto 4 ml quartz glass columns filled with HDEHP-Teflon resin to separate the Nd from the other REE. There is a 100% separation of Sm from Nd with this technique, but with significant contamination of the Nd fraction with Ce, requiring analysis of Nd metal rather than Nd oxide during mass spectrometer runs.

Isotopic ratios were determined by thermal ionization mass spectrometry (TIMS) at the Department of Earth and Planetary Sciences at Rutgers University on a GV Isoprobe-T multicollector. Sr and Nd are measured in dynamic multicollection mode, whereas Pb is measured in static multicollection. Sr and Nd isotopic ratios are normalized within each run to $^{86}Sr/^{88}Sr$ = 0.1194 and $^{146}Nd/^{144}Nd$ = 0.7219, respectively, and all errors are reported as 2 sigma of the mean. Reference material measured along with the samples gave $^{87}Sr/^{86}Sr$ = 0.710241 ± 0.000006 (n=33) for NBS987 and $^{143}Nd/^{144}Nd$ = 0.511851 ± 0.000006 (n=20) for La Jolla standards. The reproducibility of NBS 981 (n = 13) is $^{206}Pb/^{204}Pb$ = 16.896 ± 0.009, $^{207}Pb/^{204}Pb$ = 15.437 ± 0.013, $^{208}Pb/^{204}Pb$ = 36.541 ± 0.011. Pb isotope ratios were normalized to NBS 981 values of Galer and Abouchami (1998). Total chemistry blanks are <100 pg for Sr, Nd and Pb and are thus considered negligible for the amount of sample processed.

A subset of 10 samples (codes EG-, P-, and TC-; Tables 1, 2 and 3) were analyzed at IFM-GEOMAR and the University of Kiel. Samples were first crushed to small pieces, then washed in deionized water and carefully hand-picked under a binocular microscope. Major elements and some trace elements (e.g., Cr, Ni, Zr, Sr) of whole rock samples were determined on fused beads using a Philips X'Unique PW1480 X-ray fluorescence spectrometer (XRF) equipped with a Rh-tube at IFM-GEOMAR. H_2O and CO_2 were analyzed in an infrared photometer (Rosemount CSA 5003). Additional trace elements (e.g., Rb, Ba, Y, Nb, Ta, Hf, U, Th, Pb and all REE) were determined by ICP-MS on a VG Plasmaquad PQ1-ICP-MS at the Institute of Geosciences (University of Kiel) after the methods of Garbe-Schönberg (1993). Pb isotopes were determined in a Finningan MAT 262-RPQ^{2+}, Sr and Nd isotopes in a ThemoFinnigan TRITON TIMS at IFM-GEOMAR. The procedures and precision are detailed in Geldmacher et al. (2006) and Hoernle et al. (2008). Inter-lab comparison can be made with the samples TA-021206-4 analyzed by the Rutgers-Michigan State Labs and EG-1 analyzed at the IFM-GEOMAR labs. Even though the codes are different, this sample was collected by the first author in the same place and split for different lab analyses. For this particular sample (EG-1/ TA-021206-4) the different lab results are in good agreement within the analytical errors (Tables 1, 2 and 3).

Key samples were dated by step-heating $^{40}Ar/^{39}Ar$ to compliment the existing geochronology record reported in the literature (MacMillan et al., 2004; Gazel et al., 2005) (Table 4). Mineral separates, rock matrix samples and irradiation monitor TCR-2 (sanidine from Taylor Creek Rhyolite; Age = 27.87 Ma) (Lanphere and Dalrymple, 2000) were irradiated in position E6 of the FRG-1 nuclear reactor at the GKSS Research Center, Geesthacht, using a Cd shielding. Step-heating $^{40}Ar/^{39}Ar$ analyses were carried out with a 20 W argon-ion laser in a MAP 216 mass spectrometer at IFM-GEOMAR. Analysis of system blanks were measured prior to each sample and after each fifth sample heating step, typically comprising 10%, 1%, and 2% of the measured ^{36}Ar, ^{39}Ar, and ^{40}Ar isotopes, respectively. The data reported included more than 50% of ^{39}Ar in each plateau.

3. Data and Results

The main crystalline phases in the Oligocene-Middle Miocene samples are zoned plagioclase and clinopyroxene. Olivine is present in the basalts and basaltic andesites, typically altered to chlorite or iddingsite. Matrix textures in the lavas range from trachytic to interstitial and are composed of plagioclase, pyroxene and magnetite. In general, the Oligocene-Middle Miocene samples display some degree of low temperature alteration (chlorite + zeolites). The petrography shows only one major temporal change, the appearance of orthopyroxene as a phenocryst phase during the Late Miocene.

We report 76 new major element analyses and 72 new trace element analyses presented in Tables 1 and 2. The analyzed samples include basalts, basaltic-andesites, some andesites, and one dacite (Fig. 4). The Oligocene-Middle Miocene samples belong to the calc-alkaline series, similar to the Nicaraguan volcanic front lavas, whereas most of the Late Miocene-Pliocene samples belong to the high-K calc-alkaline to transitional shoshonitic series, similar to the Central Costa Rican volcanic front lavas (Fig. 4). With the exception of lower Ba, Th, U, and Pb, the Oligocene-Middle Miocene rocks are very similar to lavas from the Nicaraguan volcanic front and have more depleted compositions than lavas from the central Costa Rica volcanic front (Fig. 5). The Late Miocene-Pliocene samples have incompatible-element abundances closer the central Costa Rica volcanic front lavas (Fig. 5).

The Sr-Nd-Pb isotopes data are presented in Table 3. The radiogenic isotope ratios were age-corrected (Faure, 1986) assuming that ages reported in the literature or in this study (Table 1) apply uniformly within each geologic unit. The corrected isotopic ratios in Table 3 are plotted in Figs. 6, 8 and 10. The most radiogenic Pb isotopic ratios occur in the Late Miocene-Pliocene units (e.g. $^{206}Pb/^{204}Pb > 18.8$ and $^{208}Pb/^{204}Pb > 38.5$; Fig. 6). $^{87}Sr/^{86}Sr$ increased from 0.7035 in the Oligocene samples to 0.7042 in the Middle Miocene samples and decreased to 0.7035 in the Late Miocene-Pliocene units.

$^{143}Nd/^{144}Nd$ increased from 0.51298 in the Oligocene to 0.51302 in Middle Miocene and decreased to 0.51295 by Late Miocene-Pliocene (Fig. 6).

New $^{40}Ar/^{39}Ar$ step-heating ages are reported in Table 4. Age spectra are provided in Fig. 7. The new ages from the Trinidad area (Fig. 3) (sample P-126 matrix and sample P-217 plagioclase separate) are the oldest reliable $^{40}Ar/^{39}Ar$ ages for in situ remnants of arc magmatism in Costa Rica and range from 28.43±0.44 to 29.2±1.30 Ma. The oldest $^{40}Ar/^{39}Ar$ age previously reported from the intrusives of the Dominical area was 17.5±0.10 Ma, (Fig. 3) (MacMillan et al., 2005). A new $^{40}Ar/^{39}Ar$ age (plagioclase separate) from an andesitic dike from this area provides a slightly older age of 18.3±0.33 Ma. The matix of a diabase from the Cerro de la Muerte area (Fig. 3) yields an $^{40}Ar/^{39}Ar$ age of 13.77±0.43 Ma and the matrix from a nearby olivine basalt yields an age of 14.1±1.0 Ma. Both of these ages are in agreement with the ones published by MacMillan et al. (2005) for volcanic and subvolcanic rocks from the Talamanca Range in this area. The matrix from a basaltic sill from the La Garita Formation (Fig. 3) yielded a $^{40}Ar/^{39}Ar$ age of 6.47±0.21 Ma. The locations of these geologic units are show in Fig. 3.

4. Discussion

The new major observation reported here is the temporal magmatic evolution in Costa Rica. We first describe the geochemical changes over time in Costa Rica and along the volcanic front from central Costa Rica to Nicaragua. We then explain these geochemical and petrological changes to be related to arc-hotspot interaction. To make quantitative estimation of our geological model of arc-hotspot interaction, we use Pb isotope systematics to define the percentage of contribution of the subducting Galapagos hostpot tracks. Based on the Pb isotopic sytematics, we model the entire suite of incompatible trace elements presented here and reported in the literature (Carr et al., 2007) using significant input from subducting Cocos Plate sediments and contributions from the subduction Galapagos Hotspot tracks off Costa Rica.

4.1 Temporal Magmatic evolution in Costa Rica

As mentioned in Section 3, the Late Miocene to Pliocene lavas are mineralogically, petrologically and geochemically distinct from the Oligocene through Middle Miocene lavas. The appearance of orthopyroxene as a phenocryst phase in the Late Miocene-Pliocene lavas could be the result of increasing silica content of the magmas via fractionation or by a metasomatic addition to the mantle source by silica-rich melts (melt-rock reaction) (e.g., Kelemen et al., 1992). Orthopyroxene-rich mantle peridotites from subduction zones are too high in SiO_2 and depleted in Al_2O_3 to be considered residues. Therefore, they are interpreted to be produced by the reaction of the mantle with melts from the subduction zone (Herzberg, 2004). Melting of this metasomatized source will produce lavas that can crystallize orthopyroxene at the initial stages of crystallization; orthopyroxene bearing basaltic lavas are common in central Costa Rica since the Late Miocene. It is likely that the appearance of this mineral reflects a change in the source by metasomatic addition of silicate-rich melts to the mantle source. Based on the trace element compositions of volcanic rocks and olivine-hosted melt inclusions, recent studies have also argued that a component with melt-like characteristics (e.g. with low Ba/La but high La/Yb, La/Nb and probably also Cl, S and F) controls many of geochemical peculiarities of the Costa Rican magmas (Sadofsky et al., 2008).

The change in geochemical character between the Oligocene-Middle Miocene and the Late Miocene-Quaternary volcanic rocks is also evident in major (Fig. 4) and trace elements (Fig. 5). The magmas change from low-K calc-alkaline series during the Oligocene-Middle Miocene, to high-K calc-alkaline to transitional shoshonitic series in the Late Miocene-Quaternary volcanic rocks (Fig. 4). Primitive mantle-normalized trace element patterns (Fig. 5) reveal slightly lower Y and heavy REE abundances in the Late Miocene to Quaternary central Costa Rican volcanic front lavas compared to the Oligocene-Middle Miocene samples. The lower Y and heavy REE abundances are possibly due to greater amounts of garnet in the residue (subduction oceanic cust and/or veins of garnet pyroxenite) as suggested by Feigenson and Carr (1986). For elements to the left of Ti in Fig. 5, the Oligocene-Middle Miocene samples show patterns that mimic the modern Nicaraguan volcanic front lavas, with the exception of some of the fluid mobile elements Ba, U, and Pb (Fig. 5). The higher values for these fluid mobile elements in the modern Nicaraguan arc can be explained by the subduction of different sediments over time, as suggested by Patino et al. (2000) and Plank et al. (2002). It is also worth noting that the Sr isotope ratio begins decreasing after the “carbonate crash”, believed to have been caused by an ~800 m rise in the carbonate compensation depth as the Central American isthmus gateway began to close around 10 Ma ago (Plank et al. 2002). The addition of hemipelagic sediments to the sediment column may have reduced the concentration of Sr in the overall sediment pile. Compared to the older Costa Rica samples and the modern Nicaraguan volcanic front lavas, Central Costa Rican samples younger than 6 Ma are strongly enriched in most incompatible elements, including fluid (e.g. Ba, K, Sr, K, etc.) and melt (e.g. Nb, Ta, Ce, Nd, Zr, etc.) mobile incompatible elements.

The temporal evolution of the key geochemical parameters (Pb, Nd, Sr isotopes and La/Yb) were summarized above and are shown in Fig. 6. The Galapagos-OIB signature in Costa Rica volcanic-front rocks is characterized by $^{206}Pb/^{204}Pb \geq 18.9$, $^{208}Pb/^{204}Pb > 38.5$, $^{143}Nd/^{144}Nd \leq 0.51298$ and La/Yb>10 (Fig. 6). This signature is first evident in the Late Miocene (~6 Ma) samples. The Oligocene-Middle Miocene samples have $^{206}Pb/^{204}Pb < 18.8$, $^{208}Pb/^{204}Pb < 38.4$, $^{143}Nd/^{144}Nd > 0.51297$ and La/Yb <6 values, typical of normal arc volcanic rocks and close to the Nicaraguan volcanic front lavas (Fig. 6). The appearance of the Galapagos-OIB signature in central Costa Rica at ~6 Ma correlates with the eruption of alkaline basalts in the back-arc and adakites in southern Costa Rica and Panama. The isotopic and trace element ratios of the alkaline basalts and adakites overlap with and extend to even higher La/Yb and Pb isotope ratios and lower Nd isotope ratios than the Costa Rican volcanic front lavas (Fig. 6). This geochemical change coincides in central Costa Rica with a tectonic discordance reported by Denyer and Arias (1991) between the La Cruz Formation (11.35-10.90 Ma) (MacMillan et al., 2004) and the Grifo Alto Formation (5.10-4.04 Ma) (Marshall et al., 2003; MacMillan et al., 2004). Samples from the Grifo Alto Formation have the enriched isotopic ratios and trace element values representative of the modern Galapagos-OIB signature in central Costa Rica (Figs. 5 and 6).

4.2 Geochemical Components of the Southern Central American lavas

The subducting crust on the incoming plates outboard of Nicaragua, Costa Rica and Panama is geochemically heterogeneous (Fig. 1). The crust in front of Nicaragua was formed at the East Pacific Rise-Cocos spreading center and has a normal MORB-type geochemical composition (Werner et al., 2003) (Fig. 1). The subducting crust in front of central Costa Rica and Panama is covered by Galapagos Hotspot tracks that preserve the geochemical zonation of the Galapagos Hotspot domains (Hoernle et al., 2000; Werner et al., 2003). The subducting Seamount Province in front of central Costa Rica includes a series of small seamounts and submerged oceanic islands. These Seamount Province lavas show an OIB-alkaline composition and an isotopic signature belonging to the Northern Galapagos Domain (Hoernle et al., 2000; Werner et al., 2003, Harpp et al., 2005) (Fig. 1). The subducting Cocos and Coiba ridges have an OIB-tholeiitic composition and are more isotopically heterogeneous (Central, Eastern and Southern Galapagos domains). However, the dominant isotopic domain in these ridges is the Central Galapagos Domain (Hoernle et al., 2000; Werner et al., 2003) (Fig 1).

The B, Be and Th isotope systematics of the volcanic front lavas require the contribution of the subducted sediments (Leeman et al., 1994; Reagan et al., 1994).

Similarly, the Sr isotopes are controlled by melts and/or hydrous fluids from the subducting sedimentary section of the Cocos Plate (Patino et al., 2002) and fluids from the subducting oceanic crust and de-serpentinization of the subducting mantle (Ranero et al., 2003). Nd isotope systematics in Central America are more complicated. In Nicaragua, Carr et al., (1990) modeled the volcanic front lavas as a mix of a DM component and a small amount of sediment. However, this mix does not provide sufficient Nd to explain the Nd concentrations of the erupted lavas, thus some Nd is required from the subducting oceanic crust (Patino et al., 2000 and this study).

In contrast to other isotopic systems, Pb isotope systematics show no convincing evidence for contribution of subducted sediments (Hoernle et al., 2008). This may be due to decoupling between highly fluid-mobile Pb flushed at shallower levels (fore-arc vents?) and the relatively fluid-immobile Be, Th, and Nd possibly released at deeper levels. Alternatively, the integrated slab fluid that reacts with the mantle wedge does not shift the Pb isotope composition of the mixture because the subducting sediments are close to the composition of DM (Feigenson et al., 2004). Therefore, Pb isotope systematics in southern Central America are mostly controlled by the interaction between the subducting oceanic crust and DM (Hoernle et al., 2008 and Fig. 8).

In summary the Pb isotope systematics of the data presented here (Fig. 8) are explained by three main components. The first is an un-radiogenic component that could either be normal subducting Cocos/Nazca oceanic crust or depleted mantle (DM) in the wedge. The other two components are highly radiogenic and derived from the Galapagos Hotspot. These two radiogenic components are the subducting Seamount Province

(Northern Galapagos Domain) and the subducting Cocos/Coiba Ridge (Central Galapagos Domain) (Fig.8). Nd isotopes require the afore-mentioned components as well as an input from subducting sediments (Fig. 8). Most of the isotopic ratios of the samples >10 Ma can be explained by the interaction of normal oceanic crust or DM and subducted sediments (for Nd isotopes), analogous to those from the Nicaraguan volcanic front lavas. The samples from the Upper Miocene-Pliocene units (La Garita Fm., Grifo Alto Fm., and Paso Real Fm., $^{206}Pb/^{204}Pb>18.8$; Fig. 8) trend toward a composition intermediate between the Cocos/Coiba Ridge and the Seamount Province components. This intermediate composition suggests that mixing between the two Galapagos components occurred in the mantle wedge (Section 4.3). The data from the modern central Costa Rica volcanic front and the alkaline basalts require a Seamount Province component whereas adakites and alkaline lavas from southern Costa Rica and Panama are in range with the Cocos/Coiba Ridge component (Hoernle et al., 2008).

4.3 Arc-hotspot interaction

The interaction between a subduction system and a hotspot can occur in at least two different tectonic scenarios. An enriched mantle plume could flow into the wedge of a subduction zone if the arc passes over or is merely close to it. A different interaction can occur when the eruptive products of a plume (e.g. seamount tracks or aseismic ridges), subduct beneath an arc. Subduction of hotspot tracks can "re-fertilize" the arc mantle source by metasomatic processes (fluids and/or melts). Subsequent melting of this metasomatized mantle could produce lavas with an OIB signature.

Wendt et al. (1997) reported Pb isotopes and trace element evidence for the interaction of the northern segment of the Tonga-Kermadec arc with two hotspot components. The Samoa mantle plume flows into the northern segment of the arc and the Louisville seamount chain subducts into the central part of the arc. In both cases the erupting lavas show an enriched geochemical signature. The OIB signature in alkaline lavas from the Mexican volcanic belt has been explained as a consequence of an arc-hotspot interaction involving plume activity below the arc (Márquez et al., 1999). Bryant et al. (2006) reported Pb, Sr, and Nd isotopic and trace element evidence for the interaction between melts from the Carnegie Ridge (Galapagos Hotspot track) (Fig. 1) and the mantle wedge in the northern Andean volcanic zone in Ecuador with minor continental crust assimilation. Independent of the nature of the interaction between an arc and a hotspot, the result will be arc lavas with an anomalous enriched geochemical signature.

The present day geographic distribution of the Galapagos signature in the volcanics of Costa Rica and Panama is onshore from the ongoing collision of Galapagos hotspot tracks with the Middle American Trench (Fig. 1). In central Costa Rica, where the Seamount Province has been subducted (see projected lines and blue areas in Fig. 1), the samples from the volcanic front and the back-arc alkaline lavas (Fig. 1) require a Seamount Province (Northern Galapagos Domain) geochemical component (Fig. 8), whereas the southern Costa Rica and Panama adakites and alkaline lavas are in the isotopic range of the Cocos/Coiba Ridge component (Central Galapagos Domain) (Fig. 7). Geophysical studies reveal that not only the subducting tracks may interact with the southern Central American margin, but also there may be interaction with the Galapagos Hotspot plume material; since a low velocity seismic anomaly is detected up to southern Costa Rica margin (Montelli et al., 2006). However, the central Costa Rican volcanic front lavas show significant Nb, Ta and Ti depletions typical of arc volcanism (e.g., Carr et al., 2007), indicating that at least in the volcanic front the enriched Galapagos Hotspot component went through the subduction process that separated those elements from the other incompatible elements and thus possibly represent a subduction input and not a mantle composition.

The isotopic and trace element data described here indicate that the central Costa Rican Galapagos-OIB signature results from metasomatism of the mantle wedge by melts and/or fluids from the subducting Galapagos Hotspot tracks. The intermediate Pb isotopic values ($^{206}Pb/^{204}Pb$=18.7-18.8; Figs. 6 and 8) of some of the samples from the Middle Miocene might be explained as an input from the subduction of older Galapagos Hotspot tracks that collided with southern Central America during the Miocene (Hoernle et al., 2002).

Estimates for the timing of the collision of the Cocos Ridge, the Seamount Province, and possibly older tracks with southern Central America range from 10-1 Ma (Gardner et al., 1995; Johnston and Thorkelson, 1997; Gräfe et al., 2002; Silver et al., 2004; MacMillan et al., 2004). Our new data show that the Galapagos-OIB signature appears in central Costa Rica at ~ 6 Ma ago (sample P-95 from La Garita Formation).

This particular geochemical signature allows us to constrain the initial collision of the Galapagos Hotspot tracks at ~8 Ma, allowing ~ 2 Ma for the subducted tracks to move from the trench to a melt generating depth of ~ 100 km beneath the arc (using the current average convergence rate of 80 mm/y). This calculation agrees with the geophysical evidence of a major tectonic event in the Pacific coast of southern Costa Rica circa 8-10 Ma, possibly triggered by the collision of the margin with Galapagos Hotspot tracks (Silver et al., 2004) as with elevated subduction erosion rates beginning ~6 Ma ago (Vannuchi et al., 2006).

The southern Central American margin has been interacting with the Galapagos Hotspot throughout its geologic history. This interaction began with the formation of the Caribbean Large Igneous Province (CLIP) (139-85 Ma, Hoernle et al., 2000; Denyer et al., 2006). Subsequently, oceanic islands and aseismic ridges were accreted during the Eocene and Miocene (Hoernle et al., 2000; Denyer et al., 2006). The interaction continues with the relatively recent subduction of the hotspot tracks. The mantle wedge enrichment produced by the subduction of the hotspot tracks can be considered an important stage in the global cycle of oceanic crust recycling and mantle re-fertilization by metasomatic processes.

4.4 Isotopic and trace element modeling of the arc-hotspot interaction in southern Central America

To evaluate the implications of our subduction-hotspot interaction model, we estimate the regional and temporal contribution of the Galapagos Hotspot to magmatism in southern Central America. According to Peacock et al. (2005) the thermal properties of the subduction zone of Costa Rica and Nicaragua allow the subducting sediments and the uppermost part of subducting oceanic crust to partially melt. We consider melting of the subducting slab an important part of the metasomatic processes inferred from the previous discussion of the spatial and temporal geochemical changes in southern Central America.

The melting model used in this study is aggregated fractional melting (Shaw, 1970) and the partition coefficients used in our modeling (peridotite and eclogite sources) are from the compilation of Kelemen et al. (2003). The first modeling requirement is a mantle wedge with a DM composition that makes an appropriate isotopic and trace element end-member. We obtained a locally appropriate DM by inverting using a melt fraction of 8% the sample SO-144-1 (Fig. 9) from the EPR-Cocos crust off Nicaragua (Werner et al., 2003). This DM is similar to the modal and trace element composition reported by Workman and Hart (2005). The Galapagos Hotspot contributions were modeled from the mean values of the subducting Seamount Province and the Cocos/Coiba Ridge reported by Hoernle et al. (2000) and Werner et al. (2003), using 20% melting in the eclogite facies (Fig. 9). The final components are two sediment melts based on the sediment compositions of Patino et al. (2000) and a melt fraction of 20%. Pr and Ta, not included in the original data, were interpolated from adjacent elements normalized to McDonough and Sun (1995) values. Pr_N (Ce_N, Nd_N) for the hemipelagics, Pr_N (L_N, Nd_N) for the carbonates, and Ta_N(~Nb_N) for both sediments. The first sediment melt consists of a mix of 30% mean carbonate and 70% mean hemipelagic sediments (Fig. 9). Because we do not have the actual composition of the sediment subducting during Oligocene-Pliocene, we used the same composition as sediment melt 1; but with some adjustments to fit the trace element data of the average Oligocene-Pliocene values, specifically, lower Ba, U and Pb (Fig. 9). All the modeled results and details, including melt modes and melt fractions are Table 5 and plotted in Figs. 9-11.

To constrain the Pb isotopic contribution from the subducting Galapagos Hotspot tracks, we plotted a three component diagram that shows the interaction of DM with melts from the subducting Seamount Province and the Cocos/Coiba Ridge (Fig. 10). In Fig. 10a, the Galapagos Hotspot contribution decreases systematically along the volcanic front from central Costa Rica to NW Nicaragua. The samples from southern Costa Rica and Panama are close to the mixing line between the subducting Cocos/Coiba Ridge and DM (Fig. 10a). Along the volcanic front of Costa Rica and Nicaragua, the Galapagos Hotspot contribution is actually a mix between the highly enriched subducting Seamount Province and the volumetrically major Cocos/Coiba Ridge. There are two clusters of data in the central Costa Rica volcanic front and both require >1% of the Galapagos Hotspot contribution. The less radiogenic cluster, represented by samples from Barva, Irazú and Turrialba volcanoes requires a mix of 20% Seamount Province + 80% Cocos/Coiba

Ridge melts (Fig. 9a). The second cluster includes samples from Poás and Platanar volcanoes, which are located directly above the subducting Seamount Province. This group requires a mix of 40% Seamount Province + 60% Cocos/Coiba Ridge melts (Fig. 10a). The Galapagos Hotspot contribution decreases to 1-0.5% in NW Costa Rica, 0.5-0.1 in SE Nicaragua, and it is negligible in NW Nicaragua.

A temporal change in the contribution from the Galapagos Hotspot is shown in Fig. 10b. For most of the Oligocene-Middle Miocene samples, the Galapagos Hotspot contribution was minor. The Middle Miocene samples from the Talamanca Range (southern Costa Rica, Fig. 1) require about 0.5% of Galapagos Hotspot contribution, with a major participation of a component similar to the Cocos/Coiba Ridge (Fig. 10b). In the Late Miocene-Pliocene samples, the Galapagos Hotspot contribution ranges between 0.1-2% and must be a mix between the Seamount Province component and the Cocos/Coiba Ridge component.

To model the incompatible trace elements, we calculated average elemental concentrations of the main volcanic segments from central Costa Rica to NW Nicaragua, using the data from Carr et al. (2007) (Fig. 11). We also calculated mean values of the Oligocene-Middle Miocene samples and Late Miocene-Pliocene samples to constrain the temporal effect of the interaction of the subduction zone with the Galapagos Hotspot (Fig. 11).

The interaction between the subducting Galapagos Hotspot tracks, the sediment and the DM mantle wedge is modeled as a three stage process. The first stage includes melting of the subducting crust (sediment and/or subducting oceanic crust) in eclogite facies. The second stage is visualized as a metasomatic melt-rock reaction between the melts from the slab and the mantle wedge in the garnet stability field and modeled as multicomponent mixing. The last stage is flux melting of this metasomatized or "re-fertilized" mantle caused by fluids from the subducting slab (slab de-hydratation and/or subducting oceanic mantle de-serpentinization) possibly in a shallower level but still in the garnet stability field. The modeled Galapagos Hotspot contribution was based on the the Pb isotopes in Fig. 10. Small increments of sediment melt were added to the mantle until acceptable Rb, Ba, K, Pb, U, and Sr fits were obtained (within the modeled group range and close to the average calculation, Fig. 11). According to Thomsen and Schmidt (2008) no more than 30% of the carbonates are recycled in the sub-arc mantle region. Therefore, we used sediment melt 1 (70% hemipelagic+30% carbonate) for the trace element modeling. However, the Nd isotopic systematics (Fig.8) and some of the trace element data from the volcanic front (Patino et al., 2003) may require additional subducted carbonate. This component could be a hydrous fluid instead of a melt. The source modal composition after metasomatism is close to the original DM; however, a mass balance of clinopyroxene and garnet was required to fit the heavy REE data of each calculated mean in Fig. 11.

The different trace element models are plotted with the respective volcanic front segment means and temporal means in Fig. 11. The most important observation of the trace element modeling is that the trace element concentrations observed along the arc, south of central Nicaragua require a Galapagos Hotspot component. Trace element compositions in central Costa Rica lavas are explained by a DM metasomatized by 3% of the Galapagos Hotspot contribution and <0.1% of sediment input, melted at 8% (Fig. 10a). The trace element composition of NW Costa Rica require a DM metasomatized by about 0.6% of the Galapagos Hotspot contribution and 0.6% of sediment input, melted at 9% (Fig. 11b). The SE Nicaragua mean is controlled by the enriched composition of the two southernmost volcanoes of Conception and Maderas. This segment requires a DM metasomatized by 0.4% Galapagos Hotspot contribution and 0.4% sediment input melted at 6% (Fig. 10c). Because of the strong geochemical gradient in SE Nicaragua, the mean value provided here is less appropriate than the means for the other segments. Therefore, the last estimates should be carefully examined in the future. NW Nicaragua requires DM to be metasomatized by 0.6% of sediment melt (and possibly fluids), a melt fraction of 8%, and there is no need for Galapagos Hotspot contribution (Fig. 10d).

In the Oligocene-Middle Miocene samples the Galapagos Hotspot contribution is absent or negligible (Fig. 11e). It is not until the Late Miocene-Pliocene that a metasomatic process involving the Galapagos Hotspot melts is necessary to explain the trace element data (Fig. 11f).

Carr et al. (1990) reported a contradictory inverse correlation between degree of melting and volcano size in Central America. The degree of melting was inferred from the REE patterns and was considered high in Nicaragua and low in central Costa Rica. This conclusion was based on the assumption that source composition was the same along the volcanic front. However, a second important observation from the trace element modeling (Fig. 11 and Table 6) is that the melt fraction required to reproduce central Costa Rica is similar to the melt fractions needed in the rest of the volcanic front. Steep

REE patterns (high La/Yb) imply a lower degree of melting only if C_0 (Equations 1 and 2, Table 5) is the same for all the magmas. The C_0 modeled here is systematically different along the arc and varies from a DM mantle highly metasomatized by Galapagos tracks melts in central Costa Rica to a DM metasomatized by hydrous fluids and/or sediment melts in NW Nicaragua (Figuere 11 and Table 5 and 6). Therefore, the geochemical variations along the volcanic front (e.g. La/Yb, Ba/La, etc.) reflect the extent and type of metasomatic processes caused by the subducting input not just the degree of partial melting. The higher volcanic volumes in Costa Rica (Carr et al., 2007) are possibly related to a more fertile metasomatized mantle (enriched veins from melts of the subducting Galapagos Hotspot tracks). While in Nicaragua the Galapagos Hotspot contribution is subordinate or insignificant and the resulting metasomatized mantle will be less fertile. Melting of this mantle will produce volcanoes with smaller volumes in Nicaragua.

The main purpose of the modeling presented here was to estimate the effect of the interaction for the Galapagos Hotspot with the arc in southern Central America. Our models have several limitations; for example, they do not include the effect of hydrous fluids and fractional crystallization of the primary magmas. According to Eiler et al. (2005) a hydrous fluid dominates the slab component in the Nicaraguan volcanic front. Therefore, constraining and modeling the effect of this component will likely refine the fits in some of fluid mobile elements (e.g. Ba, U, K, Pb and Sr in Fig. 11). Missfits occur in P, Zr, and Ti but could be explained by fractional crystallization of apatite (P) and titano-magentite/illmenite (Zr, Ti), possibly at crustal levels. Given the limitations of the modeling, the isotopic and trace element models of the Galapagos Hotspot contributions along the volcanic front are remarkably similar and the excellent fits in the central Costa Rica segment argue for an arc-hotspot interaction model.

4.5 Evaluation of the previous models that explain the Galapagos-OIB signature in southern Central America.

Russo and Silver (1994) suggested that a trench-parallel flow of Pacific mantle through the Nazca Plate may feed the growing reservoir of the Atlantic mantle. Herrstrom et al. (1995) used this model to explain the enriched nature of the central Costa Rica lavas. However, the maximum $^{208}Pb/^{204}Pb$ signal is not present in eastern Panama (Fig. 7), as would be expected for northward flow beneath the Nazca Plate, but is instead present in the central Costa Rican volcanic front, directly below the projected subduction of the Galapagos Hotspot Seamount Province (Fig.1).

Abratis and Wörner (2001) proposed that a slab window in the subducting Cocos-Nazca plates, proposed by Johnston and Thorkelson (1997), allowed hot Galapagos mantle to rise into the mantle wedge below southern Costa Rica and Panama, producing the enriched geochemical signature in central Costa Rica. The main weakness in this model is that it does not explain the intermediate values found in some of the Early-Middle Miocene samples from the Talamanca Range (Fig. 6 and 8). A possible variation on this model could involve flow of hot asthenosphere following a detachment of the subducting slab, as suggested by the OIB magmas in the Trans-Mexican volcanic belt

(Ferrari, 2004; Orozco-Esquivel et al., 2007). In this model, the interaction will be between upwelling asthenosphere following the slab detachment and the subducting Seamount Province and the Cocos/Coiba Ridge. Models that suggest direct flow from the Galapagos Hotspot plume below southern Costa Rica and Panama via a slab or slab detachment remain interesting ideas whose implications need to be defined and tested.

The oceanic complexes of the Pacific shore of Costa Rica are related to the Caribbean Large Igneous Province (CLIP) and are interpreted to have originated at the Galapagos Hotspot (e.g. Hauff et al., 2000a; Hoernle et al., 2002; Denyer et al., 2006).. The Costa Rican volcanic front developed on the westernmost part of the CLIP. This geologic history and the high Pb isotopic ratios in eastern Nicaragua and Costa Rican back-arc lavas led Feigenson et al. (2004) to propose that the Galapagos-OIB signature is produced by melting CLIP mantle. Our new data contradict this model because we found that the OIB signature is a recent development (Middle Miocene in the Talamanca Range, Late Miocene-Pliocene in central Costa Rica; Figs. 6 and 8). If residual CLIP had melted, we would expect the Galapagos-OIB signature to be present since the Oligocene (or even earlier). Also, samples <6 Ma in the central Costa Rica are more enriched in $^{208}Pb/^{204}Pb$ and lower in $^{143}Nd/^{144}Nd$ at a given $^{206}Pb/^{204}Pb$ than the fore-arc CLIP complexes of the Costa Rican Pacific shore (Fig. 8). Therefore, melting residual CLIP mantle is not a good source for the OIB signature in southern Central America.

Goss and Kay (2006) proposed that the Galapagos-OIB signature results from incorporating portions of the CLIP fore-arc oceanic complexes into the mantle wedge by tectonic erosion. This model can explain the timing of the appearance of the enriched geochemical signature in central Costa Rica lavas only if tectonic erosion initiated with subduction of the Galapagos tracks. However, as mentioned in the preceding paragraph, samples <6 Ma in the central Costa Rica are more enriched in $^{208}Pb/^{204}Pb$ and lower in $^{143}Nd/^{144}Nd$ at a given $^{206}Pb/^{204}Pb$ than the fore-arc CLIP complexes of the Costa Rican fore-arc CLIP complexes. Furthermore, the modern Costa Rican volcanic front and alkaline basalts require a Seamount Province component (Fig. 8). As a result, the Goss and Kay (2006) model does not explain the isotope and trace element geochemistry of the Late Miocene-recent volcanic in central Costa Rica.

5. Conclusions

Most of the Oligocene-Middle Miocene samples from Costa Rica are normal calc-alkaline arc lavas, geochemically similar to the Nicaraguan volcanic front The modern central Costa Rican Galapagos-OIB signature ($^{206}Pb/^{204}Pb>18.8$, $^{143}Nd/^{144}Nd<0.513$, LaYb>10) is evident in the units younger than 6 Ma ago. We propose that this anomalous signature is the result of metasomatic processes related with the subduction of Galapagos Hotspot tracks that most likely began to collide with the margin ~8 Ma ago. The intermediate values ($^{206}Pb/^{204}Pb=18.7$-18.8, La/Yb=6-10) of some of the samples from the Middle Miocene could represent the effect of the interaction of older Galapagos Hotspot tracks that collided with the southern Central American margin during the Miocene.

The southern part of the Central American margin has been interacting with the Galapagos Hotspot throughout its geologic history. The relatively recent interaction of the subducting Galapagos Hotspot tracks (the Seamount Province, the Cocos/Coiba Ridge, and possible older Galapagos tracks) with the mantle wedge has changed the composition of the erupted lavas in southern Central America producing a Hotspot signature (Galapagos-OIB) in a volcanic arc.

The Galapagos Hotspot contribution is mix between the volumetrically major Cocos/Coiba Ridge component and the highly enriched Seamount Province. The most enriched isotopic signature is present in central Costa Rica, directly above the subducting Seamount Province. There is a systematic decrease in the influence of the Galapagos Hotspot along the volcanic front from central Costa Rica to NW Nicaragua. The interaction of the southern Central American segments of the arc with the eruptive products of the Galapagos Hotspot, subducting beneath Costa Rica, is strongly favored by the geochemical and geochronological data presented here, therefore more complex models are not required.

6. Acknowledgments

Field work logistics supported by P. Denyer, G. Alvarado and T. Aguilar from the Central American School of Geology at the University of Costa Rica. Revisions by L. Patino, I. Saginor, N. Sou, and S. Whattam improved the manuscript. Reviews and comments by I. Smith, O. Ishizuka and V. Salters are highly appreciated. This research is the result of collaboration between the Department of Earth and Planetary Sciences at Rutgers University, IFM-GEOMAR and Michigan State University. This work was supported through the NSF Margins Program, grants EAR0203388 and NSF OCE 0505924, the German Science Foundation Collaborative Research Center (SFB574, contribution 145) and by the Rutgers University Graduate School Pre-Dissertation award.

7. References

Abratis, M., and G. Wörner (2001), Ridge collision, slab-window formation, and the flux of Pacific asthenosphere into the Caribbean realm. *Geology* 29 (2), 127-130.

Alvarado, G. E., C. Dengo, U. Martens, J. Bundschuh, T. Aguilar, and S. B. Bonis (2007), Stratigraphy and geologic history, in *Central America Geology, Resources and Hazards,* edited by J. Bundschuh and G. E, Alvarado, pp. 345-394, Taylor and Francis, Leiden.

Bindeman I.N., J.M Eiler., G.M Yogodzinski., Y Tatsumi., C.R Stern., T.L. Grove, M. Portnyagin., K. Hoernle, and L.V .Danyushevsky (2005), Oxygen isotope evidence for slab melting in modern and ancient subduction zones. Earth Planet. Sci. Lett. 235, 480-496.

Bryant, J. A., G. M. Yogodzinski, M. L. Hall, J. L. Lewicki, and D. G. Bailey (2006), Geochemical constrains on the origin of volcanic rocks from the Andean northern volcanic zone, Ecuador. *J. Petrol.* 47(6), 1147-1175.

Calvo, C., and A. Bolz (1994), The oldest calc-alkaline island arc volcanism in Costa Rica. Marine tephra from the Loma Chumico Formation (Albian to Campanian). *Profil* 7, 235-264.

Carr, M. J., M. D. Feigenson, and E. A. Bennett (1990), Incompatible element and isotopic evidence for tectonic control of source mixing and melt extraction along the Central American arc. *Contrib. Mineral. Petrol.* 105, 369-380.

Carr, M. J., M. D. Feigenson, L. C. Patino, and J. A. Walker (2003), Volcanism and geochemistry in Central America: Progress and problems, in *Inside the Subduction Factory, Geophys. Monogr. Ser.*, vol 138, edited by J. Eiler and G. Abers, pp. 153-179, AGU, Washington, D. C.

Carr, M. J., I. Saginor, G. E. Alvarado, L. Bolge, F. Lindsay, K. Milidakis, B. Turrin, M. D. Feigenson, and C. C. Swisher III (2007), Element fluxes from the volcanic front of Nicaragua and Costa Rica. *Geochem. Geophys. Geosyst*. 8(6), Q06001, doi:10.1029/2006GC001396.

DeBoer, J. Z., M. Drumond, M. J. Bordelon, M. J. Defant, H. Bellon, and R. C. Maury (1995), Cenozoic magmatic phases of the Costa Rica island arc (Cordillera de Talamanca), in *Geologic and Tectonic Development of the Caribbean Plate Boundary in Southern Central America*, *Geol. Soc. Am. Spec. Pap., 295*, edited by P. Maan, pp. 35-36.

DeMets, C. (2001), A new estimate for present-day Cocos–Caribbean Plate motion: Implications for slip along the Central American volcanic arc. *Geophys. Res. Lett.* 28, 4043-4046.

Denyer, P., and O. Arias (1991) Estratigrafía de la región central de Costa Rica. *Rev. Geol. Am. Cent.*, 12, 1-59, http://www.geologia.ucr.ac.cr/revista-geol.htm.

Denyer, P., P. O. Baumgartner, and E. Gazel (2006), Characterization and tectonic implications of Mesozoic-Cenozoic oceanic assemblages of Costa Rica and Western Panama. *Geologica Acta* 4, 1-2, 203-218.

Denyer, P., and G. E. Alvarado (2007), Mapa Geologico de Costa Rica, Liberia Francesa S.S., San Jose, Costa Rica.

Ehrenborg, J. (1996), A new stratigraphy for the Tertiary volcanic rocks of the Nicaraguan Highland. *Geol. Soc. Am. Bull.* 108(7), 830-842.

Eiler, J. M., M. J. Carr, M. Reagan and E. Stolper (2005), Oxygen isotope constraints on the sources of Central American arc lavas. *Geochem. Geophys. Geosyst.* 6, Q07007, doi:10.1029/2004GC000804.

Faure, G. (1986), *Principles of Isotope Geology*, 2nd ed., 589 pp., John Willey & Sons, New York.

Feigenson, M. D., and M. J. Carr (1986), Positively correlated Nd and Sr isotope ratios of lavas from the Central American Volcanic Front. *Geology* 14, 79-82

Feigenson, M. D., and M. J. Carr (1993), The source of Central American lavas: Inferences from geochemical inverse modeling. *Contrib. Mineral. Petrol.* 133, 226-235.

Feigenson, M. D., M. J. Carr, S. V. Maharaj, S. Juliano, and L. L. Bolge (2004), Lead isotope composition of Central American volcanoes: Influence of the Galapagos plume. *Geochem. Geophys. Geosyst.* 5, Q006001, doi:10.1029/2003GC000621.

Ferrari, L. (2004), Slab detachment control on mafic volcanic pulses and mantle heterogeneity in Central Mexico. *Geology* 32, 77-80.

Galer, S. J. G., and W. Abouchami (1998), Practical application of lead triple spiking for correction of instrumental mass discrimination. *Min. Mag.* 62A, 491-492.

Gardner, T. W., D. Verdonk, N. M. Pinter, R. L. Slingerland, K. P. Furlong, T. F. Bullard, and S. G. Wells (1992), Quaternary uplift astride of aseismic Cocos Ridge, Pacific Coast, Costa Rica,. *Geol. Soc. Am. Bull*. 104, 219-232.

Gazel, E. (2003), Las series alcalinas del Plioceno de Costa Rica: Distribución espacial y relación con una fuente mantelica tipo OIB. *Rev. Geol. Am. Cent. 29*, 87-94, http://www.geologia.ucr.ac.cr/revista-geol.htm.

Gazel, E., G. E. Alvarado, J. Obando, and A. Alfaro (2005), Evolución magmática del arco de Sarapiquí, Costa Rica. *Rev. Geol. Am. Cent.* 32, 13-31, http://www.geologia.ucr.ac.cr/revista-geol.htm.

Geldmacher, J., K. Hoernle, A. Klügel, P. van den Bogaard, F. Wombacher, and B. Berning (2006), Origin and geochemical evolution of the Madeira-Tore Rise (eastern north Atlantic). *J. Geophys. Res.* 111, doi:10.1029/2005JB003931.

Goss, A. R., and S. M. Kay (2006), Steep REE patterns and enriched Pb isotopes in southern Central American arc magmas: Evidence for forearc subduction erosion? *Geochem. Geophys. Geosyst*. 7, Q05016, doi:10.1029/2005GC001163.

Gräfe, K., W. Frisch, I. M. Villa, and M. Meschede (2002), Geodynamic evolution of southern Costa Rica related to low-angle subduction of the Cocos Ridge: Constrains from thermochronology. *Tectonophysics* 348, 187-204.

Hannah R. S., T. A. Vogel, L. C. Patino, and G. E. Alvarado (2002), The Origin of the chemically variable 0.33 Ma Valle Central Ash-flow tuff, Costa Rica. *Bull. Volcanol.* 64, 117-133.

Hauff, F., K. A. Hoernle, P. van den Bogaard, G. E. Alvarado, and D. Garbe-Schönberg (2000), Age and geochemistry of basaltic complexes in western Costa Rica: Contributions to the geotectonic evolution of Central America. *Geochem. Geophys. Geosyst.* 1, doi: 10.1029/1999GC000020.

Harpp KS, Wanless V, Otto R, Hoernle K, Werner R (2005), The Cocos and Carnegie aseismic ridges: A trace element record of long-term plume-spreading center interaction. *Jour. Petrol*. 46, 109-133.

Hart, S. R., and C., Brooks (1974), Clinopyroxene-matrix partitioning of K, Rb, Cs, and Ba. *Geochim. Cosmochim. Acta* 38, 1799-1806.

Herrstrom, E. A., M. K. Reagan, and J. D. Morris (1995), Variations in lava composition associated with flow of asthenosphere beneath southern Central America. *Geology* 23, 617-620.

Herzberg, C. (2004), Geodynamic information in peridotite petrology. *J. Petrol*. 45(12), 2507-2530.

Hoernle, K. A., R. Werner, J. P. Morgan, J. Bryce, and J. Mrazek (2000), Existence of a complex spatial zonation in the Galápagos plume for at least 14.5 Ma. *Geology* 28, 435-438.

Hoernle, K., P. van den Bogaard, R. Werner, B. Lissinna, F. Hauff, G. E. Alvarado, and D. Garbe-Schönberg (2002), Missing history (16-71 Ma) of the Galapagos hotspot: Implications for the tectonic and biological evolution of the Americas. *Geol. Soc. Am. Bull*. 30(9), 795-798.

Hoernle, K., F. Hauff, and P. van den Bogaard (2004), A 70 Myr history (139-69 Ma) for the Caribbean large igneous province. *Geology* 32, 697-700.

Hoernle, K., D. L. Abt, K. M. Fischer, H. Nichols, F. Hauff, G. A. Abers, P. van den Bogaard, G. Alvarado, M. Protti, and W. Strauch (2008), Arc-parallel flow in the mantle wedge beneath Costa Rica and Nicaragua. *Nature* 451, 1094-1097, doi: 10.1038/nature06550.

Johnston, S. T., and D. J. Thorkelson (1997), Cocos-Nazca slab window beneath Central America. *Earth Planet. Sci. Lett.* 146, 465-474.

Kay, R. W. (1978), Aleutian magnesian andesites: Melts from the subducted Pacific Ocean crust. *J. Volcanol. Geotherm. Res.* 4, 117-132.

Kelemen, P. B., H. J. B. Dick, and J. E. Quick (1992), Formation of harzburguite by pervasive melt/rock reaction in the upper mantle. *Nature* 358, 635-641, doi:10.1038/358635ao.

Kelemen, P. B., G. M. Yogodzinski, and D. Scholl (2003), Along-strike variation in the Aleutian island arc: Genesis of high Mg# andesites and implications for continental crust, in *Inside the Subduction Factory, Geophys. Monogr. Ser.,* vol 138, edited by J. Eiler and G. Abers, pp. 223-276, AGU, Washington, D. C.

Kerr, A. C., R. V. White, P. M. E. Thompson, J. Tarney, and A. D. Saunders (2003), No Oceanic plateau - no Caribbean plate? The seminal role of oceanic plateau(s) in Caribbean plate evolution, in *The Gulf of Mexico and Caribbean Region: Hydrocarbon Habitats, Basin Formation and Plate Tectonics*, *Am. Assoc. Petrol. Geol. Mem.,* 79, edited by C. Bartolini, R. T. Buffler, and J. Blickwede, pp. 126-268.

Kussmaul, S., J. Tournon, and G. E. Alvarado (1994), Evolution of the Neogene to Quaternary igneous rocks of Costa Rica. *Profil* 7, 97-123.

Lanphere, M. A., and G. B. Dalrymple (2000), First-principles calibration of ^{38}Ar tracers; Implications for the ages of ^{40}Ar/^{39}Ar fluence monitors. *U.S. Geol. Surv. Prof. Pap.* 1621, 1-10.

Leeman, W. P., M. J. Carr, and J. D. Morris (1994), Boron geochemistry of the Central American arc: Constraints on the genesis of subduction-related magmas. *Geochim. Cosmochim. Acta* 58, 149-168.

MacMillan, I., P. B. Gans, and G. Alvarado (2004), Middle Miocene to present plate tectonic history of the southern Central American volcanic arc. *Tectonophysics* 392, 325-348.

Márquez, A., R. Oyarzun, M. Doblas, and S. P. Verma (1999), Alkalic (ocean-island type) and calc-alkalic volcanism in the Mexican volcanic belt: A case for plume-related magmatism and propagating rifting at an active margin? *Geology* 27(1), 51-54.

Marshall, J.S., B.D. Idlemann, T. Garner, and D.M. Fisher (2003), Landscape evolution within retreating volcanic arc, Costa Rica, Central America. *Geology* 31(5), 419-422.

McDonough, W. F., and S. S. Sun (1995), The composition of the Earth. *Chem. Geol.* 120, 223-253.

Montelli, R., G. Nolet, F. A. Dahlen, and G. Masters (2006), A catalogue of deep mantle plumes: New results from finite-frequency tomography. *Geochem. Geophys. Geosyst*. 7, Q11007, doi:10.1029/2006GC001248.

Orozco-Esquivel, T., C. M. Petrone, L. Ferrari, T. Tagami, and P. Manetti (2007), Geochemical and isotopic variability in lavas from eastern Trans-Mexican volcanic belt: Slab detachment in a subduction zone with varying dip. *Lithos* 93, 149-174, doi: 10.1016/j.lithos.2006.06.006.

Patino, L. C., M. J. Carr, and M. D. Feigenson (2000), Local and regional variations in Central American arc lavas controlled by variations in subducted sediment input. *Contrib. Mineral. Petrol*. 138, 265-283.

Peacok, S. M., P. E. van Keken, S. D. Holloway, B. R. Hacker, G. A. Abers, and R. L. Fergason (2005), Thermal structure of the Costa Rica-Nicaragua subduction zone. *Earth Planet. Sci. Lett.* 149, 187-200.

Plank, T., V. Balzer, and M. J. Carr (2002), Nicaraguan volcanoes record paleoceanographic changes accompanying closure of the Panama gateway,.*Geology* 30, 1087-1090.

Protti, M., F. Guendel, and K. McNally (1995), Correlation between the age of the subducting Cocos plate and the geometry of the Wadati-Benoiff zone under Nicaragua Costa Rica, in *Geologic and Tectonic Development of the Caribbean Plate Boundary in Southern Central America*. *Geol. Soc. Am. Spec. Pap., 295*, edited by P. Maan, pp. 309-326.

Ranero, C. R., and R. von Huene (2000), Subduction erosion along the Middle America convergent margin. *Nature* 404, 748-752.

Ranero, C. R., J. P. Morgan, K. McIntosh, and C. Reichert (2003), Bending-related faulting and mantle serpentinization at the Middle America trench. *Nature* 425, 367-373.

Reagan, M. K., and J. G. Gill (1989), Coexisting of calc-alkaline and high-niobium basalts from Turrialba volcano, Costa Rica: Implications for residual titanites in arc magmas sources. *J. Geophys. Res*. 94, 4691-4633.

Reagan, M. K., J. D. Morris, E. A. Herrstrom, and M. T. Murrel (1994), Uranium series and beryllium isotope evidence for an extended history of subduction modification of the mantle below Nicaragua. *Geochem. Cosmochem. Acta* 58, 4199-4212.

Russo, R. M., and P. G. Silver (1994), Trench-parallel flow beneath the Nazca plate from seismic anisotropy. *Science* 263, 1105-1111.

Shaw, D. M. (1970), Trace element fractionation during anatexis. *Geochim. Cosmochim. Acta* 34, 237-243.

Silver, E., P. Costa Pisani, M. Hutnak, A. Fisher, H. DeShon, and B. Taylor (2004), An 8-10 Ma tectonic event on the Cocos Plate offshore Costa Rica: Result of the Cocos Ridge collision. *Geophys. Res. Lett.* 31, L18601, doi: 10.1029/2004GL020272.

Syracuse, E. M., and G. A. Abers (2006), Global compilation of variation in slab depth beneath arc volcanoes and implications. *Geochem. Geophys. Geosyst*. 7, Q05017, doi: 10.1029/2005GC001045.

Sadofsky S., M. K. Portnyagin. K. Hoernle and P. van den Bogaard, (2008), Subduction cycling of volatiles and trace elements through the Central American Volcanic Arc: Evidence from melt inclusions. *Contrib. Min. Petrol*. 155, 433-456. doi: 10.1007/s00410-007-0251-3.

Thomsen B. T. and M.W. Schmidt (2008), Melting of carbonated pelites at 2.5-5.0 GPa, silicate-carbonate liquid immiscibility, and potassium-carbon metasomatism of the mantle. *Earth Planet. Sci. Lett.* 267, 17-31.

Tournon, J., and G. Alvarado (1997), Mapa geológico de Costa Rica, Edit. Tecnológica, Cartago, Costa Rica.

Vannucchi, P., Fisher, D.M. Bier, S., and Gardner, T.W. (2006), From seamount accretion to tectonic erosion: Formation of Osa Mélange and the effects of Cocos Ridge subduction in southern Costa Rica. *Tectonics* 25, TC2004. doi: 10.1029/2005TC001855,

Wendt, J. I., M. Regelous, K. D. Collerson, and A. Ewart (1997), Evidence for a contribution from two mantle plumes to island-arc lavas from northern Tonga. *Geology* 25(7), 611-614.

Werner, R., K. Hoernle, P. van den Bogaard, C. Ranero, R. von Hune (1999), Drowned 14 m.y.-old Galapagos archipelago off the coast of Costa Rica: Implications for tectonic and evolutionary models. *Geology* 2(6), 499-502.

Werner, R., K. Hoernle, U. Barckhausen, and F. Hauff (2003), Geodynamic evolution of the Galapagos hotspot system (central East Pacific) over the past 20 m.y.: Constraints from morphology, geochemistry, and magnetic anomalies. *Geochem. Geophys. Geosyst.* 4, 1108, doi: 10.1029/2003GC000576.

Weyl, R. (1980), *Geology of Central America*, 2nd ed., 372 pp., Gebrüder Borntraeger, Berlin-Stuttgart.

Wiesemann, G. (1975), Remarks on the geologic structure of the Republic of El Salvador, Central America. *Mitt. Geol. Palaőnt. Inst. Univ. Hamburg* 44, 557-574.

Workman, R. K., and S. Hart (2005), Major and trace element composition of the depleted MORB mantle (DMM). *Earth Planet. Sci. Lett*. 231, 53-72.

Figures captions

Figure 1

Tectonic setting of Central America (Hoernle et al., 2008; Alvarado et al., 2007; Carr et al., 2003). The Galapagos hotspot and tracks, both bathymetry and isotopic domains, are from Hoernle et al. (2000) and Werner et al. (2003). Note that the isotopic compositions of the eruptive lavas in southern Central America match with the isotopic domains of the subducting Galapagos hotspot tracks in front of the trench. The central Costa Rican volcanic front lavas and alkaline basalts require the input of the subducting Seamount Province (Northern Galapagos Domain-blue areas) and the southern Costa Rican and Panamanian adakites and alkaline basalts are in the range of the subducting Cocos and Coiba ridges (Central Galapagos Domain-green areas) (Hoernle et al., 2008 and this study). CCR: central Costa Rica, CNS: Cocos-Nazca Spreading Center, EPR: East Pacific Rise, NAP: North American Plate, SCR: southern Costa Rica, VF: Volcanic front.

Figure 2

Selected trace element and isotopic ratios for the different segments of the Central American Volcanic Front. The range of subducting sediments, Pacific MORB and Galapagos hotspot lavas are plotted in the Y-axis for comparison. The maximum subducting sediment signal (Ba/La) is located in the NW Nicaragua segment and the minimum in central Costa Rica. The La/Yb and $^{206}Pb/^{204}Pb$ ratios of central Costa Rica are in range with the Galapagos OIB hotspot lavas while the rest of the arc show La/Yb and $^{206}Pb/^{204}Pb$ ratios in the range of a MORB source and subducting sediments. Data for the volcanic front from Carr et al. (2003), Feigenson et al. (2004) and Hoernle et al (2008), for the subducting sediments from Patino et al. (2000), Pacific MORB and Galapagos hotspot data from Georoc database (http://georoc.mpch-mainz.gwdg.de).

Figure 3

Simplified geologic map modified from Denyer and Alvarado (2007) that shows the different units sampled for this study. The locations of the samples are reported in Table 1. Bathymetric features from Ranero and von Huene (2000). The chrono-stratigraphic range of the different units mention in the text and in Tables 1-3 is included to the right of the geologic map. Ages from MacMillan et al. (2004), Gazel et al. (2005), and this study. VF: Volcanic Front.

Figure 4

Geochemical classification for the Oligocene to Pliocene samples. Note that most the Upper Miocene-Pliocene samples are higher in K_2O at a given SiO_2, generally having high-K calc-clkaline to shoshonitic compostions similar to the Costa Rican volcanic front. Most Oligocene-Middle Miocene samples have calc-alkaline compositions similar to Quaternary Nicaragua lavas. Fields for the modern volcanic fronts of central Costa Rica (gray) and Nicaragua (light red) are from Carr et al. (2003). All samples normalized on a volatile free basis.

Figure 5

Primitive-mantle normalized diagram of the Oligocene-Middle Miocene (a) and Late Miocene-Pliocene (b) samples, compared to incompatible-element patterns of the volcanic fronts of Nicaragua and central Costa Rica (Carr et al., 2003; Carr et al., 2007). The Oligocene-Middle-Miocene and Late Miocene-Pliocene sample means include lavas with SiO_2< 63 wt% reported in Tables 1 and 2. Note that the Oligocene-Middle Miocene samples from Costa Rica have patterns similar to the modern Nicaraguan volcanic front lavas and are relatively depleted compared to modern central Costa Rican lavas. The Late Miocene-Pliocene samples have patterns similar to the central Costa Rican volcanic front (VF) lavas.

Figure 6

La/Yb and age-corrected Pb, Sr, and Nd isotopic ratios of Oligocene to Pliocene arc-related volcanic rocks are plotted against age in Ma. The range for modern volcanic fronts of central Costa Rica (CCR) and Nicaragua (NVF) are shown on the Y-axis. The appearance of alkaline basalts from the central Costa Rica area and alkaline basalts and adakites from southern Costa Rica and Panama coincide with the appearance of the new source about ~6 Ma ago. The time frame for accretionary processes and the collision of the Cocos Ridge and Seamount Province is shown at the bottom on the X-axis and discussed in the text. Data for the volcanic front, alkaline basalts and adakites are from Hoernle et al. (2008). Ages of the Galapagos hotspot accreted terrains in Panamá are from Hauff et al. (2000) and Hoernle et al. (2002). Symbols are the same as Fig. 4.

Figure 7

Age spectra for the new $^{40}Ar/^{39}Ar$ ages presented in this study.

Figure 8

Age-corrected Pb and Nd isotopic ratios for samples and possible sources of the Oligocene-Pliocene samples, the central Costa Rican and Nicaraguan volcanic front lavas, and alkaline basalts and adakites from Costa Rica and Panama. Additional data for the Seamount Province, Cocos/Coiba Ridge, and Cocos/Nazca Plate are from Hoernle et al. (2000) and Werner et al. (2003). The fore-arc CLIP oceanic complexes are from Hauff et al. (2000) and Hoernle et al. (2004), and subducting sediments from Feigenson et al. (2004). The volcanic front lavas and alkaline basalts from central Costa Rica require a subducting Seamount Province component (Northern Galapagos Domain, also see Fig. 1). The alkaline basalts and adakites from southern Costa Rica and Panama are in range with the subducting Cocos/Coiba Ridge (Central Galapagos Domain, also see Fig.1). The modern Galapagos-OIB signature in central Costa Rica appears in the Late Miocene-Pliocene units (~6 Ma). Intermediate values ($^{206}Pb/^{204}Pb$=18.7-18.8) in the Oligocene-Middle Miocene samples possibly reflect the effect of the interaction of older Galapagos hotspot tracks with southern Central America.

Figure 9

Trace element compositions of the different modeled components for this study (model data in Appendix 2). DM was inverted with a melt fraction of 8% from the sample SO 144-1 (Werner et al., 2003) with a modal composition of 60%olivine+25% orthopyroxene+13%clinopyroxene+2%spinel. Melts from the mean subducting Cocos/Coiba Ridge and Seamount Province (Hoernle et al., 2000; Werner et al., 2003) were modeled with melt fraction of 20% with a modal composition of 83%clinopyroxene+15%garnet+2% rutile. Sediment melt 1 was modeled from a mix of a 70% mean hemipelagic+30% mean carbonate from Patino et al. (2000). The sediment melt 1 was modeled with melt fraction of 20% and a modal composition of 84.6% clinopyroxene+15%garnet+0.4rutile. There is no information about the subducting sediments during the Oligocene-Pliocene. Thus, sediment melt 1 composition was empirically adjusted (reducing Ba, U and Pb) to fit the average value of the Oligocene-Pliocene samples.

Figure 10

Mixing lines connect the modeled mean Seamount Province melt ($^{143}Nd/^{144}Nd$= 0.51286, $^{206}Pb/^{204}Pb$= 19.390, $^{208}Pb/^{204}Pb$= 39.284, N= 14) and the mean Cocos/Coiba Ridge melt ($^{143}Nd/^{144}Nd$= 0.51297, $^{206}Pb/^{204}Pb$= 19.296, $^{208}Pb/^{204}Pb$= 38.930, N= 17) (Hoernle et al., 2000; Werner et al., 2003) with the DM (inverted from sample SO 144-1) from Werner et al. (2003). Notice that the Galapagos hotspot contribution decreases systematically along the volcanic front (a) and in the older samples (b). The relative recent Galapagos OIB signature (with $^{206}Pb/^{204}Pb > 18.8$) appears in the Late Miocene-Pliocene samples (b). The intermediate $^{206}Pb/^{204}Pb$ (18.7-18.8) from some of the Middle Miocene Talamanca Range (b) could be explained by the interaction of the arc with older Galapagos hotspot tracks during the Miocene. The Galapagos hotspot participation is a mix between the volumetrically major Cocos Ridge and the less voluminous but highly enriched Seamount Province. GC1= Galapagos hotspot component for the volcanic front. It was modeled as 40% Seamount Province+60%Cocos/Coiba Ridge. GC2= Galapagos hotspot component for the Late Miocene-Pliocene units and was modeled as 20% Seamount Province+80% Cocos/Coiba Ridge.

Figure 11

Trace element models compared with the mean (denoted by line with symbols) and range (denoted by shaded field enclosing the mean line) for each volcanic segment from Central Costa Rica to NW Nicaragua. The dashed blue lines show model melts derived from a DM mantle source metasomatized by melts from subducting sediments. Metasomatized mantle models that require a Galapagos hotspot component and liquids derived form that source are plotted as continuous blue lines. There is a good agreement between the models and the data. Misfits in P, Zr, and Ti could be explained by fractional crystallization at crustal levels. The Galapagos hotspot component was approximated from Fig. 8 and represents a mix between melts of the Seamount Province (SP) and the Cocos/Coiba Ridge (CCR). GC1: Galapagos hotspot component for the volcanic front. It was modeled as 40% SPM+60%CCR. GC2: Galapagos hotspot component for the Late

Miocene-Pliocene units and was modeled as 20% SP+80% CCR. SedM1: sediment melt 1, SedM2: sediment melt 2(Oligocene-Miocene). F: melt fraction in percent

Tables Captions

Table 1

Geologic units, sample locations, ages, major and trace elements results. *Ages from Gazel et al. (2005), **ages from MacMillan et al. (2004). Lit: lithology, a: andesite, ab: aphyric basalt, b: basalt, ba: basaltic andesite, d: dacite, di: diabase, gb: gabbro, ol: olivine-rich basalt.

Table 2

ICP-MS trace element results.

Table 3

Radiogenic isotopes ratios results. Age-corrected ratios in **bold**. *Pb, Sr and Nd concentrations for age-correction assumed the same as sample from sample P-125. **Data from Hoernle et al. (2008). The initial ratios were calculated with the average ages reported in the literature or in this study (Table 1) for each geologic unit.

Table 4

Complete step heating experimets $^{40}Ar/^{39}Ar$ data for the new ages in this study, the plateau steps are shown in **bold**.

Table 5

Modeled components and melts for the southern Central American lavas. The melting model used in this study was aggregated fractional melting (Shaw, 1970) described by the following equation: $C_L/C_0=1/F\times(1-(1-F)^{1/D0})$. Where C_L is the average concentration of the element in the liquid, C_0 is the initial concentration of the element in the source, F is the melt fraction, and D_0 is the initial bulk partition coefficient. Equation 1 is derived from the mass balance equation $C_0=F\times C_L+(1-F)C_S$, and the bulk partition coefficient $D = C_S/C_L$. Where C_S is the concentration of the element in the solid phase. The partition coefficients used in our modeling (peridotite and eclogite sources) are from the compilation of Kelemen et al. (2003). The DM composition was inverted from sample SO-144-1 from Werner et al. (2003). Modeled melts in eclogite facies from the subducting Seamount Province and Cocos/Coiba Ridge were based on the average calculation of the data published by Hoernle et al. (2000) and Werner et al. (2003). The subducting sediments were obtained from Patino et al. (2000) and the melt modeled was produced from a 30% carbonate (carb.) and a 70% hemipelagic (hemi.) sediment mix. Average TiO_2 concentrations in the subducting plate were used as a proxy for rutile in the residue. The trace element patterns are plotted in Figs. 9 and 11, and other details of the modeling are in section 4.4. cpx: clinopyroxene, ga:garnet;, ol:olivine, opx:orthopyroxene, rut: rutile, spn: spinel. C_0: Composition of the metasomatized mantle, C_L: Composition of the melts from the metazomatized mantle, F: melt fraction in percent

Table 6

Summary of the different models shown in Fig. 11. The Galapagos contribution and sediment refer to the metasomatic additions to a DM mantle from melts the subducting slab. Notice that the degree of partial meting used in each model is in the same order of magnitude and does not change significantly along the volcanic front. The modal garnet needed to fit the heavy REE patterns only occurs along with the metasomatic contribution of the Galapagos hotspot.

Figure 1

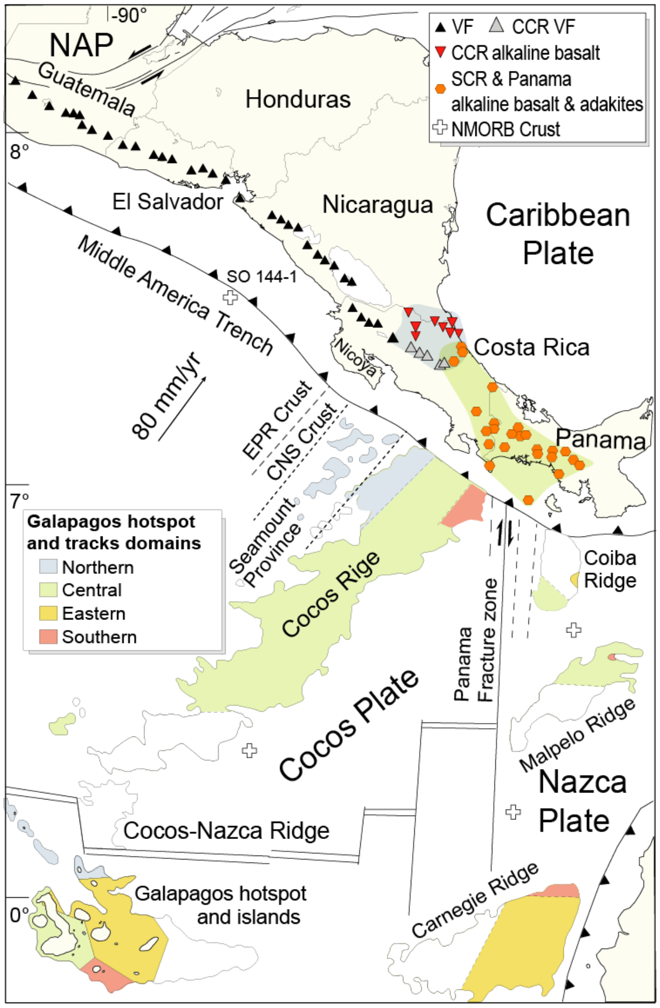

-90°
NAP
Guatemala
Honduras
8°
El Salvador
Nicaragua
Caribbean Plate
VF
CCR VF
CCR alkaline basalt
SCR & Panama alkaline basalt & adakites
NMORB Crust
Middle America Trench
SO 144-1
Nicoya
Costa Rica
80 mm/yr
EPR Crust
CNS Crust
Panama
7°
Galapagos hotspot and tracks domains
Northern
Central
Eastern
Southern
Seamount Province
Cocos Rige
Coiba Ridge
Panama Fracture zone
Cocos Plate
Malpelo Ridge
Nazca Plate
Cocos-Nazca Ridge
Galapagos hotspot and islands
0°
Carnegie Ridge

Figure 2

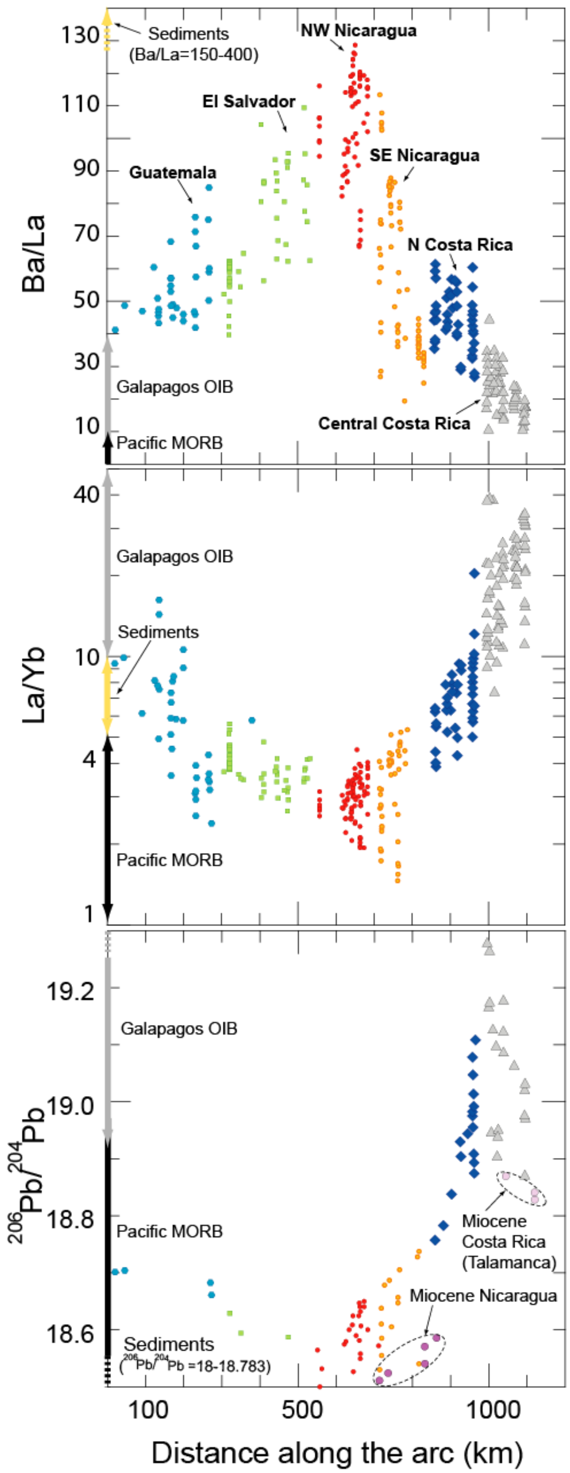

Sediments
(Ba/La=150-400)
NW Nicaragua
El Salvador
Guatemala
SE Nicaragua
N Costa Rica
Galapagos OIB
Pacific MORB
Central Costa Rica
Ba/La
130
110
90
70
50
30
10
La/Yb
40
10
4
1
Sediments
Miocene Costa Rica (Talamanca)
Miocene Nicaragua
Sediments
($^{206}Pb/^{204}Pb$ =18-18.783)
$^{206}Pb/^{204}Pb$
19.2
19.0
18.8
18.6
100
500
1000
Distance along the arc (km)

Figure 3

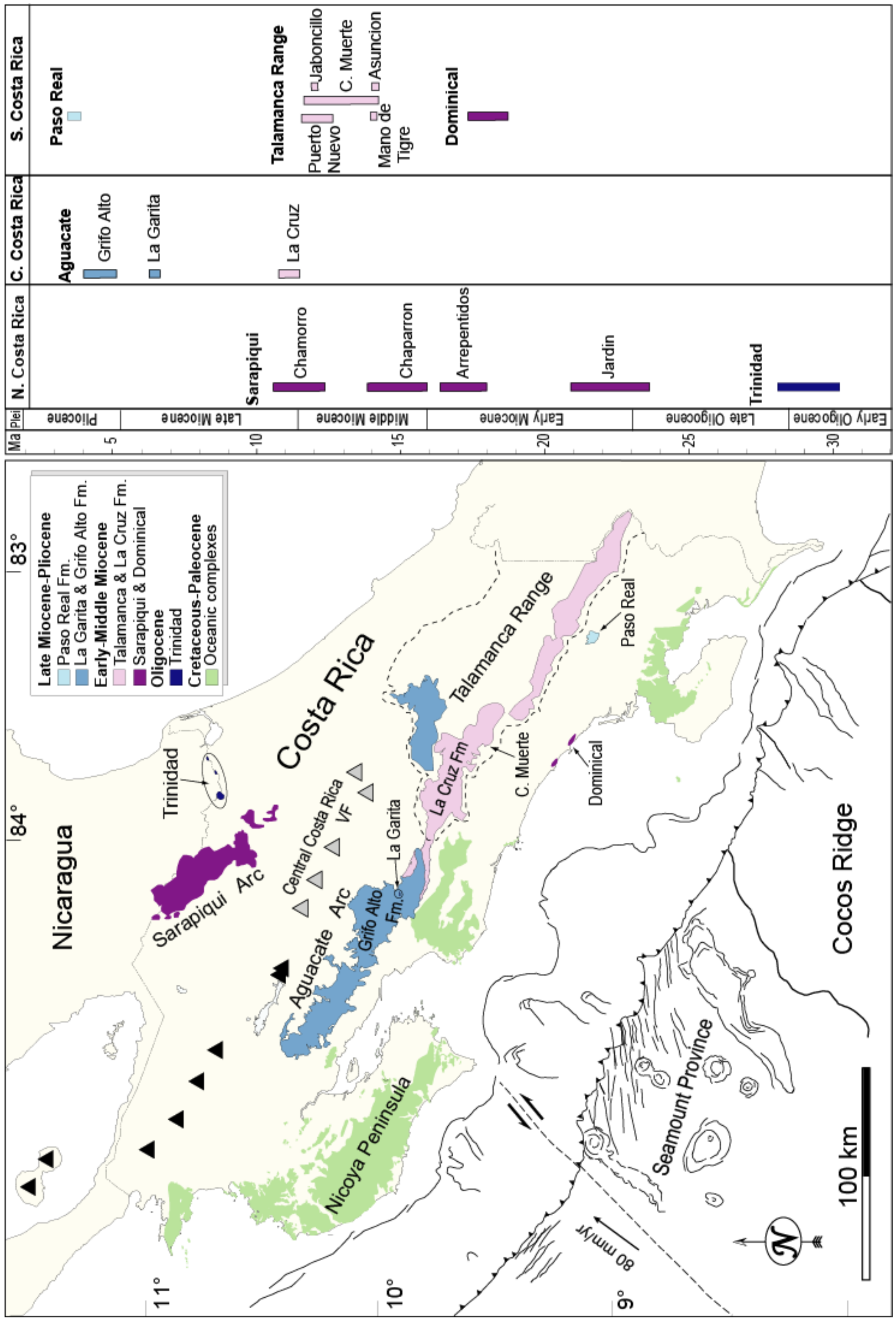
Late Miocene-Pliocene
Paso Real Fm.
La Garita & Grifo Alto Fm.
Early-Middle Miocene
Talamanca & La Cruz Fm.
Sarapiqui & Dominical
Oligocene
Trinidad
Cretaceous-Paleocene
Oceanic complexes
Nicaragua
Costa Rica
Sarapiqui Arc
Trinidad
Central Costa Rica VF
Aguacate Arc
Grifo Alto Fm.
La Garita
La Cruz Fm
Talamanca Range
C. Muerte
Dominical
Paso Real
Nicoya Peninsula
Seamount Province
Cocos Ridge
80 mm/yr
100 km
84°
83°
11°
10°
9°
Ma
Plei
Pliocene
Late Miocene
Middle Miocene
Early Miocene
Late Oligocene
Early Oligocene
5
10
15
20
25
30
N. Costa Rica
Sarapiqui
Chamorro
Chaparron
Arrepentidos
Jardin
Trinidad
C. Costa Rica
Aguacate
Grifo Alto
La Garita
La Cruz
S. Costa Rica
Paso Real
Talamanca Range
Puerto Nuevo
Jaboncillo
C. Muerte
Asuncion
Mano de Tigre
Dominical

Figure 4

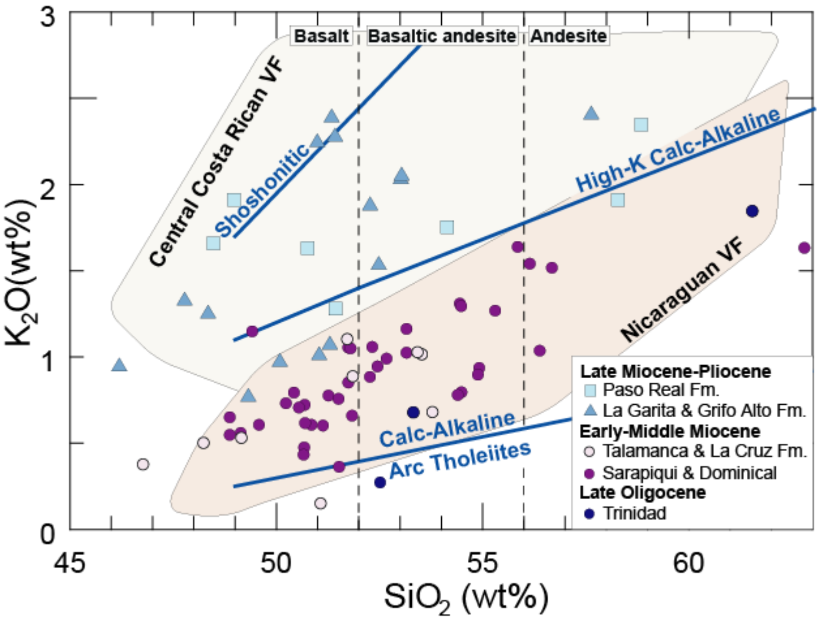
Basalt
Basaltic andesite
Andesite
Central Costa Rican VF
Shoshonitic
High-K Calc-Alkaline
Nicaraguan VF
Calc-Alkaline
Arc Tholeiites
Late Miocene-Pliocene
Paso Real Fm.
La Garita & Grifo Alto Fm.
Early-Middle Miocene
Talamanca & La Cruz Fm.
Sarapiqui & Dominical
Late Oligocene
Trinidad
K2O(wt%)
SiO2 (wt%)
0
1
2
3
45
50
55
60

Figure 5

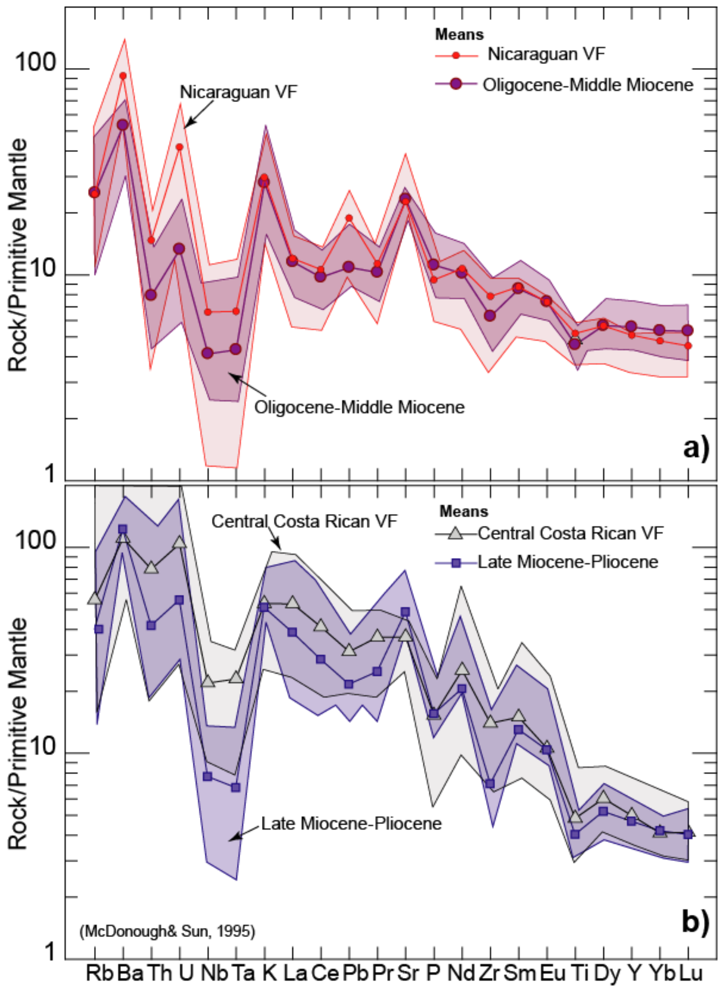
Means
Nicaraguan VF
Oligocene-Middle Miocene
Nicaraguan VF
Oligocene-Middle Miocene
Rock/Primitive Mantle
100
10
1
a)
Central Costa Rican VF
Means
Central Costa Rican VF
Late Miocene-Pliocene
Late Miocene-Pliocene
Rock/Primitive Mantle
(McDonough& Sun, 1995)
b)
Rb Ba Th U Nb Ta K La Ce Pb Pr Sr P Nd Zr Sm Eu Ti Dy Y Yb Lu

Figure 6

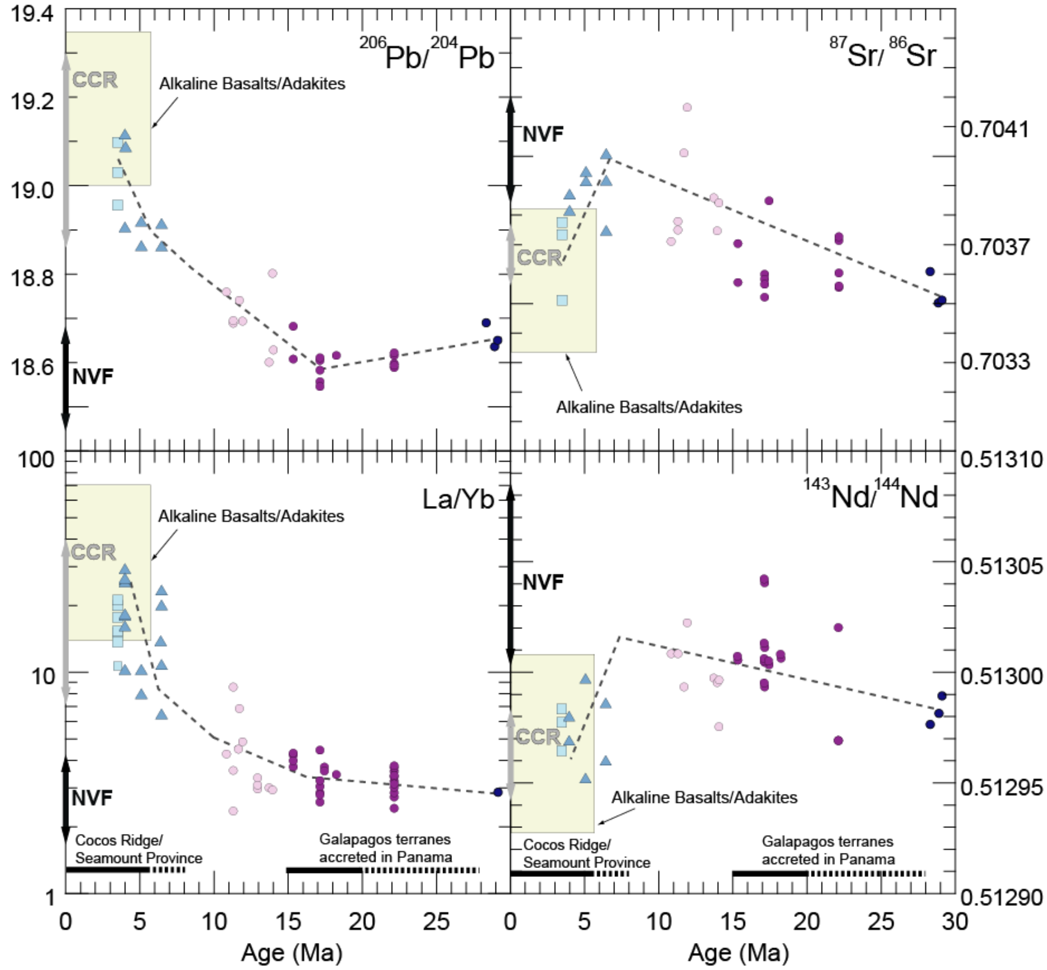

$^{206}Pb/^{204}Pb$
$^{87}Sr/^{86}Sr$
La/Yb
$^{143}Nd/^{144}Nd$
CCR
NVF
Alkaline Basalts/Adakites
Cocos Ridge/ Seamount Province
Galapagos terranes accreted in Panama
Age (Ma)

Figure 7

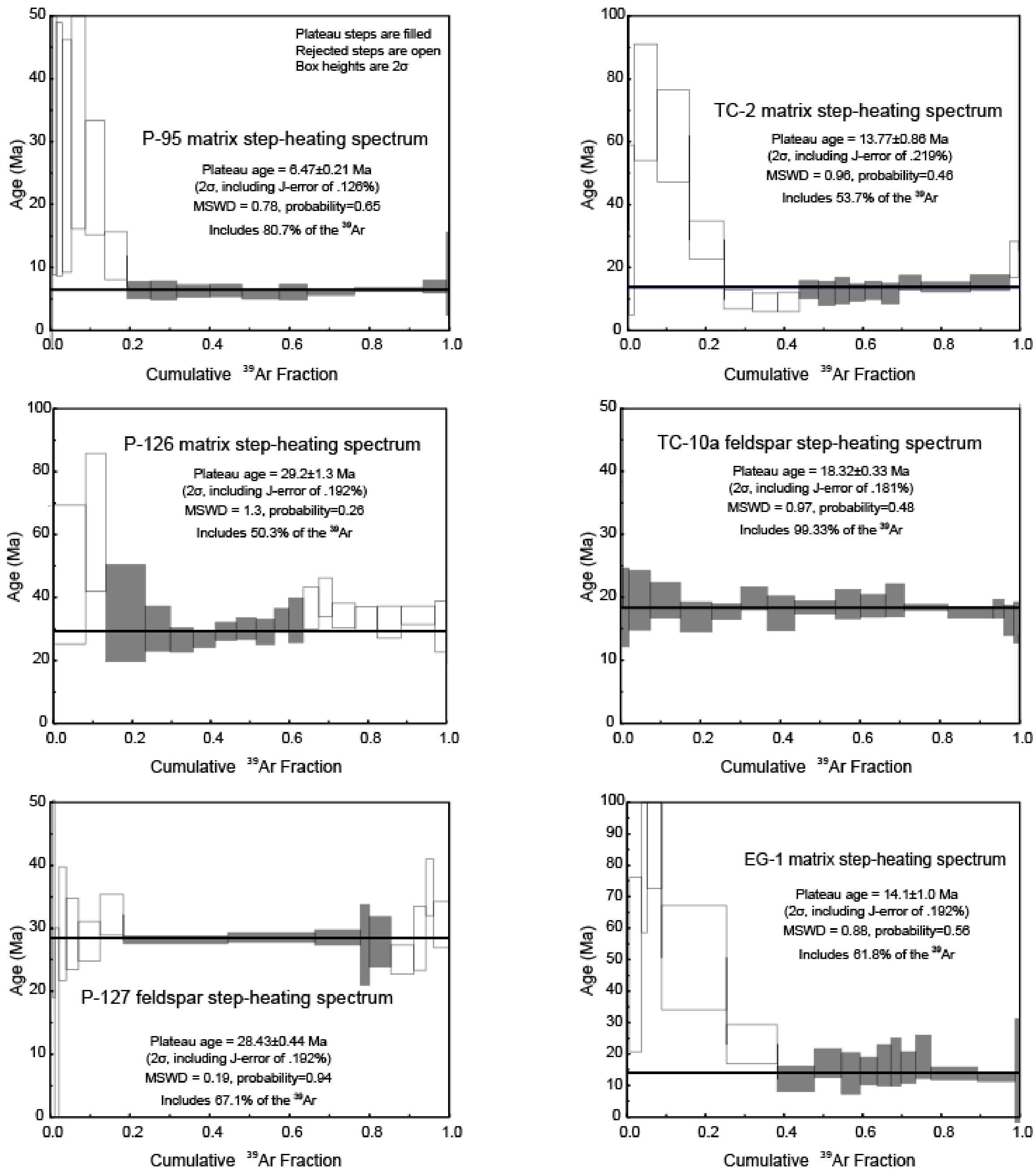

Plateau steps are filled
Rejected steps are open
Box heights are 2σ
P-95 matrix step-heating spectrum
Plateau age = 6.47±0.21 Ma
(2σ, including J-error of .126%)
MSWD = 0.78, probability=0.65
Includes 80.7% of the 39Ar
Age (Ma)
Cumulative 39Ar Fraction
TC-2 matrix step-heating spectrum
Plateau age = 13.77±0.86 Ma
(2σ, including J-error of .219%)
MSWD = 0.96, probability=0.46
Includes 53.7% of the 39Ar
P-126 matrix step-heating spectrum
Plateau age = 29.2±1.3 Ma
(2σ, including J-error of .192%)
MSWD = 1.3, probability=0.26
Includes 50.3% of the 39Ar
TC-10a feldspar step-heating spectrum
Plateau age = 18.32±0.33 Ma
(2σ, including J-error of .181%)
MSWD = 0.97, probability=0.48
Includes 99.33% of the 39Ar
P-127 feldspar step-heating spectrum
Plateau age = 28.43±0.44 Ma
(2σ, including J-error of .192%)
MSWD = 0.19, probability=0.94
Includes 67.1% of the 39Ar
EG-1 matrix step-heating spectrum
Plateau age = 14.1±1.0 Ma
(2σ, including J-error of .192%)
MSWD = 0.88, probability=0.56
Includes 61.8% of the 39Ar

Figure 8

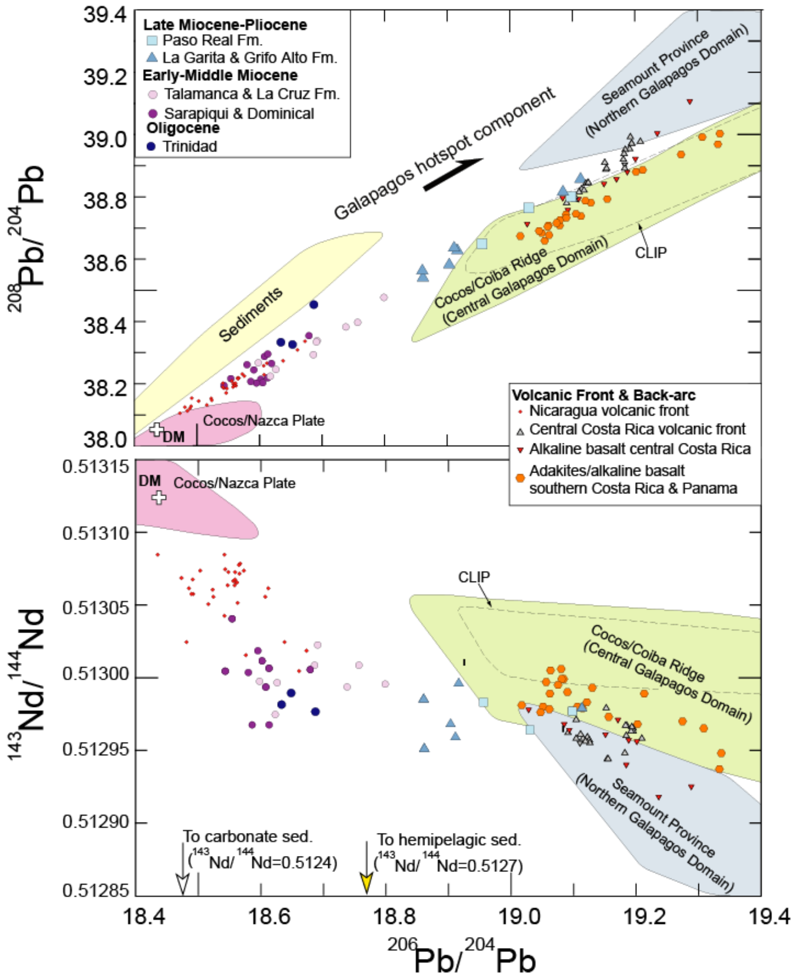

Late Miocene-Pliocene
Paso Real Fm.
La Garita & Grifo Alto Fm.
Early-Middle Miocene
Talamanca & La Cruz Fm.
Sarapiqui & Dominical
Oligocene
Trinidad
Galapagos hotspot component
Seamount Province (Northern Galapagos Domain)
Cocos/Coiba Ridge (Central Galapagos Domain)
CLIP
Sediments
Cocos/Nazca Plate
DM
Volcanic Front & Back-arc
Nicaragua volcanic front
Central Costa Rica volcanic front
Alkaline basalt central Costa Rica
Adakites/alkaline basalt southern Costa Rica & Panama
To carbonate sed. (143Nd/144Nd=0.5124)
To hemipelagic sed. (143Nd/144Nd=0.5127)
208Pb/204Pb
143Nd/144Nd
206Pb/204Pb

Figure 9

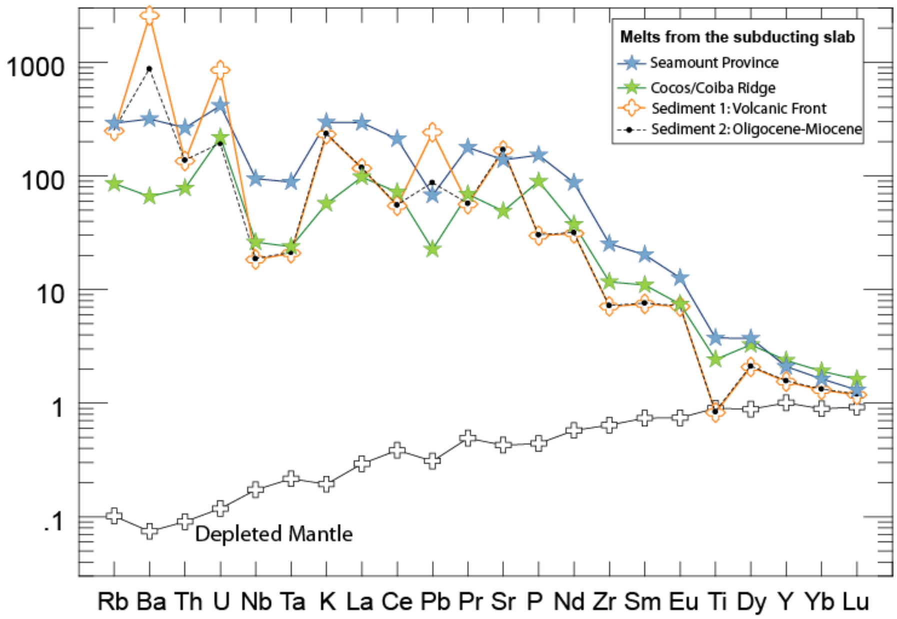
Melts from the subducting slab
Seamount Province
Cocos/Coiba Ridge
Sediment 1: Volcanic Front
Sediment 2: Oligocene-Miocene
1000
100
10
1
.1
Depleted Mantle
Rb Ba Th U Nb Ta K La Ce Pb Pr Sr P Nd Zr Sm Eu Ti Dy Y Yb Lu

Figure 10

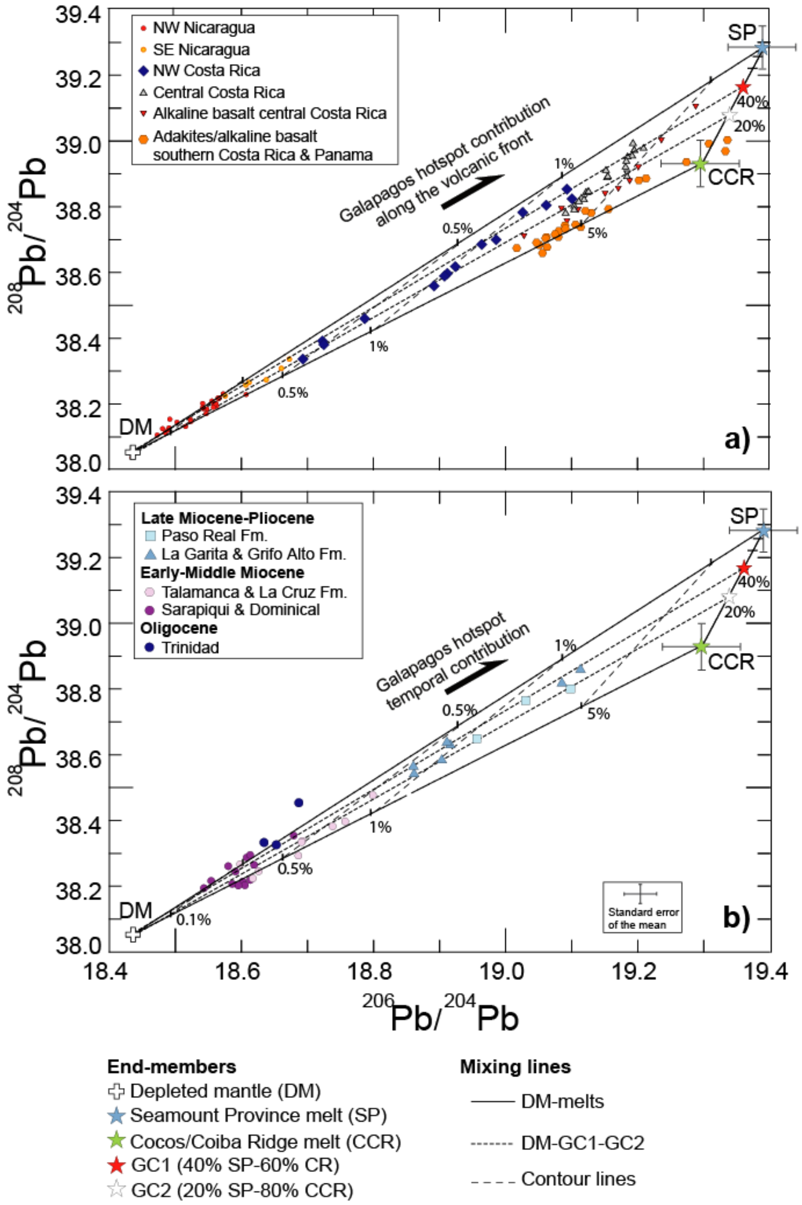

NW Nicaragua
SE Nicaragua
NW Costa Rica
Central Costa Rica
Alkaline basalt central Costa Rica
Adakites/alkaline basalt southern Costa Rica & Panama
Galapagos hotspot contribution along the volcanic front
SP
CCR
DM
40%
20%
1%
0.5%
5%
a)
Late Miocene-Pliocene
Paso Real Fm.
La Garita & Grifo Alto Fm.
Early-Middle Miocene
Talamanca & La Cruz Fm.
Sarapiqui & Dominical
Oligocene
Trinidad
Galapagos hotspot temporal contribution
0.1%
Standard error of the mean
b)
208Pb/204Pb
206Pb/204Pb
End-members
Depleted mantle (DM)
Seamount Province melt (SP)
Cocos/Coiba Ridge melt (CCR)
GC1 (40% SP-60% CR)
GC2 (20% SP-80% CCR)
Mixing lines
DM-melts
DM-GC1-GC2
Contour lines

Figure 11

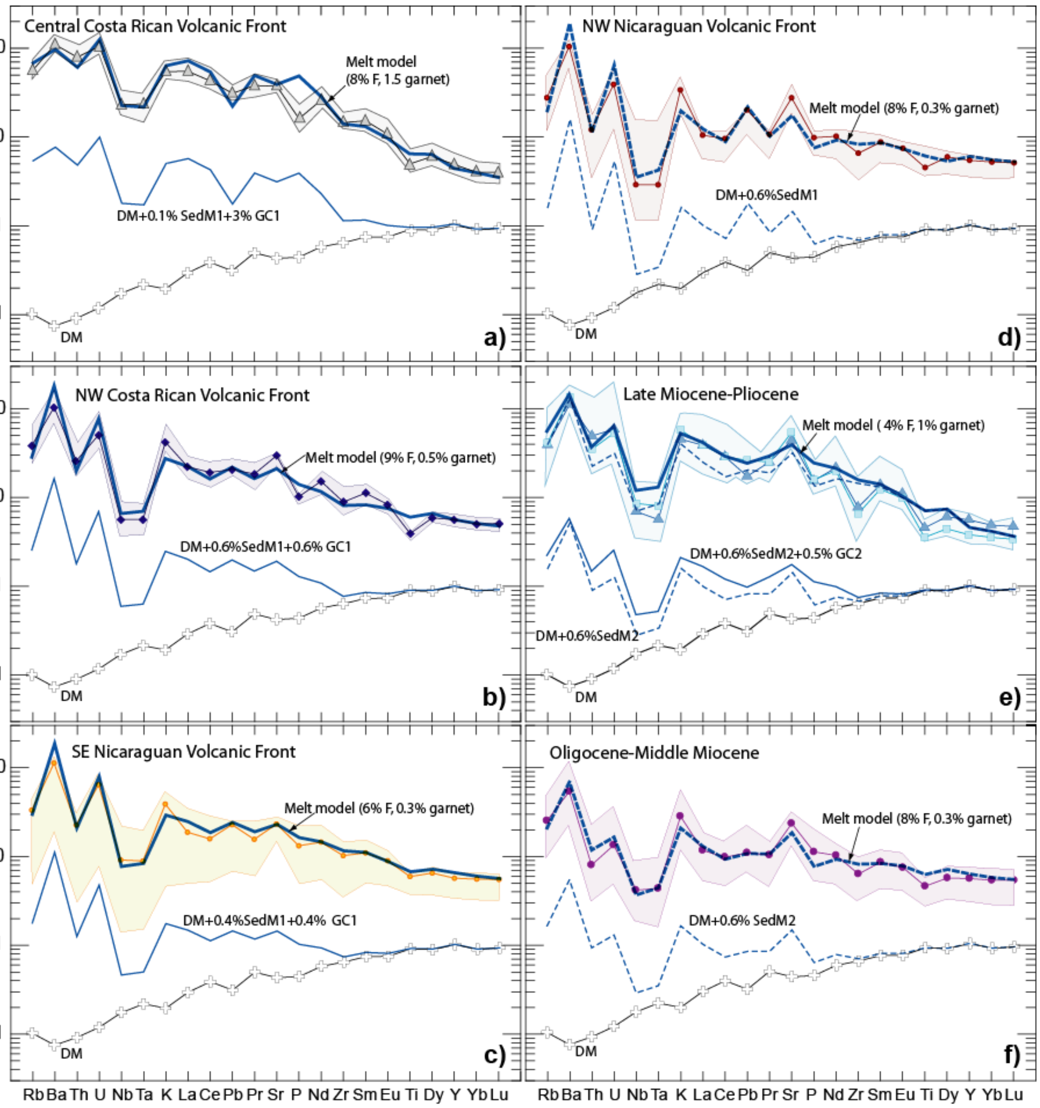

Central Costa Rican Volcanic Front
Melt model
(8% F, 1.5 garnet)
DM+0.1% SedM1+3% GC1
DM
a)
NW Nicaraguan Volcanic Front
Melt model (8% F, 0.3% garnet)
DM+0.6%SedM1
DM
d)
NW Costa Rican Volcanic Front
Melt model (9% F, 0.5% garnet)
DM+0.6%SedM1+0.6% GC1
DM
b)
Late Miocene-Pliocene
Melt model (4% F, 1% garnet)
DM+0.6%SedM2+0.5% GC2
DM+0.6%SedM2
DM
e)
SE Nicaraguan Volcanic Front
Melt model (6% F, 0.3% garnet)
DM+0.4%SedM1+0.4% GC1
DM
c)
Oligocene-Middle Miocene
Melt model (8% F, 0.3% garnet)
DM+0.6% SedM2
DM
f)
100
10
1
.1
Rb Ba Th U Nb Ta K La Ce Pb Pr Sr P Nd Zr Sm Eu Ti Dy Y Yb Lu

Table 1

Sample	Unit	Age (Ma)	Lat	Lon	Lit.	SiO2	TiO2	Al2O3	Fe2O3	MnO	MgO	CaO	Na2O	K2O	P2O5	Tot	LOI	Cr	Ni	Cu	Zn	Rb	Sr
Tinidad																							
P-125	Trinidad		10.7142	-83.9347	ba	52.43	0.9	19.26	9.14	0.16	3.9	9.86	2.71	0.66	0.2	99.33	0.81	30	18	76	71	11	388
P-126		29.20±1.3	10.7252	-83.8855	ba	51.25	0.93	18.68	9.93	0.24	4.04	10.58	2.45	0.26	0.19	98.71	1.21	-	-	-	-	-	-
P-127		28.43±0.44	10.7501	-83.8341	a	60.56	0.68	15.92	7.02	0.18	3.36	6.47	2.94	1.81	0.15	99.25	0.69	-	-	-	-	-	-
Sarapiqui																							
BT-020406-2	Jardin	22.20±1.15*	10.6826	-84.2249	b	47.07	0.87	19.53	10.03	0.16	4.61	10.79	2.12	0.57	0.16	95.91	3.96	89	31	185	66	9	495
IN-020506-1			10.7872	-84.3425	b	49.36	0.98	17.84	10.06	0.16	4.81	9.29	2.63	1	0.24	96.37	3.5	110	41	152	73	18	471
IN-020506-2			10.7652	-84.293	b	50.33	0.92	17.01	9.76	0.2	5.44	9.09	2.6	0.94	0.21	96.5	3.36	112	65	147	68	18	439
IN-020506-3			10.7872	-84.3425	b	50.65	1.01	17.88	10.58	0.19	4.95	9.58	2.7	1.02	0.25	98.81	1.05	102	44	143	74	21	467
IN-020506-5			10.7564	-84.2726	b	47.79	1.06	17.79	11.27	0.19	5.27	9.36	2.6	0.69	0.22	96.24	3.64	100	41	183	77	12	503
IN-020506-6			10.7566	-84.2718	b	49.35	1.15	17.54	12.24	0.22	5.25	9.52	2.78	0.77	0.24	99.06	0.82	97	38	190	81	15	497
IN-020506-7			10.7568	-84.2729	b	48.33	1.15	16.98	12.05	0.2	5.31	9.1	2.76	0.67	0.24	96.79	3.08	100	37	201	82	14	500
IN-020506-8			10.7729	-84.2749	b	48.07	0.89	18.63	8.72	0.18	3.38	8.87	2.68	0.86	0.21	92.49	7.38	-	-	-	-	-	-
IN-020806-1			10.7446	-84.2611	b	45.84	0.79	15.97	8.53	0.15	5.17	8.85	2.25	0.77	0.21	88.53	11.32	113	43	112	63	24	431
IN-020806-2			10.7702	-84.2214	b	44.17	0.62	20.68	7.69	0.15	4.17	11.19	1.82	0.49	0.14	91.12	8.78	131	44	96	51	8	523
IN-020806-3			10.7789	-84.201	b	48.58	0.94	16.79	10.12	0.18	7.95	9.37	2.34	0.41	0.2	96.88	2.98	-	123	99	62	0	364
IN-020806-4			10.7739	-84.2115	b	46.19	0.7	20.88	7.99	0.19	4.61	11.55	1.98	0.52	0.16	94.77	5.11	137	46	108	53	7	521
IN-020806-5			10.7438	-84.2457	b	48.24	0.85	16.7	9.18	0.18	5.4	9	2.34	0.97	0.22	93.08	6.81	144	58	54	67	20	428
PS-020706-1			10.9108	-84.3835	b	47.19	0.88	18.14	9.52	0.18	4.39	9.63	2.55	0.55	0.19	93.22	6.66	95	34	156	69	6	468
PS-020706-2			10.9342	-84.3598	b	50.53	0.91	17.82	8.39	0.15	3.06	8.14	2.87	0.82	0.19	92.88	6.99	94	22	117	69	16	403
AR-020206-1	Arrepentidos	17.20±0.80*	10.4598	-84.0283	b	49.27	1.01	19.37	10.09	0.22	3.74	9.61	2.83	0.74	0.21	97.09	2.77	-	27	201	74	12	494
AR-020206-2			10.463	-84.0284	b	49.38	1	19.39	10.02	0.18	3.73	9.42	2.8	0.72	0.21	96.85	3	103	27	155	71	11	490
AR-020206-3			10.4688	-84.0297	b	49.6	1	18.25	9.9	0.34	4.31	9.78	2.61	0.81	0.22	96.82	3.04	114	38	117	70	13	439
AR-020206-4			10.4743	-84.0301	b	49.99	0.98	17.96	11.92	0.2	5.09	9.99	2.56	0.59	0.19	99.47	0.41	96	31	243	72	9	469
AR-020206-5			10.477	-84.0331	ba	49.21	1.01	18.21	10.44	0.25	3.86	9.37	2.78	0.62	0.2	95.95	3.93	91	25	131	69	10	484
AR-020206-6			10.4791	-84.0358	ba	53.14	1.04	17.53	9.72	0.22	3.71	7.74	3.42	0.9	0.29	97.71	2.17	89	21	33	82	16	496
AR-020206-7			10.4905	-84.0399	ba	55.29	0.97	17.81	8.87	0.26	3.19	7.5	3.69	1.01	0.33	98.92	0.95	85	21	38	83	19	496
AR-020206-8			10.4655	-84.0084	ba	54.76	0.9	17.48	8.68	0.15	4.04	8.45	2.6	1.6	0.23	98.89	0.96	102	36	126	61	38	439
CH-020406-1	Chaparron	15.40±0.6*	10.5501	-84.2084	ba	54.9	0.89	17.42	8.69	0.17	3.88	8.37	2.56	1.5	0.25	98.63	1.23	85	27	85	65	26	446
CH-020406-2			10.5501	-84.2084	ba	50.61	0.88	19.34	8.35	0.32	3.14	9.34	2.85	0.97	0.22	96.02	3.83	100	30	124	60	16	503
CH-020406-3			10.5501	-84.2084	ba	52.25	0.87	16.43	8.71	0.16	5.42	9.07	2.4	1.25	0.25	96.81	3.05	-	-	-	-	-	-
CH-020406-4			10.5501	-84.2084	ba	53.27	0.88	16.58	8.96	0.17	5.53	9.32	2.43	1.26	0.25	98.65	1.2	181	58	109	62	28	417
CH-020406-5			10.5831	-84.1805	ba	60.64	0.73	15.91	6.18	0.14	2.68	5.58	3.53	1.57	0.2	97.16	2.71	88	25	51	56	29	365
CH-020406-6			10.5392	-84.2192	a	55.54	0.9	17.45	8.26	0.17	3.83	8.34	2.57	1.48	0.25	98.79	1.07	-	-	-	-	-	-
BT-020406-3	Hito Sar	-	10.6859	-84.2116	ab	53.18	1	17.9	9.55	0.23	3.9	7.92	3.65	0.77	0.43	98.53	1.34	74	19	10	86	12	613
BT-020406-5			10.7316	-84.2032	di	50.49	0.69	15.42	10	0.17	9.02	10.77	1.95	0.35	0.11	98.97	0.93	372	105	111	60	6	262
BT-020406-6			10.7571	-84.1886	ab	48.64	0.85	16.83	10.45	0.17	7.4	9.74	2.3	0.45	0.17	97	2.86	270	103	112	112	6	363
BT-020406-7			10.6773	-84.2371	di	49.53	0.85	20.34	8.35	0.14	4.8	10.98	2.63	0.7	0.21	98.53	1.36	124	49	147	55	12	528
BT-020406-8			10.6683	-84.197	ab	52.04	0.98	17.66	9.29	0.22	3.86	7.77	3.59	0.74	0.42	96.57	3.3	83	20	11	84	11	610
IN-020506-4			10.7522	-84.2918	ab	51.94	1	17.54	11.02	0.2	4.52	8.23	2.97	1.13	0.24	98.79	1.06	87	24	108	80	22	480
BT-020406-10			10.6683	-84.2417	di	48.14	0.96	17.93	10.5	0.18	5.1	9.93	2.46	0.58	0.2	95.98	3.91	95	35	161	73	11	470
BT-020406-9	Boca Tapada	-	10.6683	-84.2417	gb	52.17	1.13	15.84	10.34	0.19	3.59	7.25	3.33	1.19	0.31	95.34	4.53	83	26	154	79	22	407
PS-020706-3	Chamorro	11.40±0.90*	10.9554	-84.391	a	56.08	0.56	16.17	6.2	0.1	2.6	6.02	3.24	0.86	0.16	91.99	7.91	-	-	-	-	-	-
Talamanca																							
TA-021206-3	C. Asuncion	14.10±1.0	9.5829	-83.7634	b	46.08	0.75	18.39	9.53	0.17	3.64	10.21	2.08	0.13	0.17	91.15	8.71	82	24	180	76	0	654
TA-021206-4			9.5761	-83.7604	ob	44.18	0.64	13.86	12.4	0.2	10.92	11.68	1.34	0.35	0.11	95.68	4.21	172	79	151	67	4	444
EG-1			9.5761	-83.7604	ob	-	-	-	-	-	-	-	-	-	-	-	-	93	53	105	74	4	513
TA-021206-6	C. Muerte	10.5±0.9 to 13.00±0.20**	9.5732	-83.9109	di	48.56	0.72	16.32	10.1	0.2	5.58	9.53	2.66	1.03	0.18	94.88	4.95	97	32	83	45	15	537
TC-1	C. Jaboncillo	11.98±0.06**	9.6019	-83.788	d	65.44	0.42	14.41	3.98	0.1	1.03	3.42	3.59	2.73	0.11	98.5	3.27	2	2	43	52	87	399
TC-2	C. Muerte	13.77±0.86	9.4646	-83.7095	b (dike)	51.07	0.81	18.24	9.5	0.17	3.94	8.94	2.41	0.64	0.16	98.73	2.85	7	6	96	72	8	572
TC-4	Mano de Tigre	14.1±0.15**	9.032	-83.2911	b	47.73	0.86	20.56	10.68	0.19	3.98	11.19	2.3	0.51	0.15	99.09	0.94	3	6	140	80	4	545

Table 1 continued

Sample	Unit	Age (Ma)	Lat	Lon	Lit.	SiO2	TiO2	Al2O3	Fe2O3	MnO	MgO	CaO	Na2O	K2O	P2O5	Tot	LOI	Cr	Ni	Cu	Zn	Rb	Sr
TC-9	Puerto Nuevo Fm.	11.76±0.12**	8.965	-83.4374	b (dike)	-	-	-	-	-	-	-	-	-	-	-	-	8	11	212	45	33	686
Paso Real																							
GE-021306-4	Paso Real Fm.	3.59±0.06 to 3.65±0.30**	9.073	-83.2916	a	56.16	0.63	17.05	6.3	0.11	3.48	6.59	3.26	2.24	0.26	96.08	3.66	93	38	167	58	37	1014
GE-021306-5			9.073	-83.2916	b	46.12	0.75	18.6	10.37	0.25	5.17	9.31	2.4	1.8	0.46	95.23	4.53	76	26	197	72	41	941
GE-021306-6			9.0657	-83.2902	b	47.04	0.72	17.03	9.73	0.2	5.51	9.05	2.55	1.51	0.32	93.66	6.1	98	36	177	70	22	988
GE-021306-7			9.0426	-83.3004	ba	55.82	0.63	17.65	6.69	0.12	3.34	6.82	3.3	1.83	0.25	96.45	3.32	82	30	152	63	28	892
GE-021306-8			9.0369	-83.2868	ba	51.62	0.67	18.01	8.45	0.17	4.02	8.16	3.07	1.67	0.36	96.2	3.52	94	30	210	76	24	1105
GE-021306-9			9.065	-83.3179	ba	44.16	0.87	16.51	10.25	0.22	6	9.96	2.27	1.51	0.39	92.14	7.51	99	33	220	74	8	1629
GE-021306-10			9.0803	-83.2834	ba	49.09	0.78	18.01	9.66	0.18	4.96	9.5	2.73	1.22	0.29	96.42	3.36	82	29	207	72	15	1028
Dominical																							
DO-021406-1	Dominical	17.50±0.10**	9.2061	-83.8015	gb	44.15	1.12	15.28	12.09	0.17	4.62	9.21	2.68	1.02	0.19	90.53	9.3	99	27	490	68	17	417
DO-021406-2			9.1399	-83.7208	gb	44.78	0.77	19.72	9.56	0.16	4	10.75	2.1	0.59	0.13	92.56	7.3	93	28	242	74	7	556
TC-10a		18.32±0.33**	9.1358	-83.7177	a (dike)	-	-	-	-	-	-	-	-	-	-	-	-	2.33	7	390	119	30	477
Aguacate																							
CA-021106-1	La Cruz Fm.	10.90±0.10-11.35±0.10**	9.7944	-84.2116	b	45.73	0.86	18.03	10.79	0.17	6	11.64	2.02	0.47	0.15	95.86	3.98	95	47	195	63	4	528
CA-021106-2			9.793	-84.2344	ba	49.87	1.45	14.13	13.34	0.31	3.6	7.47	3.09	0.94	0.28	94.48	5.34	106	21	157	114	13	376
CA-021106-3			9.7932	-84.2385	ab	49.17	1.43	14.31	13.21	0.25	3.61	7.12	3.02	0.94	0.28	93.34	6.47	75	20	143	112	13	374
CA-021106-4			9.8027	-84.1934	b	49.4	0.7	17.58	9.45	0.18	5.17	10.53	2.22	0.84	0.12	96.19	3.65	106	39	168	60	15	479
CA-021106-5	Grifo Alto Fm.	5.10±0.10-4.04±0.04**	9.8507	-84.3799	b	47.03	0.8	19.03	10.84	0.18	4.92	10.31	2.37	0.73	0.24	96.45	3.38	96	32	158	67	10	802
CA-021106-6			9.8507	-84.3799	ba	49.62	0.84	19.4	10.34	0.2	3.97	10.03	2.62	0.98	0.27	98.27	1.54	83	22	172	70	15	850
CA-021106-7			9.8589	-84.3813	ba	48.58	0.85	19.23	10.8	0.2	4.67	9.9	2.6	0.94	0.32	98.09	1.7	89	29	152	70	12	883
CA-021106-8			9.8756	-84.3842	ba	49.91	0.75	18.28	10.31	0.18	5.08	9.85	2.72	1.04	0.22	98.34	1.41	-	-	-	-	-	-
ACZ			10.0864	-84.436		51.78	0.82	18.26	9.34	0.18	3.93	8.81	3.09	1.98	0.42	98.61	1.13	-	-	118	69	37	980
CLC-1			10.057	-84.4556	b	50.99	0.87	18.78	8.93	0.15	4.11	9.87	2.62	1.83	0.3	98.45	1.28	-	-	177	65	28	1228
CC-1			10.0406	-84.4142	b	49.95	0.85	18.18	9.53	0.17	4.41	9.97	2.45	2.21	0.38	98.1	1.63	-	-	14	66	40	1046
CC-2			10.0406	-84.4142	b (dike)	49.13	0.84	18.14	9.86	0.17	4.59	9.7	2.38	2.16	0.38	97.35	2.36	-	-	244	69	38	1046
CA-1			10.0272	-84.4072	b	51.77	0.82	18.61	9.13	0.18	3.71	8.84	3.05	2	0.43	98.54	1.22	-	-	122	68	36	992
FR-1			10.0524	-84.4584	b	51.06	0.82	18.1	9.93	0.19	4.51	9.33	2.62	1.49	0.25	98.3	1.5	-	-	146	66	29	813
SM-1			10.066	-84.4123	a	55.16	0.64	14.78	6.19	0.14	5.51	8.21	2.91	2.3	0.5	96.34	3.35	177	89	97	52	56	1106
LG-040105-1	La Garita Fm.	6.47±0.21	9.9879	-84.3467	ob (sill)	43.06	1.1	14.89	12.9	0.19	8.37	12.11	2.26	0.65	0.33	95.86	3.87	79	70	152	74	25	1393
LG-040105-2			9.9879	-84.3467	b (dke)	49.49	1.05	17.83	10.3	0.24	3.9	8.62	3.22	2.3	0.49	97.44	2.31	-	-	165	76	42	905
LC-010405-3			10.0739	-84.4509	b	46.85	0.86	17.53	11.19	0.17	6.71	11.37	1.89	1.21	0.26	98.04	1.77	-	-	90	63	20	861
LC-1			10.0725	-84.4511	b (dike)	44.63	0.92	16.2	12.45	0.21	8.68	11.55	1.84	0.91	0.49	97.88	1.88	79	30	190	73	36	1095
P-95			9.9865	-84.3446	ob (sill)	46.18	1.03	17.87	11.46	0.19	6.46	10.73	2.33	1.28	0.29	98.06	1.79	35.66	38	173	85	30	869
Standards																							
JB-1a						51.68	1.25	14.2	8.8	0.14	7.78	9.17	2.66	1.4	0.26	97.34	2.47	336	134	54	69	36	428
JB-1a						51.91	1.27	14.32	8.87	0.15	7.84	9.25	2.67	1.41	0.26	97.95	1.86	356	136	62	69	37	435
JB-1a						52.05	1.26	14.25	8.87	0.14	7.83	9.24	2.63	1.41	0.26	97.94	1.89	331	136	63	69	37	435
JB-1a						51.77	1.24	14.15	8.79	0.14	7.78	9.16	2.62	1.4	0.27	97.32	2.5	327	133	53	68	37	430

Table 2

Sample	V	Y	Zr	Nb	Ba	La	Ce	Pr	Nd	Sm	Eu	Gd	Tb	Dy	Ho	Er	Yb	Lu	Hf	Ta	Pb	Th	U
Trinidad																							
P-125	261.22	22.65	65.57	2.77	227.72	6.93	15.36	2.56	11.85	3.19	1.02	3.62	0.61	3.89	0.81	2.32	2.43	0.37	1.78	0.17	1.80	0.64	0.27
Sarapiqui																							
BT-020406-2	299.71	19.14	45.43	1.62	231.12	5.06	11.44	1.88	9.60	2.76	0.93	3.00	0.46	3.10	0.60	1.84	1.87	0.27	1.28	0.09	1.32	0.38	0.12
IN-020506-1	272.78	24.99	69.33	2.90	365.48	8.30	17.86	2.85	13.82	3.74	1.18	3.96	0.61	4.03	0.76	2.34	2.35	0.36	1.85	0.17	1.49	0.70	0.22
IN-020506-2	258.14	30.26	70.52	2.88	322.48	7.86	16.96	2.72	13.44	3.68	1.14	3.93	0.60	3.94	0.79	2.45	2.42	0.37	1.90	0.17	1.52	0.76	0.33
IN-020506-3	279.96	25.77	69.94	2.95	369.89	8.78	18.97	3.00	14.45	3.85	1.22	4.16	0.64	4.07	0.78	2.43	2.42	0.38	1.86	0.16	1.54	0.71	0.24
IN-020506-4	283.62	28.46	76.69	2.76	418.93	8.71	18.07	2.88	14.12	3.93	1.28	4.17	0.66	4.31	0.86	2.68	2.76	0.43	1.97	0.16	2.21	0.78	0.26
IN-020506-5	293.59	26.06	61.48	2.19	255.42	7.87	17.01	2.80	13.72	3.70	1.18	4.00	0.63	4.16	0.81	2.51	2.59	0.40	1.70	0.12	1.28	0.54	0.14
IN-020506-6	312.40	26.61	66.45	2.39	273.89	8.30	17.83	2.97	14.53	3.86	1.22	4.13	0.65	4.25	0.83	2.59	2.60	0.39	1.84	0.13	1.42	0.59	0.18
IN-020506-7	309.91	26.66	68.57	2.44	286.66	8.72	18.85	3.11	15.11	3.97	1.26	4.31	0.65	4.35	0.84	2.64	2.65	0.39	1.81	0.13	1.29	0.58	0.27
IN-020806-1	228.29	24.58	72.00	2.82	378.05	8.66	18.45	2.97	13.43	3.80	1.16	3.93	0.64	3.85	0.75	2.23	2.36	0.37	2.11	0.20	1.55	0.82	0.41
IN-020806-2	206.86	15.35	37.23	2.23	203.45	4.31	10.14	1.55	7.85	2.18	0.80	2.41	0.36	2.39	0.46	1.46	1.44	0.22	1.11	0.17	1.62	0.41	0.18
IN-020806-3	249.02	19.80	61.00	4.76	223.87	6.85	14.42	2.14	10.26	2.69	0.98	2.99	0.48	3.03	0.61	1.79	1.83	0.28	1.47	0.27	1.10	0.41	0.18
IN-020806-4	319.44	28.17	92.77	6.04	325.03	9.25	19.81	3.10	15.00	4.04	1.36	4.29	0.69	4.41	0.87	2.69	2.73	0.42	2.25	0.36	1.74	0.57	0.18
IN-020806-5	171.77	13.67	33.69	1.22	180.38	3.97	8.97	1.39	7.07	2.06	0.68	2.19	0.32	2.27	0.41	1.25	1.28	0.19	0.89	0.06	0.87	0.27	0.1
PS-020706-1	267.88	23.79	55.45	1.71	313.82	6.28	13.78	2.30	11.50	3.28	1.09	3.66	0.57	3.71	0.72	2.28	2.22	0.35	1.53	0.10	1.40	0.48	0.16
PS-020706-2	220.03	22.73	77.98	4.48	419.39	7.71	17.11	2.54	12.01	3.24	1.09	3.44	0.55	3.57	0.69	2.23	2.31	0.35	2.04	0.27	1.90	0.79	0.23
AR-020206-1	311.39	22.92	-	2.11	298.16	7.21	15.22	2.37	11.63	3.09	1.12	3.34	0.54	3.49	0.69	2.09	2.25	0.34	1.35	0.12	1.46	0.53	0.29
AR-020206-2	291.02	24.12	55.45	2.04	300.08	6.96	15.30	2.48	12.17	3.34	1.15	3.62	0.57	3.66	0.71	2.28	2.30	0.36	1.47	0.11	1.29	0.59	0.29
AR-020206-3	297.66	28.33	63.02	2.75	333.10	7.42	15.96	2.58	12.45	3.49	1.14	3.91	0.61	4.16	0.86	2.70	2.89	0.47	1.71	0.16	1.89	0.72	0.2
AR-020206-4	350.81	20.79	47.39	1.82	205.09	5.65	12.46	2.04	10.36	2.88	1.01	3.21	0.49	3.29	0.64	1.98	2.00	0.31	1.33	0.12	1.55	0.44	0.19
AR-020206-5	316.42	24.25	54.87	2.15	262.15	6.26	13.51	2.23	11.18	3.14	1.06	3.41	0.53	3.68	0.71	2.27	2.26	0.34	1.46	0.12	1.38	0.40	0.2
AR-020206-6	194.65	29.87	73.79	2.81	349.87	9.07	19.54	3.26	15.91	4.26	1.39	4.69	0.73	4.72	0.94	2.89	3.00	0.47	1.95	0.16	1.82	0.62	0.39
AR-020206-7	152.32	29.24	79.75	3.71	386.43	9.70	20.84	3.45	16.61	4.39	1.44	4.73	0.73	4.66	0.91	3.00	3.02	0.46	2.09	0.23	2.59	0.71	0.39
AR-020206-8	223.76	27.49	123.88	3.84	470.59	11.68	24.52	3.80	17.11	4.24	1.14	4.38	0.70	4.26	0.82	2.61	2.65	0.41	3.11	0.25	2.83	1.68	0.74
CH-020406-1	229.53	25.61	96.37	3.65	462.38	10.48	21.94	3.37	16.13	4.45	1.31	4.17	0.65	4.10	0.79	2.42	2.50	0.38	2.45	0.22	2.23	1.07	0.47
CH-020406-2	229.85	27.00	81.46	2.90	395.35	9.26	19.45	3.06	14.31	3.71	1.19	4.03	0.61	4.06	0.78	2.45	2.50	0.39	2.07	0.17	1.63	0.85	0.39
CH-020406-4	228.46	25.51	94.63	3.37	410.31	9.80	20.87	3.25	15.14	3.95	1.17	4.13	0.64	4.07	0.78	2.41	2.48	0.37	2.39	0.20	2.15	1.05	0.38
CH-020406-5	150.01	26.02	126.79	4.67	631.70	12.18	25.09	3.69	16.30	4.14	1.17	4.20	0.66	4.14	0.81	2.57	2.85	0.45	3.17	0.31	3.14	1.54	0.49
BT-020406-3	145.25	31.42	67.21	2.25	314.88	7.84	18.47	3.17	16.57	4.75	1.68	5.18	0.81	5.24	1.03	3.17	3.24	0.48	1.81	0.12	1.94	0.54	0.42
BT-020406-5	229.46	15.90	39.54	1.49	147.70	3.44	7.88	1.18	6.04	1.79	0.65	2.12	0.34	2.48	0.47	1.49	1.51	0.24	1.01	0.08	1.03	0.25	0.14
BT-020406-6	272.67	20.09	55.88	2.42	216.39	5.50	12.03	1.89	9.31	2.62	0.92	2.94	0.47	3.16	0.61	1.91	1.94	0.30	1.42	0.14	1.99	0.35	0.16
BT-020406-7	253.07	18.53	55.57	2.40	265.20	6.38	14.27	2.20	10.86	2.87	1.03	3.00	0.45	2.96	0.55	1.72	1.76	0.26	1.44	0.21	2.61	0.50	0.35
BT-020406-8	146.38	30.83	65.01	2.17	304.22	7.46	17.39	2.99	15.69	4.49	1.62	5.01	0.78	5.02	0.98	3.10	3.10	0.47	1.80	0.11	1.54	0.50	0.16
BT-020406-9	237.24	31.95	100.44	3.60	447.33	10.56	22.69	3.70	17.72	4.79	1.45	5.21	0.83	5.13	1.01	3.05	3.12	0.48	2.65	0.22	1.49	1.07	0.31
BT-020406-10	279.91	22.42	52.00	1.87	246.36	5.95	13.30	2.15	11.02	3.21	1.07	3.47	0.54	3.60	0.70	2.12	2.13	0.34	1.42	0.11	1.28	0.48	0.21
Talamanca																							
TC-1	50.61	26.83	203.11	6.50	1560.60	14.52	31.22	4.38	17.55	4.07	0.68	4.13	0.67	4.28	0.90	2.67	3.02	0.47	5.32	0.36	7.51	4.85	2.43
TA-021206-3	247.62	20.67	28.00	1.29	255.38	5.92	12.76	2.10	10.23	2.98	1.06	3.15	0.52	3.32	0.67	2.02	2.01	0.31	1.15	0.03	1.11	0.42	0.32
TA-021206-4	295.39	14.04	17.00	0.71	297.47	4.20	8.90	1.45	7.15	2.14	0.79	2.27	0.39	2.42	0.48	1.46	1.37	0.19	0.71	0.02	0.89	0.34	0.18
EG-1	342.04	14.08	24.07	0.69	339.46	4.46	9.80	1.67	8.10	2.31	0.66	2.57	0.42	2.56	0.51	1.40	1.35	0.20	0.77	0.04	0.92	0.41	0.23
TA-021206-6	253.92	21.28	57.00	2.01	718.08	9.22	18.39	2.90	12.73	3.49	1.10	3.52	0.57	3.51	0.69	2.01	2.07	0.32	1.67	0.11	0.81	0.90	0.53
TC-2	265.89	17.74	34.63	1.36	391.84	5.42	12.42	1.99	9.51	2.62	0.95	2.97	0.48	3.09	0.64	1.82	1.82	0.27	1.08	0.08	1.42	0.53	0.3
TC-4	315.08	16.61	33.54	1.51	406.87	4.98	11.39	1.77	8.43	2.41	0.89	2.78	0.45	2.90	0.60	1.69	1.71	0.26	1.05	0.08	1.71	0.66	0.28
TC-9	323.10	29.71	94.22	6.08	1826.11	19.71	42.38	6.03	25.43	5.95	1.50	5.85	0.88	5.27	1.04	2.91	2.90	0.43	2.75	0.28	1.56	2.76	1.08
Paso Real																							
GE-021306-4	169.40	13.90	101.00	8.03	988.91	27.42	51.75	6.28	22.33	4.28	1.25	4.37	0.59	2.57	0.47	1.39	1.37	0.20	2.48	0.45	6.17	4.07	2.24
GE-021306-5	279.91	17.41	99.00	8.00	799.04	28.47	54.32	7.17	27.70	5.50	1.68	5.21	0.68	3.19	0.58	1.62	1.61	0.23	2.45	0.39	2.53	3.55	1.37
GE-021306-6	257.87	16.94	57.00	4.50	833.80	24.32	46.02	6.28	24.82	5.14	1.53	4.77	0.63	3.03	0.56	1.60	1.61	0.23	1.82	0.22	3.42	2.54	0.82
GE-021306-7	172.15	13.36	80.00	5.99	885.25	20.60	39.21	4.88	18.30	3.68	1.14	3.73	0.53	2.44	0.46	1.34	1.34	0.20	2.14	0.36	4.56	2.51	0.94
GE-021306-8	226.03	17.11	51.00	4.33	964.00	22.96	43.30	5.86	23.21	4.72	1.47	4.53	0.62	3.00	0.56	1.63	1.68	0.25	1.67	0.23	4.10	1.48	0.57
GE-021306-9	303.35	19.50	60.00	5.53	1090.65	37.47	70.83	9.76	39.24	7.73	2.28	6.96	0.84	3.79	0.66	1.76	1.77	0.25	2.22	0.26	4.51	3.91	1.17

Table 2 continued

Sample	V	Y	Zr	Nb	Ba	La	Ce	Pr	Nd	Sm	Eu	Gd	Tb	Dy	Ho	Er	Yb	Lu	Hf	Ta	Pb	Th	U
GE-021306-10	258.06	17.07	37.00	3.29	706.64	17.82	34.40	4.81	19.71	4.33	1.38	4.12	0.57	3.04	0.56	1.63	1.67	0.25	1.39	0.16	2.41	1.44	0.5
Dominical																							
DO-021406-1	450.28	20.89	45.00	1.55	310.55	7.47	14.28	2.38	11.15	3.15	1.03	3.26	0.54	3.40	0.67	2.01	2.02	0.31	1.51	0.10	0.79	0.74	0.37
DO-021406-2	316.76	15.44	29.00	1.14	394.55	5.43	10.97	1.77	8.37	2.37	0.87	2.50	0.42	2.58	0.52	1.57	1.53	0.23	1.08	0.03	1.56	0.52	0.32
TC-10a	463.52	24.60	53.24	1.88	767.07	8.52	19.13	3.12	14.49	3.95	1.30	4.35	0.70	4.40	0.88	2.47	2.49	0.37	1.70	0.11	3.33	0.88	0.45
Aguacate																							
CA-021106-1	280.03	18.15	47.22	2.38	417.94	7.11	14.34	2.11	10.30	2.76	0.94	3.00	0.45	3.00	0.56	1.71	1.68	0.26	1.22	0.12	1.30	0.85	0.17
CA-021106-2	261.57	42.82	107.33	4.56	696.59	10.41	22.44	3.88	20.00	5.93	1.81	6.69	1.09	7.13	1.43	4.52	4.45	0.69	3.10	0.25	2.87	1.33	0.39
CA-021106-3	226.84	18.66	58.36	1.97	522.75	6.31	12.97	1.92	9.04	2.52	0.83	2.78	0.45	2.88	0.55	1.74	1.77	0.27	1.48	0.12	1.61	0.95	0.27
CA-021106-4	294.16	28.01	50.53	2.14	559.45	18.03	27.52	4.47	20.56	4.59	1.51	4.80	0.65	3.85	0.74	2.25	2.12	0.32	1.17	0.08	1.87	1.11	0.23
CA-021106-5	269.42	21.31	57.54	2.54	635.97	15.12	29.63	4.27	19.18	4.41	1.39	4.23	0.58	3.42	0.62	1.89	1.92	0.29	1.36	0.09	2.30	1.57	0.38
CA-021106-6	255.59	20.42	66.44	3.88	568.51	18.05	35.97	5.01	21.64	4.79	1.46	4.51	0.61	3.40	0.61	1.81	1.78	0.27	1.50	0.15	2.09	1.80	0.42
CA-021106-7	239.37	17.89	51.09	1.92	837.84	17.13	30.13	3.92	16.94	3.65	1.19	3.53	0.48	2.81	0.52	1.67	1.69	0.26	1.34	0.09	3.02	4.69	0.86
LG-040105-1	463.00	19.11	59.00	3.81	618.00	20.62	46.50	6.30	27.43	5.58	1.74	5.08	0.65	3.29	0.59	1.58	1.52	0.22	1.39	0.15	2.68	1.33	0.77
LG-040105-2	208.87	26.88	85.00	5.52	1113.69	23.17	46.61	6.52	28.96	6.06	1.90	5.62	0.77	4.80	0.75	2.35	2.17	0.36	1.81	0.18	2.65	2.99	1.18
LC-010405-3	300.40	17.22	61.00	4.22	590.73	27.38	52.09	6.46	27.21	5.25	1.55	4.83	0.60	3.36	0.49	1.38	1.38	0.17	1.38	0.17	2.09	5.42	1.38
ACZ	199.04	21.95	125.00	6.66	893.37	34.89	67.62	8.53	34.79	7.94	1.96	5.91	0.76	4.12	0.64	1.86	1.96	0.29	2.45	0.29	2.61	5.29	2.16
CLC-1	238.11	14.24	91.00	5.77	863.53	28.37	54.15	6.51	26.77	4.79	1.47	4.70	0.57	2.82	0.40	0.98	0.98	0.12	1.72	0.25	3.01	5.53	1.6
CC-1	284.41	18.72	132.00	6.49	1020.27	51.36	95.71	11.40	43.93	7.53	2.20	6.40	0.73	3.77	0.52	1.46	1.99	0.21	2.41	0.31	3.01	10.67	3.66
CC-2	260.35	19.56	128.00	6.69	1025.92	52.72	95.50	11.40	45.19	7.74	2.20	6.75	0.81	3.97	0.60	1.57	2.09	0.21	2.62	0.31	4.54	10.88	2.62
CA-1	198.00	22.22	126.00	6.65	876.33	34.03	66.27	8.43	35.41	6.45	1.98	5.90	0.77	4.07	0.65	1.79	1.88	0.30	2.58	0.30	2.76	5.46	1.69
LC-1	294.01	20.70	104.00	5.91	654.70	40.52	79.61	10.07	41.72	7.88	2.30	6.97	0.85	4.27	0.63	1.53	1.75	0.22	1.75	0.22	2.61	4.93	1.53
FR-1	235.53	19.92	88.00	5.12	741.78	28.54	53.09	6.50	26.67	5.04	1.54	4.77	0.63	3.50	0.53	1.71	1.79	0.24	1.79	0.24	2.30	4.31	1.38
SM-1	155.92	23.66	164.00	8.54	1192.17	54.63	112.82	14.65	55.52	10.70	3.12	10.03	1.16	4.60	0.74	1.92	2.08	0.30	3.39	0.49	5.59	6.64	2.5
P-95	351.19	19.61	55.51	2.55	675.61	11.68	24.77	3.71	16.55	4.08	1.02	4.12	0.62	3.64	0.71	1.93	1.83	0.27	1.48	0.12	2.79	1.51	0.59
Standards																							
JB-1a	201.75	28.34	-	32.16	512.37	41.93	66.29	7.30	27.29	5.13	1.42	5.47	0.79	4.45	0.86	2.39	2.20	0.34	4.00	2.05	4.87	11.61	1.42
JB-1a	193.84	22.94	-	29.85	500.91	36.88	66.22	7.42	27.67	5.21	1.50	5.24	0.75	4.00	0.78	2.14	2.09	0.30	3.46	1.87	4.90	9.60	1.47
JB-1a	190.37	24.55	-	29.84	502.50	38.21	65.22	7.37	28.08	5.49	1.52	5.69	0.81	4.22	0.84	2.35	2.21	0.33	3.76	1.96	4.80	10.08	1.44
JB-1a	203.23	22.00	-	26.94	507.39	38.62	66.89	6.86	23.72	4.87	1.44	5.48	0.75	3.82	0.69	2.05	2.14	0.17	3.11	1.65	6.38	8.43	1.35
JB-1a	195.00	22.88	-	26.98	508.39	38.32	66.69	7.44	25.48	5.09	1.47	5.51	0.78	3.93	0.72	2.06	2.12	0.32	3.26	1.77	6.12	8.94	1.4
JB-1a	194.28	23.10	-	26.77	500.23	38.23	66.10	7.42	25.54	5.12	1.49	5.51	0.79	3.95	0.73	2.09	2.14	0.32	3.26	1.79	6.25	9.03	1.41
JB-1a	194.84	23.13	-	26.76	501.13	38.72	66.48	7.49	25.86	5.09	1.48	5.63	0.79	3.87	0.72	2.13	2.19	0.32	3.30	1.79	6.37	9.14	1.43
JB-1a	190.20	23.64	-	26.63	501.92	38.71	65.87	7.43	25.39	5.05	1.50	5.57	0.81	4.00	0.76	2.15	2.13	0.32	3.25	1.74	6.18	8.99	1.36
JB-1a	189.46	23.69	-	26.84	495.26	38.55	65.62	7.43	25.72	5.04	1.48	5.51	0.79	4.06	0.76	2.17	2.18	0.34	3.32	1.80	6.15	9.05	1.34

Table 3

Sample	87/86Sr	2σ	87/86Sr	143/144Nd	2σ	143/144Nd	206/204Pb	2σ	207/204Pb	2σ	208/204Pb	2σ	206/204Pb	207/204Pb	208/204Pb
Trinidad															
P-125	0.703534	0.000005	0.703501	0.513012	0.000006	0.512981	18.677	0.002	15.562	0.002	38.364	0.005	18.634	15.560	38.330
P-126*	0.70354	0.000002	0.703507	0.51302	0.000002	0.512989	18.692	0.001	15.554	0.001	38.354	0.003	18.649	15.552	38.320
P-127*	0.703636	0.000002	0.703604	0.513007	0.000003	0.512976	18.73	0.002	15.587	0.002	38.486	0.004	18.688	15.585	38.453
Sarapiqui															
BT-020406-2	0.703618	0.000008	0.703601	0.513018	0.000008	0.513018	18.616	0.001	15.516	0.001	38.221	0.003	18.596	15.515	38.200
IN-020506-2	0.703589	0.000006	0.703552	-	-	-	18.662	0.006	15.514	0.005	38.253	0.011	18.614	15.512	38.217
IN-020506-6	0.703585	0.000008	0.703557	0.51299	0.000008	0.512967	18.615	0.006	15.509	0.005	38.235	0.012	18.587	15.508	38.205
PS-020706-1	0.703723	0.000008	0.703711	-	0.000016	-	18.645	0.004	15.535	0.004	38.288	0.008	18.62	15.534	38.263
IN-020806-1	0.703775	0.000011	0.703724	-	-	-	18.65	0.007	15.526	0.006	38.28	0.014	18.592	15.523	38.242
AR-020206-2	0.703613	0.000011	0.703597	0.513021	0.000008	0.513003	18.619	0.011	15.562	0.01	38.285	0.025	18.581	15.560	38.259
AR-020206-3	0.703584	0.000025	0.703563	0.51303	0.000003	0.513011	18.621	0.002	15.528	0.002	38.234	0.004	18.603	15.527	38.212
AR-020206-4	0.703533	0.000006	0.703519	0.513059	0.000025	0.51304	18.576	0.005	15.536	0.004	38.23	0.001	18.555	15.535	38.214
AR-020206-6	0.703603	0.000007	0.703580	0.513022	0.000002	0.513004	18.58	0.003	15.53	0.002	38.211	0.006	18.544	15.528	38.192
AR-020206-7	0.70359	0.000007	0.703563	0.513011	0.000006	0.512993	18.635	0.009	15.556	0.007	38.3	0.019	18.609	15.555	38.285
CH-020406-2	0.703589	0.000008	0.703569	-	-	-	18.642	0.004	15.526	0.003	38.227	0.008	18.606	15.524	38.201
CH-020406-5	0.703751	0.000007	0.703701	0.51302	0.000008	0.513005	18.704	0.002	15.554	0.002	38.377	0.005	18.68	15.553	38.352
Talamanca															
TA-021206-4	0.703843	0.000008	0.703838	0.512996	0.000016	0.512998	18.655	0.001	15.503	0.008	38.238	0.002	18.627	15.502	38.220
TC-1**	0.704269	0.000003	0.704162	0.513022	0.000002	0.513022	18.73	0.001	15.538	0.001	38.357	0.001	18.692	15.536	38.332
TC-2**	0.703864	0.000003	0.703856	0.512997	0.000002	0.512997	18.628	0.001	15.538	0.001	38.282	0.003	18.599	15.537	38.265
TC-4**	0.703749	0.000003	0.703744	0.512995	0.000002	0.512995	18.822	0.001	15.55	0.001	38.492	0.002	18.8	15.549	38.475
TC-9**	0.704031	0.000003	0.704008	0.512993	0.000002	0.512993	18.819	0.001	15.542	0.001	38.447	0.001	18.739	15.539	38.380
EG-1**	0.703844	0.000003	0.703839	0.512974	0.000019	0.512975	18.658	0.004	15.53	0.003	38.263	0.007	18.624	15.528	38.243
Paso Real															
GE-021306-4	0.70378	0.000008	0.703775	0.51298	0.000017	0.512977	19.111	0.002	15.575	0.001	38.809	0.003	19.098	15.575	38.801
GE-021306-8	0.703737	0.000006	0.703734	0.512986	0.000006	0.512983	18.961	0.014	15.519	0.01	38.653	0.022	18.956	15.519	38.649
GE-021306-9	0.703512	0.000006	0.703511	0.512967	0.000017	0.512964	19.039	0.009	15.574	0.007	38.775	0.018	19.03	15.574	38.765
Dominical															
TC-10a	0.704565	0.000003	0.704518	0.513025	0.000003	0.513006	18.638	0.001	15.548	0.001	38.309	0.002	18.614	15.547	38.293
Aguacate															
CA-021106-1	0.703711	0.000009	0.703708	0.513019	0.000042	0.513008	18.772	0.004	15.54	0.003	38.418	0.008	18.758	15.539	38.395
CA-021106-2	0.703763	0.000006	0.703747	0.513021	0.00003	0.513008	18.702	0.005	15.532	0.003	38.308	0.007	18.687	15.531	38.291
CA-021106-4	0.703783	0.000008	0.703776	-	-	-	18.699	0.003	15.527	0.003	38.346	0.007	18.693	15.527	38.336
CA-021106-5	0.703914	0.000008	0.703911	0.512956	0.000023	0.512951	18.869	0.015	15.527	0.012	38.553	0.03	18.861	15.527	38.541
CA-021106-6	0.703947	0.000008	0.703943	0.513	0.000005	0.512996	18.926	0.001	15.547	0.001	38.643	0.003	18.916	15.547	38.629
CA-021106-7	0.703868	0.000007	0.703866	0.512971	0.000007	0.512968	18.914	0.001	15.537	0.001	38.603	0.002	18.903	15.536	38.583
CA-021106-8	-	-	-	-	-	-	19.096	0.001	15.573	0.001	38.837	0.003	19.085	15.573	38.817
LG-040105-1	0.704045	0.000007	0.704040	0.512991	0.000024	0.512986	-	-	-	-	-	-	-	-	-
CC-2	0.703817	0.000007	0.703811	0.512982	0.000006	0.512979	19.136	0.006	15.572	0.004	38.89	0.011	19.113	15.571	38.858
LC-1	0.703922	0.000006	0.703913	0.512986	0.000005	0.512959	18.949	0.009	15.536	0.007	38.677	0.019	18.911	15.534	38.637
P-95	0.703752	0.000007	0.703743	0.512991	0.000004	0.512985	18.873	0.001	15.557	0.001	38.575	0.002	18.86	15.556	38.564

Table 4

Sample	P-95 matrix step-heating analysis									
Mass	8.513 mg									
J =	3.75E-03	±	4.72E-06	(0.126 Percent; 2 Sigma)						
Heating step	Laser power [W]	40Ar/39Ar	37Ar/39Ar	36Ar/39Ar	Mol 39ArK	Ca/K	% 40ArA	Cum 39ArK	Age [Ma]	2 Sigma
1	0.15	5.70E+03	-1.55E+00	1.92E+01	1.08E-17	-3	99.7	5.54E-05	9.84E+01	7.41E+02
2	0.25	4.71E+03	4.11E+00	1.58E+01	1.05E-16	8.1	99.5	5.96E-04	1.68E+02	3.25E+02
3	0.4	1.10E+03	2.86E+00	3.71E+00	8.58E-16	5.6	99.4	5.00E-03	4.78E+01	5.06E+01
4	0.5	2.83E+02	2.67E+00	9.44E-01	1.87E-15	5.2	98.3	1.46E-02	3.21E+01	2.31E+01
5	0.6	1.07E+02	2.84E+00	3.47E-01	2.99E-15	5.6	96	3.00E-02	2.89E+01	2.01E+01
6	0.7	1.50E+02	3.59E+00	4.96E-01	4.53E-15	7.1	97.3	5.32E-02	2.78E+01	1.84E+01
7	0.8	1.83E+02	4.03E+00	6.05E-01	6.70E-15	7.9	97.2	8.77E-02	3.44E+01	1.82E+01
8	0.9	1.12E+02	2.79E+00	3.67E-01	9.43E-15	5.5	96.8	1.36E-01	2.43E+01	9.04E+00
9	1	4.58E+01	1.92E+00	1.50E-01	1.10E-14	3.8	96.1	1.93E-01	1.20E+01	3.78E+00
10	**1.1**	**1.78E+01**	**1.46E+00**	**5.76E-02**	**1.13E-14**	**2.9**	**94.5**	**2.51E-01**	**6.57E+00**	**1.31E+00**
11	**1.2**	**9.79E+00**	**1.26E+00**	**3.04E-02**	**1.29E-14**	**2.5**	**90.1**	**3.17E-01**	**6.53E+00**	**1.47E+00**
12	**1.35**	**5.93E+00**	**1.10E+00**	**1.73E-02**	**1.63E-14**	**2.2**	**84**	**4.01E-01**	**6.41E+00**	**9.49E-01**
13	**1.5**	**4.33E+00**	**1.01E+00**	**1.18E-02**	**1.55E-14**	**2**	**77.9**	**4.80E-01**	**6.48E+00**	**9.25E-01**
14	**2**	**4.15E+00**	**1.48E+00**	**1.17E-02**	**1.83E-14**	**2.9**	**78.9**	**5.74E-01**	**5.93E+00**	**7.85E-01**
15	**3**	**4.56E+00**	**3.97E+00**	**1.41E-02**	**1.35E-14**	**7.8**	**79.8**	**6.44E-01**	**6.23E+00**	**1.21E+00**
16	**5**	**3.80E+00**	**3.50E+00**	**1.13E-02**	**2.31E-14**	**6.9**	**76**	**7.62E-01**	**6.19E+00**	**4.51E-01**
17	**10**	**3.45E+00**	**3.98E+00**	**1.01E-02**	**3.34E-14**	**7.8**	**71.7**	**9.34E-01**	**6.63E+00**	**3.06E-01**
18	**20**	**3.36E+00**	**5.81E+00**	**1.04E-02**	**1.16E-14**	**11.4**	**68.9**	**9.93E-01**	**7.10E+00**	**1.01E+00**
19	**25**	**3.54E+00**	**6.20E+00**	**1.01E-02**	**1.22E-15**	**12.2**	**61.9**	**1.00E+00**	**9.16E+00**	**6.60E+00**
20	27.5	-6.81E-01	1.19E+01	-3.90E-02	5.89E-17	23.6	1908.4	1.00E+00	8.29E+01	1.62E+02
Total gas	Age	9.98	±	0.21	Ma (2s, steps 1 through 20)					
Isochron	Age	6.23	±	0.29	Ma (2s, steps 1 through 20)					
	Initial 40Ar/36Ar	298.89	±	0.73	MSWD = 1.529					
Plateau	**Age**	**6.47**	**±**	**0.21**	**Ma (2s, including J-error of 0.126%)**					
	Stats				**MSWD = 0.78, probability = 0.65**					
	Size				**80.7% of the 39Ar, steps 10 through 20**					

Sample	P-126 matrix step-heating analysis									
Mass	6.528 mg									
J =	3.74E-03	+/-	7.19E-06	(0.192 Percent; 2 Sigma)						
Heating step	Laser power [W]	40Ar/39Ar	37Ar/39Ar	36Ar/39Ar	Mol 39ArK	Ca/K	% 40ArA	Cum 39ArK	Age [Ma]	2 Sigma
1	0.15	2.91E+01	9.33E-01	7.49E-02	3.53E-15	1.8	75.6	8.08E-02	4.75E+01	2.20E+01
2	0.25	4.77E+01	1.77E+00	1.30E-01	2.23E-15	3.5	79.8	1.32E-01	6.40E+01	2.18E+01
3	**0.4**	**1.95E+01**	**2.08E+00**	**4.91E-02**	**4.40E-15**	**4.1**	**73**	**2.33E-01**	**3.52E+01**	**1.53E+01**
4	**0.5**	**1.34E+01**	**3.56E+00**	**3.15E-02**	**2.77E-15**	**7**	**66.2**	**2.96E-01**	**3.03E+01**	**7.08E+00**
5	**0.6**	**1.07E+01**	**5.39E+00**	**2.53E-02**	**2.53E-15**	**10.6**	**63.1**	**3.54E-01**	**2.67E+01**	**3.88E+00**
6	**0.7**	**1.03E+01**	**6.76E+00**	**2.43E-02**	**2.49E-15**	**13.3**	**61**	**4.11E-01**	**2.71E+01**	**2.65E+00**
7	**0.8**	**1.21E+01**	**7.73E+00**	**2.96E-02**	**2.31E-15**	**15.3**	**64**	**4.64E-01**	**2.94E+01**	**2.78E+00**
8	**0.9**	**1.60E+01**	**8.09E+00**	**4.24E-02**	**2.21E-15**	**16**	**71.9**	**5.14E-01**	**3.03E+01**	**3.46E+00**
9	**1**	**2.18E+01**	**9.19E+00**	**6.30E-02**	**2.02E-15**	**18.2**	**80.1**	**5.60E-01**	**2.93E+01**	**3.97E+00**
10	**1.1**	**2.57E+01**	**9.37E+00**	**7.47E-02**	**1.63E-15**	**18.5**	**81.1**	**5.98E-01**	**3.29E+01**	**3.83E+00**
11	**1.2**	**2.87E+01**	**9.79E+00**	**8.51E-02**	**1.60E-15**	**19.4**	**83**	**6.34E-01**	**3.29E+01**	**7.05E+00**
12	1.35	3.17E+01	1.11E+01	9.36E-02	1.75E-15	22	82.8	6.74E-01	3.68E+01	6.56E+00
13	1.5	3.38E+01	1.11E+01	9.90E-02	1.49E-15	21.9	82.3	7.09E-01	4.02E+01	6.13E+00
14	2	3.54E+01	1.37E+01	1.09E-01	2.57E-15	27.2	85.6	7.67E-01	3.45E+01	3.93E+00
15	3	3.61E+01	1.29E+01	1.11E-01	2.44E-15	25.6	86.4	8.23E-01	3.32E+01	3.95E+00
16	5	3.33E+01	1.26E+01	1.02E-01	2.66E-15	25	85.7	8.84E-01	3.24E+01	5.05E+00
17	10	3.25E+01	1.34E+01	9.86E-02	3.79E-15	26.6	84.3	9.71E-01	3.45E+01	2.89E+00
18	20	3.30E+01	1.38E+01	1.02E-01	1.22E-15	27.5	86.2	9.99E-01	3.09E+01	8.13E+00
19	25	3.58E+01	2.16E+01	7.34E-02	5.50E-17	43.2	52.6	1.00E+00	1.13E+02	9.40E+01
20	>	-1.68E+02	-4.35E+01	-1.02E-01	-5.46E-18	-81.8	14.6	1.00E+00	-1.30E+03	3.94E+03
Total gas	Age	35.2	±	1	Ma (2s, steps 1 through 20)					
Isochron	Age	25.8	±	0.27	Ma (2s, steps 1 through 20)					
	Initial 40Ar/36Ar	309.5	±	6	MSWD = 1.50					
Plateau	**Age**	**29.2**	**±**	**1.3**	**Ma (2s, including J-error of 0.192%)**					
	Stats				**MSWD = 1.3, probability = 0.26**					
	Size				**50.3% of the 39Ar, steps 3 through 11**					

Table 4 continued

Sample	**P-127 feldspar step-heating analysis**									
Mass	6.441 mg									
J =	3.74E-03	+/-	7.19E-06	(0.192 Percent; 2 Sigma)						
Heating step	Laser power [W]	40Ar/39Ar	37Ar/39Ar	36Ar/39Ar	Mol 39ArK	Ca/K	% 40ArA	Cum 39ArK	Age [Ma]	2 Sigma
1	0.15	6.61E+02	2.05E+00	1.93E+00	2.97E-18	4	86.1	6.29E-05	5.34E+02	1.41E+03
2	0.25	5.49E+03	7.32E+01	1.80E+01	3.09E-18	154.7	96.9	1.28E-04	9.52E+02	1.75E+03
3	0.4	3.39E+03	1.91E+01	1.13E+01	3.25E-17	38.2	98.6	8.16E-04	2.95E+02	3.84E+02
4	0.5	3.01E+03	1.28E+01	9.88E+00	2.74E-17	25.5	96.8	1.40E-03	5.65E+02	1.69E+02
5	0.6	1.51E+03	8.98E+00	5.02E+00	4.02E-17	17.8	98	2.25E-03	2.00E+02	3.11E+02
6	0.8	5.67E+02	7.71E+00	1.92E+00	1.51E-16	15.2	99.9	5.45E-03	2.67E+00	9.42E+01
7	1	1.27E+02	7.42E+00	4.12E-01	3.13E-16	14.7	95.5	1.21E-02	3.84E+01	1.93E+01
8	1.2	3.83E+01	7.45E+00	1.28E-01	4.44E-16	14.7	95.9	2.15E-02	1.06E+01	1.95E+01
9	1.5	1.74E+01	7.13E+00	4.65E-02	8.54E-16	14.1	73.7	3.96E-02	3.08E+01	9.01E+00
10	2	6.04E+00	6.97E+00	8.84E-03	1.44E-15	13.8	28.2	7.00E-02	2.92E+01	5.64E+00
11	3	5.00E+00	6.92E+00	5.92E-03	2.55E-15	13.7	16.9	1.24E-01	2.80E+01	3.19E+00
12	4	4.67E+00	8.14E+00	3.24E-03	2.77E-15	16.1	-2.3	1.83E-01	3.22E+01	3.23E+00
13	**6**	**4.32E+00**	**8.80E+00**	**4.32E-03**	**1.24E-14**	**17.4**	**2.9**	**4.45E-01**	**2.83E+01**	**6.12E-01**
14	**8**	**4.22E+00**	**9.30E+00**	**4.06E-03**	**1.03E-14**	**18.4**	**-0.4**	**6.63E-01**	**2.86E+01**	**7.36E-01**
15	**10**	**4.19E+00**	**8.80E+00**	**3.73E-03**	**5.38E-15**	**17.4**	**-1.1**	**7.77E-01**	**2.86E+01**	**1.21E+00**
16	**12**	**4.20E+00**	**8.81E+00**	**4.34E-03**	**1.06E-15**	**17.4**	**3.2**	**7.99E-01**	**2.74E+01**	**6.35E+00**
17	**15**	**4.19E+00**	**8.92E+00**	**4.16E-03**	**2.55E-15**	**17.6**	**1.5**	**8.54E-01**	**2.79E+01**	**3.97E+00**
18	20	4.20E+00	9.27E+00	5.75E-03	2.71E-15	18.3	11.6	9.11E-01	2.51E+01	2.30E+00
19	25	4.20E+00	9.13E+00	4.00E-03	1.43E-15	18.1	-0.2	9.41E-01	2.84E+01	5.09E+00
20	>	4.20E+00	9.04E+00	-1.43E-04	9.07E-16	17.9	-29.2	9.60E-01	3.65E+01	4.48E+00
21	>>	4.22E+00	9.21E+00	2.97E-03	1.81E-15	18.2	-7.7	9.99E-01	3.06E+01	3.66E+00
22	>>>	4.15E+00	7.63E+00	2.37E-02	5.74E-17	15.1	145.2	1.00E+00	-1.28E+01	9.98E+01
Total gas	Age	29.2	±	0.4	Ma (2s, steps 1 through 22)					
Isochron	Age	28.44	±	0.64	Ma (2s, steps 1 through 22)					
	Initial 40Ar/36Ar	302.5	±	3.16	MSWD = 2.30					
Plateau	**Age**	**28.43**	**±**	**0.44**	**Ma (2s, including J-error of 0.192%)**					
	Stats				**MSWD = 0.19, probability = 0.94**					
	Size				**67.1% of the 39Ar, steps 13 through 17**					

Sample	**EG-1 matrix step-heating analysis**									
Mass	6.023 mg									
J =	3.74E-03	+/-	7.19E-06	(0.192 Percent; 2 Sigma)						
Heating step	Laser power [W]	40Ar/39Ar	37Ar/39Ar	36Ar/39Ar	Mol 39ArK	Ca/K	% 40ArA	Cum 39ArK	Age [Ma]	2 Sigma
1	0.15	6.96E+03	4.40E+00	2.34E+01	4.46E-17	8.7	99.2	1.07E-03	3.57E+02	2.38E+02
2	0.25	2.32E+03	5.70E+00	7.81E+00	1.66E-16	11.2	99.4	5.06E-03	8.85E+01	1.17E+02
3	0.4	6.13E+02	5.20E+00	2.05E+00	1.28E-15	10.2	98.8	3.57E-02	4.87E+01	2.76E+01
4	0.5	2.73E+02	3.34E+00	8.76E-01	5.58E-16	6.6	94.5	4.91E-02	9.82E+01	3.95E+01
5	0.6	1.71E+02	2.92E+00	5.24E-01	1.56E-15	5.7	90.6	8.66E-02	1.05E+02	3.22E+01
6	0.7	1.88E+02	3.72E+00	6.11E-01	6.90E-15	7.3	95.9	2.53E-01	5.08E+01	1.64E+01
7	0.8	6.33E+01	4.33E+00	2.04E-01	5.38E-15	8.5	94.5	3.82E-01	2.34E+01	6.17E+00
8	**0.9**	**2.91E+01**	**3.93E+00**	**9.40E-02**	**3.91E-15**	**7.7**	**93.7**	**4.76E-01**	**1.24E+01**	**4.06E+00**
9	**1**	**1.99E+01**	**3.75E+00**	**6.01E-02**	**2.90E-15**	**7.4**	**87**	**5.46E-01**	**1.74E+01**	**4.54E+00**
10	**1.1**	**1.64E+01**	**3.45E+00**	**4.98E-02**	**1.95E-15**	**6.8**	**87.2**	**5.93E-01**	**1.41E+01**	**6.47E+00**
11	**1.2**	**1.48E+01**	**3.63E+00**	**4.43E-02**	**1.77E-15**	**7.1**	**85.1**	**6.36E-01**	**1.49E+01**	**4.26E+00**
12	**1.35**	**1.47E+01**	**4.70E+00**	**4.35E-02**	**1.49E-15**	**9.3**	**83.2**	**6.71E-01**	**1.67E+01**	**6.47E+00**
13	**1.5**	**1.45E+01**	**6.04E+00**	**4.29E-02**	**1.07E-15**	**11.9**	**81.9**	**6.97E-01**	**1.77E+01**	**7.58E+00**
14	**2**	**1.52E+01**	**1.00E+01**	**4.78E-02**	**1.55E-15**	**19.8**	**84.5**	**7.34E-01**	**1.60E+01**	**4.95E+00**
15	**3**	**1.37E+01**	**1.42E+01**	**4.31E-02**	**1.62E-15**	**28.2**	**79.3**	**7.73E-01**	**1.94E+01**	**6.84E+00**
16	**5**	**1.02E+01**	**1.48E+01**	**3.39E-02**	**4.90E-15**	**29.4**	**79.6**	**8.91E-01**	**1.41E+01**	**2.02E+00**
17	**10**	**9.51E+00**	**2.44E+01**	**3.65E-02**	**4.05E-15**	**48.9**	**80**	**9.89E-01**	**1.31E+01**	**1.53E+00**
18	**20**	**1.08E+01**	**4.09E+01**	**4.75E-02**	**4.34E-16**	**83.5**	**80.3**	**9.99E-01**	**1.50E+01**	**1.64E+01**
19	**25**	**1.71E+01**	**6.97E+01**	**6.45E-02**	**3.38E-17**	**146.8**	**58.2**	**1.00E+00**	**5.11E+01**	**1.05E+02**
20	>	1.02E+01	7.65E-01	9.93E-03	-1.92E-17	1.5	27.8	1.00E+00	4.90E+01	2.95E+02
Total gas	Age	28.1	±	1	Ma (2s, steps 1 through 20)					
Isochron	Age	13.57	±	2.24	Ma (2s, steps 1 through 20)					
	Initial 40Ar/36Ar	299.3	±	2.26	MSWD = 4.35					
Plateau	**Age**	**14.1**	**±**	**1**	**Ma (2s, including J-error of 0.192%)**					
	Stats				**MSWD = 0.88, probability = 0.56**					
	Size				**61.8% of the 39Ar, steps 8 through 19**					

Table 4 continued

Sample	**TC-2 matrix step-heating analysis**									
Mass	1.540 mg									
J =	3.46E-03	+/-	7.57E-06	(0.219 Percent; 2 Sigma)						
Heating step	Laser power [W]	40Ar/39Ar	37Ar/39Ar	36Ar/39Ar	Mol 39ArK	Ca/K	% 40ArA	Cum 39ArK	Age [Ma]	2 Sigma
1	0.13	1.69E+03	7.64E+00	5.63E+00	1.16E-16	15.1	98.2	2.47E-03	1.83E+02	7.44E+01
2	0.2	3.90E+02	6.73E+00	1.30E+00	6.70E-16	13.3	98.7	1.68E-02	3.21E+01	2.69E+01
3	0.3	7.94E+01	4.17E+00	2.31E-01	2.73E-15	8.2	85.1	7.50E-02	7.25E+01	1.84E+01
4	0.4	5.37E+01	4.24E+00	1.50E-01	3.79E-15	8.3	81.3	1.56E-01	6.20E+01	1.46E+01
5	0.5	3.17E+01	3.60E+00	9.32E-02	4.21E-15	7.1	85.3	2.46E-01	2.90E+01	6.12E+00
6	0.6	1.20E+01	3.19E+00	3.66E-02	3.40E-15	6.3	86.4	3.18E-01	1.02E+01	3.00E+00
7	0.7	8.81E+00	2.74E+00	2.60E-02	3.03E-15	5.4	83.2	3.83E-01	9.22E+00	2.87E+00
8	0.8	9.03E+00	2.66E+00	2.66E-02	2.59E-15	5.2	83.4	4.38E-01	9.34E+00	3.06E+00
9	**0.9**	**8.74E+00**	**2.91E+00**	**2.36E-02**	**2.31E-15**	**5.7**	**75.5**	**4.88E-01**	**1.33E+01**	**2.77E+00**
10	**1**	**9.39E+00**	**3.02E+00**	**2.66E-02**	**1.93E-15**	**5.9**	**79.5**	**5.29E-01**	**1.20E+01**	**3.79E+00**
11	**1.1**	**9.73E+00**	**3.23E+00**	**2.73E-02**	**1.73E-15**	**6.3**	**78.8**	**5.66E-01**	**1.29E+01**	**4.13E+00**
12	**1.2**	**9.23E+00**	**3.03E+00**	**2.59E-02**	**1.83E-15**	**5.9**	**78.6**	**6.05E-01**	**1.23E+01**	**2.73E+00**
13	**1.35**	**9.40E+00**	**3.17E+00**	**2.61E-02**	**2.04E-15**	**6.2**	**77.9**	**6.49E-01**	**1.30E+01**	**2.80E+00**
14	**1.5**	**9.24E+00**	**3.68E+00**	**2.64E-02**	**2.08E-15**	**7.2**	**79.2**	**6.93E-01**	**1.20E+01**	**3.26E+00**
15	**2**	**8.46E+00**	**3.33E+00**	**2.17E-02**	**2.65E-15**	**6.5**	**70.7**	**7.50E-01**	**1.54E+01**	**2.36E+00**
16	**3**	**1.18E+01**	**3.78E+00**	**3.38E-02**	**5.86E-15**	**7.4**	**80.8**	**8.75E-01**	**1.41E+01**	**1.58E+00**
17	**5**	**1.66E+01**	**4.78E+00**	**5.00E-02**	**4.70E-15**	**9.4**	**85.1**	**9.75E-01**	**1.55E+01**	**2.48E+00**
18	10	2.15E+01	7.24E+00	6.37E-02	1.07E-15	14.3	83	9.98E-01	2.28E+01	5.64E+00
19	15	2.13E+01	6.51E+00	3.31E-02	8.88E-17	12.8	41.9	1.00E+00	7.62E+01	5.07E+01
20	20	-9.19E+01	-2.96E+01	-4.00E-01	-6.01E-18	-56.5	124.5	1.00E+00	1.32E+02	5.50E+02
Total gas	Age	22.7	±	0.8	Ma (2s, steps 1 through 20)					
Isochron	Age	12.33	±	2.48	Ma (2s, steps 1 through 20)					
	Initial 40Ar/36Ar	302.5	±	5.47	MSWD = 8.18					
Plateau	**Age**	**13.77**	**±**	**0.86**	**Ma (2s, including J-error of 0.219%)**					
	Stats				**MSWD = 0.96, probability = 0.46**					
	Size				**53.7% of the 39Ar, steps 9 through 17**					

Sample	**TC-10a feldspar step-heating analysis**									
Mass	1.349 mg									
J =	3.63E-03	+/-	6.55E-06	(0.181 Percent; 2 Sigma)						
Heating step	Laser power [W]	40Ar/39Ar	37Ar/39Ar	36Ar/39Ar	Mol 39ArK	Ca/K	% 40ArA	Cum 39ArK	Age [Ma]	2 Sigma
1	0.13	5.49E+02	2.07E+00	1.82E+00	5.22E-16	4.1	98	3.70E-03	6.97E+01	3.13E+01
2	**0.2**	**1.11E+02**	**9.78E-01**	**3.67E-01**	**2.35E-15**	**1.9**	**97.5**	**2.04E-02**	**1.85E+01**	**6.18E+00**
3	**0.3**	**5.09E+01**	**8.56E-01**	**1.62E-01**	**7.53E-15**	**1.7**	**94.1**	**7.38E-02**	**1.96E+01**	**4.73E+00**
4	**0.4**	**3.85E+01**	**1.12E+00**	**1.21E-01**	**1.05E-14**	**2.2**	**92.2**	**1.48E-01**	**1.96E+01**	**2.82E+00**
5	**0.5**	**2.93E+01**	**1.21E+00**	**9.08E-02**	**1.12E-14**	**2.4**	**91.1**	**2.28E-01**	**1.70E+01**	**2.35E+00**
6	**0.6**	**3.14E+01**	**1.01E+00**	**9.73E-02**	**1.02E-14**	**2**	**91.3**	**3.00E-01**	**1.78E+01**	**1.27E+00**
7	**0.7**	**3.13E+01**	**1.13E+00**	**9.62E-02**	**9.46E-15**	**2.2**	**90.3**	**3.67E-01**	**1.99E+01**	**1.82E+00**
8	**0.8**	**2.49E+01**	**1.55E+00**	**7.58E-02**	**9.49E-15**	**3**	**89.2**	**4.35E-01**	**1.75E+01**	**2.75E+00**
9	**1**	**2.36E+01**	**1.49E+00**	**7.09E-02**	**1.45E-14**	**2.9**	**88**	**5.38E-01**	**1.85E+01**	**1.04E+00**
10	**1.2**	**2.37E+01**	**1.25E+00**	**7.08E-02**	**8.95E-15**	**2.5**	**87.7**	**6.01E-01**	**1.90E+01**	**2.31E+00**
11	**1.35**	**2.44E+01**	**1.26E+00**	**7.34E-02**	**8.76E-15**	**2.5**	**88.2**	**6.63E-01**	**1.87E+01**	**1.77E+00**
12	**1.5**	**2.63E+01**	**9.25E-01**	**7.91E-02**	**6.58E-15**	**1.8**	**88.5**	**7.10E-01**	**1.96E+01**	**2.61E+00**
13	**2**	**1.63E+01**	**8.90E-01**	**4.59E-02**	**1.55E-14**	**1.7**	**82.6**	**8.20E-01**	**1.85E+01**	**4.83E-01**
14	**3**	**1.45E+01**	**1.18E+00**	**4.05E-02**	**1.59E-14**	**2.3**	**81.3**	**9.33E-01**	**1.77E+01**	**9.19E-01**
15	**4**	**1.13E+01**	**1.46E+00**	**2.95E-02**	**3.81E-15**	**2.9**	**75.2**	**9.60E-01**	**1.83E+01**	**1.48E+00**
16	**6**	**1.13E+01**	**8.61E-01**	**3.01E-02**	**3.43E-15**	**1.7**	**77.7**	**9.84E-01**	**1.64E+01**	**2.40E+00**
17	**8**	**1.10E+01**	**6.73E-01**	**2.90E-02**	**1.79E-15**	**1.3**	**77.5**	**9.97E-01**	**1.61E+01**	**3.23E+00**
18	10	1.27E+01	1.79E+00	4.40E-02	2.98E-16	3.5	100.9	9.99E-01	-7.44E-01	1.50E+01
19	12	1.48E+01	1.33E+00	7.73E-02	4.99E-17	2.6	153.4	1.00E+00	-5.24E+01	8.50E+01
20	15	1.05E+01	2.37E+00	4.12E-02	7.32E-17	4.6	112.9	1.00E+00	-8.88E+00	5.96E+01
Total gas	Age	18.5	±	0.3	Ma (2s, steps 1 through 20)					
Isochron	Age	17.55	±	0.8	Ma (2s, steps 1 through 20)					
	Initial 40Ar/36Ar	297.6	±	1.88	MSWD = 1.47					
Plateau	**Age**	**18.32**	**±**	**0.33**	**Ma (2s, including J-error of 0.181%)**					
	Stats				**MSWD = 0.97, probability = 0.48**					
	Size				**99.3% of the 39Ar, steps 2 through 17**					

Table 5

Model	Rb	Ba	Th	U	Nb	Ta	K2O	La	Ce	Pb	Pr	Sr	P2O5	Nd	Zr	Sm	Eu	Y	TiO2	Dy	Yb	Lu
DM (SO 144-1) 8%F (60ol25opx12cpx3spn)	0.061	0.491	0.007	0.002	0.114	0.008	0.006	0.19	0.645	0.046	0.125	8.499	0.009	0.718	6.733	0.3	0.114	4.333	0.181	0.596	0.393	0.062
Mean Semount Province melt (SP) 20%F (83cpx15ga2rut)	174.7	2094.676	21.047	8.438	62.217	3.268	8.6	190.473	353.951	10.141	45.302	2755.231	3.148	108.962	265.09	8.209	1.951	9.026	0.753	2.51	0.723	0.088
Mean Cocos/Coiba Ridge melt (CCR) 20%F (83cpx15ga2ru)	51.4	435.095	6.199	4.444	17.168	0.883	1.65	63.342	120.672	3.396	17.539	974.121	1.849	46.803	122.595	4.445	1.146	10.214	0.488	2.203	0.844	0.11
Galapagos Component 1 (SP40+CCR 60%)	100.72	1098.927	12.138	6.042	35.188	1.837	4.43	114.194	213.984	6.094	28.644	1686.565	2.368	71.666	179.593	5.95	1.468	9.739	0.594	2.326	0.795	0.101
Galapagos Component 2 (SP20%+CCR80%)	76.06	767.011	9.169	5.243	26.178	1.36	3.04	88.768	167.328	4.745	23.092	1330.343	2.108	59.234	151.094	5.197	1.307	9.977	0.541	2.265	0.82	0.105
Sediment Melt1 (30Carb+70Hemi) 20%F (D15garnet84.6cpx0.4rut)	149.15	17013.203	10.738	17.313	12.073	0.771	6.71	75.445	91.411	36.251	14.314	3329.281	0.615	38.92	74.387	3.031	1.087	6.648	0.166	1.402	0.576	0.08
SedMelt 2(Oligocene-Miocene) (30Carb+70Hemi) 20%F (D15garnet84.6cpx0.4rut)	149.15	5671.06	10.738	3.85	12.073	0.771	6.71	75.445	91.411	12.86	14.314	3329.281	0.615	38.92	74.387	3.031	1.087	6.648	0.166	1.402	0.576	0.08
Central Costa Rica C_0 (60ol25opx13.5cpx1.5ga)	3.23	50.457	0.382	0.201	1.178	0.064	0.145	3.685	7.136	0.264	0.995	62.162	0.081	2.885	11.986	0.472	0.156	4.497	0.194	0.649	0.406	0.064
Central Costa Rica C_L	40.371	630.712	4.773	2.511	14.721	0.795	1.813	46.062	89.087	3.299	12.26	769.112	0.971	34.147	134.825	4.87	1.475	18.989	1.293	4.424	1.748	0.236
NW Costa Rica C_0 (60ol25opx14.5cpx0.5ga)	1.559	109.158	0.144	0.142	0.396	0.024	0.072	1.325	2.47	0.3	0.381	38.492	0.027	1.373	8.176	0.35	0.128	4.379	0.184	0.611	0.397	0.063
NW Costa Rica C_L	17.325	1212.868	1.604	1.583	4.398	0.262	0.804	14.724	27.42	3.332	4.193	424.387	0.292	14.618	85.78	3.331	1.146	23.874	1.193	4.384	2.224	0.319
SE Nicaragua C_0 (60ol25opx14.7cpx0.3ga)	1.06	72.936	0.099	0.096	0.302	0.018	0.05	0.947	1.862	0.215	0.296	28.494	0.021	1.155	7.695	0.333	0.124	4.364	0.183	0.606	0.396	0.063
SE Nicaragua C_L	17.663	1215.597	1.644	1.597	5.024	0.306	0.835	15.77	30.715	3.574	4.681	454.579	0.319	16.801	109.711	3.992	1.354	27.916	1.338	5.096	2.618	0.377
NW Nicaragua C_0 (60ol25opx14.7cpx0.3ga)	0.955	102.568	0.072	0.106	0.185	0.013	0.046	0.641	1.19	0.264	0.21	28.424	0.013	0.947	7.139	0.316	0.12	4.347	0.181	0.601	0.395	0.062
NW Nicaragua model C_L	13.247	911.697	1.233	1.197	3.771	0.23	0.626	11.833	23.223	2.691	3.632	351.082	0.253	13.54	89.099	3.413	1.181	26.178	1.237	4.638	2.448	0.355
Late Miocene-Pliocene $C_0$1(60ol25opx14cpx1ga)	1.335	38.347	0.117	0.052	0.316	0.019	0.061	1.084	2.023	0.147	0.325	35.033	0.023	1.24	7.861	0.341	0.126	4.375	0.183	0.609	0.397	0.063
Late Miocene-Pliocene C_L1	33.383	958.68	2.935	1.292	7.805	0.478	1.525	26.959	48.439	3.581	7.064	776.119	0.467	23.387	136.179	4.862	1.582	23.022	1.436	5.154	2.144	0.293
Late Miocene-Pliocene $C_0$2(60ol25opx14cpx1ga)	0.955	34.515	0.072	0.025	0.185	0.013	0.046	0.641	1.19	0.123	0.21	28.424	0.013	0.947	7.139	0.316	0.12	4.347	0.181	0.601	0.395	0.062
Late Miocene-Pliocene C_L2	23.883	862.865	1.79	0.637	4.583	0.311	1.146	15.945	28.485	3.008	4.568	629.698	0.256	17.869	123.674	4.512	1.507	22.874	1.422	5.084	2.133	0.292
Oligocene-Pliocene C_0 (60ol25opx14.7cpx0.3ga)	0.955	34.515	0.072	0.025	0.185	0.013	0.046	0.641	1.19	0.123	0.21	28.424	0.013	0.947	7.139	0.316	0.12	4.347	0.181	0.601	0.395	0.062
Oligocene-Pliocene C_L	11.942	431.433	0.895	0.319	2.317	0.157	0.573	8.014	14.842	1.54	2.58	350.211	0.153	11.108	82.659	3.237	1.147	26.076	1.226	4.597	2.44	0.355

Table 6

Segment	Galapagos hotspot contribution	Sediment component	Degree of melting	Garnet in the source
Central Costa Rica	3.00%	0.10%	8%	1.50%
NW Costa Rica	0.60%	0.60%	9%	0.50%
SE Nicaragua	0.40%	0.40%	6%	0.30%
NW Nicaragua	-	0.60%	8%	0.30%
Late Miocene-Pliocene	0.50%	0.60%	4%	1.00%
Oligocene-Mid. Miocene	-	0.60%	8%	0.30%

Chapter 4

Petrological and Geochemical Evidence of Galapagos Asthenosphere Upwelling in Southern Central America

To be submitted to the Journal of Petrology by:

Esteban Gazel[1]*, Kaj Hoernle[2], Michael J. Carr[1], Claude Herzberg[1], Ian Saginor[3], Carl Swisher III[1], Mark Feigenson[1], Folkmar Hauff[2], Paul van den Bogaard[2]

1. Department of Earth and Planetary Sciences, Rutgers University, 610 Taylor Road, Piscataway, NJ 08854-8066 U.S.A.
2. IFM-GEOMAR, Wischhofstrasse 1-3, 24148 Kiel, Germany
3. Keystone College, La Plume, PA, 188440-1099 U.S.A

*Corresponding author: Tel: (732) 445-2124, Fax (732) 445-3374, E-mail: egazel@rutgers.edu (E. Gazel).

Abstract

The interaction between a mantle plume and an arc system usually can generate arc lavas with an enriched OIB-like geochemical signature. The Central Costa Rican volcanic front is well known for its Galapagos OIB-type geochemical signature. This study focuses on minor alkaline and contemporaneous sub-alkaline magmatic rocks that

appeared ~6 Ma, at the same time the Galapagos signature is first evident in the volcanic front lavas. The regional correlation between La/Yb and Pb-isotopes along both the volcanic front and back-arc suggests that the geochemical variations are controlled by the composition of the magma sources (mantle and recent recycled oceanic crust). The geochemical variations of the magmas across the arc (e.g. Nb/Nb*, Pb/Pb*) depend on the absence of a subducting slab or the distance from it. Recent adakites (<4.5 Ma) are located above the edge of the subducting slab between Costa Rica and Panama. The alkaline magmas are restricted to areas were there is no clear seismic evidence of a subducting slab, with a geochemical signature controlled mostly by upwelling mantle with some contributions of the subduction component. The isotopic composition of the alkaline basalt suggests an important Galapagos Plume component. Mantle potential temperatures calculated from olivine-phyric alkaline basalt are higher (~1390- 1430 ˚C) than expected from ambient mantle decompression. We calculated the initial and final melting pressures from the units that yield successful primary magma solutions. The initial meting pressures 3.0-2.7 GPa are in the garnet-spinel transition depth, and the final melting pressures range between 2.5-2.1 GPa. The length of the upwelling melt column positively correlates with the computed melt fractions. The final meting pressure ~85-70 km (~2.5-2.1 GPa) suggest that the lithosphere-asthenosphere boundary is possibly the upper limit of the melting column. The geochemical signature and the petrological characteristics of these lavas are consistent with the geophysical evidence that suggests a broad interaction between Galapagos Plume, the Cocos Ridge (and associated seamount provinces), and the arc in southern Central America. We report a younging age progression of the back-arc volcanism towards the north, consistent with arc-parallel mantle flow models, and an age progression in the opposite direction in the adakitic unites possibly related to the east-west migration of the Panama Fracture Zone. A model that involves mantle metasomatism by slab derived melts, follow by slab detachment after the collision of the arc with the Galapagos tracks (~ 10-8 Ma) and the influx of the hotter enriched asthenosphere, is preferred to explain the composition of the erupted alkaline lavas and the temperature requirements for slab melts (recent oceanic crust recycling) in the southern Central American arc.

Keywords

Central America, Galapagos Plume, alkaline basalt, adakite, petrology, mantle potential temperatures, lithosphere, geochemistry, Sr-Nd-Pb isotopes

1 Introduction

Mantle plumes near subduction systems can cause geochemical and geodynamic deviations from normal arc magmatism. Direct arc-plume interaction can occur if the arc passes over the plume or if the arc is close to the influence of the mantle plume. For example, geophysical and geochemical evidence suggest that the Samoa mantle plume flows beneath the Lau Basin into the northern segment of the Tonga-Kermadec arc (Went et al., 1997; Turner and Hawkesworth, 1998, Smith et al., 2001). A less direct interaction that can cause similar geochemical results occurs when the eruptive products of a plume (e.g. seamount tracks) subduct beneath an arc. Subduction of hotspot tracks can "re-fertilize" the arc mantle source by metasomatic processes related to oceanic crust recycling. Subsequent melting of this metasomatized mantle can produce lavas with an OIB signature in an arc setting (Gazel et al., 2009). Wendt et al. (1997) reported Pb isotopes and trace element evidence for this type of interaction in the central Tonga-Kermadec arc impacted by the subducting Louisville seamount track. The OIB signature in alkaline lavas from the Mexican volcanic belt has been attributed to plume activity below the arc (Márquez et al., 1999). Recent evidence, however, suggests that this signature in Mexico is caused by mantle re-fertilization by oceanic crust recycling (Straub et al., 2008) rather than a mantle plume. Bryant et al. (2006) reported Pb, Sr, and Nd isotopic and trace element evidence for the interaction between melts from the subducting Carnegie Ridge (Galapagos Plume track) and the mantle wedge in the northern Andean volcanic zone in Ecuador. In the northern Marianas the subduction of the Wake and Magellan seamounts (Koppers et al., 1998) also correlates with an enriched geochemical and Pb-isotopic signature of the eruptive lavas (Peate and Pearce, 1998; Ishizuka et al., 2007; Benjamin et al., 2007). In summary, independent of the nature of the interaction between an arc and a mantle plume (or the eruptive products of a plume), the result will be arc lavas with an anomalous enriched OIB-like geochemical signature in a subduction setting.

The central Costa Rican volcanic front lavas are well-known for their enriched OIB-like signature (e.g., Reagan and Gill, 1989; Herrstrom et al., 1995; Gazel, 2003; Feigenson et al., 2004; Hoernle et al., 2008, Gazel et al., 2009). Herrstrom et al. (1995) suggested that trench-parallel mantle flow above the subducting Nazca Plate, proposed by Russo and Silver (1994), brings this enriched component from the mantle wedge beneath

South America. Abratis and Wörner (2001) suggested that a “slab window” in the subducting Cocos Plate, originally proposed by Johnston and Thorkelson, (1997), allows Galapagos-modified asthenosphere to flow below southern Costa Rica and Panama. Feigenson et al. (2004) explained the OIB signature by re-melting of mantle modified by the Galalapagos Hostpot beneath central Costa Rica and Panama. Goss and Kay (2006) proposed the OIB-like signature of the central Costa Rican volcanic front by the incorporation of fore-arc oceanic complexes into the mantle wedge by tectonic erosion. Recent studies, however, have provided convincing evidence that this anomalous signature in the volcanic front is derived from the interaction of the mantle wedge with the Galapagos Hostpot tracks subducting beneath Costa Rica and Panama (Benjamin et al., 2007; Hoernle et al., 2008; Gazel et al., 2009).

Most of the former studies focus on the active Central American volcanic front. This study focuses on volumetrically minor alkaline basalts and adakites that appear in, behind or near the arc after ~6 Ma, the same time that the OIB signature is first evident in the volcanic front lavas. Here we will evaluate from a petrologic and geochemical perspective different models that attempt to explain the occurrence of these alkaline basalts and adakites in southern Central America and their relation to the Galapagos Plume.

1.1 Tectonic setting of southern Central America

The Central American volcanic front extends parallel to the Middle American Trench from the Mexico-Guatemalan border to central Costa Rica, followed by a gap in recent volcanic activity from central Costa Rica to Panama (Fig. 1). The northwest segment of the arc (Guatemala) is located on Paleozoic continental crust, while the southeast segment (Costa Rica-Panama) develops on the western-most edge of the Caribbean Large Igneous Province (CLIP) (Dengo, 1985; Hauf et al., 2000; Alvarado et al. 2007). The Central American volcanic front results from the subduction of the Cocos Plate beneath the Caribbean Plate. The convergence rate between the Cocos and Caribbean plates increases toward the southeast from ~60 mm/year off southern Guatemala to ~90 mm/year off southern Costa Rica (DeMets, 2001). The depth and angle of the Wadati-Benoiff zone beneath the volcanic front ranges from ~200 km and 80° beneath Nicaragua to ~125 km and 60° beneath central Costa Rica (Protti et al., 1994; Husen et al., 2003; Syracuse and Abers, 2006). Seismicity associated with the subducting Cocos Plate ends abruptly south of central Costa Rica, where seismicity reaches a maximum depth of ~50 km (Fig. 1) (Protti et al., 1994). Normal mid-ocean ridge basalt (MORB) crust produced at the East Pacific Rise subducts beneath Guatemala to northwestern Costa Rica. In contrast, the oceanic crust subducting beneath central Costa Rica and Panama was formed at the Cocos-Nazca spreading center. This crust has been overprinted by the Galapagos Hostpot tracks and it is characterized by large oceanic discontinuities caused by several fracture zones. The Middle American Trench off Costa Rica is characterized by seamount subduction and tectonic erosion (Ranero and von Huene, 2000; Vannucchi et al., 2001; Husen and Kissling, 2002; Ranero et al., 2003, Vannucchi et al., 2006). The subducting Galapagos Hostpot tracks offshore of Costa Rica (Fig. 1) range in age between 13.0-14.5 Ma (Werner et al., 1999, O'Connor et al., 2007). The subducting Galapagos Seamount Province out-board of central Costa Rica has an

OIB-alkaline composition and an isotopic signature belonging to the Northern Galapagos Domain, similar to volcanic rocks from the Wolf-Darwin Lineament in the Galapagos Archipelago (Hoernle et al., 2000; Werner et al., 2003, Harpp et al., 2005). The subducting Cocos and Coiba ridges have an OIB-tholeiitic composition with a dominant isotopic component of the Central Galapagos Domain (Hoernle et al., 2000; Werner et al., 2003) (Fig 1).

1.2 Geochemical variations along the volcanic front in Central America

It is widely accepted that the magmatic production in a volcanic arc result from the partial meting of the mantle wedge triggered by fluids from the subducted slab. Along the volcanic front in Central America the geochemical indicators of subducting sediments (e.g. Ba/La, U/Th and $^{10}Be/^{9}Be$) define a maximum in northwest to central Nicaragua and a minimum in central Costa Rica (Carr et al., 1990; Leeman et al., 1994; Patino et al., 2000). Feigenson and Carr (1993) suggested two mantle reservoirs for Central America. The most common reservoir is analogous to depleted mantle (DM). The second reservoir has a more enriched composition and was visualized as garnet-bearing pyroxenitic veins within the DM reservoir. Melting of this veined mantle triggered by interaction with the subduction fluids produced magmas with a typical arc signature in most of the volcanic front (Carr et al., 2003; Feigenson et al., 2004). This signature is dominant along most of the volcanic front. Nevertheless, central Costa Rica lavas have an anomalous enriched OIB-like geochemical signature (Regan and Gill, 1989; Herrstrom et al., 1995; Gazel, 2003; Feigenson et al., 2004; Hoernle et al., 2008, Gazel et al., 2009).

The enriched signature of the central Costa Rican volcanic front was also recognized by the steep REE patterns (high La/Yb) of the erupted lavas (Carr et al., 1990). Higher La/Yb implies a lower degree of partial melting or derivation from a more enriched source. The overall correlation between La/Yb and radiogenic isotope ratios (Gazel et al., 2009) indicates that more enriched sources are present where La/Yb is higher (beneath central Costa Rica and Panama). The mirror image in the along the arc variations of La/Yb, Ba/La and $^{206}Pb/^{204}Pb$ suggests that the subducted sediment component, characterized by high Ba/La but low La/Yb and $^{206}Pb/^{204}Pb$ (possibly as a fluid) is dominant beneath Nicaragua and that an enriched OIB-type component, with low Ba/La but high La/Yb and $^{206}Pb/^{204}Pb$ (possibly as a melt), is dominant beneath central Costa Rica (Hoernle et al., 2008; Sadofsky et al., 2008). Therefore, the geochemical variations along the volcanic front reflect the extent and type of metasomatic processes caused by the subducting input and magma source composition and not just the degree of partial melting (Gazel et al., 2009).

2 Results

2.1 Age relations and progression

To study the age relations between the alkaline units, the adakites and the volcanic front lavas, we determined 25 $^{40}Ar/^{39}Ar$ step-heating ages. The analytical methods, data and examples of age spectrum are provided in the Supplementary Materials (Table 1 and details in Tables 4 and 5). The new age data define an age progression in the back-arc units from southern Costa Rica to Nicaragua (Fig. 1). The oldest back-arc magmas, located in southern Costa Rica, have a minor subduction signature but also display a clear Galapagos geochemical signature. This unit, known as the Victoria dike swarm (Dengo, 1962), includes a series of shallow intrusions and basaltic flows. The basaltic matrix from one of these dikes yields an age of 6.49±0.03 Ma, slightly older than the age reported by Abratis and Worner (2001) for this same unit. The ages of the alkaline back-arc rocks become progressively younger to the north (Fig. 1).

New ages for alkaline basalts from the Guayacan Formation, the unit directly north of the Victoria Dikes, range between 4.48±0.19-4.33±0.03 Ma, confirming the K/Ar ages reported by Bellon and Tournon (1978) for this unit. Contemporaneous volcanic front lavas in the La Garita Fomation (6.47±0.21 Ma, Gazel et al., 2009) and Paso Real Formation (4.23±0.02 Ma, this study) are the first on the volcanic front to have the Galapagos signature (Gazel et al., 2009).

The next pulse of back-arc activity, the Azules unit, is preserved to the north of the Guayacan Formation. Two lavas from this unit collected in the Lomas Azules provided ages that range between 3.60±0.03-3.23±0.03 Ma. Further north, a sample from this unit collected in the Cerro Coronel provided a slightly younger age of 3.06±0.08 Ma. North of Lomas Azules, near the Costa Rican-Nicaraguan border there are a series of isolated hills known as the Lomas del Colorado that possibly represent the last pulse of the Azules unit. The new dated samples range between 3.13±0.06-2.01±0.11 Ma.

The northern-most dated unit is the Cukra Hill Unit, in the Pear Lagoon area of Nicaragua. One sample from Cukra Hill yielded an age of 0.74±0.03Ma. The most recent volcanic activity is possibly <<1 Ma and is represented by small cinder cones near the Caribbean coast of Costa Rica (Cerro Tortuguero) and in the Pearl Lagoon area of Nicaragua (Volcan Blue). This interpretation is based on the cone morphology and the state of preservation of the rocks (mostly fresh tephra with olivine phenocrysts) in these localities and the fact that the collected samples are too young to be dated by $^{40}Ar/^{39}Ar$ techniques. With the possible exception of Tortuguero, our data support the age progession of volcanism at 40 mm/yr proposed for the Costa Rica back-arc by Abratis and Wörner (2001) and extend this age progression in volcanism further to the NNW. Abratis and Wörner (2001) interpreted this age progression to reflect mantle flow through a slab window to north beneath the Costa Rica back-arc. Combining the results from seismic anisotropy and correlations in isotopic composition with distance along the volcanic front from central Costa Rica to NW Nicaragua, Hoernle et al. (2008) propose NW mantle flow at a rate 60-190 mm/yr. Gazel et al. (2009) have shown that the Seamount Province Component of the subducting Galapagos Hostpot Track first appeared in Costa Rica 6 Ma ago, constraining the rate to be c. 50-60 cm/yr

The alkaline lavas in Panama occur in the forearc and volcanic front but are absent in the back-arc (Fig. 1). Their tectonic setting is more complicated than of the back-arc of Costa Rica and Nicaragua, which explains the fact that there is no clear age progression in the Panamanian alkaline suites. Nevertheless, our new ages suggest a correlation between the first recorded adakites in southern Costa Rica and Panama (4.54±0.64-3.558±0.0043 Ma) and the first pulse of alkaline basalt in Panama (4.45±0.35 Ma). In contrast, the adakites show a progression of decreasing ages to the southeast from 4.54±0.32-3.558±0.0043 Ma in southern Costa Rica/Panama to 0.77±0.37-0.21±0.07 Ma to the southeastin Panama at a rate of 20-30 mm/yr. It has been shown that the Panama Fracture Zone (Fig. 1) have been migrating toward the east (Meschede et al., 1998; MacMillan et al., 2004), suggesting a link between the adakite age progression, possibly resulting from melting of the slab edge, and the eastward movement of the Panama Fracture Zone.

2.2 Petrology results

The main crystalline phases in the alkaline samples are olivine, clinopyroxene, and plagioclase. Olivine is typically unaltered and commonly bears melt and spinel inclusions. Clinopyroxene is Ti-augite or aegirine. Plagioclase is abundant in the shallow intrusions and generally high in Ca (An>50%). The matrix is generally trachytic, composed of plagioclase, clinopyroxene, olivine, magnetite, glass and occasionally traces of biotite. In the low silica samples, feldspathoids (generally analcime) are also present in the matrix. Feldspathoids (analcime and hauyne) are also common in the shallow intrusion together with amphibole and traces of biotite. We found five new localities with spinel-bearing mantle peridotite and pyroxenite inclusions with reaction rims with the olivine-rich alkaline basalt host. The adakites are composed of clinopyroxene together with orthopyroxene in an interstitial matrix of plagioclase, pyroxenes and glass. Some adakites (trachy-andesites, Fig. 2A) are also composed of amphibole and biotite with cumulates of the same minerals in a trachytic matrix.

For this study we produced 123 new major element analyses (wt%). The analytical methods and data are included in the Supplementary Materials (Table 1). The back-arc samples from Costa Rica and Nicaragua and the alkaline basalts from Panama range from picritic basalts and basanites to basaltic trachy-andesites. They are characterized by lower SiO_2 and higher alkali contents than the volcanic front lavas (Fig. 2A). The low-silica (<45% SiO_2) samples are characterized by high CaO contents, similar to experimental data of magmas produced by melting of a carbonated peridotite (addition of CO_2 to the mantle) (Dasgupta et al., 2007) (Fig. 2B). There is also a minor population of samples (generally in the sub-alkaline lavas, Fig. 2 A) with lower CaO and higher SiO_2 contents to be produced by melting mantle peridotite (Fig. 2B). Modeled liquid lines of descent (Fig. 2B) also suggest that these samples are not the result of normal fractional crystallization of a primary magma produced by melting a peridotite source. Therefore, these samples possibly require either a second stage pyroxenite component (Fig 2B) or large amounts of pyroxene fractionation possibly in the mantle (Albarède et al., 1997; Herzberg and Asimow, 2008). More detailed work (e.g., olivine composition analyses) is required to determine if indeed this is a pyroxenitic component. For now we can infer that, if there is a pyroxenitic component, it may be in the form of veins that result from the reaction of silica-rich melts with a mantle peridotite (Feigenson and Carr, 1993; Sobolev et al., 2005; Herzberg, 2006). The adakite samples are basaltic andesites to andesites and fall on the high-K trend of the central Costa Rican volcanic front lavas, interpreted to be the result of mantle metasomatism by slab-derived melts (Hoernle et al., 2008; Gazel et al., 2009). The high-silica adakite end-members have compositions close to experimental eclogite melts (Petermann and Hirschmann, 2003) (Fig. 2B).The low silica adakites possibly represent a mix between mantle melts (by subduction released fluids) and slab melts (Fig.2B).

2.3 Petrological information from peridotite primary magmas from the alkaline basalts

A primary magma is a silicate liquid that initially separates from a mantle source. In most cases primary magmas are modified by crystallization during transport to the surface and eruption (e.g., O'Hara, 1968). To reconstruct a primary magma composition, it is necessary to find the most magnesian liquid that can be identified in a given rock suite on an olivine control trend. Once the composition of a primary magma is obtained (see Supplementary Materials, Table 6 for details), we can use that composition to infer petrological information such as, mantle potential temperatures (T_P), melt fractions and melting pressures. In an arc setting, it is a major task to obtain lava compositions that fulfill the requirements of Herzberg and Asimow (2008) (Supplementary Materials) for primary magmas, because most rocks are too fractionated to be used to model primary compositions. However, we were able to obtain 14 successful primary magma solutions through vigorous sampling and selection of olivine-phyric basalt in the alkaline suites of Costa Rica (13) and Panama (1).

The MgO content of a volatile-deficient primary magma from a peridotite source positively correlates with the temperature of the mantle source (e.g., Langmuir et al., 1992, Putirka, 2005; Herzberg et al., 2007; Herzberg and Asimow, 2008) and provides a petrological record of the mantle potential temperature. The term mantle potential temperature (T_P) defines the temperature that a mass of mantle will obtain if it rises adiabatically without melting to the surface of the Earth (McKenzie and Bickle, 1988).

From a primary magma composition (Supplementary Materials, Table 6), we can determine if a primary magma is derived from a normal ambient mantle (T_P 1350±50 ˚C), typical of the mid-ocean ridge system, or from a restricted mantle thermal anomaly like a mantle plume with a higher T_P (e.g. ~1500 ˚C for the T_P maximum in the Galapagos Hostpot) (McKenzie et al, 2005; Herzberg et al., 2007; Herzberg and Asimow, 2008).

The T_P computed for the alkaline basalts in Costa Rica and Panama, ranges between ~1390- 1430 ˚C, higher than ambient mantle temperatures (T_P 1350±50 ˚C) (Fig. 3). These mantle potential temperature results are the same as the lower end of those determined for the Galapagos Hotspot and near the T_Ps calculated for the Cocos and Carnegie ridges (Galapagos tracks) (Fig. 3) (Herzberg and Gazel, 2009). Even though Weins et al. (2006) used a different method for mantle potential temperature calculation, they also reported mantle potential temperatures higher than ambient mantle of 1450 ˚C in the Lau Basin and 1430˚C in the North Fiji Basin. In the case of the Lau basin this authors interpreted the higher mantle potential temperatures as the result of the influx of the Samoa Plume into the mantle wedge of the Tonga Arc. The process that produced mantle potential temperatures higher than ambient mantle in the North Fiji Basin is unknown. On the other hand, the computed mantle potential temperatures from the Mariana Trough and the East Scotia Ridge are expected ambient mantle potential temperatures (1350 ˚C) (Weins et al., 2006).

We calculated the initial and final melting pressures of the primary magmas of the alkaline basalts, using the geobarometers described in Herzberg and Gazel (2009). The initial melting pressures for the units that yield successful petrological solutions (Supplementary Materials) range between 3.0-2.7 GPa, lying at the garnet-spinel transition depth, and the final melting pressures range between 2.5-2.1 GPa. The length of the melting column ranges between ~40-14 km and correlates positively with the computed melt fractions (Fig. 4). Magmas aggregated during upwelling in longer melting columns have higher melt fractions (Fig. 4). The average final meting pressure calculations suggest that boundary is variable lying between ~85-70 km (~2.5-2.1 GPa). This upper limit of the melting column is possibly the lithosphere-asthenosphere boundary (Fig. 5). The calculated results agree with estimates of the lithosphere-asthenosphere boundary from recent geophysical studies in oceanic settings that yield average thicknesses of ~70 km (Rychert and Shearer, 2009; Kawakatsu et al., 2009). The calculated melting pressures are also consistent with the mineralogy of mantle peridotite xenoliths found in the back-arc alkaline basalts. The presence of spinel, as an Al-phase instead of garnet or plagioclase, suggests that the alkaline melts produced at about 100 km (~ 3GPa) "collected" the xenoliths from the lithospheric mantle (~70-40 km) (Herzberg and Gasparik, 1991) during transport to the surface (Fig. 5).

2.4 Geochemical variations between the volcanic front and the back-arc: Slab Signature vs. Mantle Control.

We produced 73 new trace element analyses. The analytical methods and data are included in the Supplementary Material (Table 2). Primitive-mantle normalized trace element patterns are plotted in Fig. 6, compared with both OIB and arc lava reference patterns. Plots of distance along the volcanic front versus $^{206}Pb/^{204}Pb$ and La/Yb (Fig. 7A and B) reveal similar correlations, suggesting that the geochemical variations along the volcanic front and back-arc are related to changes in the magma source composition and not just the degree of melting. Along the volcanic front the lowest $^{206}Pb/^{204}Pb$ and La/Yb are in the Nicaraguan samples and the highest $^{206}Pb/^{204}Pb$ and La/Yb are in Costa Rica and Panama (Fig. 7, A and B).

Fractionation of high field strength elements (HFSE, eg. Nb, Ta, Zr, Ti, Hf) relative to other trace elements is well known for convergent margin igneous rocks (e.g. the northwest Nicaragua and central Costa Rica arc pattern in Fig. 6). This fractionation is related to subduction processes in which a residual mineral phase in the subducting slab (e.g., rutile) or mantle wedge holds the HFSE (e.g., Ringwood, 1990, Foley et al., 2000). The Nb/Nb* denotes the variations in the depletion of Nb relative to U and La, normalized to the McDonough and Sun (1995) primitive mantle composition. Magmas derived from the mantle wedge in a subduction zone through flux melting have Nb/Nb* <1, whereas magmas produced by mantle upwelling with no subduction signature are characterized by Nb/Nb* ≥1. The volcanic front lavas of Costa Rica and Nicaragua and the adakites from Panama have a significant subduction signatures with Nb/Nb* <0.5 (Fig. 5C). The back-arc lavas in Nicaragua have positive Nb and Ta anomalies (Fig. 6), which is reflected in Nb/Nb*>1 (Fig. 7C). Therefore, lavas with Nb/Nb*>1 possibly represent partial melts of upwelling mantle, with a minor subduction component. Alkaline basalts in Panama and back-arc lavas from Costa Rica have transitional Nb/Nb* (0.5-1). This suggests that these lavas were produced by mantle upwelling but with some influence of the subduction process. Fig. 1 and 7C show that HFSE depletions (Nb/Nb* <0.5) only occur at geographic locations directly above the subducting slab inferred from seismicity (contours in Fig. 1). HFSE depletions are common in the volcanic front of

Costa Rica and robust in the volcanic front lavas of Nicaragua and the adakites in southern Costa Rica/Panama (Fig. 7C). The samples with Nb/Nb* >0.5 are located in areas with no seismic evidence of the subducting slab (Panama) or well-behind it (the back-arc regions of Costa Rica and Nicaragua). These spatial-geochemical correlations are consistent with the HFSE depletions in the arc magmatism being controlled by the presence of a HFSE retaining phase (e.g. residual rutile) in the subducting slab.

Pb is a fluid mobile element. Magmas produced by arc volcanism are also characterized by having Pb enrichments relative to other trace elements. In contrast, the behavior of Pb is the opposite in OIB magmas (see reference patterns in Fig. 6). Previous studies have showed that the Pb geochemistry and Pb isotope systematics in the Central American volcanic front are largely controlled by the interaction between the subducting oceanic crust and the mantle (Feigenson et al., 2004; Hoernle et al., 2008; Gazel et al., 2009). Based on these results, we follow a similar approach to the one previously discussed for Nb but with Pb. The Pb/Pb* indicates the variations of Pb relative to Ce and Pr. Pb/Pb*>1 indicates positive Pb anomalies typical of arc magmatism whereas Pb/Pb* <0.5 indicates a depleted Pb signature that is typical of intraplate (OIB-type) magmatism. Intermediate Pb/Pb* (0.5-0.1) indicates a combination of arc and intraplate (mantle upwelling) processes. Fig. 1 and Fig. 7D show that there is a direct association between Pb/Pb* >1 and the presence of a subducting slab inferred form seismic studies. The volcanic front from Nicaragua, most of the Costa Rican volcanic front and the adakites in southern Costa Rica and in Panama have Pb/Pb* >1 controlled by Pb added from the subducting slab (Fig. 7D). On the other hand, most of the alkaline lavas in Panama and the back-arc lavas of Costa Rica and Nicaragua have major depletions in Pb (Pb/Pb*<0.5)

(Fig. 7D). These samples are interpreted to be the result of mantle upwelling processes, analogous to an intraplate-OIB-type setting. Some back-arc samples and the central Costa Rican volcanic front samples show transitional Pb/Pb* values which indicates mixing between slab melts/fluids and decompression melts from mantle upwelling (Fig. 7D).

In summary, the correlation between La/Yb and Pb-isotopes for the different arc segments suggests that these geochemical variations, both in the volcanic front and in the back-arc, are controlled by the composition of the magma sources (mantle source + subducting oceanic crustal components). The geochemical variations of the magmas across the arc depend on the absence of, or distance from, the subducting slab. The alkaline basalts are restricted to areas that have no clear seismic evidence of a subducting slab (Fig. 1). The alkaline magmas in southern Central America have geochemical signatures controlled by decompression melting of upwelling mantle with some contributions from slab components. The adakites are located on the edge of the subducting slab between Costa Rica and Panama and have an important slab signature. The subduction signature is, of course, also evident in the volcanic front in Costa Rica and Nicaragua.

2.5 Fingerprinting the magma components: Evidence from radiogenic isotopes.

Radiogenic isotopic ratios are robust tracers of magma components, because they are not fractionated by magmatic processes such as mantle melting and crystallization. Therefore, they have been an important tool in the study of the source components of Central American lavas. Previous studies show systematic regional variations in the composition of volcanic front lavas, related to the mantle composition and heterogeneities, the nature of the overriding plate, and the different subducting input components (sediments and subduting crust) (Feigenson and Carr, 1986; Regan and Gill, 1989; Feigenson et al., 2004; Hoernle et al., 2008). The isotopic composition of the volcanic front lavas in Costa Rica revels a Galapagos OIB-type geochemical signature that appeared ~6 Ma (Gazel et al. 2009). To identify the different Galapagos Plume components and complete the database published by Hoernle et al (2008), we carried out 9 new Sr-Nd-Pb isotopic analyses of the back-arc lavas. We also included 42 new Sr-isotopic analyses not included before by Hoernle et al. (2008). The data and analytical methods are detailed in the Supplementary Material (Table 3).

The Pb, Nd and Sr isotope ratios for samples from the back-arc area of Costa Rica and Nicaragua and the adakites and alkaline basalts from southern Costa Rica together with end-members of the subducting Galapagos components (Seamount Province and Cocos/Coiba Ridge) from Gazel et al. (2009) and subducting sediments form Feigenson et al. (2004) are plotted in Fig. 8. The systematic decrease in the Galapagos Plume components described in the volcanic front (Gazel et al., 2009) from Southern Central America towards Nicaragua is also present in the back-arc region in all the systems reported in Fig. 8. The highest Pb-isotope, lowest Nd-isotope and Sr-isotope ratios are present in the Panamanian adakites and central Costa Rican volcanic front and back-arc lavas (Feigenson et al., 2004; Hoernle et al., 2008; this study) (Fig. 8).

Three isotopic end-members are required to explain the Pb-isotopic composition of southern Central American lavas, a depleted component (either depleted mantle – DM – in the mantle wedge or depleted subducting ocean crust/lithosphere) and two enriched components, the subducting Seamount Province and the Cocos/Coiba Ridges of the

Galapagos Hostpot Tracks (Hoernle et al., 2008; Gazel et al., 2009) (Fig. 8). The isotopic end-members from the Seamount Province and Cocos/Coiba Ridge were originally interpreted to be melts from the subducting slab (Hoernle et al., 2008; Gazel et al., 2009). All the evidence suggests that the Seamount Province Component is indeed a recent (~ 6 Ma) recycled component from the subducting Galapagos tracks in front of Costa Rica (Gazel et al., 2009). Melts/fluids from this component produced the metasomatic enrichment of the mantle wedge and possibly also the lithosphere of central Costa Rica. The adakites in Panama/Costa Rica are the result of the reaction of melts from the subducting Cocos and Coiba ridges with the mantle wedge, also resulting in a metasomatic enrichment of the mantle wedge and the lithosphere. As mentioned before, most of the alkaline basalts from Panama and the back-arc lavas from Costa Rica and Nicaragua were produced by mantle upwelling with some subduction contribution (Fig. 7C and D). The Sr-isotope ratios (and somehow the Nd-isotopes) also suggest that there are slab derived components (fluids from the subducting sediments and altered oceanic crust) in the back-arc lavas from Costa Rica and the alkaline lavas of Panama. This suggests that the Galapagos signature is a combination two recent inputs; the recycling of Galapagos tracks and upwelling of Galapagos modified asthenosphere, at least in southern Costa Rican and Panama.

3 Discussions

The geologic record shows that alkaline magmas, adakites and volcanic front lavas with geochemical characteristics similar to the subducting Seamount Province

(Gazel et al., 2009) and Cocos Ridge of the subducting Galapagos Hostpot track appeared in Costa Rica for the first time at ~6 Ma. From petrology we can infer two main source lithologies for lavas collected in this study. The alkaline lavas in Costa Rica and Panama require a fertile mantle peridotite source. Nevertheless, the samples with high CaO and low SiO_2 (Figure 2B) require that the mantle peridotite was metasomatized by CO_2. The adakites, on the other hand, were produced by direct partial melting of the subducting slab in the eclogite facies, leaving behind a garnet-rich residue with a HFSE-retaining phase (rutile?). The geochemical signature of the adakites is also consistent with the petrologic interpretation, because all the common geochemical indicators (e.g., steep REE, high La/Yb and Sr/Y) indicate high-pressure melting of a mafic protolith (e.g., Kay, 1978; Defant and Drummond, 1990). The volcanic front lavas were produced largely by flux melting, resulting from the hydration the metasomatized peridotitic mantle wedge by fluids from the subducting slab (Fig. 2B). The petrological and geochemical indicators slab-derived-hydrous melts are more evident in the adakites from southern Costa Rica/Panama, but they are also an important component in the central Costa Rican volcanic front lavas (Gazel et al., 2009). The adakite upper-mantle-like oxygen isotope ratios require mixing of slab melts from the upper low-temperature and lower high-temperature altered parts of the subducting crust (Bindeman et al., 2005). Slab melts in this part of the arc can be explained by melting of relatively young subducting Galapagos Hostpot tracks (13.0-14.5 Ma) (Werner et al., 1999) under a hot mantle regime. The petrology and geochemistry presented here suggest that the alkaline basalts in southern Central America are primarily derived through decompression melting and the interaction of this melts with the subduction-metasomatized lithosphere. The alkaline lavas are restricted to areas where the seismic evidence indicates that there is no subducting slab, therefore the metasomatic processes inferred with the geochemistry (Nb/Nb*>1, Sr and Nd-isotopes) pre-date the mantle upwelling. Contemporaneous adakites, on the other hand, appear to be restricted to the area above the Panama Fracture Zone.

Johnston and Thorkelson (1997) explained the OIB-like signature of the Costa Rican volcanic front lavas by the opening of a "window" in the subducting slab following the collision of the Cocos Ridge (or older Galapagos-related tracks). A slab window can be produced when an active oceanic spreading center subducts beneath an arc producing a gap between the two subducting plates (Thorkelson and Taylor, 1989; Thorkelson, 1996). Slab windows are formed mostly by the interaction of a spreading center with a subduction zone. The dominant melting mechanism above a slab window is adiabatic mantle decompression, controlled by the extension in the lithosphere above the slab free area. As a result, these areas in general are not related to "active mantle upwelling" like the one found in mantle plumes (Thorkelson, 1996). The volume of magma production above a slab window is generally small compared to a mid-ocean ridge or arc setting. The petrology of the erupted lavas above a "slab-free" region range from adakites and high Nb-basalts close to the edge of the subducting slab (Calmus et al., 2003, Aguillón-Robles et al., 2001; Defant et al. 1991) to alkaline and tholeiitic mafic volcanism produced by extension-related mantle upwelling (Hole et al., 1991; Gorring et al., 1997; Pallares et al., 2007). Based on the slab window model, we expect a MORB geochemical signature in the erupted lavas in southern Central America and mantle potential temperatures in the range of the ambient mantle of ~ 1350±50 °C (McKenzie et al, 2005; Herzberg et al., 2007; Herzberg and Asimow, 2008). Therefore, a simple slab-window model does not adequately explain the relatively high mantle potential temperatures (1390-1430°C) computed from the alkaline basalts in Costa Rica and Panama and the Seamount Province geochemical signature in the alkaline lavas behind the Central Costa Rican Volcanic Front (Hoernle et al., 2008; Gazel et al. 2009).

Detachment of the subducting slab will also produce a “slab free” area, generally larger than a slab window caused by the subduction of an active spreading center. Structural weakness in the subducting slab can trigger a tear and lead to the rapid sinking of the detached slab into the mantle (e.g., Davies and von Blanckenburg, 1995; Wortel and Spakman, 2000). This will produce an area free of subducting lithosphere that propagates laterally as the oceanic plate continues to tear along the strike of the subducting slab. The detached slab is replaced by upwelling asthenosphere (Levin et al., 2002; Ferrari, 2004; Pallares et al., 2007). The numerous hotspot tracks and fracture zones on the subducting Cocos and Nazca plates (Werner et al., 1999) suggests that the subducting slab below Costa Rica and Panama could be relatively easy to tear and detach. We suggest that the collision of the Galapagos Hostpot tracks with the arc beginning circa 10-8 Ma ago (Denyer and Arias, 1991; Silver et al., 2004; Gazel et al., 2009), clogged or slowed the subduction processes and triggered the detachment of a major portion of the subducting slab below Costa Rica and Panama (Fig. 9).

The detached slab was replaced by hot and buoyant asthenosphere, as suggested for northern Central America and Mexico (Rogers et al. 2002; Ferrari, 2004). This process differs in southern Central America, because the geochemical signature of the alkaline lavas (even the ones free of any slab signature) requires the contribution of a Galapagos Plume component (Fig. 9). Abratis and Wörner (2001) suggested that this signature resulted from Galapagos Plume flow beneath southern Costa Rica/Panama. O'Connor et al. (2007) showed that the standard fixed hotspot age-distance correlation is not the case for the Galapagos Plume. The Galapagos Plume continues its interaction with the Cocos Ridge at a significant distance from the plume axis (Meschede et al., 1998; O'Connor et al., 2007). An important piece of evidence of this long term plume-ridge interaction is the Cocos Island and near-by seamounts located in the middle of the Cocos Ridge, ~600 km away from modern the Galapagos Plume axis (Fig. 10) (Meschede et al., 1998; Werner et al., 2003; O'Connor et al., 2007). A classic linear age-distance progression from the plume axis (fixed at the modern day Galapagos Islands) predicts an age of ~9 m.y. for Cocos Island. Instead geochronology and paleomagnetic studies confirm an anomalously young age of ~2 m.y. (Castillo et al., 1998; O'Connor et al., 2007 and references therein).

Recent geophysical studies provide evidence of a possible thermal anomaly, located ~300 km below the Cocos. This anomaly extends ~1200 km from the Galapagos Hostpot to southern Central America (Montelli et al., 2006). These long-term broad plume-ridge interactions can be explained by plume movement within the mantle and plume capture by a ridge (Tarduno et al., 2009). Hoernle et al. (2008) show geophysical and geochemical evidence of arc-parallel flow in the mantle wedge beneath Costa Rica towards Nicaragua. The "slab-free area" in southern Costa Rica and Panama (see contours in Fig. 1) may indeed be a window that allows Galapagos mantle to flow beneath southern Costa Rica and Panama (Fig 9).

The "slab-free area" correlates with the highest elevations in southern Central America. A change from 85 to 70 km in lithosphere thickness calculated form the primary magmas of the alkaline basalts will not explain elevations above the sea level al almost 4 km (Fig. 5). Therefore, these elevations (e.g., the Talamanca Cordillera) are possibly related to the isostatic effect produced by hot mantle upwelling after the slab detachment in this area together with shortening related to the collision of the Cocos Ridge. These interpretations are also consistent with the progression of decreasing ages in the back-arc from southern Costa Rica to Nicaragua (Fig. 1). The age progression and arc-parallel mantle flow possibly represent northern flow of a thermal anomaly related to Galapagos-modified asthenosphere. The age progression of back-arc magmatism in Costa Rica and Nicaragua can be explained by the interaction of this Galapagos-modified "hot" asthenosphere and volatile-rich ambient mantle and lithosphere. As the Galapagos-modified asthenosphere moved towards the northwest (following the strike of the subducting slab) triggered melting in the ambient and lithospheric mantle. As the ambient mantle and lithosphere were depleted in volatiles and metasomaitic veins, the Galapagos-modified asthenospehere was not able to produce more extensive melting,

It has been argue that the source of alkaline and high Nb-basalt is amphibole bearing veins or cumulates at lithospheric pressures (Defant et al., 1992; Médard et al., 2006; Pilet et al., 2008). Even though some of low pressure experimental data from Médard et al. (2006) and Pilet et al. (2008) overlap the data of alkaline basalt from southern Central America produced in this study (Fig. 11). We argue based on the petrology (Fig. 2) and trace element composition (Fig. 12) of the alkaline lavas that the metasomatic veins are possibly dominated by a pyroxenitic component. These pyroxenites are "frozen metasomatic melts" from the interaction between lithosphere mantle and the subducting carbonated eclogite, the recycled Galapagos Tracks.

4. Conclusions

Petrology indicates that there are three main source lithologies for the lavas collected in this study. For the alkaline lavas in Costa Rica and Panama the source is mantle peridotite (sometimes metasomatized by CO_2) and pyroxenite viens located in the lithospheric mantle. The geochemical and isotopic evidence suggest that those veins represent subduction metasomatism by fluids/melts from subducting Galapagos Hotspot Tracks. The adakites were produced by direct partial melting of the edge of the subducting slab in the eclogite facies, leaving behind a garnet-rich residue with a HFSE-holding phase, such as titanite or rutile. The volcanic front lavas from Central Costa Rica reflect a mixture between hydrous slab melts from the subducting Seamount Province of the Galapagos Hotspot Track and DM mantle peridotite.

Mantle potential temperatures from primary magmas of olivine-phyric alkaline basalts that yield successful petrologic solutions (peridotite source, no important metasomatic addition, no cpx-plag fractionation, etc.) from Costa Rica and Panama are higher than ambient mantle and range between ~1390- 1430˚C. Initial melting pressures for calculated primary magmas range between 3.0-2.7 GPa (~100-85 Km) in the garnet-spinel transition depth. The final melting pressures range between 2.5-2.1 GPa (~ 85-70 km). These pressures suggest that the melting column varies between ~40-15 km. The extent of the melting column positively correlates with the calculated melt fractions. We interpret that the upper limit of the melt column (final melting pressures) as the lithosphere-asthenosphere boundary at ~85-70 km depth.

Radiogenic isotope systematics together with trace element data suggest that the Seamount Province Component is a recently arrived (~6 Ma) recycled component from the subducting Galapagos tracks in front of central Costa Rica (Hoernle et al., 2008; Gazel et al., 2009). This component can be traced in the volcanic front lavas from Costa Rica to southeast Nicaragua. The adakites in Panama/Costa Rica are also the result of the reaction of melts from the subducting Cocos/Coiba Ridge with the mantle wedge. Most of the alkaline basalts from Panama and the back-arc lavas from Costa Rica and Nicaragua were produced by upwelling mantle that interacted with a subduction metasomatized lithosperic mantle. We consider that the best way to explain the new data presented here is a model that involves slab detachment triggered by the collision of the Galapagos Hostpot tracks with the arc (primarily the buoyant Cocos Ridge), followed by the influx of hot, Galapagos modified asthenosphere that interacted with a subduction-metasomatized lithosphere.

5. Acknowledgments

Field work supported by G. Alvarado from the Central American School of Geology at the University of Costa Rica and O. Arias, F. Cervantes from the Instituto Costarricence de Electricidad. Field assistance by S. T. Carr is gratefully acknowledged. D. Symanski and S. Hauff provided valuable analytical support. L. Danyushevsky kindly provided the new version of Petrolog software. Revisions by N. Sou and L. Patino improved the original manuscript. This research is the result of collaboration between the Department of Earth and Planetary Sciences at Rutgers University and the German Science Foundation (DFG) Collaborative Research Center (SFB574). This work was supported through the NSF Margins Program, grants EAR0203388 and NSF OCE 0505924, the DFG Collaborative Research Center (SFB574, contribution 145) and by the Geological Society of America Student Award.

6. References

Abratis, M., and G. Worner (2001), Ridge collision, slab-window formation, and the flux of Pacific asthenosphere into the Caribbean realm, *Geology*, *29*(2), 127-130.

Aguillon-Robles, A., T. Calmus, M. Benoit, H. Bellon, R. O. Maury, J. Cotten, J. Bourgois, and F. Michaud (2001), Late miocene adakites and Nb-enriched basalts from Vizcaino Peninsula, Mexico: Indicators of East Pacific Rise subduction below Southern Baja California?, *Geology*, *29*(6), 531-534.

Albarède, F., B. Luais, G. Fitton, M. Semet, E. Kaminski, B. G. J. Upton, P. Bachelery, and J. L. Cheminee (1997), The geochemical regimes of Piton de la Fournaise volcano (Reunion) during the last 530,000 years, *Journal of Petrology*, *38*(2), 171-201.

Alvarado, G. E., C. Dengo, U. Martens, J. Bundschuh, T. Aguilar and B.Bonis, Stratigraphy and geologic history, in Central America: Geology, Resources and Hazards (eds Bundschuh, J. & Avarado, G.) 345–394 (Taylor and Francis, Leiden, 2007).

Bindeman I.N., J.M Eiler., G.M Yogodzinski., Y Tatsumi., C.R Stern., T.L. Grove, M. Portnyagin., K. Hoernle, and L.V .Danyushevsky (2005), Oxygen isotope evidence for slab melting in modern and ancient subduction zones. Earth Planet. Sci. Letters 235, 480-496.

Bryant, J. A., G. M. Yogodzinski, M. L. Hall, J. L. Lewicki, and D. G. Bailey (2006), Geochemical constrains on the origin of volcanic rocks from the Andean northern volcanic zone, Ecuador. *J. Petrol.*, 47(6), 1147-1175.

Calmus, T., A. Aguillon-Robles, R. C. Maury, H. Bellon, M. Benoit, J. Cotten, J. Bourgois, and F. Michaud (2003), Spatial and temporal evolution of basalts and magnesian andesites ("bajaites") from Baja California, Mexico: the role of slab melts, *Lithos*, *66*(1-2), 77-105.

Carr, M. J., M. D. Feigenson, L. C. Patino, and J. A. Walker (2003), Volcanism and geochemistry in Central America: Progress and problems, in *Inside the Subduction Factory, Geophys. Monogr. Ser*., vol 138, edited by J. Eiler and G. Abers, pp. 153-179, AGU, Washington, D. C.

Carr, M. J., M. D. Feigenson, and E. A. Bennett (1990), Incompatible element and isotopic evidence for tectonic control of source mixing and melt extraction along the Central American arc, *Contributions to Mineralogy and Petrology*, *105*(4), 369-380.

Castillo, P., R. Batiza, D. Vanko, E. Malavassi, J. Barquero, and E. Fernandez (1988), Anomalously young volcanoes on old hot-spot traces: Geology and Petrology of Cocos island, *Geological Society of America Bulletin*, *100*(9), 1400-1414.

Dasgupta, R., M. M. Hirschmann, and N. D. Smith (2007), Partial melting experiments of peridotite CO2 at 3 GPa and genesis of alkalic ocean island basalts, *Journal of Petrology*, *48*(11), 2093-2124.

Davies, J. H., and F. Von Blanckenburg (1995), Slab breakoff: A model of lithosphere detachment and its test in the magmatism and deformation of collisional orogens, *Earth and Planetary Science Letters*, *129*(1-4), 85-102.

Defant, M. J., and M. S. Drummond (1990), Derivation of some modern arc magmas by melting of young subducted lithosphere, *Nature*, *347*(6294), 662-665.

Defant, M. J., P. M. Richerson, J. Z. Deboer, R. H. Stewart, R. C. Maury, H. Bellon, M. S. Drummond, M. D. Feigenson, and T. E. Jackson (1991), Dacite genesis via both slab melting and differentiation: Petrogenesis of La Yeguada volcanic complex, Panama, *Journal of Petrology*, *32*(6), 1101-1142.

Defant, M. J., T. E. Jackson, M. S. Drummond, J. Z. Deboer, H. Bellon, M. D. Feigenson, R. C. Maury, and R. H. Stewart (1992a), The Geochemistry of young volcanism throughout western Panama and Southern Costa Rica-An overview, *Journal of the Geological Society*, *149*, 569-579.

DeMets, C. (2001), A new estimate for present-day Cocos-Caribbean plate motion: Implications for slip along the Central American volcanic arc, *Geophysical Research Letters*, *28*(21), 4043-4046.

Dengo, G., 1962, Tectonic-igenuos sequence in Costa Rica. In: Engel, A. E. J., James, H. J., Leonard, B. F. (Eds.), A volume to honor A. F. Budington. Geological Society of America Special Volume, pp. 133-161.

Dengo, G., 1985. Mid America; Tectonic setting for the Pacific margin from southern Mexico to northwestern Columbia. In: Nairn, A.E.M., Stechli, F.G. (Eds.), The ocean basins and margins. Plenum Press, New York, pp. 123-180.

Denyer, P., and O. Arias (1991) Estratigrafía de la región central de Costa Rica. *Rev. Geol. Am. Cent.*, 12, 1-59, http://www.geologia.ucr.ac.cr/revista-geol.htm.

Eiler, J. M., M. J. Carr, M. Reagan, and E. Stolper (2005), Oxygen isotope constraints on the sources of Central American arc lavas, *Geochemistry Geophysics Geosystems*, *6*. Feigenson, M. D., and M. J. Carr (1993), The source of Central American lavas: Inferences from geochemical inverse modeling, *Contributions to Mineralogy and Petrology*, *113*(2), 226-235.

Feigenson, M. D., and M. J. Carr (1986), Positively correlated Nd and Sr isotope ratios of lavas from the Central American volcanic front, *Geology*, 14, 79-82.

Feigenson, M. D., and M. J. Carr (1993), The source of Central American lavas: Inferences from geochemical inverse modeling, *Contrib. Mineral. Petrol.,* 133, 226-235.

Feigenson, M. D., M. J. Carr, S. V. Maharaj, S. Juliano, and L. L. Bolge (2004), Lead isotope composition of Central American volcanoes: Influence of the Galapagos plume, *Geochem. Geophys. Geosyst.,* 5, Q006001, doi:10.1029/2003GC000621.

Ferrari, L. (2004), Slab detachment control on mafic volcanic pulse and mantle heterogeneity in central Mexico, *Geology*, *32*(1), 77-80.

Foley, S. F., M. G. Barth, and G. A. Jenner (2000), Rutile/melt partition coefficients for trace elements and an assessment of the influence of rutile on the trace element characteristics of subduction zone magmas, *Geochimica et Cosmochimica Acta*, *64*(5), 933-938.

Foley, S., M. Tiepolo, and R. Vannucci (2002), Growth of early continental crust controlled by melting of amphibolite in subduction zones, *Nature*, *417*(6891), 837-840.

Gazel, E., M. J. Carr, K. Hoernle, M. D. Feigenson, D. Szymanski, F. Hauff, and P. van den Bogaard (2009), Galapagos-OIB signature in southern Central America: Mantle refertilization by arc-hot spot interaction, *Geochemistry Geophysics Geosystems*, *10*, 32.

Gazel, E. (2003), Las series alcalinas del Plioceno de Costa Rica: Distribución espacial y relación con una fuente mantelica tipo OIB. *Rev. Geol. Am. Cent., 29* , 87-94, http://www.geologia.ucr.ac.cr/revista-geol.htm.

Geldmacher, J., B. B. Hanan, J. Blichert-Toft, K. Harpp, K. Hoernle, F. Hauff, R. Werner, and A. C. Kerr (2003), Hafnium isotopic variations in volcanic rocks from the Caribbean Large Igneous Province and Galapagos hot spot tracks, *Geochemistry Geophysics Geosystems*, *4*.

Gorring, M. L., S. M. Kay, P. K. Zeitler, V. A. Ramos, D. Rubiolo, M. I. Fernandez, and J. L. Panza (1997), Neogene Patagonian plateau lavas: Continental magmas associated with ridge collision at the Chile Triple Junction, *Tectonics*, *16*(1), 1-17.

Harpp, K. S., and W. M. White (2001), Tracing a mantle plume: Isotopic and trace element variations of Galapagos seamounts, *Geochemistry Geophysics Geosystems*, *2*.

Hauff, F., K. A. Hoernle, P. van den Bogaard, G. E. Alvarado, and D. Garbe-Schönberg (2000), Age and geochemistry of basaltic complexes in western Costa Rica: Contributions to the geotectonic evolution of Central America, *Geochem. Geophys. Geosyst.*, 1

Herrstrom, E. A., M. K. Reagan, and J. D. Morris (1995), Variations in lava composition associated with flow of asthenosphere beneath southern Central America, *Geology*, *23*(7), 617-620.

Herzberg, C. (2006), Petrology and thermal structure of the Hawaiian plume from Mauna Kea volcano, *Nature*, *444*(7119), 605-609.

Herzberg, C., and T. Gasparik (1991), Garnet and pyroxenes in the mantle: A test of the majorite fractionation hypothesis, *Journal of Geophysical Research-Solid Earth*, *96*(B10), 16263-16274

Herzberg, C., P. D. Asimow, N. Arndt, Y. L. Niu, C. M. Lesher, J. G. Fitton, M. J. Cheadle, and A. D. Saunders (2007), Temperatures in ambient mantle and plumes: Constraints from basalts, picrites, and komatiites, *Geochemistry Geophysics Geosystems*, *8*.

Herzberg, C., and P. D. Asimow (2008), Petrology of some oceanic island basalts: PRIMELT2.XLS software for primary magma calculation, *Geochemistry Geophysics Geosystems*, *9*.

Herzberg, C., and E. Gazel (2009), Petrological evidence for secular cooling in mantle plumes, *Nature*, *458*(7238), 619-U683.

Hoernle, K., R. Werner, J. P. Morgan, D. Garbe-Schonberg, J. Bryce, and J. Mrazek (2000), Existence of complex spatial zonation in the Galapagos plume for at least 14 m.y, *Geology*, *28*(5), 435-438.

Hoernle, K., et al. (2008), Arc-parallel flow in the mantle wedge beneath Costa Rica and Nicaragua, *Nature*, *451*(7182), 1094-U1094.

Hole, M. J., G. Rogers, A. D. Saunders, and M. Storey (1991), Relation between alkalic volcanism and slab-window formation, *Geology*, *19*(6), 657-660.

Husen, S., E. Kissling, and R. Quintero (2002), Tomographic evidence for a subducted seamount beneath the Gulf of Nicoya, Costa Rica: The cause of the 1990 Mw=7.0 Gulf of Nicoya earthquake, *Geophysical Research Letters*, *29*(8).

Husen, S., R. Quintero, E. Kissling, and B. Hacker (2003), Subduction-zone structure and magmatic processes beneath Costa Rica constrained by local earthquake tomography and petrological modelling, *Geophysical Journal International*, *155*(1), 11-32.

Ishizuka, O., R. N. Taylor, M. Yuasa, J. A. Milton, R. W. Nesbitt, K. Uto, and I. Sakamoto (2007), Processes controlling along-arc isotopic variation of the southern Izu-Bonin arc, *Geochemistry Geophysics Geosystems*, *8*.

Johnston, S. T., and D. J. Thorkelson (1997), Cocos-Nazca slab window beneath Central America, *Earth and Planetary Science Letters*, *146*(3-4), 465-474.

Kay, R. W. (1978), Aleutian magnesian andesites: Melts from the subducted Pacific Ocean crust, *J. Volcanol. Geotherm. Res.,* 4, 117-132.

Kawakatsu, H., P. Kumar, Y. Takei, M. Shinohara, T. Kanazawa, E. Araki, and K. Suyehiro (2009), Seismic Evidence for Sharp Lithosphere-Asthenosphere Boundaries of Oceanic Plates, *Science*, *324*(5926), 499-502.

Koppers, A. A. P., H. Staudigel, J. R. Wijbrans, and M. S. Pringle (1998), The Magellan seamount trail: implications for Cretaceous hotspot volcanism and absolute Pacific plate motion, *Earth and Planetary Science Letters*, *163*(1-4), 53-68.

Langmuir, C.H., Klein, E.M. and Plank, T. (1992) in Mantle Flow and Melt Generation at Mid-Ocean Ridges (eds Morgan, J.P., Blackman, D.K. and Sinton J.M.) Vol. 71, 183-280 *Geophys. Monogr. Ser., AGU*, Washington DC.

Leeman, W. P., M. J. Carr, and J. D. Morris (1994), Boron geochemistry of the Central American arc: Constraints on the genesis of subduction-related magmas, *Geochimica Et Cosmochimica Acta*, *58*(1), 149-168.

Levin, V., N. Shapiro, J. Park, and M. Ritzwoller (2002), Seismic evidence for catastrophic slab loss beneath Kamchatka, *Nature*, *418*(6899), 763-767.

MacMillan, I., P. B. Gans, and G. Alvarado (2004), Middle Miocene to present plate tectonic history of the southern Central American volcanic arc, *Tectonophysics,* 392, 325-348.

Marquez, A., R. Oyarzun, M. Dobias, and S. P. Verma (1999), Alkalic (ocean-island basalt type) and calc-alkalic volcanism in the Mexican volcanic belt: A case for plume-related magmatism and propagating rifting at an active margin?, *Geology*, *27*(1), 51-54.

McDonough, W. F., and S. S. Sun (1995), The composition of the Earth, *Chem. Geol.,* 120, 223-253.

McKenzie, D., and M. J. Bickle (1988), The volume and composition of melt generated by extension of the lithosphere, *Journal of Petrology*, *29*(3), 625-679.

McKenzie, D., J. Jackson, and K. Priestley (2005), Thermal structure of oceanic and continental lithosphere, *Earth and Planetary Science Letters*, *233*(3-4), 337-349.

Medard, E., M. W. Schmidt, P. Schiano, and L. Ottolini (2006), Melting of amphibole-bearing wehrlites: An experimental study on the origin of ultra-calcic nepheline-normative melts, *Journal of Petrology*, *47*(3), 481-504.

Meschede, M., U. Barckhausen, and H. U. Worm (1998), Extinct spreading on the Cocos Ridge, *Terra Nova*, *10*(4), 211-216.

Montelli, R., G. Nolet, F. A. Dahlen, and G. Masters (2006), A catalogue of deep mantle plumes: New results from finite-frequency tomography, *Geochemistry Geophysics Geosystems*, *7*.

O'Connor, J. M., P. Stoffers, J. R. Wijbrans, and T. J. Worthington (2007), Migration of widespread long-lived volcanism across the Galapagos Volcanic Province: Evidence for a broad hotspot melting anomaly?, *Earth and Planetary Science Letters*, *263*(3-4), 339-354.

O'Hara, M.J. (1968), Are ocean floor basalts primary magmas? *Nature* 220, 683-686.

Pallares, C., R. C. Maury, H. Bellon, J. Y. Royer, T. Calmus, A. Aguillon-Robles, J. Cotten, M. Benoit, F. Michaud, and J. Bourgois (2007), Slab-tearing following ridge-trench collision: Evidence from Miocene volcanism in Baja California, Mexico, *Journal of Volcanology and Geothermal Research*, *161*(1-2), 95-117.

Patino, L. C., M. J. Carr, and M. D. Feigenson (2000), Local and regional variations in Central American arc lavas controlled by variations in subducted sediment input, *Contributions to Mineralogy and Petrology*, *138*(3), 265-283.

Peate, D. W., and J. A. Pearce (1998), Causes of spatial compositional variations in Mariana arc lavas: Trace element evidence, *Island Arc*, *7*(3), 479-495.

Pertermann, M., and M. M. Hirschmann (2003), Anhydrous partial melting experiments on MORB-like eclogite: Phase relations, phase compositions and mineral-melt partitioning of major elements at 2-3 GPa, *Journal of Petrology*, *44*(12), 2173-2201.

Pilet, S., M. B. Baker, and E. M. Stolper (2008b), Metasomatized lithosphere and the origin of alkaline lavas, *Science*, *320*(5878), 916-919.

Putirka, K. D. (2005), Mantle potential temperatures at Hawaii, Iceland, and the mid-ocean ridge system, as inferred from olivine phenocrysts: Evidence for thermally driven mantle plumes, *Geochemistry Geophysics Geosystems*, *6*.

Ranero, C. R., and R. von Huene (2000), Subduction erosion along the Middle America convergent margin, *Nature*, *404*(6779), 748-752.

Ranero, C. R., J. P. Morgan, K. McIntosh, and C. Reichert (2003), Bending-related faulting and mantle serpentinization at the Middle America trench, *Nature*, *425*(6956), 367-373.

Reagan, M. K., and J. B. Gill (1989), Coexisting of calc-alkaline and high-Nb basalts from Turrialba volcanoe, Costa Rica: Implications for residual titanates in arc magma sources, *Journal of Geophysical Research-Solid Earth and Planets*, *94*(B4), 4619-4633.

Ringwood, A. E. (1990), Slab mantle interactions: Petrogenesis of intraplate magmas and structure of the upper mantle, *Chemical Geology*, *82*(3-4), 187-207.

Rogers, R. D., H. Karason, and R. D. van der Hilst (2002), Epeirogenic uplift above a detached slab in northern Central America, *Geology*, *30*(11), 1031-1034.

Russo, R. M., and P. G. Silver (1994), Trench-parallel flow beneath the Nazca plate from seismic anisotropy, *Science*, *263*(5150), 1105-1111.

Rychert, C. A., and P. M. Shearer (2009), A Global View of the Lithosphere-Asthenosphere Boundary, *Science*, *324*(5926), 495-498.

Sadofsky, S. J., M. Portnyagin, K. Hoernle, and P. van den Bogaard (2008), Subduction cycling of volatiles and trace elements through the Central American volcanic arc: evidence from melt inclusions, *Contributions to Mineralogy and Petrology*, *155*(4), 433-456.

Silver, E., P. C. Pisani, M. Hutnak, A. Fisher, H. DeShon, and B. Taylor (2004), An 8-10 Ma tectonic event on the Cocos Plate offshore Costa Rica: Result of Cocos Ridge collision?, *Geophysical Research Letters*, *31*(18).

Smith, G. P., D. A. Wiens, K. M. Fischer, L. M. Dorman, S. C. Webb, and J. A. Hildebrand (2001), A complex pattern of mantle flow in the Lau back-arc, *Science*, *292*(5517), 713-716

Sobolev, A. V., A. W. Hofmann, S. V. Sobolev, and I. K. Nikogosian (2005), An olivine-free mantle source of Hawaiian shield basalts, *Nature*, *434*(7033), 590-597.

Straub, S. M., A. B. LaGatta, A. Pozzo, and C. H. Langmuir (2008), Evidence from high-Ni olivines for a hybridized peridotite/pyroxenite source for orogenic andesites from the central Mexican Volcanic Belt, *Geochemistry Geophysics Geosystems*, *9*.

Syracuse, E. M., and G. A. Abers (2006), Global compilation of variations in slab depth beneath arc volcanoes and implications, *Geochemistry Geophysics Geosystems*, *7*.

Syracuse, E. M., G. A. Abers, K. Fischer, L. MacKenzie, C. Rychert, M. Protti, V. Gonzalez, and W. Strauch (2008), Seismic tomography and earthquake locations in the Nicaraguan and Costa Rican upper mantle, *Geochemistry Geophysics Geosystems*, *9*.

Tarduno, J., H. P. Bunge, N. Sleep, and U. Hansen (2009), The Bent Hawaiian-Emperor Hotspot Track: Inheriting the Mantle Wind, *Science*, *324*(5923), 50-53.

Thorkelson, D. J. (1996), Subduction of diverging plates and the principles of slab window formation, *Tectonophysics*, *255*(1-2), 47-63.

Thorkelson, D. J., and R. P. Taylor (1989), Cordilleran slab windows, *Geology*, *17*(9), 833-836.

Turner, S., and C. Hawkesworth (1998), Using geochemistry to map mantle flow beneath the Lau Basin, *Geology*, *26*(11), 1019-1022.

Vannucchi, P., D.M. Fisher, S. Bier, and T.W. Gardner (2006), From seamount accretion to tectonic erosion: Formation of Osa Mélange and the effects of Cocos Ridge subduction in southern Costa Rica Tectonics 25, TC2004. doi: 10.1029/2005TC001855.

Vannucchi, P., D.W. Scholl, M. Meschede, and K. McDougall-Reid, (2001), Tectonic erosion and consequent collapse of the Pacific margin of Costa Rica: Combined implications from ODP Leg 170, seismic offshore data and regional geology of the Nicoya Peninsula. Tectonics 20, 649-668.

Wendt, J. I., M. Regelous, K. D. Collerson, and A. Ewart (1997), Evidence for a contribution from two mantle plumes to island-arc lavas from northern Tonga, *Geology*, *25*(7), 611-614.

Werner, R., K. Hoernle, P. van den Bogaard, C. Ranero, and R. von Huene (1999), Drowned 14-m.y.-old Galapagos archipelago off the coast of Costa Rica: Implications for tectonic and evolutionary models, *Geology*, *27*(6), 499-502.

Werner, R., K. Hoernle, U. Barckhausen, and F. Hauff (2003), Geodynamic evolution of the Galapagos hot spot system (Central East Pacific) over the past 20 m.y.: Constraints from morphology, geochemistry, and magnetic anomalies, *Geochemistry Geophysics Geosystems*, *4*.

Wiens, D. A., K. A. Kelley, and T. Plank (2006), Mantle temperature variations beneath back-arc spreading centers inferred from seismology, petrology, and bathymetry, *Earth and Planetary Science Letters*, *248*(1-2), 30-42.

Wortel, M. J. R., and W. Spakman (2000), Geophysics - Subduction and slab detachment in the Mediterranean-Carpathian region, *Science*, *290*(5498), 1910-1917.

Figure Captions

Figure 1

Tectonic setting of southern Central America and sample locations. The Galapagos hotspot tracks and other bathymetric features are from Werner et al. (2003). The depth contours of the subducting slab are from Protti et al. (1994). Note that the alkaline basalts in Panama and the back-arc units are restricted to areas with either no clear seismic evidence of a subducting slab or in the back-arc. The adakites and alkaline basalts erupted at some of the same locations of the volcanic front in Panama. The adakites are restricted to the southern-edge of the subducting Cocos Plate. The right panel shows the age-progression of volcanism from the back-arc of Nicaragua through the back-arc of Costa Rica to western Panama. These units have clear Galapagos-type geochemical signatures. The oldest unit is the ~6.5 Ma Victoria dikes in Costa Rica near the northern border with Panama; the rest of the units get progressively younger towards the northwest. The rate of the NNW age progression of alkaline volcanism in the Costa Rica and Nicaragua is 40-60 cm/y.. There is also an age progression in the opposite direction from the Victoria dikes, observed in adakites from southern Costa Rican and western Panama. This progression is possibly related to the east-west progression of the Panama Fracture Zone and thus the segment of the slab that melted to produce adakites. Based on this new age control the rate of Panama Fracture Zone migration is about 2-3 cm/y. CNS: Cocos-Nazca Spreading Center, EPR: East Pacific Rise, PFZ: Panama Fracture Zone.

Figure 2

A) Geochemical classification and comparison to the volcanic front lavas of Carr et al. (2003). The back-arc samples from Costa Rica and Nicaragua and the alkaline basalt from Panama range from picritic basalts and basanites to basaltic trachy-andesites. The adakites range from basaltic andesites to andesites, with compositions similar to the high-K trend of the Central Costa Rica volcanic front (Gazel et al., 2009). **B)** Petrological discrimination of magma sources for primary magmas. The two diagonal lines separate magmas melted from carbonated (metasomatized) peridotite, garnet lherzolites and pyroxenites. The low silica (<45% SiO_2) samples are characterized by high CaO contents, similar to experimental compositions of magmas produced by melting a carbonated peridotite (Dasgupta et al., 2007). The population with lower CaO and higher SiO_2 show similar compositions to magmas produced by melting second-stage pyroxenite (Sobolev et al., 2005; Herzberg, 2006) or high pressure pyroxene fractionation (Albarède et al., 1997; Herzberg and Asimow, 2008). The high-silica adakite end-members have compositions simillar to experimental eclogite melts (Petermann and Hirschmann, 2003). The low-silica adakites possibly represent a mixture of mantle wedge melts, with melting being triggered by subduction-released fluids, and slab melts. The shaded circular field surrounded by a thick black line in both figures represents the composition of calculated primary magmas for alkaline lavas that yield successful pretological solutions in the Supplementary Materials, produced by melting a garnet lherzolite (e.g., Herzberg and Asimow, 2008). The liquid lines of descent (LLD) of a representative primary magma were modeled using Petrolog Software (Supplementary Materials).

Figure 3

Mantle potential temperatures of alkaline lavas of Panama and Costa Rica, compared to the mantle potential temperatures of the modern day Galapagos Hotspot (Galapagos Islands) and the Cocos and Carnegie Ridges (Galapagos tracks) (Herzberg and Gazel 2009). The calculated temperatures from alkaline basalt from Costa Rica and Panama are at the lower end of the range of the Galapagos hotspot mantle potential temperatures.

Figure 4

The melt fraction computed from the primary magma composition of the alkaline basalts correlates positively with melt column length. The melt column for each primary magma was calculated by subtracting the final melting pressure from the initial melting pressures. The melting pressures calculations for the primary magmas follow Herzberg and Gazel (2009) and are detail in the Supplementary Materials. AFM, Aggregated Fractional Melting.

Figure 5

A) Elevation profile along a southeast-northwest transect through southern Central America. **B)** Schematic model that show the structure of the lithosphere boundary based on the initial and final melting pressures calculated from the primary magmas of alkaline lavas from Costa Rica and Panama (Supplementary Material, Table 6). The initial melting pressure is in the garnet-spinel transition zone. The final melting pressures are interpreted as the lower boundary of the lithosphere. The pressures are averages for each locality; the standard deviation of the mean is smaller than the "star" symbols of the initial and final meting pressures. The lithosphere boundary topography is variable and decreases into the back-arc. Note a possibly correlation between lithosphere thickness (B) and elevation (A) on the across–arc profiles. These elevations are possibly related to the isostatic effect produced by hot mantle upwelling in this area together with shortening related with the collision of the Cocos Ridge. The thickness of the crust of ~40 for Costa Rica is from Sallares et al. (2001). A similar same crustal thickness was assumed for Panama.

Figure 6

Primitive-mantle-normalized incompatible element patterns. The adakites from southern Costa Rica/Panama are the only samples with the typical arc-type depletions in Nb and Ta (see NW Nicaragua pattern in the lower right panel) and enrichment in Pb. In contrast, the Volcan Blue/Cukra Hill samples are enriched in Nb and Ta and depleted in Pb. With the exception of enrichments (peaks) for Ba and Sr, the Volcan Blue/Cukra Hill patterns are similar to those of typical ocean-island-basalts (OIBs). All of the other alkaline rocks have characteristics intermediate between the subduction-zone and OIB reference patterns. The adakites also have the most dramatic large ion lithophile element enrichments (Sr, Ba, U, etc) and HREE (eg., Yb, Lu) and HSFE(e.g. Nb, Ta) depletions, consistent with a mafic protolith with residual garnet and a HFSE holding phase (amphibole and/or titanite/rutile). The reference patterns for the volcanic arc from Carr et al. (2007) and the OIB reference is from Sun and McDonough (1989). Primitive Mantle from McDonough and Sun (1995).

Figure 7

Pb-isotope and trace element variations along the volcanic front from Nicaragua to western Panama (A and B) and across (B and C) the subduction zone in southern Central America. The left panel reveals similar variations in $^{206}Pb/^{204}Pb$ and La/Yb with distance along the volcanic front. The HFSE depletion and Pb enrichments (Fig. 3) typical of an arc setting were evaluated across the subduction zone. Magmas produced with a significant subducting slab component will have Nb/Nb* <1, magmas with evident Nb depletions will have values Nb/Nb*<0.5 and magmas produced by mantle upwelling with no/minor subduction signature will have Nb/Nb* >1. Pb/Pb*>1 indicate positive Pb anomalies typical of arc magmatism (Fig. 6 reference patters for the volcanic front) and Pb/Pb* <0.5 indicates a depleted Pb signature that is typical of intraplate (OIB-type, Fig. 6, reference patterns) magmatism. Intermediate Pb/Pb* (0.5-0.1) indicate a combination between arc and intraplate processes. The Galapagos OIB range is from Georoc database (http://georoc.mpch-mainz.gwdg.de) and the volcanic front data are from Carr et al., (2003), Hoernle et al. (2008) and this study.

Figure 8

Pb, Nd and Sr isotopes systematics for the magmas of southern Central America. Data from this study, Feigenson et al., 2004 and Hoernle et al., 2008). At least four end-members are required to explain the Pb, Nd and Sr data (Hoernle et al., 2008; Gazel et al., 2009). Mixing lines connect the required end-members, depleted mantle (DM), the Seamount Province (Northern Galapagos Domain) and the Cocos/Coiba Ridge (Central Galapagos Domain) and slab derived fluids/melts (sediments). The Galapagos signature systematically decreases to the northwest both along the volcanic front and in the back-arc region from Central Costa Rica/Panama towards Nicaragua.

Figure 9

S Schematic model of the different geologic processes required to explain the Galapagos signature in the lavas of southern Central America. Galapagos tracks initially collided with the convergent margin and clogged/slowed the subduction system during the upper Miocene (~ 10-8 Ma) (Denyer and Arias, 199, Silver et al., 2004, Gazel et al., 2009). This collision triggered a detachment of the subducting slab. The detachment was followed by the influx of the relatively hot mantle (including the Galapagos-modified asthenosphere) below southern Central America. The clear age progression, mantle potential temperatures higher than ambient mantle, and the Galapagos signature is consistent with arc-parallel flow of a thermal anomaly determined by geophysical evidence (Hoernle et al. 2008). Therefore, interaction with asthenosphere affected by or originating from the Galapagos plume is consistent with geochemical and geophysical evidence. The alkaline magmas were produced by Galapagos-modified asthenosphere upwelling through the "slab free-area" in southern Costa Rica and then through northward flow of this hotter asthenosphere. The adakites were produced by the interaction of upwelling mantle with the edge of the subducting Cocos Ridge. The geochemical signature of Central Costa Rican volcanic front lavas is also consistent with the reaction of melts from the subducting Seamount Province and upwelling mantle. The structure of the subduction zone is based on the work of Protti et al (1994). PFZ, Panama Fracture Zone; EPR, East-Pacific Rise; QSC, Quesada Sharp Contortion Tear.

Figure 10

Schematic model showing the flow of Galapagos plume material parallel to the Cocos Ridge and then the influx of this Galapagos-modified asthenosphere into the mantle wedge beneath southern Central America.

Figure 11

Possible alkaline basalt sources and the effect of fractional crystallization. The alkaline basalt and volcanic front arrays (Carr et al., 2003) (dashed ovals) are compared to two low pressure (<1 GPa) experimental melting trends; amphibole-bearing wherlite (Médard et al., 2006); and clinopyroxene bearing hornblendite (Pilet et al., 2008) and to primary garnet lherzolite melts modeled in this study (Supplementary Materials). Some of the low pressure melting experiments overlap the alkaline basalt array at high CaO/Al_2O_3 suggesting that hornblende bearing metasomatic veins (reaction between slab derived melts and peridotite in the lithosphere) are the source of some of the alkaline magmas. Nevertheless, from petrology the sources of alkaline magmas appears to be upwelling mantle peridotite (primary magmas derived from garnet lherzolites) and metasomatized peridotite by CO_2 (see Fig 2).

Figure 12

NB/Ta, Zr/Sm source discrimination diagram modified from Foley et al. (2002). A) Possible source compositions: amphibolite and eclogite sources and melts form Foley et al. (2002), Primitive Mantle (PM) from McDonough and Sun (1995), DM and subducting carbonated composition are from Gazel et al. (2009) and references therein. B) The

Ontong-Java Plateau (OJP) and Caribbean Large Igneous Province (CLIP) as reference of peridotite source lavas data is from Georoc database. The carbonated eclogite is a mix of about 10% subducting carbonate and 90% rutile-bearting eclogite. Notice how some of the adakites and much of the alkaline lavas required a carbonated eclogite source together with mantle peridotite (C and D). Therefore is possible that the source of CO_2 that metasomatized the mantle peridotite was the subducting oceanic crust, producing veins of carbonated peridotite (flux) and pyroxenite in the lithosphere (melts). The samples that yield successful petrological primary magma solutions (Supplementary Materials) are close to primitive mantle compositions (D), supporting the petrology that suggest a fertile garnet lherzolite source.

Figure 1

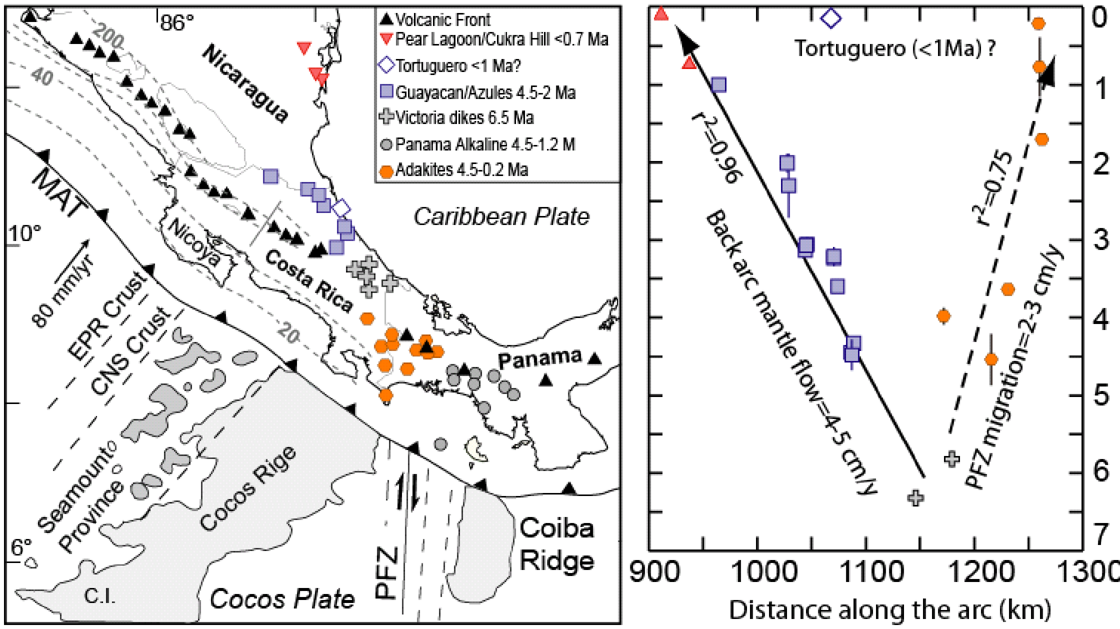

Volcanic Front
Pear Lagoon/Cukra Hill <0.7 Ma
Tortuguero <1 Ma?
Guayacan/Azules 4.5-2 Ma
Victoria dikes 6.5 Ma
Panama Alkaline 4.5-1.2 M
Adakites 4.5-0.2 Ma
86°
10°
6°
200
40
20
Nicaragua
Costa Rica
Nicoya
Panama
Caribbean Plate
MAT
80 mm/yr
EPR Crust
CNS Crust
Seamount Province
Cocos Rige
Cocos Plate
C.I.
PFZ
Coiba Ridge
Tortuguero (<1Ma) ?
r2=0.96
Back arc mantle flow=4-5 cm/y
r2=0.75
PFZ migration=2-3 cm/y
Age (Ma)
Distance along the arc (km)

Figure 2

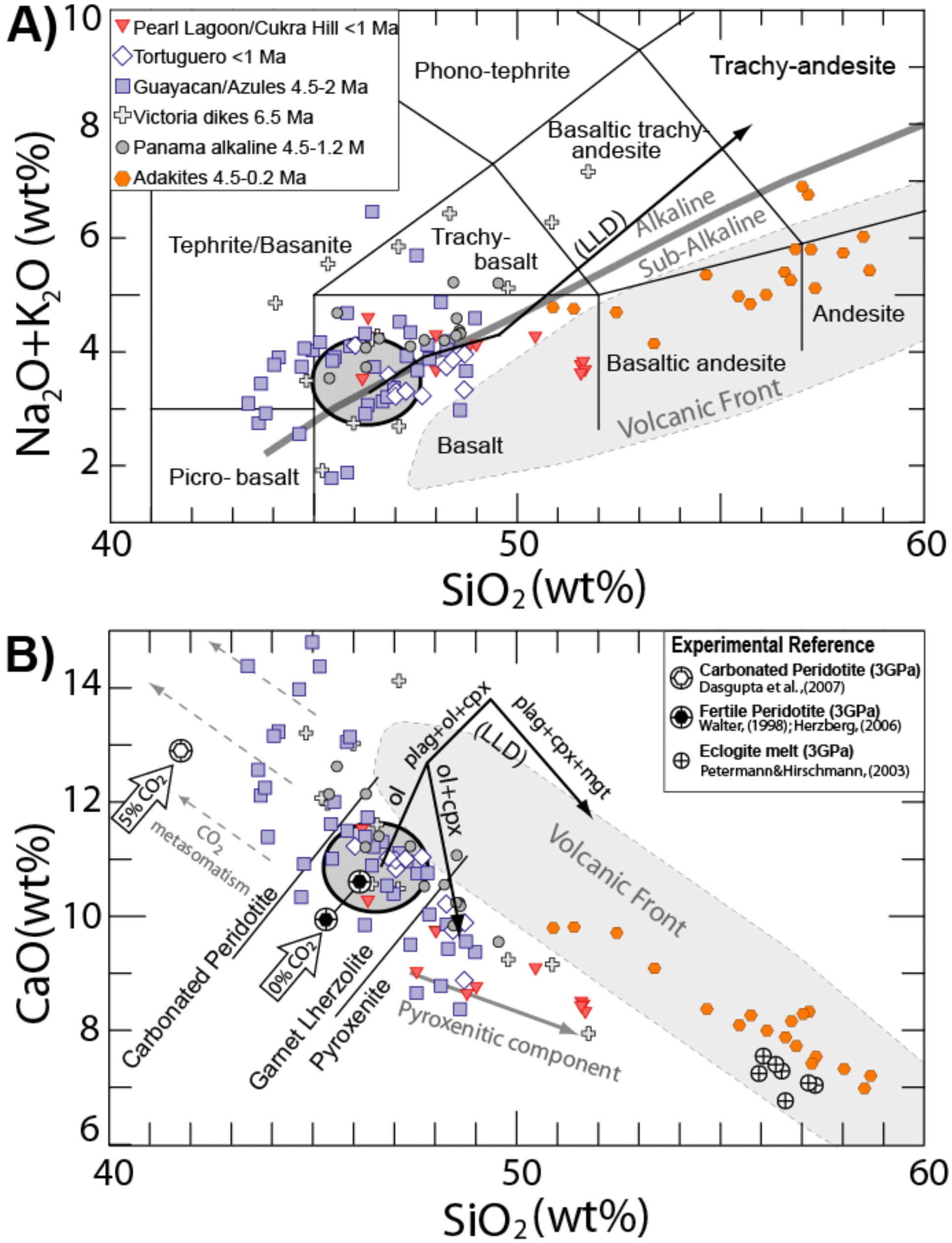
A)
Pearl Lagoon/Cukra Hill <1 Ma
Tortuguero <1 Ma
Guayacan/Azules 4.5-2 Ma
Victoria dikes 6.5 Ma
Panama alkaline 4.5-1.2 M
Adakites 4.5-0.2 Ma
Phono-tephrite
Trachy-andesite
Basaltic trachy-andesite
Tephrite/Basanite
Trachy-basalt
(LLD)
Alkaline
Sub-Alkaline
Andesite
Basaltic andesite
Volcanic Front
Basalt
Picro- basalt
Na2O+K2O (wt%)
SiO2 (wt%)
B)
Experimental Reference
Carbonated Peridotite (3GPa) Dasgupta et al.,(2007)
Fertile Peridotite (3GPa) Walter, (1998); Herzberg, (2006)
Eclogite melt (3GPa) Petermann&Hirschmann, (2003)
plag+ol+cpx
plag+cpx+mgt
(LLD)
ol
ol+cpx
5% CO2
CO2 metasomatism
Volcanic Front
Carbonated Peridotite
0% CO2
Garnet Lherzolite
Pyroxenite
Pyroxenitic component
CaO(wt%)
SiO2 (wt%)

Figure 3

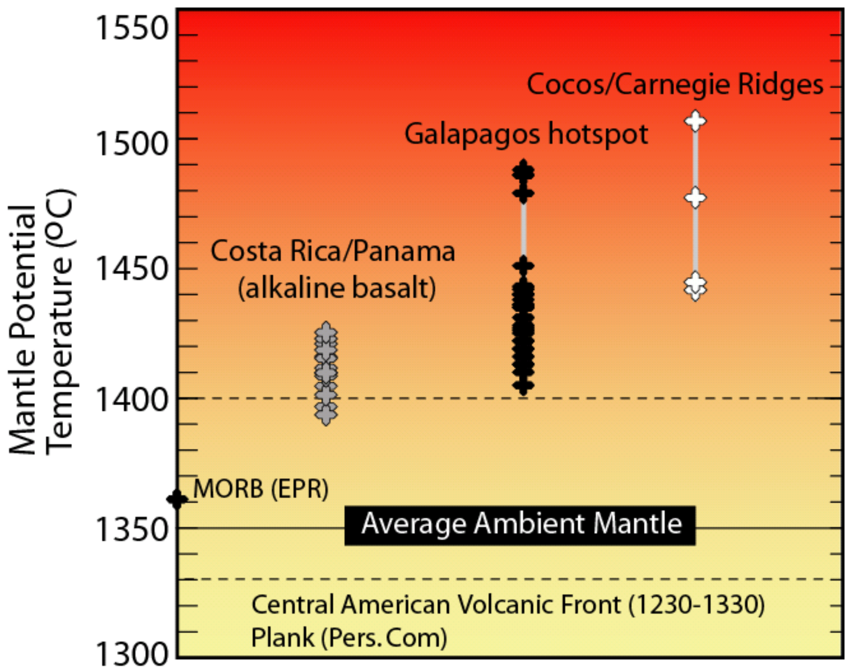
1550
1500
1450
1400
1350
1300
Mantle Potential Temperature (°C)
Cocos/Carnegie Ridges
Galapagos hotspot
Costa Rica/Panama (alkaline basalt)
MORB (EPR)
Average Ambient Mantle
Central American Volcanic Front (1230-1330)
Plank (Pers. Com)

Figure 4

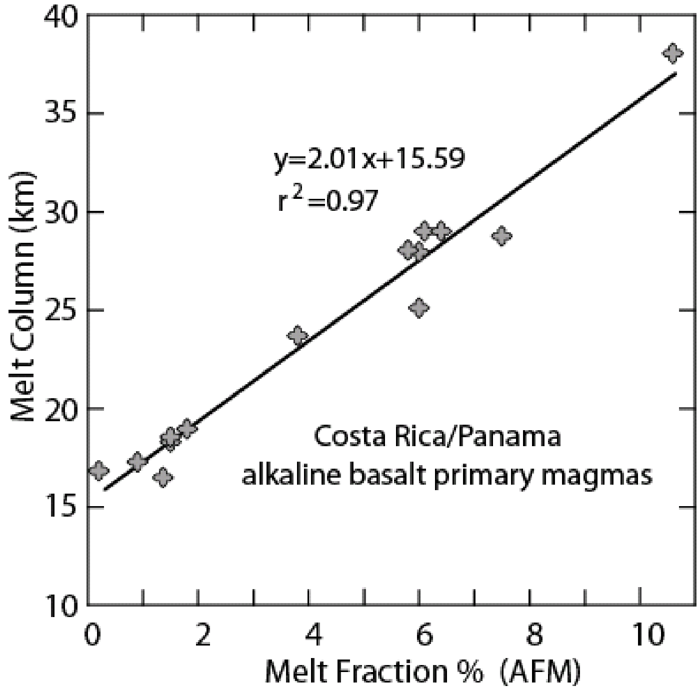
y=2.01x+15.59
r 2 =0.97
Costa Rica/Panama
alkaline basalt primary magmas
Melt Column (km)
Melt Fraction % (AFM)
40
35
30
25
20
15
10
0
2
4
6
8
10

Figure 5

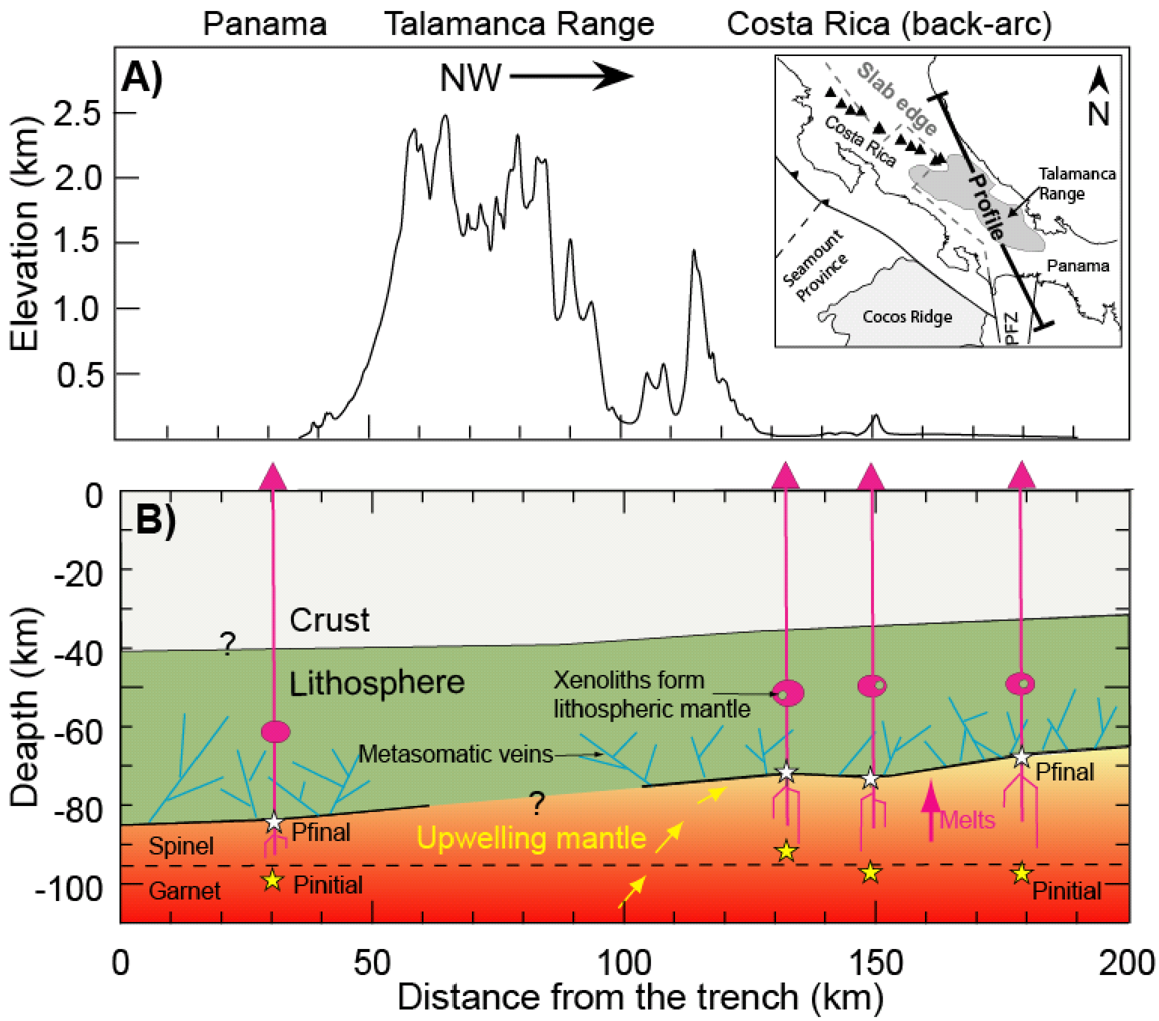

Panama
Talamanca Range
Costa Rica (back-arc)
A)
NW
Elevation (km)
2.5
2.0
1.5
1.0
0.5
Slab edge
Costa Rica
Profile
Talamanca Range
Panama
Seamount Province
Cocos Ridge
PFZ
N
B)
0
-20
-40
-60
-80
-100
Deapth (km)
Crust
Lithosphere
Xenoliths form lithospheric mantle
Metasomatic veins
Pfinal
Upwelling mantle
Melts
Spinel
Garnet
Pinitial
0
50
100
150
200
Distance from the trench (km)

Figure 6

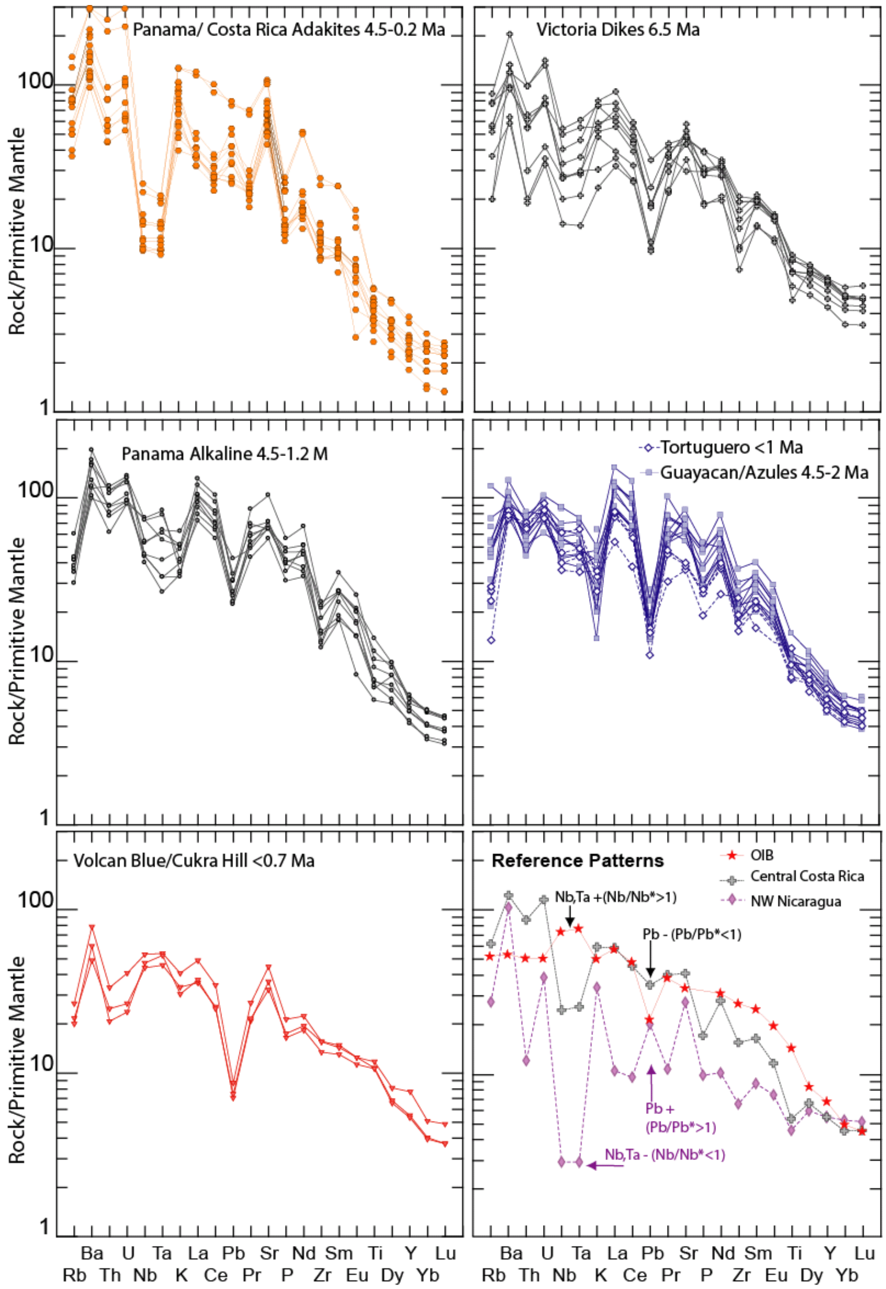
Panama/ Costa Rica Adakites 4.5-0.2 Ma
Victoria Dikes 6.5 Ma
Panama Alkaline 4.5-1.2 M
Tortuguero <1 Ma
Guayacan/Azules 4.5-2 Ma
Volcan Blue/Cukra Hill <0.7 Ma
Reference Patterns
OIB
Central Costa Rica
NW Nicaragua
Nb,Ta +(Nb/Nb*>1)
Pb - (Pb/Pb*<1)
Pb +
(Pb/Pb*>1)
Nb,Ta - (Nb/Nb*<1)
Rock/Primitive Mantle
100
10
1
Rb Ba Th U Nb Ta K La Ce Pb Pr Sr P Nd Zr Sm Eu Ti Dy Y Yb Lu

Figure 7

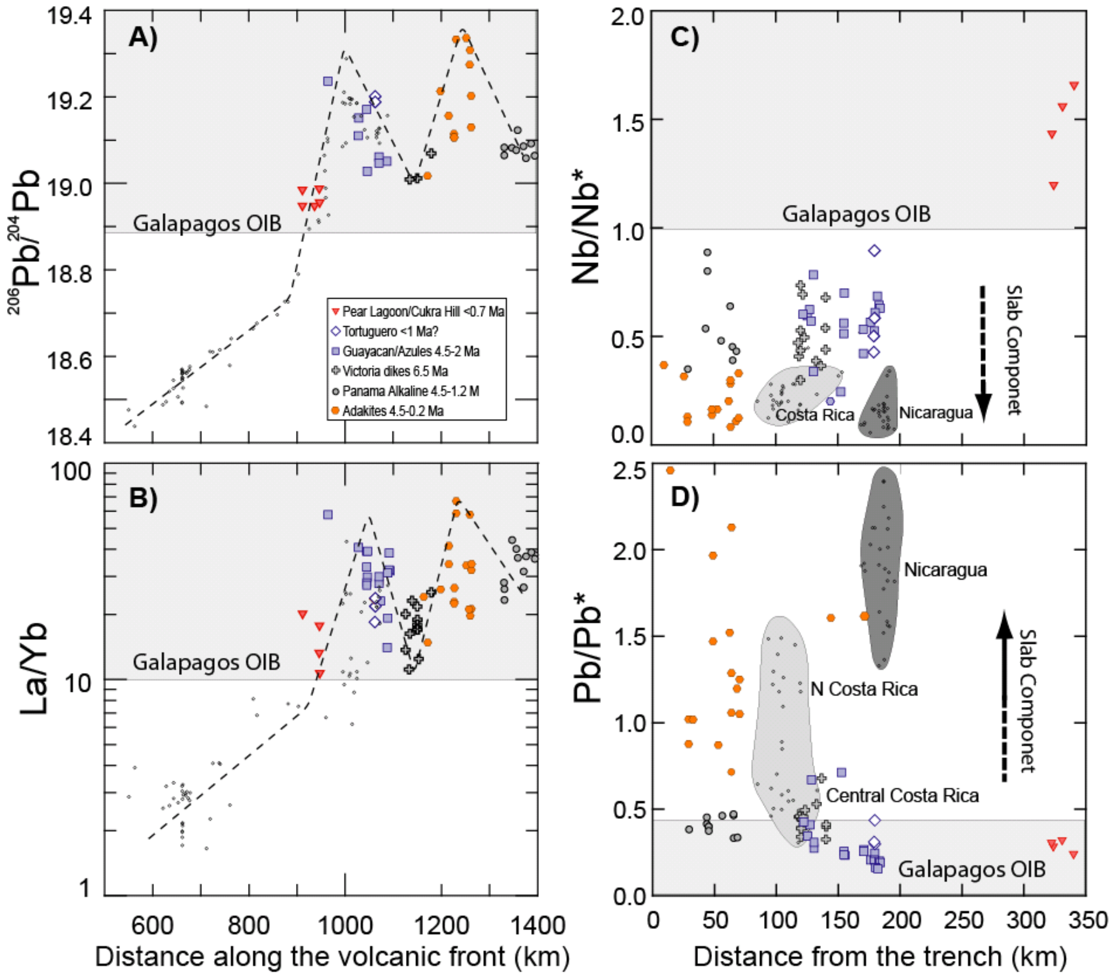
A)
B)
C)
D)
$^{206}Pb/^{204}Pb$
La/Yb
Nb/Nb*
Pb/Pb*
Galapagos OIB
Pear Lagoon/Cukra Hill <0.7 Ma
Tortuguero <1 Ma?
Guayacan/Azules 4.5-2 Ma
Victoria dikes 6.5 Ma
Panama Alkaline 4.5-1.2 M
Adakites 4.5-0.2 Ma
Costa Rica
Nicaragua
N Costa Rica
Central Costa Rica
Slab Componet
Distance along the volcanic front (km)
Distance from the trench (km)

Figure 8

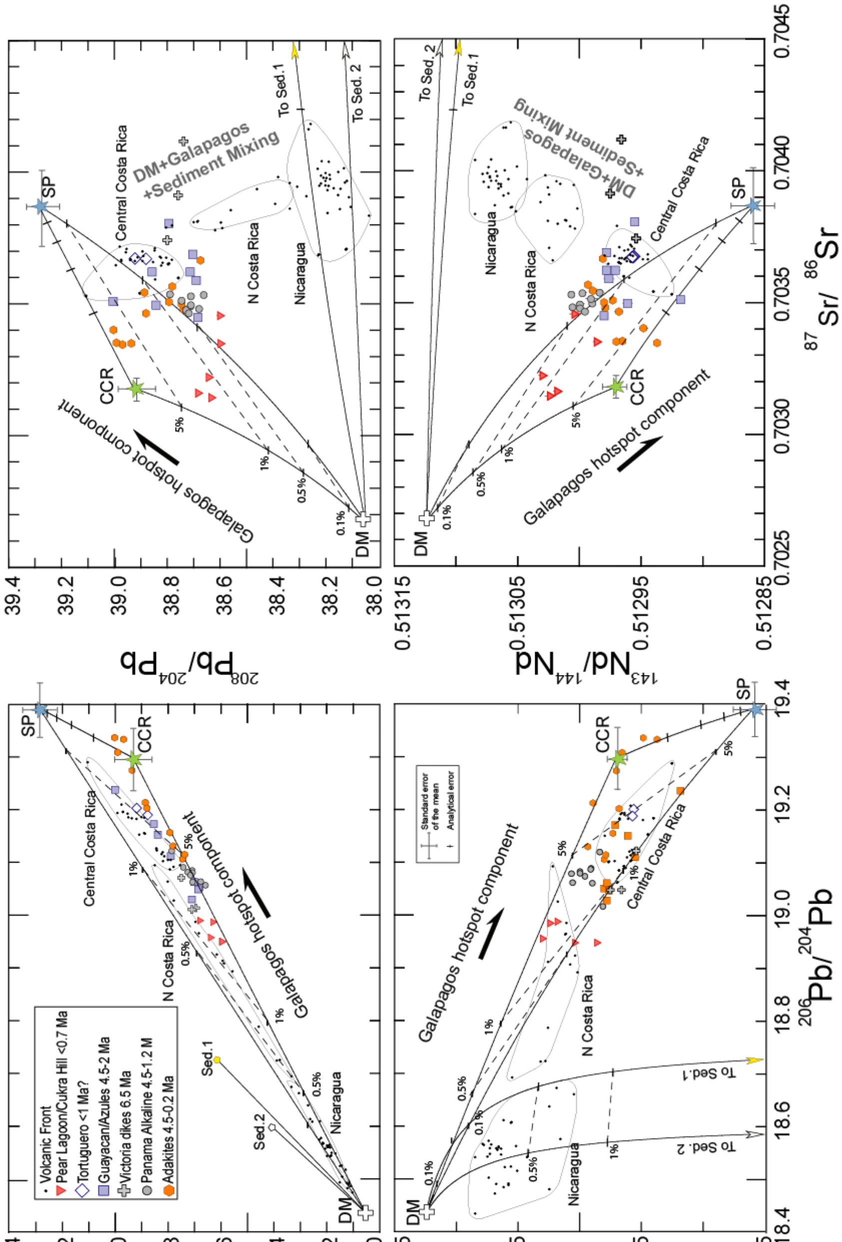

Volcanic Front
Pear Lagoon/Cukra Hill <0.7 Ma
Tortuguero <1 Ma?
Guayacan/Azules 4.5-2 Ma
Victoria dikes 6.5 Ma
Panama Alkaline 4.5-1.2 M
Adakites 4.5-0.2 Ma
Galapagos hotspot component
DM+Galapagos +Sediment Mixing
Central Costa Rica
N Costa Rica
Nicaragua
To Sed.1
To Sed. 2
Sed.1
Sed.2
SP
CCR
DM
Standard error of the mean
Analytical error
208Pb/204Pb
143Nd/144Nd
206Pb/204Pb
87Sr/86Sr

Figure 9

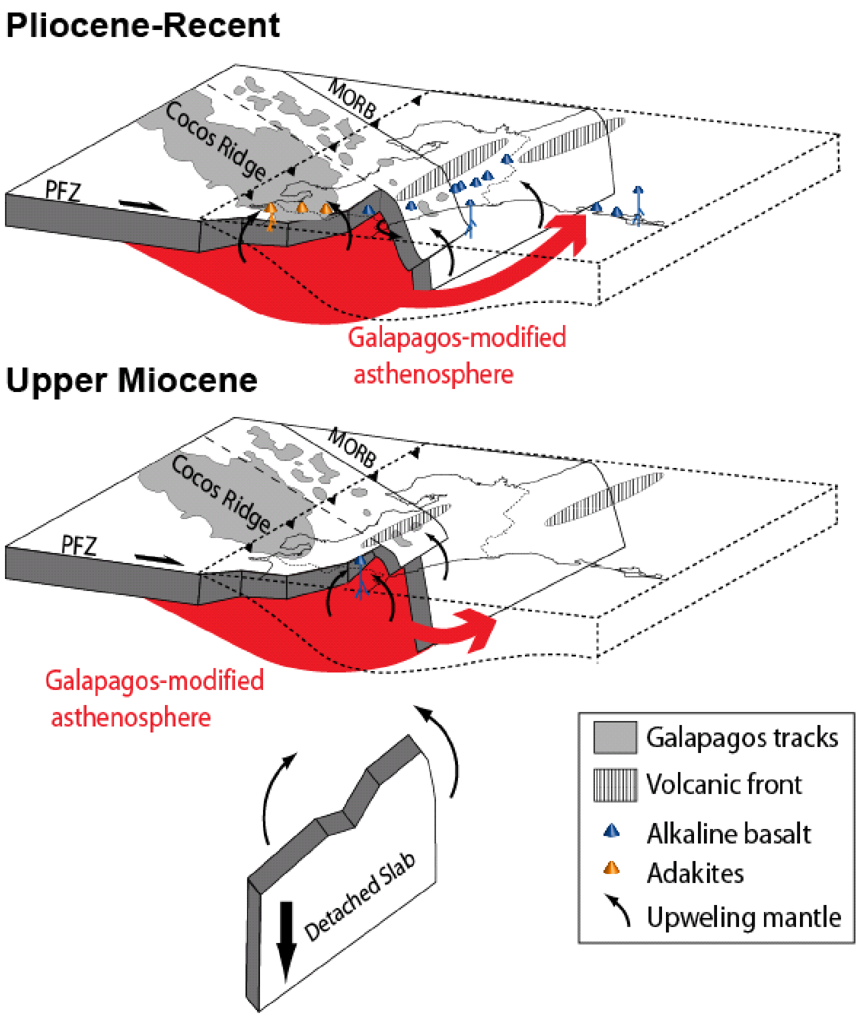
Pliocene-Recent
MORB
Cocos Ridge
PFZ
Galapagos-modified
asthenosphere
Upper Miocene
MORB
Cocos Ridge
PFZ
Galapagos-modified
asthenosphere
Detached Slab
Galapagos tracks
Volcanic front
Alkaline basalt
Adakites
Upweling mantle

Figure 10

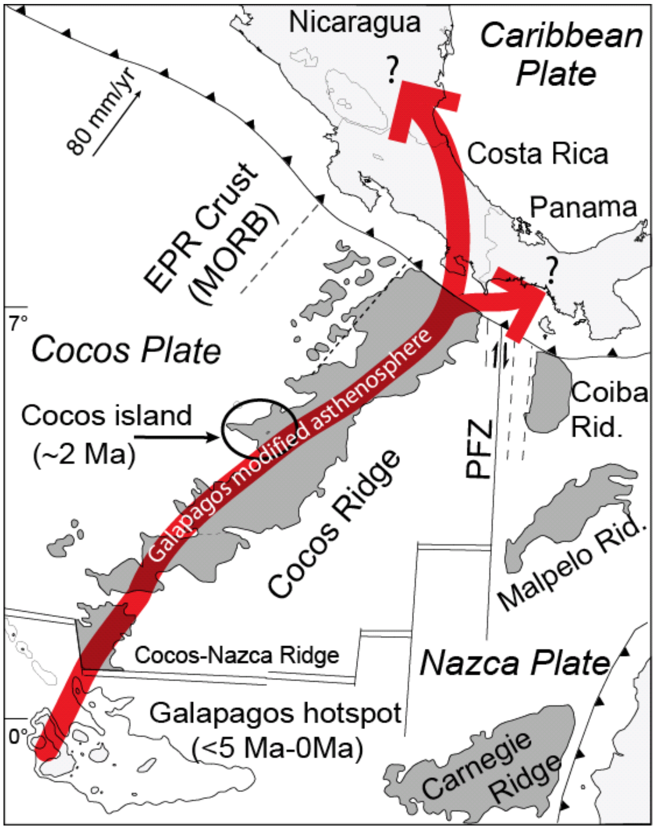
Nicaragua
Caribbean Plate
?
80 mm/yr
Costa Rica
Panama
EPR Crust (MORB)
?
7°
Cocos Plate
Galapagos modified asthenosphere
Cocos island (~2 Ma)
Coiba Rid.
PFZ
Cocos Ridge
Malpelo Rid.
Cocos-Nazca Ridge
Nazca Plate
Galapagos hotspot (<5 Ma-0Ma)
0°
Carnegie Ridge

Figure 11

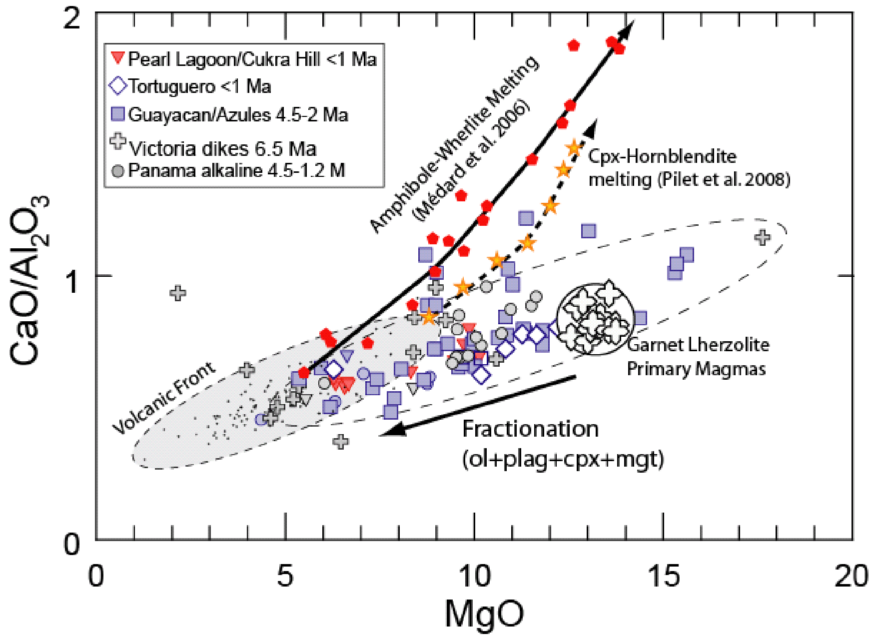
Pearl Lagoon/Cukra Hill <1 Ma
Tortuguero <1 Ma
Guayacan/Azules 4.5-2 Ma
Victoria dikes 6.5 Ma
Panama alkaline 4.5-1.2 M
Amphibole-Wherlite Melting
(Médard et al. 2006)
Cpx-Hornblendite
melting (Pilet et al. 2008)
Garnet Lherzolite
Primary Magmas
Volcanic Front
Fractionation
(ol+plag+cpx+mgt)
CaO/Al2O3
MgO
0
5
10
15
20
0
1
2

Figure 12

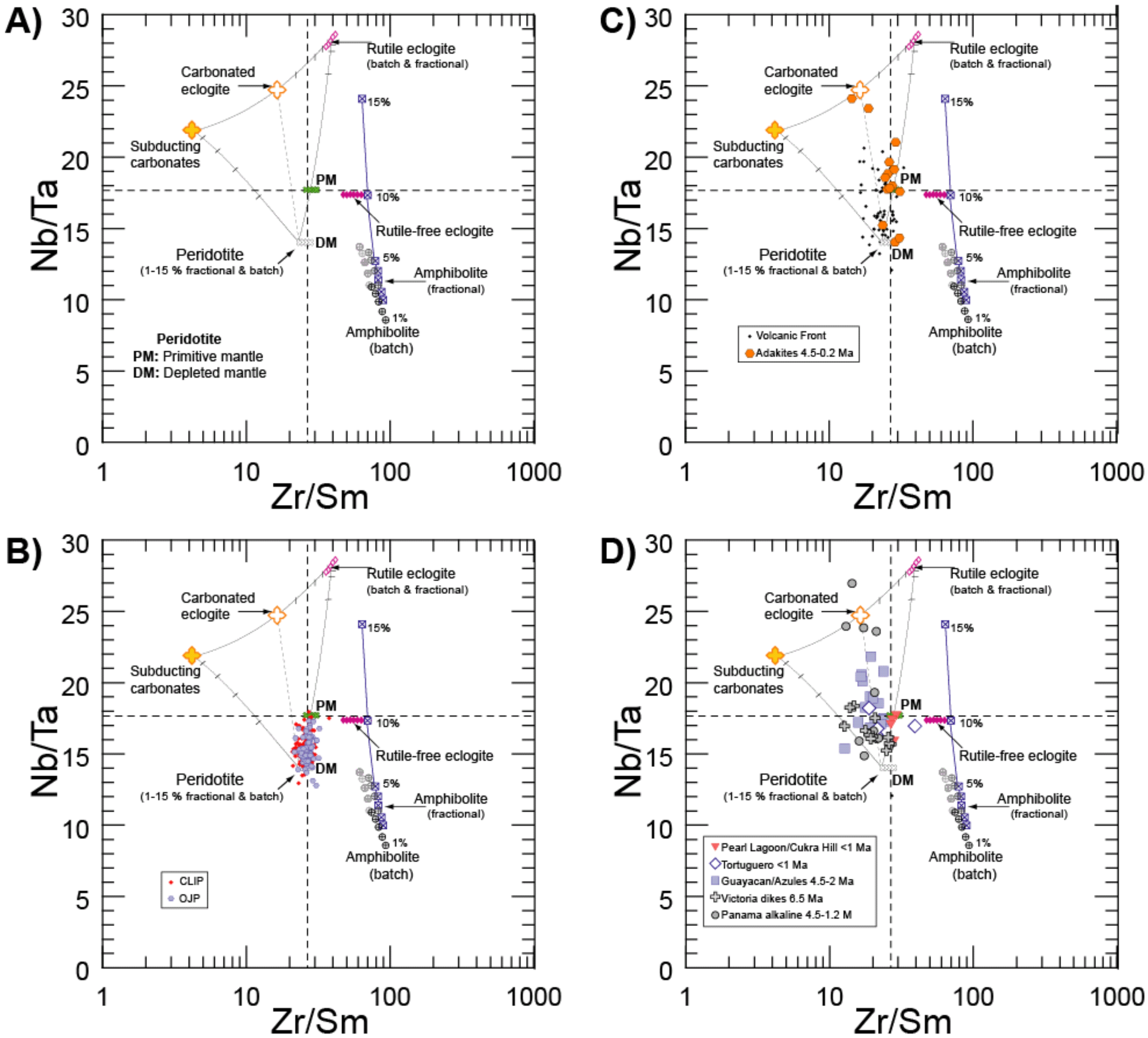
A)
B)
C)
D)
Nb/Ta
Zr/Sm
Carbonated eclogite
Subducting carbonates
Rutile eclogite
(batch & fractional)
Rutile-free eclogite
Peridotite
(1-15 % fractional & batch)
Amphibolite
(fractional)
Amphibolite
(batch)
PM
DM
15%
10%
5%
1%
Peridotite
PM: Primitive mantle
DM: Depleted mantle
CLIP
OJP
Volcanic Front
Adakites 4.5-0.2 Ma
Pearl Lagoon/Cukra Hill <1 Ma
Tortuguero <1 Ma
Guayacan/Azules 4.5-2 Ma
Victoria dikes 6.5 Ma
Panama alkaline 4.5-1.2 M

Supplementary Materials

1. Data and analytical methods

Outcrops of olivine-bearing lavas and shallow intrusions were sampled from quarries, river beds, and road cuts in Nicaragua, Costa Rica and Panama. Adakites were sampled close to the Costa Rican-Panamanian border and along the Panamanian volcanic front (GPS locations are included in Table 1).

1.1 Major and trace element data

Samples with no visible weathering, as verified by petrographic studies, were crushed in an alumina jaw crusher and washed with de-ionized water in an ultrasonic bath. Alteration-free rock chips (e.g. those free of oxides, veins, and zeolites) were selected under stereoscopic microscope and powdered in an alumina mill. Because of the collaborative nature of this study some samples were analyzed for major and trace element at Michigan State University and some by IFM-GEOMAR/Kiel University, Germany. Inter-lab comparison can be made with the samples CS-082106-1 analyzed by the Michigan State Labs and TC-8 analyzed at the IFM-GEOMAR/Kiel University labs. Even though the codes are different, this sample was collected at the same locality and split for different lab analyses. The different lab results are in good agreement within the analytical errors (Tables 1 and 2).

At Michigan State University, major and trace element analyses (sample codes CH-, D, RB-,ES-,AM-,BS-,BO-,CO-,TO, Tables 1 and 2) were obtained from glass disks created by fusing each powdered sample with lithium tetraborate ($Li_2B_4O_7$). The disks were then analyzed for major elements and selected trace elements (e.g. Cr, Cu, Ni, Sr, Rb, Zr, and Zn) by X-ray fluorescence (XRF) in a Bruker S4 Pioneer. Additional trace elements were measured in the same glass disks using laser ablation inductively-coupled plasma mass spectrometry (LA-ICP-MS) with a Micromass Platform ICP-MS with a Cetac LSX 200+ Nd:YAG laser (266 nm). The methods and precision and accuracy are reported by Hannah et al. (2002).

At IFM-GEOMAR , major elements and selected trace elements (e.g., Cr, Ni, Zr, Sr) of whole rock samples (sample codes Azul-, P-, CR,CP, M, SO-TC-, Tables 1 and 2) were determined on fused beads using a Philips X'Unique PW1480 X-ray fluorescence spectrometer (XRF) equipped with a Rh-tube at IFM-GEOMAR. H_2O and CO_2 were analyzed in an infrared photometer (Rosemount CSA 5003). Additional trace elements (e.g., Rb, Ba, Y, Nb, Ta, Hf, U, Th, Pb and all REE) were determined by ICP-MS on a VG Plasmaquad PQ1-ICP-MS at the Institute of Geosciences (University of Kiel) after the methods of Garbe-Schönberg (1993).

1.2 Sr, Nd and Pb isotopes

Sr-Nd-Pb isotope measurements were carried out on whole rock powders. About 100 mg of sample were weighed into a Teflon beaker and then dissolved for 2 days in a 5:1 mixture of HF and HNO_3 at 150°C. Sample dissolution and element chromatography were carried out at IFM-GEOMAR in Kiel (Germany) in Class 1000 clean rooms, equipped with Class 100 laminar flow hoods. All reagents used were either double distilled in a PicoTrace Teflon distillery (HCl and HNO_3) or certified ultra pure HF and HBr acids from SEASTAR©. An ELGA© purifying system provided 18.2MΩ water.

The ion chromatography followed established standard procedures e.g. (Hart and Brooks, 1974). These included a two-pass Pb separation and clean-up using 100 µl Teflon micro-columns filled with BIORAD© AG 1x8 (100-200 mesh) resin that equilibrated with 1M HBr for highest Pb retention and from which Pb is released with 1ml of 6N HCl. The rest of the sample collected during Pb chromatography was then loaded in 2.5N HCl into 6ml quartz glass columns filled with BIORAD© AG50W-X8 (100-200 mesh) resin to separate Sr. The rare earth elements (REE) were obtained in 6ml 6N HCl at the final washout of the Sr columns. The REE collection was then loaded in 0.25N HCl onto 4ml quartz glass columns filled with EICHROM© Ln-Spec resin (100-150 µm) to obtain the Nd fraction.

Isotopic ratios (Table 3) were determined by thermal ionization mass spectrometry (TIMS) at IFM-GEOMAR on a TRITON (Sr-Nd) and MAT262 RPQ^{2+} TIMS (Pb). Both instruments operated in static multi-collection mode. Sr and Nd isotopic ratios are normalized within each run to $^{86}Sr/^{88}Sr = 0.1194$ and $^{146}Nd/^{144}Nd = 0.7219$, respectively and all errors are reported as 2 sigma of the mean. Reference material measured along with the samples were normalized and gave $^{87}Sr/^{86}Sr = 0.710250 \pm 0.000008$ (n=13) for NBS987 and $^{143}Nd/^{144}Nd = 0.511850 \pm 0.000006$ (N=8) for La Jolla. Sr-Nd replicate analyses of sample JK117 were within the external errors of the reference material. The long-term reproducibility of NBS 981 (n = 197) is $^{206}Pb/^{204}Pb = 16.899 \pm 0.008$, $^{207}Pb/^{204}Pb = 15.437 \pm 0.009$, $^{208}Pb/^{204}Pb = 36.525 \pm 0.029$. Pb isotope ratios are normalized to NBS 981 values of Galer and Abouchami (1998). Pb replicate analyses of sample JK117 is better than 0.01%/amu. Total chemistry blanks are <50 pg for Sr-Nd and Pb and thus are considered negligible.

1.3 Step-heating $^{40}Ar/^{39}Ar$ ages

$^{40}Ar/^{39}Ar$ age determinations at Rutgers University (Table 4) were made on samples selected on the basis of no visible weathering and minimal interstitial glass, determined by evaluation of thin sections. The samples were crushed using a steel plated micro jaw crusher and sieved to >300 μm and <425 μm and prepared following the methods reported in Carr et al. (2007). A cleaned fraction of the sample matrix was then loaded into individual sample wells of aluminum irradiation disks, along with the irradiation monitor mineral Alder Creek (AC-1). The loaded sample disks were wrapped in Al foil, sealed in quartz glass tubes, and then irradiated for 0.25 hours in the Cadmium-Lined, In-Core Irradiation Tube (CLICIT) facility of the Oregon State University Triga Research Reactor (OSTR).

Ten to 80 milligrams of the irradiated samples were loaded into individual six mm diameter wells in ~60 mm diameter stainless steel disks, loaded onto one of the two extraction line sample chambers, and baked out at approximately 100° C for six hours. Gases were extracted using a 40 watt CO_2 laser to apply stepwise incremental heating. The laser is focused through a II-VI ZnSe faceted transmissive beam integrator lens resulting in a 6 mm square flat top beam profile with minimal temperature gradients. The use of the CO_2 laser to heat samples permits the heating of 10 to 80 milligrams of sample and provides adequate "clean-up" of extracted gases for up to 10 minutes without significantly raising background values, a problem with larger volume metal resistance furnaces.

Calibration and determination of the irradiation parameter J was determined by multiple total fusion analyses of the co-irradiated monitor mineral, Alder Creek Rhyolite Sanidine (ACS-1), using a published reference age of 1.194 ± 0.006 Ma (Turrin et al., 1994; Renne et al., 1998). Interference isotopes produced from Ca during irradiation of the samples using the Oregon TRIGA were corrected using previously published values $(^{36}Ar/^{37}Ar)_{Ca} = 2.72 \pm 0.06$ $(\times 10^{-4})$ and $(^{39}Ar/^{37}Ar)_{Ca} = 7.11 \pm 0.02$ $(\times 10^{-4})$ (Renne et al., 1998; Deino et al., 2002). During the analysis of the samples and standards, mass discrimination was regularly monitored through measurement of air aliquots delivered via an on-line automated air pipette system and varied between 1.000 and 1.007 AMU. System baselines, Ar isotope backgrounds and mass discrimination measured for a typical sample loading and run period (approximately one week) were time averaged though linear regressions of the measured data. Resultant curves were then applied to the standards and unknown sample measurements. This approach of "modeling" baseline, background, and mass discrimination throughout the run period significantly improves the analytical data for both the standard and unknowns by minimizing spurious low signal measurements on backgrounds and blanks due to electronic and mechanical noise. Automated laser heating, gas extraction and clean-up, spectrometer measurement and data reduction were made using software written by A. Deino.

A subset of samples was dated by step-heating $^{40}Ar/^{39}Ar$ at IFM-GEOMAR (Table 5). Mineral separates, rock matrix samples and irradiation monitor TCR-2 (sanidine from Taylor Creek Rhyolite; Age = 27.87 Ma) (Lanphere and Dalrymple, 2000) were irradiated in position E6 of the FRG-1 nuclear reactor at the GKSS Research Center, Geesthacht, using a Cd shielding. Step-heating $^{40}Ar/^{39}Ar$ analyses were carried out with a 20 W argon-ion laser in a MAP 216 mass spectrometer at IFM-GEOMAR. Analysis of system blanks were measured prior to each sample and after each fifth sample heating step, typically comprising 10%, 1%, and 2% of the measured ^{36}Ar, ^{39}Ar, and ^{40}Ar isotopes, respectively. The data reported included more than 50% of ^{39}Ar in each plateau.

2. Methods for primary magma calculation

Table 6 reports the primary magmas, mantle potential temperatures, source melt fractions and mantle potential temperatures modeled from the alkaline lavas from Panama and Costa Rica. All modeled data are based on the implementation of PRIMELT2.XLS (Herzberg and Asimow, 2008). PRIMELT2.XLS provides for each primary magma the olivine liquidus temperature T_{OL} at 1 atmosphere and the mantle potential temperature T_P. Adiabatic melting paths of Iwamori et al. (1995) were used to obtain: $T_P(^oC) = 1463 + 12.74MgO – 2924/MgO$ (Herzberg et al., 2007). Because both T_{OL} and T_P are dependent on the MgO content of the primary magma (Herzberg et al., 2007), the accuracy of the former is a guide to the precision of the latter. For any specific peridotite composition, accuracy of T_{OL} is ± 31°C at the 2σ level of confidence (Herzberg et al., 2007).

The source of the lavas needs to be a volatile free mantle peridotite. The data is filtered based on the parameters described by Sobolev et al., (2005), Herzberg 2006 and Dasgupta et al., (2007). We assumed that they melted from peridotite having the average FeO contents of ~8.0% for natural fertile and depleted peridotite (Herzberg and O'Hara, 2002). Uncertainties of the FeO content of peridotite can propagate to an uncertainty of ± 50-70°C in T_P. Melting of depleted peridotite propagates to calculated melt fractions that are too high, but with a negligible error in mantle potential temperature. Melt fraction is more difficult to quantify than mantle potential temperature because it is strongly dependent on the composition of the source (Herzberg and O'Hara 2002; Herzberg et al., 2007; Herzberg and Asimow, 2008). A detail discussion of the effects of variation of FeO composition of the mantle peridotite source in the calculation of primary magmas can be found in Herzberg and Gazel (2009). Fractional crystallization does not preserve in the geochemistry the T-P conditions of melt formation in the mantle. PRIMELT2 only provides successful information about source temperature if the primary magma gained or lost only olivine before solidifying to a primitive rock. Most basalts have crystallized clinopyroxene and plagioclase together with olivine and those samples can not be modeled accurately at the present state-of-knowledge. Fe_2O_3 is calculated based on OIB-like $Fe_2O_3/TiO_2 \sim 1$ (Herzberg and Asimow, 2008).

3. References for the Supplementary Materials

Ariskin A.A. and G. S. Barmina (1990). Equilibria thermometry between plagioclases and basalt and andesite magmas. *Geochemica International*, 27(10), 129-134.

Ariskin A.A. and G. S. Barmina (1999), An empirical model for the calculation of spinel-melt equilibria in mafic igneous systems at atmospheric pressure: 2. Fe-Ti oxides. *Contribuitions to Mineralogy and Petrology*, 134, 251-263.

Ariskin A.A., M.Y. Frenkel, G.S. Barmina and R. Nielsen (1993), COMAGMAT: a *Fortran* program to model magma differentiation processes, *Computers and Geoscience*, 19, 1155-1170.

Beattie, P. (1993), Olivine-melt and orthopyroxene-melt equilibria, *Contribuitions to Mineralogy and Petrology,* 115, 103-111.

Bindeman I.N., J.M Eiler., G.M. Yogodzinski., Y. Tatsumi., C.R Stern., T.L. Grove, M. Portnyagin., K. Hoernle, and L.V .Danyushevsky (2005), Oxygen isotope evidence for slab melting in modern and ancient subduction zones. Earth Planet. Sci. Letters 235, 480-496.

Dasgupta, R., M. M. Hirschmann, and N. D. Smith (2007), Partial melting experiments of peridotite CO2 at 3 GPa and genesis of alkalic ocean island basalts, *Journal of Petrology*, *48*(11), 2093-2124.

Deino, A., L. Tauxe, M. Monaghan, and A. Hill (2002),40Ar/39Ar geochronology and paleomagnetic stratigraphy of the Lukeino and lower Chemeron Formations at Tabarin and Kapcheberek, Tugen Hills, Kenya, *Journal of Human Evoution*, 42, 117–140.

Galer, S. J. G., and W. Abouchami (1998), Practical application of lead triple spiking for correction of instrumental mass discrimination, *Min. Mag.,* 62A, 491-492.\

Garbe-Schönberg, C.D. (1993), Simultaneous determination of thirty-seven trace elements in twenty-eitgh international rock standards by ICP-MS, *Geostand. Newsl.* 17, 81-97.

Hannah, R. S., T. A. Vogel, L. C. Patino, G. E. Alvarado, W. Perez, and D. R. Smith (2002), Origin of silicic volcanic rocks in Central Costa Rica: a study of a chemically variable ash-flow sheet in the Tiribi Tuff, *Bulletin of Volcanology*, *64*(2), 117-135.

Hart, S. R., and C. Brooks (1974), Clinopyroxene-matrix partitioning of K, Rb, Cs, and Ba, *Geochim. Cosmochim.. Acta*, 38, 1799-1806.

Herzberg, C. (2006), Petrology and thermal structure of the Hawaiian plume from Mauna Kea volcano, *Nature*, *444*(7119), 605-609.

Herzberg, C., P. D. Asimow, N. Arndt, Y. L. Niu, C. M. Lesher, J. G. Fitton, M. J. Cheadle, and A. D. Saunders (2007), Temperatures in ambient mantle and plumes: Constraints from basalts, picrites, and komatiites, *Geochemistry Geophysics Geosystems*, *8*.

Herzberg, C., and P. D. Asimow (2008), Petrology of some oceanic island basalts: PRIMELT2.XLS software for primary magma calculation, *Geochemistry Geophysics Geosystems*, *9*.

Herzberg, C., and E. Gazel (2009), Petrological evidence for secular cooling in mantle plumes, *Nature*, *458*(7238), 619-U683.

Herzberg, C., and M. J. O'Hara (2002), Plume-associated ultramafic magmas of phanerozoic age, *Journal of Petrology*, 43(10), 1857-1883.

Iwamori, H., D. McKenzie, and E. Takahashi (1995), Melt generation by isentropic mantle upwelling. *Earth Planet. Sci. Lett.* 134, 253-266

Lanphere, M. A., and G. B. Dalrymple (2000), First-principles calibration of ^{38}Ar tracers; implications for the ages of $^{40}Ar/^{39}Ar$ fluence monitors, *U.S. Geol. Surv. Prof. Pap.*, 1621, 1-10.

Renne, P.R., C.C. Swisher, A.L. Deino, D.B. Karner, T.L.Owens and D.J. DePaolo (1998)Intercalibration of standards, absolute ages and uncertainties in 40Ar/ 39Ar dating, *Chemical Geology 145*, 117-152.

Sobolev, A. V., A. W. Hofmann, S. V. Sobolev, and I. K. Nikogosian (2005), An olivine-free mantle source of Hawaiian shield basalts, *Nature*, *434*(7033), 590-597.

Sun, S-S., W.F., McDonough, (1989), Chemical and isotopic systematics of oceanic basalts: Implications for mantle compositions and processes. In: Saunders, A.D., Norry, M.J. (Eds.), Magmatism in the Ocean Basins, *Geological Society, Special Paper* 42, pp. 313-345.

Stack, C. (1991), Inverse modeling of alkaline lavas from Guayacan, Costa Rica, Rutgers University, New Jersey*, MSc Thesis*, 52 pages.

Turrin, B.D., J.M. Donnelly-Nolan, B.C. Hearn Jr. (1994), 40Ar/ 39Ar ages from the rhyolite of Alder Creek, California; age of the Cobb Mountain normal-polarity subchron revisited,*Geology, 22-3*, 251-254.

Supplementary Material Figures Captions

Figure S1

Plateau spectra and inverse geochrons for representative step heating $^{40}Ar/^{39}Ar$ ages determined at Rutgers University.

Figure S2

Plateau spectra for representative step heating $^{40}Ar/^{39}Ar$ ages determined at IFM-GEOMAR. The plateau steps are in gray

Figure S3

Petrology of primary magmas and source discrimination. **A)** Alkaline lavas from Costa Rica and Panama and the primary magmas inferred from them, compared with primary magmas compositions inferred for the modern day Galapagos Plume from Galapagos Island lavas (Herzberg and Gazel, 2009). All primary magmas of fertile peridotite KR-4003 plot within the gray field (Herzberg et al., 2007, Herzberg and Asimow, 2008). The intersections of the red and blue lines identify the composition of an accumulated fractional melt at the initial and final melting pressure, respectively. The equations that described these lines are in Herzberg and Gazel (2009). The dashed lines identify the melt fractions. The small arrows show the effect of olivine addition. Notice that there is overlap between the lower temperature (also lower FeO and MgO) end of the Galapagos primary magmas and the alkaline lavas from Costa Rica and Panama. **B)** CaO-SiO_2 source composition discrimination for **primary magmas,** modified from Herzberg and

Asimow (2008). The primary magmas inferred from the alkaline basalts in Costa Rica and Panama and the primary magmas inferred from the Galapagos plume are both consistent with a volatile-free peridotite source. As suggested by Sobolev et al. (2005), mixing (solid state or reaction) between silicic melts from recycled oceanic crust and mantle peridotite can produce an array of second stage pyroxenitic source compositions (represented by the dashed line). Primary magmas from Mauna Kea are consistent with melts produced from a second stage pyroxenite source (Herzberg, 2006). The primary magmas inferred from the alkaline basalts of Panama and Costa Rica and from the primary magmas inferred from the Galapagos hotspot are in equilibrium with a garnet peridotite source. The black vectors show the effects of fractionation on magmas evolving from a primary magma, derived from a garnet lherzolite. Two fractionation trends are modeled, one includes olivine+plagioclase+clinopyroxene+magnetite and the other excludes plagioclase. The liquid lines of descent were modeled using Petrolog Software, with the parameters of Beattie (1993), Ariskin et al. (1993), Ariskin and Barmina (1990, 1999) and a QFM buffer.

Supplementary Material Tables Captions

Table 1

Geologic units, sample locations, ages, major and trace elements compositions by XRF. Additional data and plateaus for the new $^{40}Ar/^{39}Ar$ ages are found in Tables 4 and 5.

Table 2

ICP-MS trace element data.

Table 3

Radiogenic isotopic ratios. Additional data from Hoernle et al. (2008).

Table 4

Data from the new step-heating $^{40}Ar/^{39}Ar$ ages produced at Rutgers University.

Table 5

Data from the new step-heating $^{40}Ar/^{39}Ar$ ages produced at IFM-GEOMAR.

Table 6

Primary magma results from the samples that yield successful petrological solutions using the method of Herzberg and Asimow (2009). Additional samples from the Guayacan Formation from Stack (1991). Di, initial meting depth; Df, final melting depth; F, melt fraction; Mc, melt column length; Pi, initial meting pressure; Pf, final melting pressure.

Figure S1

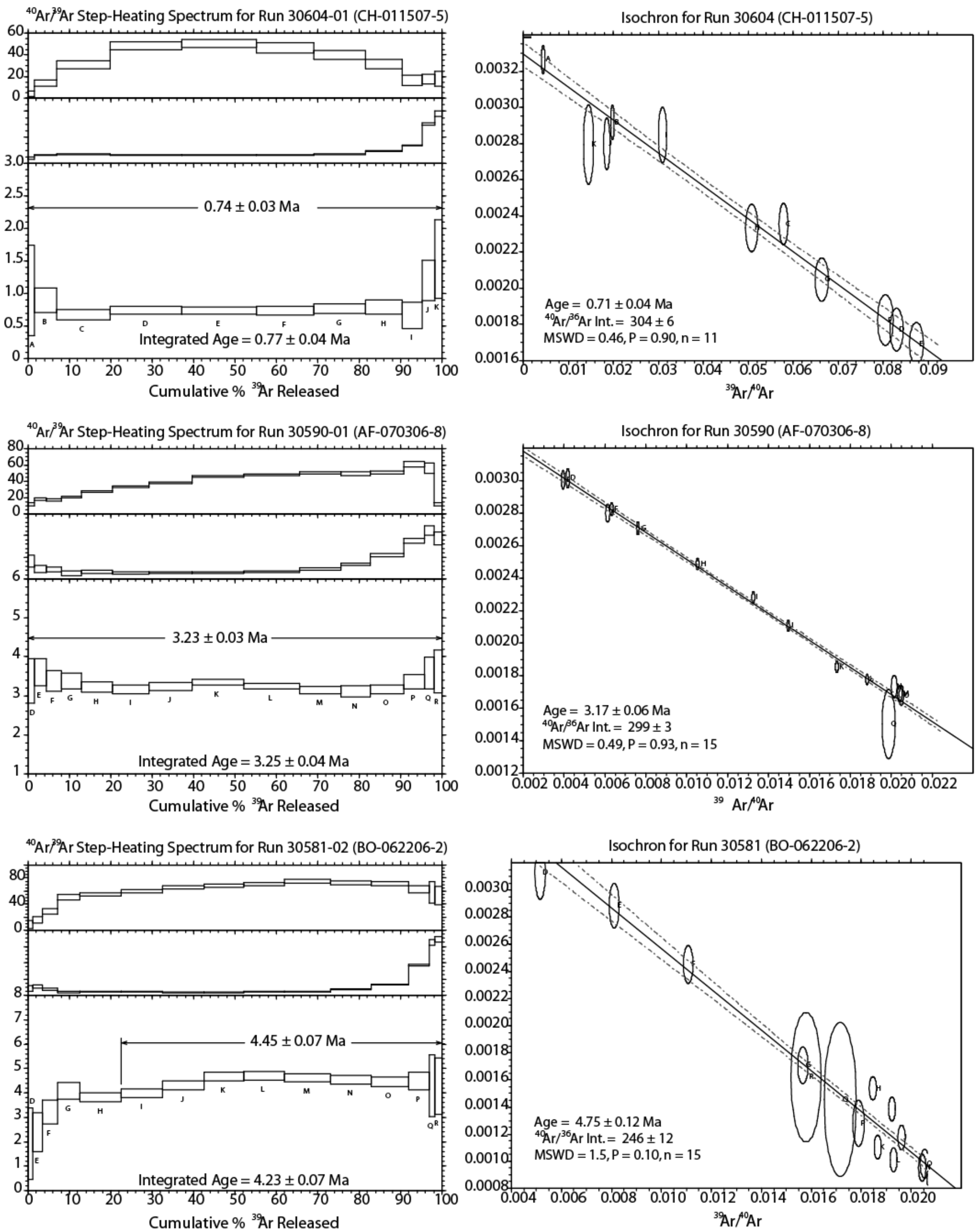

40Ar/39Ar Step-Heating Spectrum for Run 30604-01 (CH-011507-5)
0.74 ± 0.03 Ma
Integrated Age = 0.77 ± 0.04 Ma
Cumulative % 39Ar Released
Isochron for Run 30604 (CH-011507-5)
Age = 0.71 ± 0.04 Ma
40Ar/36Ar Int. = 304 ± 6
MSWD = 0.46, P = 0.90, n = 11
39Ar/40Ar
40Ar/39Ar Step-Heating Spectrum for Run 30590-01 (AF-070306-8)
3.23 ± 0.03 Ma
Integrated Age = 3.25 ± 0.04 Ma
Cumulative % 39Ar Released
Isochron for Run 30590 (AF-070306-8)
Age = 3.17 ± 0.06 Ma
40Ar/36Ar Int. = 299 ± 3
MSWD = 0.49, P = 0.93, n = 15
39 Ar/40Ar
40Ar/39Ar Step-Heating Spectrum for Run 30581-02 (BO-062206-2)
4.45 ± 0.07 Ma
Integrated Age = 4.23 ± 0.07 Ma
Cumulative % 39Ar Released
Isochron for Run 30581 (BO-062206-2)
Age = 4.75 ± 0.12 Ma
40Ar/36Ar Int. = 246 ± 12
MSWD = 1.5, P = 0.10, n = 15
39Ar/40Ar

Figure S2

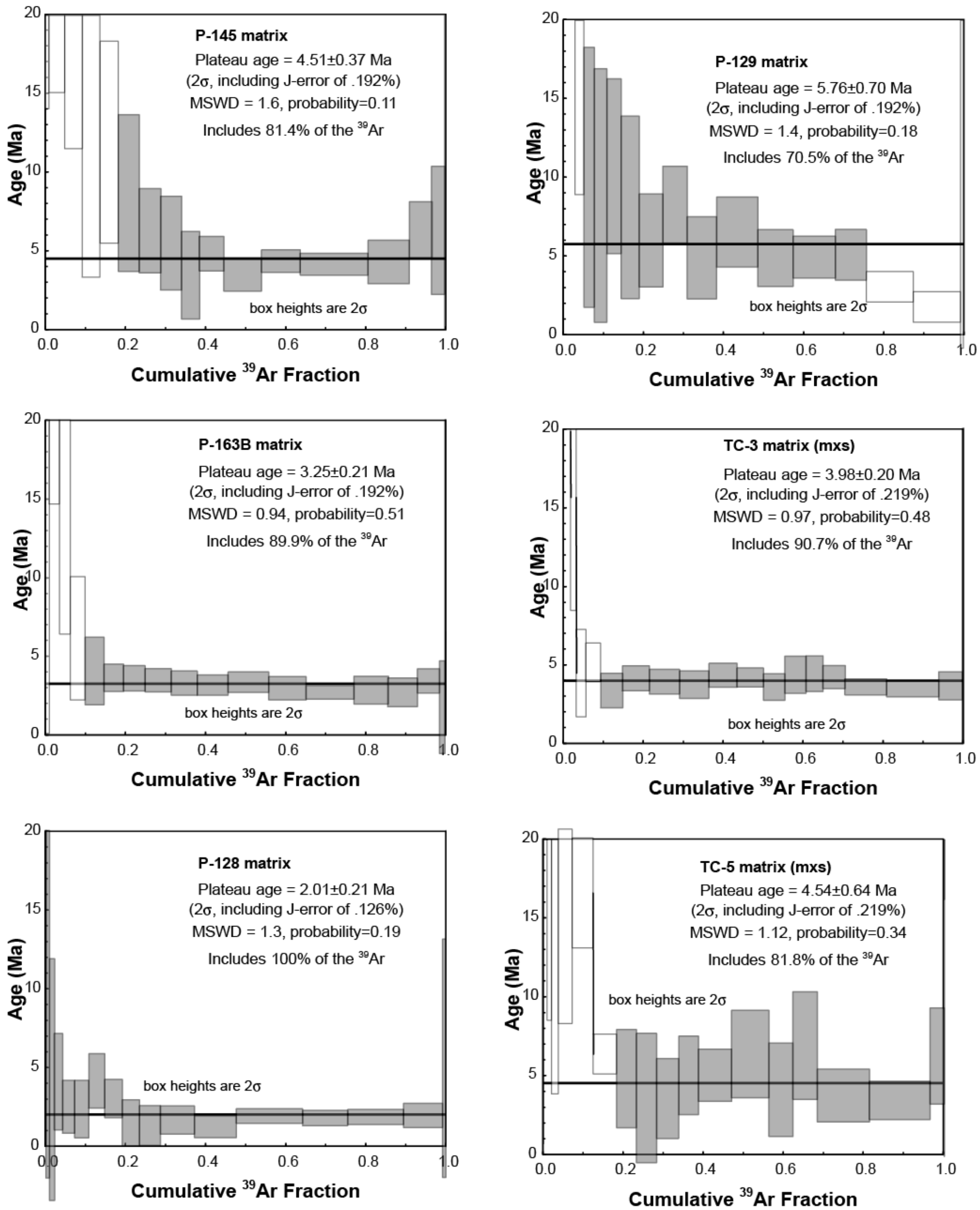
P-145 matrix
Plateau age = 4.51±0.37 Ma
(2σ, including J-error of .192%)
MSWD = 1.6, probability=0.11
Includes 81.4% of the ^{39}Ar
box heights are 2σ
Age (Ma)
Cumulative ^{39}Ar Fraction
P-129 matrix
Plateau age = 5.76±0.70 Ma
(2σ, including J-error of .192%)
MSWD = 1.4, probability=0.18
Includes 70.5% of the ^{39}Ar
box heights are 2σ
Age (Ma)
Cumulative ^{39}Ar Fraction
P-163B matrix
Plateau age = 3.25±0.21 Ma
(2σ, including J-error of .192%)
MSWD = 0.94, probability=0.51
Includes 89.9% of the ^{39}Ar
box heights are 2σ
Age (Ma)
Cumulative ^{39}Ar Fraction
TC-3 matrix (mxs)
Plateau age = 3.98±0.20 Ma
(2σ, including J-error of .219%)
MSWD = 0.97, probability=0.48
Includes 90.7% of the ^{39}Ar
box heights are 2σ
Age (Ma)
Cumulative ^{39}Ar Fraction
P-128 matrix
Plateau age = 2.01±0.21 Ma
(2σ, including J-error of .126%)
MSWD = 1.3, probability=0.19
Includes 100% of the ^{39}Ar
box heights are 2σ
Age (Ma)
Cumulative ^{39}Ar Fraction
TC-5 matrix (mxs)
Plateau age = 4.54±0.64 Ma
(2σ, including J-error of .219%)
MSWD = 1.12, probability=0.34
Includes 81.8% of the ^{39}Ar
box heights are 2σ
Age (Ma)
Cumulative ^{39}Ar Fraction

Figure S3

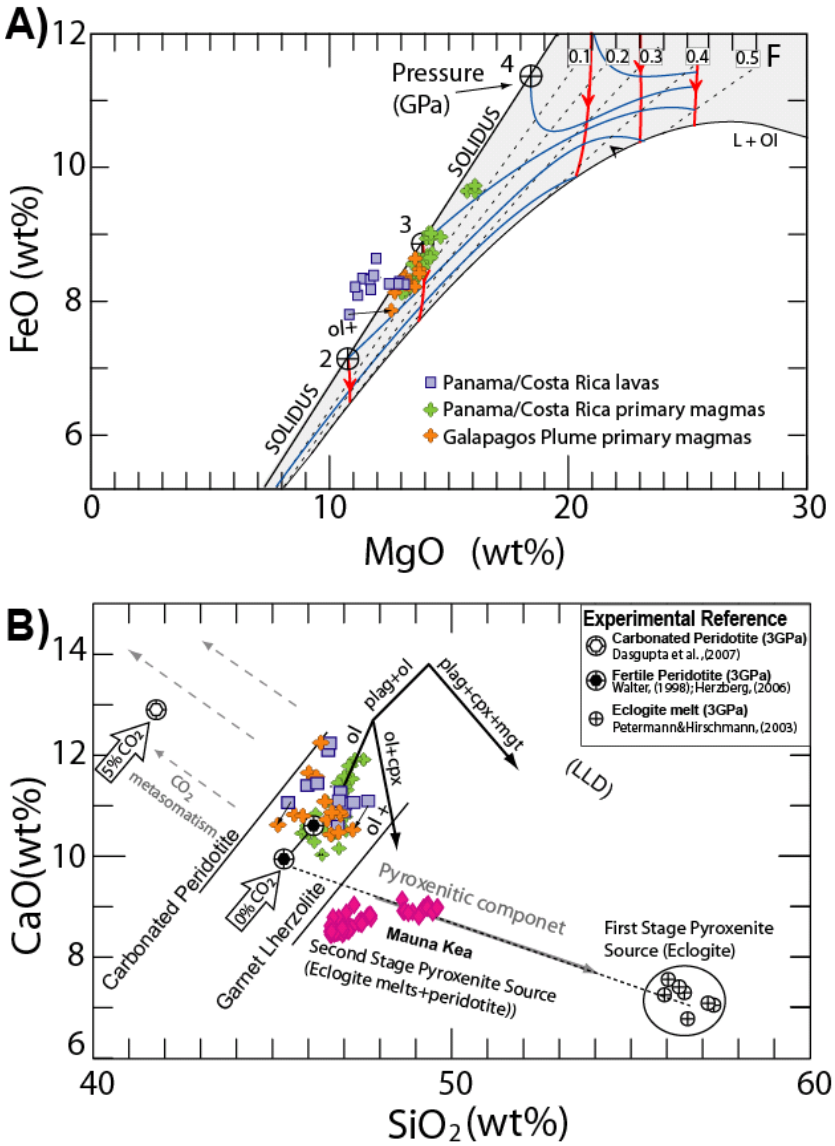
A)
Pressure (GPa)
SOLIDUS
SOLIDUS
ol+
L + Ol
0.1
0.2
0.3
0.4
0.5
F
FeO (wt%)
MgO (wt%)
Panama/Costa Rica lavas
Panama/Costa Rica primary magmas
Galapagos Plume primary magmas
B)
Experimental Reference
Carbonated Peridotite (3GPa) Dasgupta et al., (2007)
Fertile Peridotite (3GPa) Walter, (1998); Herzberg, (2006)
Eclogite melt (3GPa) Petermann&Hirschmann, (2003)
plag+ol
plag+cpx+mgt
ol
ol+cpx
ol +
(LLD)
5% CO2
CO2 metasomatism
Carbonated Peridotite
0% CO2
Garnet Lherzolite
Pyroxenitic componet
Mauna Kea
Second Stage Pyroxenite Source (Eclogite melts+peridotite))
First Stage Pyroxenite Source (Eclogite)
CaO(wt%)
SiO2 (wt%)

Table 1

Sample	Lat	Long	Age	Error	SiO2	TiO2	Al2O3	Fe2O3	MnO	MgO	CaO	Na2O	K2O	P2O5	Totals	LOI/H2O	Rb	Sr	Zr
Nicaragua-Volcan Blue																			
AZUL-2	12.5500	-83.9617			46.39	2.85	16.55	11.79	0.17	5.54	8.88	3.30	2.33	0.97	99.15	1.05	38	908	252
AZUL-5	12.5500	-83.9617			45.84	2.67	13.37	13.57	0.86	6.63	9.38	3.30	0.84	0.38	97.10	1.15	12	656	201
AZUL-4	12.5500	-83.9617			47.79	2.71	14.79	12.49	0.15	8.39	8.54	3.21	0.78	0.38	99.50	0.64	12	566	184
Nicaragua-Cukra Hill																			
CH-011507-1	12.2572	-83.7607			44.80	2.16	14.67	11.64	0.18	9.47	10.00	3.31	1.18	0.44	97.85	1.90	16	890	164
CH-011507-2	12.2923	-83.8199			50.51	3.18	14.00	12.19	0.16	6.63	8.40	3.23	0.51	0.32	99.13	0.73	7	400	208
CH-011507-3	12.2567	-83.7708			45.02	2.08	14.31	11.61	0.18	9.72	10.65	3.13	1.05	0.35	98.10	1.71	13	717	141
CH-011507-4	12.2485	-83.7704			44.37	2.14	13.86	11.87	0.22	9.86	11.14	2.46	0.97	0.34	97.23	2.59	13	722	141
CH-011507-5	12.2807	-83.8443	0.74	0.03	50.42	3.18	13.99	12.39	0.16	6.33	8.33	3.28	0.50	0.29	98.87	1.00	8	361	198
CH-011507-6	12.2987	-83.8456			50.34	3.18	14.05	12.20	0.16	6.57	8.18	3.16	0.47	0.30	98.61	1.25	6	373	203
CH-011507-7	12.3047	-83.8372			50.38	3.21	13.98	12.30	0.16	6.67	8.30	3.15	0.43	0.31	98.89	0.96	0	382	205
CH-011507-8(A)	-12.2028	-83.8263			49.35	3.30	14.55	11.71	0.16	6.28	8.96	3.39	0.83	0.43	98.96	0.88	10	531	232
CH-011507-9	12.3084	-83.7183			46.94	2.36	13.74	12.02	0.19	10.13	9.59	2.76	0.88	0.36	98.97	0.82	12	644	163
CH-011507-10	12.3084	-83.7183			47.51	3.00	13.37	12.72	0.23	8.32	8.56	3.07	0.97	0.47	98.22	1.61	14	473	233
Costa Rica-Victoria Dikes																			
D68	9.6962	-83.1299			45.15	1.46	17.09	11.13	0.20	6.47	6.36	4.34	1.69	0.61	94.50	5.28	33	590	158
D83	9.7500	-83.5000			47.64	1.45	17.66	10.52	0.19	4.79	8.90	3.21	1.72	0.65	96.73	3.04	36	993	167
D88	9.7003	-83.1240			44.21	1.68	16.96	10.54	0.16	5.36	9.90	3.37	2.15	0.62	94.95	4.82	47	1042	179
D155	9.7500	-83.5000			45.10	1.15	14.19	10.50	0.18	8.98	13.58	1.77	0.84	0.51	96.80	2.91	10	974	166
CR162	9.7500	-83.5000			40.01	1.41	16.50	11.24	0.16	3.98	10.62	4.23	0.69	0.52	89.36	10.49	15	546	154
CR271	9.8826	-83.1844			43.74	1.44	15.43	10.19	0.17	8.39	10.96	2.56	1.50	0.58	94.96	4.79	34	863	139
CR274	9.7500	-83.5000			38.44	1.80	16.04	9.58	0.17	2.16	15.01	2.33	1.94	0.75	88.22	11.53	37	982	272
RB-081606-1	9.8919	-83.1275			48.95	0.97	16.45	9.12	0.19	4.61	7.57	4.49	2.31	0.81	95.47	4.23	53	944	218
ES-081606-2	9.7114	-83.0879	6.49	0.03	44.32	1.45	15.14	11.53	0.18	9.24	12.61	1.80	0.88	0.39	97.54	2.17	12	1144	107
RB-091606-1	9.9489	-83.1619			43.57	1.83	15.30	11.98	0.19	8.42	12.90	2.04	1.39	0.80	98.42	1.40	22	933	103
AM-081906-1	9.5980	-82.8738	5.82	0.09	48.56	1.42	16.52	9.08	0.16	5.21	8.80	3.85	2.17	0.59	96.36	3.39	46	865	203
BS-011107-1	9.9849	-83.2187			43.89	1.18	10.27	11.00	0.16	17.63	11.78	1.22	0.68	0.38	98.19	1.55	12	694	78
QS-011107-1	9.9849	-83.2187			44.91	1.73	15.01	10.33	0.17	10.58	10.28	2.51	1.60	0.64	97.76	1.97	31	965	203
Costa Rica-Guayacan																			
BO-062106-1	10.0220	-83.5463			43.18	1.84	13.28	10.57	0.16	8.71	14.35	2.70	1.20	1.10	97.09	2.58	14	1681	186
BO-062106-7	10.0207	-83.5525			43.17	1.69	13.62	10.16	0.15	9.00	13.80	2.83	1.19	1.02	96.63	3.01	13	1841	166
BO-062106-8	10.0446	-83.5503			44.18	1.81	14.20	10.04	0.15	8.76	12.64	3.16	1.39	1.10	97.43	2.20	17	1882	182
BO-062206-1	10.0759	-83.5761			45.70	2.11	16.42	11.73	0.20	7.79	7.93	2.39	0.44	0.48	95.19	4.64	4	765	138
BO-062206-2	10.0761	-83.5826	4.45	0.07	43.63	1.27	13.32	10.99	0.18	14.37	11.21	1.26	0.49	0.41	97.13	2.55	6	670	111
BO-062206-3	10.0452	-83.6068			44.95	1.62	14.31	9.69	0.14	9.95	10.65	2.99	1.36	0.71	96.37	3.28	17	1753	168
BO-062206-4	10.0419	-83.6153			44.71	1.89	14.40	10.35	0.15	8.99	10.42	2.37	1.37	0.92	95.57	4.14	25	1391	195
B0-062306-1	10.0823	-83.5590			44.08	2.27	14.33	10.74	0.16	10.01	9.44	2.47	1.68	1.18	96.36	3.27	73	1768	275
B0-062306-3	10.0823	-83.5590			46.08	2.49	15.76	10.84	0.15	7.88	8.45	3.39	2.16	0.83	98.03	1.56	41	2399	252
BO-062306-4	10.0823	-83.5590			45.21	1.13	14.87	10.10	0.17	11.81	11.01	2.81	0.25	0.48	97.84	1.88	40	782	130
BO-062306-8	10.0732	-83.5597	4.33	0.07	46.18	1.98	14.97	11.23	0.16	8.66	9.07	2.84	1.19	0.43	96.71	3.07	27	959	131

Table 1 Continued

Sample	Lat	Long	Age	Error	SiO2	TiO2	Al2O3	Fe2O3	MnO	MgO	CaO	Na2O	K2O	P2O5	Totals	LOI/H2O	Rb	Sr	Zr
BO-062306-12	10.0036	-83.5753			42.49	1.66	16.40	8.78	0.16	5.36	10.02	4.08	1.86	1.57	92.38	7.10	19	2656	242
BO-062306-13	10.0413	-83.5441			44.08	1.81	14.25	10.02	0.15	8.98	12.68	2.66	1.31	1.10	97.04	2.58	14	1939	183
P-145	10.0723	-83.5781	4.48	0.19	44.16	1.30	13.31	11.10	0.19	14.02	11.14	1.26	0.59	0.41	97.86	2.33	9	680	102
Costa Rica-Lomas Azules																			
AF-070306-1	10.3277	-83.5815			41.46	1.60	16.61	10.00	0.20	5.94	10.82	5.63	2.20	1.03	95.49	4.11	37	2469	268
AF-070306-2	10.3241	-83.5720			44.82	1.68	15.35	11.60	0.17	9.29	11.41	2.29	0.71	0.59	97.91	1.82	13	1337	137
AF-070306-3	10.3115	-83.5734	3.6	0.03	45.38	1.87	14.47	11.37	0.16	9.99	11.01	2.64	1.04	0.84	98.77	0.96	15	1226	189
AF-070306-4	10.3566	-83.5865			46.24	1.90	13.55	10.96	0.17	10.85	10.51	2.23	1.38	0.53	98.32	1.36	28	1496	191
AF-070306-5	10.3612	-83.5828			43.36	2.46	13.88	11.98	0.18	10.63	10.63	2.42	1.55	0.97	98.06	1.60	27	1451	228
AF-070306-6	10.3612	-83.5828			47.30	2.12	15.85	10.62	0.16	7.31	9.11	2.94	1.53	0.70	97.64	2.05	20	1369	245
AF-070306-7	10.3736	-83.5811			46.30	1.96	14.92	10.78	0.15	9.58	9.77	2.80	0.98	0.61	97.85	1.88	20	1167	169
AF-070306-8	10.3614	-83.5823	3.23	0.03	46.83	2.02	14.39	10.78	0.17	9.67	9.62	2.88	1.07	0.65	98.08	1.63	26	1207	230
P-163B	10.3559	-83.5850	3.21	0.11	46.58	2.06	14.56	11.06	0.16	8.94	10.54	2.79	1.26	0.59	98.93	1.11	28	1477	183
P-164	10.3753	-83.5707			46.49	2.30	16.96	11.53	0.17	6.19	8.54	3.02	1.72	0.81	98.08	2.03	32	1498	216
Costa Rica-Cerro Coronel																			
CO-070206-1	10.6999	-83.6418			43.82	2.25	13.75	10.28	0.17	10.82	11.62	2.98	0.82	0.81	97.32	2.36	32	1337	325
CO-070206-2	10.6935	-83.6441	3.06	0.08	44.07	2.27	13.69	11.23	0.18	11.34	10.73	3.15	0.61	0.80	98.07	1.60	71	1338	320
CO-070206-3	10.7014	-83.6421			45.33	2.40	12.72	11.30	0.16	11.81	10.09	1.88	1.41	0.54	97.64	2.05	24	1226	216
CO-070206-4	10.7022	-83.6424			45.41	2.40	12.36	11.33	0.16	12.53	10.28	2.55	0.60	0.52	98.14	1.58	17	891	201
CO-070206-5	10.7013	-83.6445			43.30	2.24	12.89	11.73	0.17	13.15	10.15	3.08	0.58	0.76	98.05	1.66	16	1089	273
Costa Rica-Lomas del Colorado-Rio San Juan																			
P-130A	10.7023	-83.6467			42.33	2.33	12.41	11.06	0.16	10.89	12.75	2.63	1.15	1.30	97.46	2.32	34	1740	270
TO-070106-1	10.6465	-83.6891	3.13	0.06	42.16	2.16	13.08	10.62	0.17	11.02	12.66	3.05	0.60	1.32	96.84	2.73	51	2123	357
TO-070106-2	10.6685	-83.6675			44.58	2.06	13.79	11.09	0.16	11.30	11.03	2.04	0.80	0.60	97.45	2.23	33	1244	215
TO-070106-3	10.6736	-83.6673	3.07	0.06	42.35	1.99	11.66	10.31	0.16	15.31	11.80	2.74	0.63	1.00	97.95	1.64	114	1326	282
TO-070106-4	10.6742	-83.6673			41.68	1.98	11.16	10.25	0.16	15.63	12.06	2.26	0.40	0.96	96.54	3.09	45	1268	284
P-134	10.6716	-83.6652			41.75	1.99	11.21	10.34	0.16	15.36	11.73	2.14	0.68	0.97	96.78	3.13	56	1289	231
P-137	10.6189	-83.6960			42.59	2.60	10.98	12.16	0.19	11.37	13.39	2.03	0.45	0.85	97.02	3.27	33	1298	350
P-138	10.5949	-83.7011			41.87	2.04	11.90	10.63	0.16	13.02	13.94	2.18	0.84	1.00	97.99	1.98	29	1335	219
CR-85	10.9764	-84.3534																	
P-128	10.7704	-83.7962	2.01	0.11	46.07	3.00	14.36	12.23	0.17	8.07	9.30	2.79	1.47	1.00	98.87	1.47	32	1359	387
P-129	10.7755	-83.7776	2.3	0.4	47.07	2.07	15.28	12.49	0.18	7.43	9.29	2.74	0.83	0.42	98.05	2.65	21	687	165
Costa Rica-Cerro Tortuguero																			
TO-070106-5	10.6999	-83.6663			43.71	1.95	16.61	11.95	0.20	6.28	10.72	3.09	0.85	0.81	96.17	3.53	35	1624	221
TO-070206-7	10.5867	-83.5271			47.07	1.89	13.84	10.53	0.15	10.83	10.02	2.70	0.98	0.56	98.57	1.18	14	778	200
TO-072106-1	10.5866	-83.5383			46.11	1.54	13.38	10.53	0.16	12.89	10.68	2.50	0.77	0.53	99.09	0.63	8	768	178
TO-072106-2	10.5866	-83.5383			47.46	1.91	14.08	10.50	0.15	10.18	9.69	2.77	1.12	0.60	98.46	1.29	23	766	206
TO-072106-3	10.5848	-83.5383			45.94	1.56	13.51	10.52	0.16	12.56	10.79	2.37	0.81	0.54	98.76	0.98	10	779	176
TO-072106-4	10.5857	-83.5301			45.76	1.60	13.45	10.56	0.16	12.20	10.84	2.33	1.21	0.64	98.75	0.97	23	895	194
TO-072106-5	10.5911	-83.5365			46.98	2.29	13.74	11.25	0.16	9.67	9.52	2.78	1.00	0.74	98.13	1.60	19	843	244

Table 1 Continued

Sample	Lat	Long	Age	Error	SiO2	TiO2	Al2O3	Fe2O3	MnO	MgO	CaO	Na2O	K2O	P2O5	Totals	LOI/H2O	Rb	Sr	Zr
TO-072106-6	10.5911	-83.5365			46.97	2.39	13.80	11.86	0.16	10.18	8.62	2.31	0.94	0.39	97.62	2.14	16	712	253
P-132B	10.5813	-83.5289			45.84	1.59	13.68	10.32	0.15	11.27	10.67	2.12	1.02	0.53	97.54	1.78	17	781	160
P-133	10.5813	-83.5289			46.51	1.60	14.04	10.76	0.15	11.65	10.89	2.56	0.73	0.58	99.83	0.36	12	810	163
Costa Rica-Aguas Zarcas (Volcanic Front Alkaline)																			
P-152	10.3795	-84.3046			44.89	0.80	13.33	9.90	0.17	13.39	12.57	1.31	0.77	0.35	98.15	1.58	105	2507	53
P-153	10.3899	-84.3241			46.67	1.53	14.47	10.86	0.17	10.27	11.30	2.23	1.26	0.53	99.62	0.44	35	783	166
P-154B	10.4455	-84.2753			50.17	1.43	15.69	9.40	0.14	8.47	9.07	2.93	1.26	0.44	99.29	0.60	26	817	156
P-155A	10.4580	-84.3428			49.23	1.27	16.64	9.90	0.14	6.81	10.07	2.99	1.02	0.43	98.81	0.61	19	910	119
Costa Rica-Talamanca Adakites (<5 Ma)																			
TC-3	9.0907	-83.2715	3.98	0.1	49.73	0.90	17.84	9.96	0.19	4.52	9.55	2.83	1.80	0.40	97.72	1.17	38	1177	100
TC-5A	8.8498	-82.9452	4.54	0.64	56.66	0.73	15.87	7.23	0.10	4.62	7.21	3.24	2.39	0.26	98.31	0.69	48	1204	104
TC-5b	8.8498	-82.9452			53.75	1.00	16.11	7.73	0.11	5.92	7.90	3.19	1.66	0.28	97.65	0.72	30	1145	116
TC-5d	8.8498	-82.9452			60.51	0.63	16.27	4.96	0.07	2.85	5.77	3.51	2.67	0.25	97.49	1.01	50	1289	113
TC-6A	8.9143	-82.7877			54.64	0.98	16.15	7.69	0.11	5.47	7.84	3.18	1.72	0.28	98.06	0.63	32	1146	111
TC-6b	8.9143	-82.7877																	
TC-7	8.8999	-82.7894			55.44	0.77	16.09	7.10	0.11	5.79	7.78	3.36	1.96	0.23	98.63	0.28	35	1029	93
TC-8	8.6248	-82.9178	3.588	0.043	55.69	1.15	14.24	6.62	0.08	4.91	8.17	2.96	3.65	0.56	98.03	0.58	89	2134	256
TA-040107-4	9.2468	-83.2642			48.55	0.67	18.62	9.72	0.21	4.23	9.4	2.89	1.7	0.36	96.35	3.42	24	1090	70
CS-082106-1	8.6248	-82.9178			54.5	1.13	13.95	6.36	0.07	5.03	7.98	2.95	3.67	0.52	96.16	3.34	77	2076	283
Panama-Adakites																			
M38KH	8.2387	-82.1285			58.52	0.89	15.90	6.19	0.09	3.19	5.74	3.63	2.97	0.52	98.98	1.31		1591	150
M44KH	8.6690	-82.6210			54.91	0.73	15.77	7.35	0.11	7.04	8.20	3.19	1.61	0.29	99.20	0.23	30	1120	91
M53KH	8.7940	-82.5850			59.83	0.68	16.43	6.19	0.10	3.61	6.65	2.97	3.01	0.25	99.72	0.14	56	1528	133
M55KH	8.7960	-82.4740			55.91	0.76	16.44	7.28	0.12	5.11	8.10	3.29	1.92	0.29	99.22	0.34	47	1370	126
M57aKH	8.7960	-82.4740			52.40	0.86	15.62	8.18	0.13	8.41	8.98	2.95	1.15	0.28	98.96	0.44	22	861	92
M61a KH	8.8240	-82.7300			57.26	0.90	16.39	6.75	0.09	3.89	6.89	3.68	2.24	0.36	99.06	0.59		1298	118
M63aKH	8.1400	-82.8740			64.34	0.54	15.58	4.28	0.06	2.25	4.80	3.74	2.65	0.17	99.25	0.48	47	1019	101
M64 b KH	8.1840	-82.8770			53.61	0.95	17.41	8.47	0.17	4.42	8.27	3.09	2.19	0.31	99.98	0.47	-	1015	146
M64c KH	8.1840	-82.8770	0.77	0.37	58.18	0.73	17.38	6.68	0.10	3.87	7.20	2.85	2.56	0.21	100.08	0.23	44	1312	122
M64 f KH	8.1840	-82.8770			51.48	0.94	15.80	8.06	0.11	7.84	9.59	3.18	1.46	0.47	99.70	0.4	-	1314	130
M65a KH	8.4700	-82.7100	0.21	0.08	55.96	0.94	15.86	6.99	0.10	5.36	7.66	2.93	2.81	0.47	99.53	0.41	49	2006	182
M66a KH	8.5290	-82.6940			56.82	0.83	16.92	7.08	0.11	5.09	7.53	3.73	1.37	0.27	100.28	0.24	24	964	89
M91a KH	8.8290	-82.4860			56.49	0.90	15.88	6.43	0.09	5.91	7.38	3.68	2.07	0.46	99.81	0.47	-	1437	132
Panama-Alkaline 1-4.5 Ma																			
SO96-1	8.0730	-81.7320	1.30	0.15	47.74	1.54	14.62	10.54	0.15	9.62	10.09	3.15	1.16	0.64	99.25	0.51	25	1118	127
So-96-1II	8.0730	-81.7320			47.80	1.55	14.59	10.76	0.15	9.55	10.07	3.11	1.16	0.63	99.88	0.48	-	1125	127
SO-96-2	8.0730	-81.7320			46.81	1.63	14.13	10.92	0.15	10.21	10.36	2.99	1.15	0.77	99.62	0.46	21	1222	138
S0-96-3	8.0730	-81.7320			48.00	1.54	14.64	10.78	0.15	9.65	10.09	3.14	1.14	0.63	100.08	0.3	-	1127	124
S0-96-4	8.0730	-81.7320			47.63	1.54	14.64	10.77	0.15	9.55	10.09	3.05	1.17	0.62	100.20	0.96	-	1130	124
SO-96-5	8.0730	-81.7320			45.50	1.66	14.21	11.11	0.15	10.75	11.06	2.94	1.08	0.91	99.70	0.32	-	1326	138
CP97-1	8.2170	-81.5870	1.50	0.28	44.20	1.51	13.41	11.51	0.17	11.54	11.86	2.47	0.99	0.84	98.50	1.07	22	1304	135
M36KH	8.2742	-82.0377			47.13	2.77	13.03	10.82	0.15	9.57	10.35	3.10	1.02	0.83	98.77	1.18	23	1282	242
M37KH	8.2742	-82.0377			45.83	2.31	12.91	10.76	0.16	10.99	11.25	2.97	1.21	0.96	99.78	0.54	21	1342	222
M98a KH	8.2800	-82.0470			46.10	2.75	12.93	10.9	0.15	9.62	10.96	3.01	0.99	0.93	99.98	1.59	15	1382	238
M99a KH	8.3400	-81.8260			53.67	1.16	14.99	6.88	0.12	6.06	8.84	4.12	1.47	0.81	98.12	1.20	25	1307	154
M105 KH	8.2410	-81.7910	1.40	0.24	47.67	1.43	14.26	9.24	0.15	10.07	10.91	3.12	1.40	0.86	99.11	0.59	25	1415	160
M 118aKH	8.1290	-81.4470	1.43	0.22	47.49	1.84	13.94	10.17	0.16	9.86	9.68	3.33	1.80	0.73	99.00	0.57	36	1417	192
M118bKH	8.1290	-81.4470			48.62	1.74	14.14	9.74	0.15	9.44	9.41	3.30	1.82	0.68	99.74	0.59	37	1408	187
M121aKH	8.1880	-81.4880	4.45	0.35	44.35	2.06	12.88	10.46	0.16	10.34	12.32	3.08	1.49	1.16	98.30	0.65	26	2061	229
3-12-4-03	7.4700	-82.2380	1.59	0.21	45.11	1.38	12.92	10.70	0.17	11.66	11.87	2.70	0.95	1.01	98.86	0.39	18	1278	139

Table 2

Sample	Ba	La	Ce	Pr	Nd	Sm	Eu	Gd	Tb	Y	Dy	Ho	Er	Yb	Lu	V	Cr	Nb	Hf	Ta	Pb	Th	U
Nicaragua-Volcan Blue																							
AZUL-2	1661.68	37.07	79.78	10.78	43.39	8.65	1.67	7.75	1.07	25.55	5.46	0.94	2.32	1.84	0.25	278.74	51.08	53.15	5.48	2.99	1.63	2.66	0.82
Nicaragua-Cukra Hill																							
CH-011507-1	518	31.63	57.81	6.81	27.85	6.01	1.92	6.1	0.84	23.7	4.58	0.81	2.13	1.78	0.25	225	265	35	4.1	2	1.31	2.65	0.83
CH-011507-4	322	23.12	42.56	5.31	22.88	5.28	1.74	5.47	0.78	23.01	4.42	0.8	2.12	1.74	0.25	247	260	29	3.5	1.69	1.06	1.97	0.54
CH-011507-9	395	24.08	41.52	5.48	24.3	5.81	1.92	6.46	0.92	37.6	5.47	1.04	2.79	2.25	0.33	218	328	31	4.1	1.94	1.12	1.65	0.48
Costa Rica-Victoria Dikes																							
D68	872.95	41.19	76.26	9.23	38.43	7.9	2.31	7.26	0.93	25.83	4.71	0.8	2.21	2.18	0.33	244.88	23.45	21.72	3.49	1.34	2.79	5.22	1.56
D83	796.24	41.55	75.92	9.27	38.74	7.86	2.41	7.22	0.94	27.39	4.99	0.87	2.45	2.43	0.36	252.58	11.16	24.03	3.56	1.49	2.73	4.73	1.51
D88	642.27	38.44	73.17	9.22	39.37	8.63	2.48	7.73	0.98	27.49	5.3	0.88	2.44	2.26	0.33	317.76	9.08	18.39	3.98	1.05	2.75	4.39	1.58
D155	1159.37	42.49	84.27	11.25	50.02	11.21	3.13	9.35	1.13	29.38	5.84	0.93	2.49	2.37	0.33	285.39	177.89	13.04	3.68	0.71	2.77	3.76	1.37
CR162	414.04	41.71	77.17	9.64	41.08	8.69	2.46	8.06	1.04	30.98	5.72	0.99	2.65	2.45	0.36	275.68	13.37	19.96	3.36	1.2	2.14	5.01	1.53
CR271	788.41	35.92	65.58	8.09	34.38	7.35	2.28	6.74	0.89	26.78	4.78	0.84	2.32	2.21	0.33	259.71	205.52	17.64	3.18	1.08	2.82	4.32	1.69
CR274	756.31	57.17	108.87	13.31	55.16	10.91	3.15	9.6	1.2	32.76	6.08	1.01	2.73	2.63	0.4	223.8	23.71	42.06	5.44	2.76	3.42	5.59	1.74
RB-081606-1	1349.41	58.97	98.55	11.11	43.38	8.16	2.4	7.62	1	28.2	4.97	0.86	2.53	2.55	0.4	170.13	68.93	26.66	4.34	1.7	5.21	7.84	2.67
ES-081606-2	876.46	23.12	43.62	5.57	24.54	5.51	1.76	5.08	0.69	21.15	3.99	0.7	1.98	1.86	0.28	290.97	269.52	17.67	2.56	1.1	1.64	2.37	0.85
RB-091606-1	385.2	25.36	53.86	7.48	35.23	8.11	2.38	7.3	0.93	28.31	5.33	0.91	2.48	2.28	0.33	310.13	155.61	13.21	2.67	0.78	1.5	1.6	0.72
AM-081906-1	788.18	50.08	90.76	10.48	41.78	7.79	2.28	7.1	0.91	23.72	4.37	0.74	2.07	1.98	0.3	216.68	83.8	35.55	4.06	2.26	3.54	7.8	2.86
BS-011107-1	419.17	20.69	42.72	5.78	26.01	5.63	1.68	5.13	0.67	18.81	3.5	0.6	1.67	1.51	0.23	221.33	880.58	9.3	2.07	0.51	1.44	1.51	0.66
QS-011107-1	623.96	45.74	81.74	9.61	39.71	7.92	2.41	7.36	0.95	27.24	4.98	0.87	2.39	2.28	0.34	224.03	353.66	32.8	4.05	2.03	2.67	4.87	1.55
Costa Rica-Guayacan																							
BO-062106-1	846	72.48	130.04	15.55	62.09	11.15	3.04	9.49	1.14	27.46	5.59	0.96	2.57	2.28	0.33	256	185	37	4.5	1.8	3.58	6.52	1.62
BO-062106-8	901	70.76	126.75	15.04	59.99	10.74	2.93	9.09	1.1	26.19	5.33	0.92	2.49	2.2	0.32	242	245	38	4.4	1.89	4.14	6.08	1.57
B0-062306-1	705	76.95	134.72	15.84	63.28	11.61	3.18	9.97	1.24	31.03	6.18	1.06	2.8	2.47	0.37	199	276	55	6.0	3.14	2.94	7.23	1.95
BO-062306-4	479	39.4	73.47	8.69	35.32	8.2	2.02	6.47	0.83	23.68	4.42	0.79	2.21	2.05	0.3	229	661	16	3.1	0.93	1.8	5.82	1.6
BO-062306-12	1355	103.9	177.97	19.95	74.76	12.5	3.36	10.42	1.24	28	5.79	1.04	2.9	2.7	0.41	286	33	57	4.8	2.61	5.91	10.06	2.57
P-145	970.61	26.00	54.34	6.93	28.27	5.78	1.73	5.07	0.74	20.90	4.03	0.77	2.06	1.85	0.27	281.48	951.20	16.44	2.83	0.90	3.00	2.87	0.96
Costa Rica-Lomas Azules																							
AF-070306-2	520	44.09	87.86	11.64	51.14	10.75	3.02	8.95	1.05	24.87	5.24	0.88	2.25	1.91	0.27	289	127	12	3.5	0.78	5.25	3.8	1.67
AF-070306-4	508	56.71	109.01	13	51.6	9.22	2.59	8.06	0.99	23.33	4.94	0.85	2.28	1.98	0.28	235	395	29	4.3	1.68	2.23	3.81	1.46
AF-070306-8	673	56.5	108.93	13.38	53.53	9.65	2.7	8.34	1.02	24.6	5.08	0.89	2.4	2.03	0.29	226	304	34	5.1	1.97	2.05	4.09	1.24
P-163B	575.65	54.35	111.91	13.90	53.86	9.55	2.90	8.53	1.03	21.48	5.13	0.90	2.15	1.82	0.26			26.65	4.45	1.40	2.16	3.53	1.50
Costa Rica-Cerro Coronel																							
CO-070206-2	637	80.65	155.33	18.91	75.7	13.36	3.53	11.49	1.37	32.03	6.75	1.14	3	2.71	0.39	219	408	46	6.6	2.64	2.49	5.8	1.85
CO-070206-5	542	67.49	133.89	16.37	65.82	11.98	3.23	10.45	1.26	29.57	6.03	1.03	2.68	2.41	0.33	224	462	38	5.6	2.22	2.06	4.91	1.64

Table 2 Continued

Sample	Ba	La	Ce	Pr	Nd	Sm	Eu	Gd	Tb	Y	Dy	Ho	Er	Yb	Lu	V	Cr	Nb	Hf	Ta	Pb	Th	U
Costa Rica-Lomas del Colorado-Rio San Juan																							
TO-070106-1	711	115.74	210.78	24.74	96.86	16.36	4.21	13.92	1.6	35.39	7.5	1.27	3.31	2.96	0.42	226	314	59	7.3	3.18	3.45	9.42	2.85
TO-070106-2	608	57.63	113.15	14.31	59.42	11.22	3.04	9.45	1.13	26.13	5.48	0.93	2.43	2.11	0.3	252	458	28	4.7	1.66	2.28	4.43	1.54
TO-070106-4	598	80.41	161.41	19.73	79.69	14.15	3.7	11.97	1.38	30.93	6.35	1.07	2.76	2.43	0.34	215	600	42	5.9	2.22	2.12	4.62	1.72
P-138	598.44	76.11	167.25	19.74	75.65	13.21	3.57	10.60	1.34	27.76	6.18	1.02	2.50	1.94	0.27	264.43	586.82	37.55	5.02	1.84	3.54	6.15	1.97
CR-85	1402.41	137.60	274.40	31.16	114.84	18.17	4.12	13.60	1.68	33.92	7.44	1.23	3.08	2.38	0.34	200.48	651.67	57.88	8.66	2.78	5.47	14.65	4.17
P-128	715.97	99.68	212.84	25.99	98.65	16.38	4.54	12.40	1.64	36.44	7.79	1.31	3.23	2.44	0.34	225.11	171.29	57.97	8.28	2.79	2.66	5.60	2.10
P-129																							
Costa Rica-Cerro Tortuguero																							
TO-070206-7	518	52.12	98.38	11.95	48.76	9.31	2.61	8.63	1.09	28.9	5.59	0.99	2.68	2.39	0.33	214	474	30	4.7	1.79	2.36	5.08	1.51
TO-072106-1	510	50.09	94.84	11.29	45.21	8.41	2.33	7.59	0.96	24.87	4.91	0.88	2.39	2.12	0.3	222	626	26	4.1	1.59	2.35	5.51	1.69
TO-072106-6	486	34.46	62.92	7.72	31.89	6.44	2	6.07	0.81	21.44	4.37	0.77	2.12	1.87	0.27	199	411	40	5.8	2.36	2.22	5.26	1.68
P-132B	542.09	48.95	97.74	12.00	46.52	8.49	2.48	7.88	0.99	22.58	5.14	0.94	2.30	2.06	0.30	-	-	23.49	4.45	1.29	1.63	5.13	1.86
P-133																							
Costa Rica-Aguas Zarcas (Volcanic Front Alkaline)																							
P-152	2458.70	65.21	133.59	16.57	63.09	8.35	2.52	6.78	0.71	14.97	3.42	0.63	1.63	1.50	0.23	-	-	7.27	1.93	0.35	5.38	5.33	0.79
P-153	637.63	53.90	113.57	13.83	53.59	9.68	2.74	7.75	1.08	27.68	5.45	0.98	2.53	2.13	0.31	254.88	481.61	18.57	4.18	0.92	2.84	5.57	2.02
P-154B	600.65	39.15	80.13	9.78	37.71	6.67	1.99	6.15	0.76	17.43	3.97	0.72	1.77	1.58	0.23	-	-	19.77	4.11	1.11	2.50	4.03	1.52
P-155A	571.42	31.46	63.82	7.92	31.05	5.81	1.72	4.72	0.67	17.63	3.44	0.63	1.63	1.40	0.20	242.78	307.48	16.39	2.84	0.80	2.25	3.49	1.32
Costa Rica-Talamanca Adakites)																							
TC-3	802.24	23.69	50.10	6.56	26.42	5.33	1.57	4.64	0.62	18.12	3.41	0.63	1.71	1.60	0.24	275.37	19.90	5.15	2.23	0.22	3.64	3.13	1.20
TC-5A	915.46	26.97	53.69	6.42	23.83	4.10	1.12	3.12	0.38	9.63	1.90	0.34	0.89	0.79	0.12	186.02	142.65	6.39	2.60	0.36	6.32	6.53	2.03
TC-5b																							
TC-5d	1013.32	26.57	52.08	6.10	22.06	3.64	0.96	2.70	0.32	7.79	1.57	0.28	0.71	0.64	0.09	145.89	51.28	7.56	2.48	0.43	8.13	6.44	2.01
TC-6A	713.62	23.56	46.91	5.81	22.10	4.04	1.20	3.41	0.45	12.66	2.44	0.44	1.17	1.03	0.15	217.78	162.16	9.18	2.92	0.51	4.91	4.44	1.27
TC-6b	710.96	23.36	47.80	5.89	22.16	4.08	1.21	3.44	0.45	12.25	2.44	0.45	1.15	1.04	0.15	217.88	158.76	9.77	3.00	0.54	4.10	4.51	1.29
TC-7	802.74	20.66	41.06	5.01	18.90	3.53	1.02	2.88	0.36	9.41	1.88	0.34	0.89	0.78	0.12	206.99	201.78	7.31	2.48	0.41	5.05	4.88	1.58
TC-8	1914.59	74.21	169.00	17.80	64.66	9.77	2.39	6.53	0.73	15.04	3.28	0.55	1.38	1.11	0.15	197.54	104.82	14.54	7.12	0.74	11.25	16.93	4.63
TA-040107-4	1018	32.76	63.06	7.08	27.4	4.87	1.53	4.69	0.58	15.34	2.56	0.48	1.37	1.36	0.21	301	5	6.27	1.54	0.26	5.88	6.28	2.53
CS-082106-1	1955	78.13	151.09	16.77	62.72	9.76	2.65	8.75	0.96	16.39	3.24	0.52	1.38	1.33	0.18	213	118	16.41	6.99	0.78	11.95	19.93	7.12

Table 2 Continued

Sample	Ba	La	Ce	Pr	Nd	Sm	Eu	Gd	Tb	Y	Dy	Ho	Er	Yb	Lu	V	Cr	Nb	Hf	Ta	Pb	Th	U
Panama-Adakites																							
M44KH	759.97	23.50	43.82	5.35	19.85	3.55	0.65	2.99	0.39	10.02	2.00	0.36	0.98	0.90	0.13	185.04	237.01	6.78	2.53	0.36	5.68	4.15	1.35
M53KH	1152.20	30.33	59.82	7.05	26.59	4.63	1.33	3.53	0.47	10.16	2.18	0.40	1.03	0.90	0.13	171.02	30.24	5.19	4.51	0.37	10.14	11.41	2.94
M55KH	1291.24	33.02	62.87	7.63	27.90	4.45	0.44	3.49	0.44	11.26	2.20	0.40	1.11	1.03	0.15	205.50	117.67	6.51	3.91	0.34	6.34	7.70	2.23
M57aKH	636.59	23.56	45.24	5.57	20.78	3.75	0.81	3.24	0.45	12.06	2.37	0.44	1.18	1.11	0.16	216.00	514.66	9.65	2.45	0.52	3.85	3.54	1.07
M63aKH	1050	20.85	37.74	4.55	16.50	2.90	0.14	2.34	0.30	9.00	1.46	0.26	0.69	0.61	0.09	-	30		2.08	0.39	7.46	6.51	2.12
M64c KH	979.38	23.05	45.63	5.55	21.61	3.96	1.19	3.50	0.46	10.34	2.49	0.48	1.28	1.17	0.17	-	25.84	4.30	4.76	0.30	-	-	-
M65a KH	1438.84	66.56	127.81	14.69	52.55	7.72	2.07	6.08	0.67	11.75	3.12	0.54	1.40	1.15	0.17	-	90.79	10.66	7.04	0.70	-	-	-
M66a KH	742	24.30	45.85	5.50	21.08	3.82	1.14	3.39	0.44	10.00	2.42	0.46	1.23	1.15	0.17	-	154		3.20	0.49	3.74	3.59	1.22
Panama-Alkaline 1-4.5 Ma																							
SO96-1	677.05	46.81	94.14	10.98	41.19	7.27	2.20	6.08	0.83	21.04	4.45	0.82	2.11	1.77	0.25	-	-	28.79	3.63	1.21	3.34	4.88	1.88
SO-96-2	673	52.27	103.68	11.85	43.95	7.60	2.24	6.05	0.81	27.00	4.26	0.77	1.96	1.67	0.23	-	-	-	3.50	1.21	3.33	5.61	1.89
CP97-1	652.33	66.67	133.13	15.26	55.98	9.30	2.61	7.14	0.93	22.32	4.81	0.87	2.21	1.81	0.25	-	-	26.36	3.41	0.98	3.43	7.13	2.13
M36KH	775.85	51.28	106.08	13.65	55.97	10.91	3.23	9.76	1.27	25.41	6.57	1.15	2.85	2.22	0.31	-	360.12	49.57	6.96	3.09	3.47	6.13	1.86
M37KH	1065.66	56.34	115.75	14.73	58.52	10.83	3.13	9.47	1.19	25.16	6.14	1.08	2.75	2.17	0.31	-	436.78	48.00	6.37	2.90	3.76	6.47	1.95
M98a KH	812	58.66	117.48	14.37	57.22	10.75	3.20	9.01	1.25	26.00	6.19	1.08	2.68	2.11	0.29	-	-	-	5.87	2.74	3.51	6.27	1.79
M99a KH	1287.93	63.94	118.19	12.41	44.15	7.19	1.27	5.88	0.76	18.55	3.72	0.65	1.71	1.46	0.21	162.01	260.09	48.03	3.57	2.04	6.36	8.88	2.67
M105 KH	843.66	60.54	109.61	12.90	47.07	7.68	2.17	6.09	0.81	17.88	3.94	0.70	1.82	1.52	0.22	187.38	357.53	29.65	3.71	1.54	3.99	7.03	1.95
M 118aKH	1121.58	67.66	138.25	16.77	63.63	10.88	3.07	9.32	1.13	21.19	5.53	0.96	2.35	1.81	0.26	-	359.59	34.80	6.04	2.35	5.11	8.42	2.68
M118bKH	1180	66.33	134.72	16.38	62.03	10.64	2.99	8.98	1.11	21.00	5.42	0.94	2.34	1.85	0.25	-	-	-	5.87	2.22	5.07	8.38	2.72
M121aKH	1033.54	84.58	173.47	21.60	83.46	14.06	3.90	11.51	1.37	23.82	6.61	1.13	2.79	2.20	0.30	-	363.88	35.65	6.50	2.25	4.69	8.85	2.50
3-12-4-03	755.47	77.22	157.72	17.57	64.12	10.55	2.68	8.51	1.12	26.64	5.49	0.97	2.50	2.13	0.30	209.18	467.99	28.91	3.38	1.21	4.63	9.36	2.76

Table 3

Sample	87Sr/86Sr	error	143Nd/144Nd	error	206Pb/204Pb	error	207Pb/204Pb	error	208Pb/204Pb	error
Nicaragua-Volcan Blue										
AZUL-2	0.703457	0.000005	0.513004	0.000004	18.948	0.005	15.560	0.004	38.601	0.011
AZUL-5	0.703146	0.000003	0.513024	0.000004	18.985	0.002	15.556	0.002	38.634	0.004
Nicaragua-Cukra Hill										
CH-011507-1	0.703163	0.000003	0.513018	0.000003	18.988	0.001	15.567	0.001	38.684	0.002
CH-011507-7	0.703351	0.000003	0.512986	0.000003	18.948	0.003	15.569	0.003	38.599	0.007
CH-011507-9	0.703223	0.000004	0.513030	0.000003	18.956	0.002	15.567	0.001	38.643	0.003
CH-011507-10										
Costa Rica-Victoria Dikes										
D68	0.704119	0.000003	0.512966	0.000003	19.048	0.000	15.569	0.000	38.738	0.001
CR271	0.703914	0.000003	0.512975	0.000003	19.048	0.001	15.571	0.001	38.746	0.002
AM-081906-1	0.703744	0.000004	0.512954	0.000002	19.122	0.001	15.579	0.001	38.800	0.003
Costa Rica-Guayacan										
P-145	0.703450	0.000002	0.512980	0.000002	19.051	0.003	15.562	0.002	38.684	0.006
Costa Rica-Lomas Azules										
P-163B	0.703690	0.000002	0.512978	0.000002	19.061	0.001	15.559	0.001	38.704	0.003
P-164	0.703591	0.000005	0.512976	0.000004	19.047	0.003	15.565	0.002	38.690	0.006
Costa Rica-Lomas del Colorado-Rio San Juan										
P-130A	0.703623	0.000006	0.512971	0.000004	19.171	0.003	15.587	0.003	38.857	0.007
P-138	0.703623	0.000005	0.512978	0.000003	19.028	0.002	15.571	0.002	38.713	0.005
CR-85	0.703511	0.000003	0.512918	0.000003	19.236	0.001	15.571	0.000	39.004	0.001
P-128	0.703807	0.000002	0.512955	0.000003	19.110	0.002	15.575	0.002	38.793	0.004
P-129	0.703497	0.000005	0.512961	0.000004	19.151	0.003	15.571	0.003	38.842	0.007
Costa Rica-Cerro Tortuguero										
P-132B	0.703674	0.000003	0.512956	0.000004	19.201	0.001	15.591	0.001	38.922	0.003
P-133	0.703673	0.000006	0.512957	0.000004	19.188	0.001	15.573	0.001	38.880	0.002
Costa Rica-Aguas Zarcas (Volcanic Front Alkaline)										
P-152	0.703532	0.000005	0.512925	0.000002	19.288	0.001	15.576	0.001	39.107	0.003
P-153	0.703542	0.000003	0.512940	0.000002	19.184	0.003	15.577	0.002	38.904	0.005
P-154B	0.703600	0.000002	0.512964	0.000002	19.093	0.002	15.564	0.002	38.758	0.005
P-155A	0.703653	0.000002	0.512968	0.000002	19.085	0.002	15.577	0.002	38.796	0.005
Costa Rica-Talamanca Adakites (<5 Ma)										
TC-3	0.703667	0.000003	0.512981	0.000002	19.017	0.001	15.551	0.001	38.674	0.001
TC-5A	0.703509	0.000005	0.512973	0.000002	19.156	0.001	15.573	0.001	38.793	0.001
TC-6A	0.703481	0.000003	0.512979	0.000002	19.114	0.001	15.567	0.000	38.738	0.001
TC-6b	-	-	-	-	19.106	0.001	15.567	0.000	38.745	0.001
TC-7	0.703501	0.000004	0.512980	0.000002	19.106	0.000	15.567	0.000	38.745	0.001
TC-8	0.703347	0.000003	0.512937	0.000002	19.333	0.004	15.578	0.000	38.969	0.001
Panama-Adakites										
M38KH										
M44KH	0.703545	0.000005	0.512989	0.000003	19.213	0.001	15.581	0.001	38.886	0.001
M53KH	0.703403	0.000003	0.512948	0.000003	19.336	0.001	15.584	0.001	39.003	0.002
M55KH	0.703466	0.000005	0.512968	0.000003	19.202	0.001	15.583	0.001	38.880	0.002
M57aKH	0.703568	0.000003	0.512993	0.000002	19.130	0.001	15.568	0.001	38.781	0.003
M64c KH	0.703354	0.000004	0.512965	0.000002	19.308	0.001	15.587	0.001	38.992	0.002
M65a KH	0.703352	0.000003	0.512970	0.000002	19.274	0.001	15.580	0.001	38.936	0.003
Panama-Alkaline										
SO96-1	0.703495	0.000003	0.512999	0.000003	19.084	0.001	15.566	0.001	38.709	0.002
CP97-1	0.703538	0.000003	0.512997	0.000003	19.056	0.001	15.548	0.000	38.659	0.002
M36KH	0.703480	0.000002	0.512999	0.000003	19.081	0.001	15.574	0.001	38.726	0.003
M37KH	0.703485	0.000003	0.513005	0.000002	19.063	0.002	15.560	0.002	38.677	0.005
M99a KH	0.703533	0.000003	0.513006	0.000002	19.080	0.001	15.564	0.001	38.708	0.002
M105 KH	0.703468	0.000003	0.512995	0.000002	19.075	0.001	15.569	0.001	38.716	0.003
M 118aKH	0.703499	0.000003	0.512989	0.000001	19.062	0.002	15.568	0.002	38.708	0.004
M121aKH	0.703516	0.000003	0.512990	0.000005	19.090	0.001	15.572	0.001	38.743	0.002
3-12-4-03	0.703540	0.000005	0.512983	0.000003	19.121	0.001	15.579	0.000	38.787	0.001

Table 4

Run_ID	Sample	Ar36_Over_Ar39	Ar37_Over_Ar39	Ca_Over_K	Ar38_Over_Ar39	Ar40_Over_Ar39	Ar40Rad_Over_Ar39	PctAr40Rad	PctAr40Rad_Er	Age	Age_Er
30580-01A	GE-021306-8	4.979565	1.473424	2.887911	0.9588062	1496.951	25.63496	1.710685	0.3971407	3.299049	0.7921074
30580-01D	GE-021306-8	1.327396	2.804006	5.495852	0.2641233	421.2913	29.32925	6.947883	0.2903825	3.773983	0.1658962
30580-01E	**GE-021306-8**	**1.158836**	**2.253291**	**4.416451**	**0.2358482**	**374.4387**	**32.23526**	**8.59518**	**0.2887804**	**4.147488**	**0.1472425**
30580-01F	**GE-021306-8**	**0.676781**	**1.808934**	**3.545511**	**0.1430859**	**234.4625**	**34.6633**	**14.76519**	**0.3219966**	**4.459502**	**0.1014121**
30580-01G	**GE-021306-8**	**0.3651827**	**1.400873**	**2.74571**	**0.0799629**	**140.3422**	**32.57503**	**23.18814**	**0.6058928**	**4.191154**	**0.1105811**
30580-01H	**GE-021306-8**	**0.2607992**	**1.201938**	**2.355799**	**0.0611997**	**111.0666**	**34.12555**	**30.69923**	**0.3939748**	**4.390403**	**0.0575699**
30580-01I	**GE-021306-8**	**0.1873833**	**1.061749**	**2.081029**	**0.0475333**	**88.26489**	**33.00269**	**37.36257**	**0.4105496**	**4.246112**	**0.0474599**
30580-01J	**GE-021306-8**	**0.1367486**	**0.9570413**	**1.875801**	**0.0368388**	**72.89618**	**32.58527**	**44.67094**	**0.5321322**	**4.19247**	**0.0497046**
30580-01K	**GE-021306-8**	**0.1104643**	**0.9550367**	**1.871872**	**0.0324304**	**64.87037**	**32.32616**	**49.79863**	**0.8126107**	**4.15917**	**0.0665702**
30580-01L	**GE-021306-8**	**0.0942584**	**1.030287**	**2.019362**	**0.0293344**	**59.88142**	**32.13367**	**53.6235**	**1.201874**	**4.134433**	**0.0899277**
30580-01M	**GE-021306-8**	**0.0852537**	**1.078924**	**2.114692**	**0.0287154**	**56.80693**	**31.72487**	**55.80467**	**1.725027**	**4.081894**	**0.1215595**
30580-01N	**GE-021306-8**	**0.0885031**	**1.339422**	**2.625267**	**0.0283525**	**58.24178**	**32.22674**	**55.28065**	**1.919708**	**4.146394**	**0.1389577**
30580-01O	**GE-021306-8**	**0.1010821**	**1.754682**	**3.439177**	**0.0311961**	**61.77282**	**32.08342**	**51.87355**	**1.665278**	**4.127975**	**0.1285626**
30580-01P	**GE-021306-8**	**0.1165501**	**1.828915**	**3.584674**	**0.0343**	**66.46016**	**32.2078**	**48.39931**	**1.333626**	**4.14396**	**0.1114661**
30580-01Q	**GE-021306-8**	**0.1242826**	**1.867505**	**3.660309**	**0.0360876**	**69.27511**	**32.74253**	**47.20221**	**1.775645**	**4.212679**	**0.1545417**
30580-01R	**GE-021306-8**	**0.1134956**	**2.059495**	**4.036609**	**0.0345624**	**65.99122**	**32.66604**	**49.42862**	**3.439973**	**4.202849**	**0.2836226**

Run_ID	Sample	Ar36_Over_Ar39	Ar37_Over_Ar39	Ca_Over_K	Ar38_Over_Ar39	Ar40_Over_Ar39	Ar40Rad_Over_Ar39	PctAr40Rad	PctAr40Rad_Er	Age	Age_Er
30581-02D	BO-062206-2	0.6060112	3.911429	7.666401	0.1207356	193.5343	14.81223	7.632286	5.938486	1.906971	1.474835
30581-02E	BO-062206-2	0.3540316	5.110022	10.01564	0.0823276	122.517	18.37797	14.94592	5.023613	2.365735	0.7906976
30581-02F	BO-062206-2	0.2207339	3.399415	6.662853	0.0535483	89.84728	24.95326	27.70606	4.215581	3.211398	0.4867617
30581-02G	BO-062206-2	0.1091672	1.735695	3.401963	0.0337055	63.71771	31.63678	49.59075	4.074284	4.070574	0.3341164
30581-02H	BO-062206-2	0.0833768	1.908851	3.741348	0.0291303	54.01157	29.56676	54.66794	2.607192	3.804512	0.1811194
30581-02I	**BO-062206-2**	**0.0722439**	**2.059313**	**4.036253**	**0.0279549**	**51.90388**	**30.76597**	**59.1889**	**2.741814**	**3.958652**	**0.1827927**
30581-02J	**BO-062206-2**	**0.060128**	**1.722401**	**3.375907**	**0.0244853**	**50.89574**	**33.30657**	**65.36153**	**2.756371**	**4.285162**	**0.1802178**
30581-02K	**BO-062206-2**	**0.0592673**	**1.646902**	**3.227927**	**0.026383**	**53.50064**	**36.16155**	**67.51262**	**2.758276**	**4.652007**	**0.1899331**
30581-02L	**BO-062206-2**	**0.0526066**	**1.784105**	**3.496846**	**0.0253464**	**51.73546**	**36.37946**	**70.23**	**2.770729**	**4.680004**	**0.1844311**
30581-02M	**BO-062206-2**	**0.0425555**	**2.21684**	**4.345006**	**0.0210112**	**48.08734**	**35.74612**	**74.21974**	**2.645455**	**4.598631**	**0.1633229**
30581-02N	**BO-062206-2**	**0.0473244**	**3.530935**	**6.920632**	**0.0233362**	**48.77199**	**35.15929**	**71.90915**	**2.938692**	**4.523232**	**0.1842363**
30581-02O	**BO-062206-2**	**0.0491257**	**6.273371**	**12.29581**	**0.0226234**	**48.43156**	**34.57282**	**71.06753**	**3.221298**	**4.447876**	**0.2007215**
30581-02P	**BO-062206-2**	**0.0755383**	**18.78957**	**36.82755**	**0.0271562**	**55.0867**	**34.73895**	**62.22061**	**5.085707**	**4.469222**	**0.3638291**
30581-02Q	**BO-062206-2**	**0.0913838**	**32.86135**	**64.40825**	**0.0319888**	**56.83467**	**33.24866**	**57.13452**	**16.86352**	**4.277721**	**1.257597**
30581-02R	**BO-062206-2**	**0.1090335**	**34.7115**	**68.03455**	**0.0314033**	**61.69739**	**33.08379**	**52.29985**	**14.25594**	**4.256535**	**1.155124**

Run_ID	Sample	Ar36_Over_Ar39	Ar37_Over_Ar39	Ca_Over_K	Ar38_Over_Ar39	Ar40_Over_Ar39	Ar40Rad_Over_Ar39	PctAr40Rad	PctAr40Rad_Er	Age	Age_Er
30583-01G	BO-062306-8	3.518525	2.414218	4.731868	0.6824213	1059.467	19.97136	1.881805	1.05849	2.570701	1.447933
30583-01H	BO-062306-8	2.369056	2.362769	4.631027	0.4642537	720.564	20.73284	2.872476	0.8290183	2.668645	0.7728264
30583-01I	BO-062306-8	1.739884	2.239378	4.389182	0.34864	534.6669	20.74466	3.87375	0.7120524	2.670166	0.4938237
30583-01J	BO-062306-8	1.461319	1.813508	3.554476	0.289857	453.6294	21.98349	4.839892	0.6152961	2.829497	0.363527
30583-01Q	**BO-062306-8**	**0.2848631**	**1.025636**	**2.010246**	**0.0665194**	**117.3129**	**33.24194**	**28.31564**	**0.6612145**	**4.276858**	**0.1008615**
30583-01R	**BO-062306-8**	**0.1648355**	**1.50283**	**2.945546**	**0.043177**	**82.46045**	**33.9079**	**41.07662**	**1.1901**	**4.362436**	**0.1266201**
30583-01S	**BO-062306-8**	**0.1477549**	**2.993308**	**5.866883**	**0.0410533**	**76.88027**	**33.5301**	**43.52098**	**1.42591**	**4.313888**	**0.1414215**
30583-01T	**BO-062306-8**	**0.1216544**	**5.488091**	**10.75666**	**0.0357002**	**70.36884**	**34.99706**	**49.54017**	**2.522349**	**4.502387**	**0.2289829**
30583-01U	**BO-062306-8**	**0.0857466**	**6.507097**	**12.75391**	**0.0289961**	**60.11495**	**35.46335**	**58.72032**	**6.982353**	**4.5623**	**0.5413432**
30583-01V	**BO-062306-8**	**0.1091917**	**7.331413**	**14.36957**	**0.0309947**	**61.48823**	**29.96669**	**48.48217**	**12.27914**	**3.85592**	**0.9725879**

Table 4 Continued

Run_ID	Sample	Ar36_Over_Ar39	Ar37_Over_Ar39	Ca_Over_K	Ar38_Over_Ar39	Ar40_Over_Ar39	Ar40Rad_Over_Ar39	PctAr40Rad	PctAr40Rad_Er	Age	Age_Er
30593-01C	CO-070206-2	0.0314459	4.598944	9.01393	0.0775578	38.61758	29.79903	76.9135	14.30477	3.812911	0.705
30593-01D	CO-070206-2	0.0203263	3.038656	5.955766	0.0569189	31.93477	26.2336	81.97176	6.727351	3.357123	0.2737926
30593-01E	CO-070206-2	0.0181481	2.347878	4.60184	0.047668	29.9297	24.80032	82.72549	4.037069	3.173866	0.1540618
30593-01F	CO-070206-2	0.0171797	1.871087	3.66733	0.0358913	28.75594	23.8633	82.87723	3.75388	3.054051	0.137491
30593-01G	CO-070206-2	0.0224941	1.700384	3.332753	0.027866	30.40968	23.92903	78.59552	5.579952	3.062456	0.216037
30593-01H	CO-070206-2	0.0360854	2.35194	4.609803	0.0247213	33.27922	22.84326	68.52787	6.73527	2.923611	0.285521
30593-01I	CO-070206-2	0.0620676	1.263386	2.476236	0.0252542	36.27834	18.05463	49.72322	9.130489	2.311127	0.4216615
30593-01J	CO-070206-2	0.0410949	3.085469	6.04752	0.0228988	37.07951	25.23902	67.91926	15.68998	3.22996	0.7415463
30593-01K	CO-070206-2	0.0521483	4.58792	8.992323	0.0212724	37.76912	22.80166	60.17534	19.13011	2.918291	0.9219258
30593-01L	CO-070206-2	0.0767647	5.094354	9.984934	0.0229292	39.10726	16.89282	43.04042	20.94758	2.162495	1.045526
30593-01M	CO-070206-2	0.0558583	6.387376	12.51926	0.0229723	40.46676	24.58506	60.47884	25.05133	3.146342	1.295362
30593-01N	CO-070206-2	0.0750795	8.671398	16.99594	0.0186885	38.77657	17.39316	44.57908	29.22791	2.226507	1.450106
30593-01O	CO-070206-2	0.0779387	12.30708	24.12187	0.025797	45.49897	23.66359	51.55475	16.24693	3.028514	0.9490248
30593-01P	CO-070206-2	0.0973252	17.05309	33.42406	0.0262206	44.0949	16.90985	37.88438	13.29778	2.164674	0.7549697
30593-01Q	CO-070206-2	0.0938994	18.91457	37.07256	0.0275733	44.31713	18.33585	40.8184	15.46025	2.347101	0.8834191
30593-01R	CO-070206-2	0.1198023	19.88709	38.97869	0.03335	54.11347	20.60087	37.53194	10.04725	2.636827	0.701795

Run_ID	Sample	Ar36_Over_Ar39	Ar37_Over_Ar39	Ca_Over_K	Ar38_Over_Ar39	Ar40_Over_Ar39	Ar40Rad_Over_Ar39	PctAr40Rad	PctAr40Rad_Er	Age	Age_Er
30597-01B	TO-070106-3	0.0685111	0.9101194	1.783834	0.0411201	49.42708	29.27541	59.19202	10.95272	3.745981	0.6897947
30597-01C	TO-070106-3	0.0361248	0.9896271	1.939669	0.0312764	36.58209	26.00588	71.04043	4.57113	3.328008	0.212969
30597-01D	TO-070106-3	0.0240599	0.9889574	1.938356	0.0253295	31.33513	24.32239	77.56733	2.770786	3.112755	0.1104258
30597-01E	TO-070106-3	0.0215862	0.7591623	1.487958	0.0229852	29.99566	23.69088	78.94022	2.505841	3.032003	0.0953771
30597-01F	TO-070106-3	0.025207	0.6835829	1.339822	0.0224069	31.28757	23.90545	76.37017	3.369147	3.059442	0.1339407
30597-01G	TO-070106-3	0.0286605	1.406568	2.756872	0.0220433	30.43518	22.10103	72.54576	7.489443	2.828691	0.2901498
30597-01H	TO-070106-3	0.0335567	1.254968	2.459737	0.0181977	32.84046	23.04514	70.11191	7.742438	2.949428	0.323627
30597-01I	TO-070106-3	0.0432267	1.619962	3.175125	0.02096	35.73268	23.11541	64.61658	10.11854	2.958414	0.460425
30597-01J	TO-070106-3	0.0420375	1.309967	2.567535	0.0208391	37.80265	25.50903	67.41786	12.12821	3.264483	0.5838782
30597-01K	TO-070106-3	0.048482	2.02955	3.977917	0.0213232	41.20825	27.08335	65.62941	12.78189	3.465762	0.6713635
30597-01L	TO-070106-3	0.0556186	2.622803	5.140695	0.0239106	42.78511	26.60973	62.07894	11.7635	3.405211	0.6417741
30597-01M	TO-070106-3	0.0722292	4.243914	8.318072	0.0282221	45.90003	24.9724	54.24271	11.37713	3.195869	0.6667364
30597-01N	TO-070106-3	0.0939429	7.296213	14.30058	0.0295157	49.90236	22.84651	45.54555	10.29469	2.924026	0.6572702
30597-01O	TO-070106-3	0.1062838	9.700269	19.01253	0.0316107	53.08424	22.61229	42.30375	6.31052	2.894073	0.4294256
30597-01P	TO-070106-3	0.1369114	12.58017	24.65713	0.0308345	59.81006	20.54613	34.04542	5.545926	2.629825	0.4261066
30597-01Q	TO-070106-3	0.1598865	20.80282	40.77352	0.0402565	69.17208	23.9511	34.11359	15.49914	3.065278	1.385627
30597-01R	TO-070106-3	0.2310947	31.32912	61.40507	0.0524702	85.35078	20.02557	22.94022	15.794	2.563243	1.754976

Table 4 Continued

Run_ID	Sample	Ar36_Over_Ar39	Ar37_Over_Ar39	Ca_Over_K	Ar38_Over_Ar39	Ar40_Over_Ar39	Ar40Rad_Over_Ar39	PctAr40Rad	PctAr40Rad_Er	Age	Age_Er
30600-01C	**ES-081606-2**	**1.063517**	**4.016867**	**7.873059**	**0.2177734**	**361.8933**	**48.08417**	**13.24891**	**1.285389**	**6.148587**	**0.6059528**
30600-01D	**ES-081606-2**	**0.5982012**	**2.971777**	**5.824684**	**0.1244398**	**227.7847**	**51.36298**	**22.50133**	**1.021152**	**6.56709**	**0.3044148**
30600-01E	**ES-081606-2**	**0.4170667**	**2.471292**	**4.843733**	**0.0939392**	**174.4199**	**51.46535**	**29.45485**	**0.7951508**	**6.580156**	**0.1823404**
30600-01F	**ES-081606-2**	**0.4247453**	**2.195582**	**4.30334**	**0.0939264**	**176.7968**	**51.54095**	**29.10726**	**0.8589655**	**6.589804**	**0.2004671**
30600-01G	**ES-081606-2**	**0.298457**	**1.604974**	**3.145749**	**0.0698097**	**137.5355**	**49.52642**	**35.96901**	**0.4929762**	**6.332686**	**0.0889972**
30600-01H	**ES-081606-2**	**0.3303368**	**1.420204**	**2.783599**	**0.0755046**	**147.2835**	**49.8329**	**33.80066**	**0.3762094**	**6.371805**	**0.0743504**
30600-01I	**ES-081606-2**	**0.3466762**	**1.266226**	**2.481804**	**0.0791464**	**152.9306**	**50.63461**	**33.07987**	**0.3807016**	**6.47413**	**0.081572**
30600-01J	**ES-081606-2**	**0.3226783**	**1.231584**	**2.413904**	**0.0738761**	**146.302**	**51.09368**	**34.89302**	**0.32959**	**6.532721**	**0.0653629**
30600-01K	**ES-081606-2**	**0.3046508**	**1.208334**	**2.368335**	**0.0706998**	**138.3632**	**48.4771**	**35.00619**	**0.7143304**	**6.198745**	**0.1316992**
30600-01L	**ES-081606-2**	**0.2266144**	**1.050147**	**2.058289**	**0.0553583**	**118.2688**	**51.42643**	**43.45045**	**0.4332608**	**6.575188**	**0.0672384**
30600-01M	**ES-081606-2**	**0.208146**	**1.278389**	**2.505643**	**0.0519535**	**112.9696**	**51.61152**	**45.64494**	**0.5354283**	**6.598809**	**0.0790643**
30600-01N	**ES-081606-2**	**0.1771874**	**1.770575**	**3.470328**	**0.0466323**	**103.523**	**51.37049**	**49.56017**	**0.8316824**	**6.568049**	**0.1097778**
30600-01O	ES-081606-2	0.1409186	2.337893	4.58227	0.0404671	87.1332	45.75518	52.42489	1.059196	5.851258	0.1182102
30600-01P	ES-081606-2	0.1683342	5.692824	11.15793	0.0455562	100.7129	51.6362	51.06352	0.7635826	6.601959	0.0987025
30600-01Q	ES-081606-2	0.168639	6.833594	13.39384	0.0448671	100.2108	51.1753	50.81988	1.296667	6.543138	0.1647672
30600-01R	ES-081606-2	0.1623542	7.209306	14.13024	0.0438103	98.14334	51.00801	51.70694	2.085329	6.521788	0.2574021
										1.29E-13	1.303687

Run_ID	Sample	Ar36_Over_Ar39	Ar37_Over_Ar39	Ca_Over_K	Ar38_Over_Ar39	Ar40_Over_Ar39	Ar40Rad_Over_Ar39	PctAr40Rad	PctAr40Rad_Er	Age	Age_Er
30604-01A	**CH-011507-5**	**0.7205419**	**1.797947**	**3.523977**	**0.1502363**	**220.9073**	**8.141659**	**3.680855**	**2.381501**	**1.04256**	**0.6948**
30604-01B	**CH-011507-5**	**0.1475981**	**3.24892**	**6.367884**	**0.038307**	**50.3216**	**6.982801**	**13.84449**	**2.902565**	**0.8942018**	**0.1890355**
30604-01C	**CH-011507-5**	**0.0415563**	**3.654523**	**7.162865**	**0.0196347**	**17.23125**	**5.258054**	**30.43658**	**3.556468**	**0.6733757**	**0.0779266**
30604-01D	**CH-011507-5**	**0.0221517**	**3.308216**	**6.484104**	**0.0155229**	**12.01228**	**5.745101**	**47.71717**	**3.810165**	**0.735737**	**0.0572852**
30604-01E	**CH-011507-5**	**0.0201226**	**3.087581**	**6.051659**	**0.0149306**	**11.40067**	**5.714362**	**50.01608**	**3.80064**	**0.7318013**	**0.0540781**
30604-01F	**CH-011507-5**	**0.023386**	**3.127327**	**6.12956**	**0.015418**	**12.37173**	**5.724465**	**46.17026**	**4.521133**	**0.7330948**	**0.0699365**
30604-01G	**CH-011507-5**	**0.0316443**	**3.565358**	**6.988101**	**0.0183087**	**14.99734**	**5.947423**	**39.55784**	**3.969023**	**0.7616416**	**0.0759384**
30604-01H	**CH-011507-5**	**0.0468244**	**4.658032**	**9.129743**	**0.0207803**	**19.55735**	**6.11468**	**31.16294**	**4.284287**	**0.7830563**	**0.107628**
30604-01I	**CH-011507-5**	**0.0931832**	**6.886741**	**13.49801**	**0.0310805**	**32.09808**	**5.140611**	**15.93725**	**4.781202**	**0.658338**	**0.1987767**
30604-01J	**CH-011507-5**	**0.1528758**	**15.23443**	**29.85949**	**0.0432589**	**53.16445**	**9.314636**	**17.33087**	**4.469229**	**1.192713**	**0.3106552**
30604-01K	**CH-011507-5**	**0.1927182**	**19.30408**	**37.836**	**0.0460737**	**67.15823**	**11.92442**	**17.5122**	**6.871282**	**1.526747**	**0.6062149**

Table 5

P-145 matrix										
MASS=	7.111 mg									
J =	3.74E-03	±	7.19E-06	(2 Sigma)						
STEP	POWER (W)	40Ar/39Ar	37Ar/39Ar	36Ar/39Ar	Mol 39ArK	Ca/K	% 40ArA	Cum 39ArK	Age [Ma]	2 Sigma
1	1.50E-01	1.49E+03	3.63E+00	5.00E+00	6.54E-17	7.14E+00	99.2	7.72E-04	8.03E+01	1.45E+02
2	2.50E-01	2.82E+02	2.72E+00	9.32E-01	8.08E-16	5.34E+00	97.7	1.03E-02	4.41E+01	3.01E+01
3	4.00E-01	5.88E+01	2.44E+00	1.81E-01	3.26E-15	4.80E+00	90.5	4.88E-02	3.73E+01	2.22E+01
4	5.00E-01	2.07E+01	2.14E+00	5.43E-02	3.75E-15	4.20E+00	76.1	9.31E-02	3.32E+01	2.17E+01
5	6.00E-01	1.12E+01	1.76E+00	3.12E-02	3.80E-15	3.46E+00	80.2	1.38E-01	1.49E+01	1.15E+01
6	7.00E-01	7.05E+00	1.31E+00	1.84E-02	3.87E-15	2.57E+00	74.8	1.84E-01	1.19E+01	6.37E+00
7	**8.00E-01**	**6.15E+00**	**1.10E+00**	**1.69E-02**	**4.42E-15**	**2.15E+00**	**78.9**	**2.36E-01**	**8.75E+00**	**4.94E+00**
8	**9.00E-01**	**4.59E+00**	**9.56E-01**	**1.28E-02**	**4.52E-15**	**1.87E+00**	**79.4**	**2.89E-01**	**6.37E+00**	**2.66E+00**
9	**1.00E+00**	**4.04E+00**	**9.05E-01**	**1.13E-02**	**4.49E-15**	**1.78E+00**	**79.5**	**3.42E-01**	**5.58E+00**	**2.96E+00**
10	**1.10E+00**	**2.66E+00**	**9.67E-01**	**7.63E-03**	**3.73E-15**	**1.90E+00**	**80.1**	**3.86E-01**	**3.57E+00**	**2.77E+00**
11	**1.20E+00**	**2.76E+00**	**1.46E+00**	**7.50E-03**	**5.12E-15**	**2.87E+00**	**73.5**	**4.46E-01**	**4.93E+00**	**1.09E+00**
12	**1.35E+00**	**2.74E+00**	**2.18E+00**	**8.43E-03**	**8.02E-15**	**4.28E+00**	**80.5**	**5.41E-01**	**3.61E+00**	**1.04E+00**
13	**1.50E+00**	**2.85E+00**	**3.22E+00**	**8.81E-03**	**8.26E-15**	**6.32E+00**	**76.8**	**6.38E-01**	**4.45E+00**	**7.11E-01**
14	**2.00E+00**	**3.09E+00**	**6.67E+00**	**1.13E-02**	**1.43E-14**	**1.32E+01**	**79.7**	**8.07E-01**	**4.26E+00**	**6.81E-01**
15	**3.00E+00**	**4.60E+00**	**1.56E+01**	**2.03E-02**	**8.71E-15**	**3.11E+01**	**86.0**	**9.10E-01**	**4.40E+00**	**1.37E+00**
16	**5.00E+00**	**8.36E+00**	**1.93E+01**	**3.36E-02**	**4.76E-15**	**3.85E+01**	**88.8**	**9.66E-01**	**6.44E+00**	**1.77E+00**
17	1.00E+01	1.76E+01	3.54E+01	7.20E-02	2.68E-15	7.19E+01	94.8	**9.98E-01**	**6.40E+00**	**4.02E+00**
18	2.00E+01	8.17E+01	4.35E+01	2.79E-01	2.02E-16	8.90E+01	94.1	1.00E+00	3.36E+01	3.93E+01
Total Gas Age =	8.74E+00	±	3.71E-01	Ma (2Sigma)						

Plateau Age = 4.51 ± 0.37 Ma
(2s, including J-error of .192%)
MSWD = 1.6, probability = 0.11
81.4% of the 39Ar, steps 7 through 17

P-163B matrix										
MASS=	6.319 mg									
J =	3.74E-03	±	7.19E-06	(2 Sigma)						
STEP	POWER	40Ar/39Ar	37Ar/39Ar	36Ar/39Ar	Mol 39ArK	Ca/K	% 40ArA	Cum 39ArK	Age [Ma]	2 Sigma
1	1.50E-01	2.39E+03	1.91E+00	7.99E+00	2.38E-16	3.74E+00	98.9	1.54E-03	1.73E+02	9.30E+01
2	2.50E-01	2.10E+02	1.93E+00	6.60E-01	1.44E-15	3.79E+00	92.9	1.09E-02	9.81E+01	3.87E+01
3	4.00E-01	1.95E+01	1.65E+00	4.66E-02	3.95E-15	3.24E+00	69.6	3.66E-02	3.96E+01	2.49E+01
4	5.00E-01	7.55E+00	1.27E+00	1.78E-02	4.15E-15	2.50E+00	67.4	6.35E-02	1.66E+01	1.01E+01
5	6.00E-01	4.27E+00	9.50E-01	1.17E-02	5.74E-15	1.86E+00	78.3	1.01E-01	6.25E+00	3.91E+00
6	7.00E-01	4.11E+00	8.14E-01	1.22E-02	7.14E-15	1.60E+00	84.9	**1.47E-01**	**4.18E+00**	**2.14E+00**
7	8.00E-01	2.30E+00	7.03E-01	6.19E-03	7.58E-15	1.38E+00	75.7	**1.96E-01**	**3.76E+00**	**8.60E-01**
8	9.00E-01	1.98E+00	7.43E-01	5.14E-03	8.36E-15	1.46E+00	72.0	**2.51E-01**	**3.72E+00**	**7.89E-01**
9	1.00E+00	2.15E+00	8.58E-01	5.83E-03	9.94E-15	1.68E+00	75.2	**3.15E-01**	**3.59E+00**	**7.30E-01**
10	1.10E+00	1.91E+00	1.13E+00	5.24E-03	1.00E-14	2.22E+00	73.5	**3.81E-01**	**3.41E+00**	**7.63E-01**
11	1.20E+00	2.32E+00	1.46E+00	6.83E-03	1.19E-14	2.88E+00	78.9	**4.58E-01**	**3.29E+00**	**6.40E-01**
12	1.35E+00	2.02E+00	1.96E+00	5.94E-03	1.55E-14	3.84E+00	74.5	**5.59E-01**	**3.47E+00**	**6.45E-01**
13	1.50E+00	1.91E+00	2.43E+00	5.98E-03	1.45E-14	4.77E+00	76.0	**6.53E-01**	**3.09E+00**	**7.32E-01**
14	2.00E+00	1.89E+00	4.11E+00	6.81E-03	1.81E-14	8.09E+00	78.0	**7.71E-01**	**2.81E+00**	**4.28E-01**
15	3.00E+00	2.14E+00	4.80E+00	7.87E-03	1.32E-14	9.45E+00	79.5	**8.57E-01**	**2.96E+00**	**8.83E-01**
16	5.00E+00	2.40E+00	5.22E+00	9.01E-03	1.11E-14	1.03E+01	82.6	**9.29E-01**	**2.82E+00**	**9.06E-01**
17	1.00E+01	2.50E+00	6.58E+00	9.58E-03	8.67E-15	1.30E+01	79.0	**9.85E-01**	**3.55E+00**	**7.63E-01**
18	2.00E+01	2.68E+00	7.03E+00	1.12E-02	2.21E-15	1.39E+01	89.6	**1.00E+00**	**1.89E+00**	**2.93E+00**
19	2.50E+01	8.53E+00	8.38E+00	3.20E-02	3.77E-17	1.66E+01	98.0	**1.00E+00**	**1.17E+00**	**1.70E+02**
20	2.75E+01	1.70E+01	9.44E+00	9.26E-02	1.69E-17	1.87E+01	154.0	1.00E+00	-6.36E+01	3.67E+02
Total Gas Age =	5.82E+00	±	2.07E-01	Ma (2Sigma)						

Plateau Age = 3.25 ± 0.21 Ma
(2s, including J-error of .192%)
MSWD = 0.94, probability = 0.51
89.9% of the 39Ar, steps 6 through 19

Table 5 Continued

P-128 matrix										
MASS=	5.473 mg									
J =	3.75E-03	±	4.72E-06	(2 Sigma)				0.126 Percent		
STEP	POWER	40Ar/39Ar	37Ar/39Ar	36Ar/39Ar	Mol 39ArK	Ca/K	% 40ArA	Cum 39ArK	Age [Ma]	2 Sigma
1	1.50E-01	1.32E+03	1.83E+00	4.44E+00	5.23E-17	3.60E+00	99.6	**3.77E-04**	**3.63E+01**	**1.95E+02**
2	2.50E-01	4.27E+02	2.10E+00	1.43E+00	3.24E-16	4.12E+00	98.9	**2.72E-03**	**3.04E+01**	**4.56E+01**
3	4.00E-01	6.23E+01	1.59E+00	2.05E-01	1.21E-15	3.12E+00	97.0	**1.14E-02**	**1.25E+01**	**1.44E+01**
4	5.00E-01	1.32E+01	9.75E-01	4.29E-02	1.73E-15	1.91E+00	95.1	**2.39E-02**	**4.33E+00**	**7.66E+00**
5	6.00E-01	5.69E+00	7.08E-01	1.74E-02	2.81E-15	1.39E+00	89.0	**4.42E-02**	**4.23E+00**	**3.03E+00**
6	7.00E-01	3.99E+00	5.67E-01	1.24E-02	4.14E-15	1.11E+00	90.2	**7.40E-02**	**2.63E+00**	**1.66E+00**
7	8.00E-01	4.16E+00	5.04E-01	1.30E-02	4.87E-15	9.89E-01	91.2	**1.09E-01**	**2.48E+00**	**1.81E+00**
8	9.00E-01	3.84E+00	4.91E-01	1.11E-02	5.58E-15	9.62E-01	83.5	**1.49E-01**	**4.28E+00**	**1.71E+00**
9	1.00E+00	3.22E+00	5.15E-01	9.55E-03	6.04E-15	1.01E+00	85.5	**1.93E-01**	**3.15E+00**	**1.21E+00**
10	1.10E+00	2.40E+00	5.55E-01	7.56E-03	5.98E-15	1.09E+00	90.0	**2.36E-01**	**1.62E+00**	**1.44E+00**
11	1.20E+00	2.16E+00	7.14E-01	6.87E-03	7.25E-15	1.40E+00	90.0	**2.88E-01**	**1.46E+00**	**1.25E+00**
12	1.35E+00	1.92E+00	1.01E+00	6.05E-03	1.18E-14	1.97E+00	86.2	**3.73E-01**	**1.80E+00**	**8.85E-01**
13	1.50E+00	1.75E+00	1.50E+00	5.90E-03	1.44E-14	2.94E+00	88.4	**4.77E-01**	**1.37E+00**	**6.75E-01**
14	2.00E+00	2.08E+00	3.29E+00	7.46E-03	2.32E-14	6.46E+00	85.5	**6.44E-01**	**2.05E+00**	**4.52E-01**
15	3.00E+00	2.26E+00	4.16E+00	8.52E-03	1.53E-14	8.19E+00	87.4	**7.55E-01**	**1.93E+00**	**4.80E-01**
16	5.00E+00	2.96E+00	4.21E+00	1.09E-02	1.95E-14	8.29E+00	90.0	**8.96E-01**	**2.00E+00**	**4.67E-01**
17	1.00E+01	2.47E+00	3.90E+00	9.05E-03	1.33E-14	7.68E+00	87.6	**9.92E-01**	**2.09E+00**	**7.61E-01**
18	2.00E+01	2.92E+00	3.39E+00	8.54E-03	1.13E-15	6.67E+00	71.3	**1.00E+00**	**5.69E+00**	**7.54E+00**
19	2.50E+01	1.47E+00	1.88E+01	-3.13E+00	1.04E-18	3.75E+01	-63457.5	**1.00E+00**	**2.74E+03**	**9.74E+03**
20	2.75E+01	-2.02E+02	3.00E+02	-7.63E+00	1.74E-19	8.39E+02	1133.5	**1.00E+00**	**4.51E+03**	**6.47E+04**
Total Gas Age =	2.36E+00	±	2.13E-01	Ma (2Sigma)						
Plateau Age = 2.01±0.21 Ma										
(2s, including J-error of .126%)										
MSWD = 1.3, probability = 0.19										
100% of the 39Ar, steps 1 through 20										

P-129 matrix										
MASS=	4.910 mg									
J =	3.74E-03	±	7.19E-06	(2 Sigma)				0.192 Percent		
STEP	POWER	40Ar/39Ar	37Ar/39Ar	36Ar/39Ar	Mol 39ArK	Ca/K	% 40ArA	Cum 39ArK	Age [Ma]	2 Sigma
1	1.50E-01	1.58E+04	4.43E+00	5.28E+01	7.67E-17	8.73E+00	98.7	9.69E-04	1.05E+03	3.87E+02
2	2.50E-01	2.91E+03	2.80E+00	9.66E+00	4.10E-16	5.49E+00	98.2	6.15E-03	3.25E+02	9.83E+01
3	4.00E-01	1.81E+02	2.01E+00	5.83E-01	1.92E-15	3.95E+00	95.2	3.04E-02	5.71E+01	2.63E+01
4	5.00E-01	3.50E+01	1.51E+00	1.08E-01	1.76E-15	2.96E+00	90.5	5.27E-02	2.24E+01	1.34E+01
5	6.00E-01	4.36E+01	1.14E+00	1.43E-01	2.04E-15	2.24E+00	96.6	**7.85E-02**	**1.01E+01**	**8.18E+00**
6	**7.00E-01**	**1.16E+02**	**8.12E-01**	**3.87E-01**	**2.44E-15**	**1.59E+00**	**98.9**	**1.09E-01**	**8.92E+00**	**8.00E+00**
7	**8.00E-01**	**4.83E+01**	**7.28E-01**	**1.58E-01**	**2.86E-15**	**1.43E+00**	**96.7**	**1.46E-01**	**1.08E+01**	**5.52E+00**
8	**9.00E-01**	**4.40E+01**	**6.32E-01**	**1.45E-01**	**3.56E-15**	**1.24E+00**	**97.2**	**1.91E-01**	**8.18E+00**	**5.75E+00**
9	**1.00E+00**	**2.59E+01**	**7.41E-01**	**8.49E-02**	**4.63E-15**	**1.45E+00**	**96.5**	**2.49E-01**	**6.10E+00**	**2.92E+00**
10	**1.10E+00**	**2.15E+01**	**8.93E-01**	**6.88E-02**	**4.87E-15**	**1.75E+00**	**94.2**	**3.11E-01**	**8.35E+00**	**2.42E+00**
11	**1.20E+00**	**1.86E+01**	**1.26E+00**	**6.08E-02**	**5.83E-15**	**2.48E+00**	**96.0**	**3.84E-01**	**5.00E+00**	**2.60E+00**
12	**1.35E+00**	**1.80E+01**	**2.21E+00**	**5.85E-02**	**8.12E-15**	**4.34E+00**	**94.5**	**4.87E-01**	**6.63E+00**	**2.19E+00**
13	**1.50E+00**	**1.36E+01**	**3.59E+00**	**4.52E-02**	**6.85E-15**	**7.06E+00**	**94.6**	**5.73E-01**	**4.97E+00**	**1.79E+00**
14	**2.00E+00**	**1.23E+01**	**6.24E+00**	**4.19E-02**	**8.53E-15**	**1.23E+01**	**94.0**	**6.81E-01**	**5.04E+00**	**1.30E+00**
15	**3.00E+00**	**6.78E+00**	**7.58E+00**	**2.37E-02**	**6.09E-15**	**1.50E+01**	**88.7**	**7.58E-01**	**5.19E+00**	**1.60E+00**
16	5.00E+00	4.94E+00	6.89E+00	1.82E-02	9.19E-15	1.36E+01	90.5	8.74E-01	3.17E+00	9.60E-01
17	1.00E+01	2.09E+00	6.34E+00	8.91E-03	9.33E-15	1.25E+01	86.5	9.92E-01	1.91E+00	9.73E-01
18	2.00E+01	1.95E+00	8.01E+00	4.38E-03	6.13E-16	1.58E+01	12.7	1.00E+00	1.15E+01	1.22E+01
Total Gas Age =	9.85E+00	±	4.89E-01	Ma (2Sigma)						
au Age = 5.76±0.70 Ma										
cluding J-error of .192%)										
= 1.4, probability = 0.18										
the 39Ar, steps 5 through 15										

Table 5 Continued

TC-3 matrix (mxs)										
MASS=	1.733 mg									
J =	3.46E-03	±	7.57E-06	(2 Sigma)				0.219 Percent		
STEP	POWER	40Ar/39Ar	37Ar/39Ar	36Ar/39Ar	Mol 39ArK	Ca/K	% 40ArA	Cum 39ArK	Age [Ma]	2 Sigma
1	1.25E-01	8.82E+01	1.52E+00	2.76E-01	8.36E-16	2.98E+00	92.2	7.44E-03	4.26E+01	1.83E+01
2	2.00E-01	4.46E+01	1.91E+00	1.22E-01	1.10E-15	3.74E+00	80.3	1.72E-02	5.41E+01	1.93E+01
3	3.00E-01	2.04E+01	2.48E+00	6.17E-02	1.60E-15	4.87E+00	87.7	3.15E-02	1.56E+01	7.10E+00
4	4.00E-01	1.27E+01	2.37E+00	4.16E-02	2.62E-15	4.65E+00	94.3	5.48E-02	4.57E+00	2.74E+00
5	5.00E-01	6.82E+00	1.94E+00	2.11E-02	4.25E-15	3.80E+00	87.7	9.26E-02	5.25E+00	1.21E+00
6	**6.00E-01**	**2.26E+00**	**1.42E+00**	**6.37E-03**	**6.14E-15**	**2.79E+00**	**75.3**	**1.47E-01**	**3.47E+00**	**1.07E+00**
7	**7.00E-01**	**1.70E+00**	**1.11E+00**	**3.90E-03**	**7.62E-15**	**2.17E+00**	**59.7**	**2.15E-01**	**4.26E+00**	**7.82E-01**
8	**8.00E-01**	**1.45E+00**	**9.14E-01**	**3.12E-03**	**8.38E-15**	**1.79E+00**	**55.3**	**2.90E-01**	**4.04E+00**	**7.73E-01**
9	**9.00E-01**	**1.32E+00**	**8.61E-01**	**2.74E-03**	**8.20E-15**	**1.69E+00**	**53.0**	**3.63E-01**	**3.85E+00**	**8.51E-01**
10	**1.00E+00**	**1.34E+00**	**8.88E-01**	**2.49E-03**	**8.01E-15**	**1.74E+00**	**46.5**	**4.34E-01**	**4.44E+00**	**7.56E-01**
11	**1.10E+00**	**1.47E+00**	**9.06E-01**	**3.01E-03**	**7.27E-15**	**1.78E+00**	**52.8**	**4.99E-01**	**4.30E+00**	**5.90E-01**
12	**1.20E+00**	**1.43E+00**	**1.25E+00**	**3.38E-03**	**6.03E-15**	**2.46E+00**	**58.5**	**5.52E-01**	**3.70E+00**	**8.27E-01**
13	**1.35E+00**	**1.42E+00**	**1.46E+00**	**3.03E-03**	**5.94E-15**	**2.86E+00**	**49.7**	**6.05E-01**	**4.46E+00**	**1.16E+00**
14	**1.50E+00**	**1.48E+00**	**1.92E+00**	**3.37E-03**	**4.77E-15**	**3.78E+00**	**50.6**	**6.48E-01**	**4.54E+00**	**1.11E+00**
15	**2.00E+00**	**1.62E+00**	**2.81E+00**	**4.35E-03**	**6.26E-15**	**5.52E+00**	**57.1**	**7.03E-01**	**4.33E+00**	**7.24E-01**
16	**3.00E+00**	**2.10E+00**	**2.92E+00**	**6.35E-03**	**1.16E-14**	**5.73E+00**	**71.6**	**8.06E-01**	**3.72E+00**	**5.03E-01**
17	**5.00E+00**	**2.02E+00**	**2.76E+00**	**6.08E-03**	**1.47E-14**	**5.42E+00**	**71.5**	**9.38E-01**	**3.59E+00**	**5.00E-01**
18	**1.00E+01**	**1.81E+00**	**2.93E+00**	**5.36E-03**	**6.59E-15**	**5.76E+00**	**66.5**	**9.96E-01**	**3.79E+00**	**8.68E-01**
19	**1.50E+01**	**2.63E+00**	**2.70E+00**	**5.29E-03**	**3.33E-16**	**5.30E+00**	**46.2**	**9.99E-01**	**8.80E+00**	**1.56E+01**
20	**2.00E+01**	**3.68E+00**	**4.10E+00**	**3.81E-02**	**8.33E-17**	**8.07E+00**	**291.8**	**1.00E+00**	**-4.47E+01**	**6.55E+01**
Total Gas Age =	4.97E+00	±	1.99E-01	Ma (2Sigma)						
Plateau Age = 3.98±0.20 Ma										
(2s, including J-error of .219%)										
MSWD = 0.97, probability = 0.48										
90.7% of the 39Ar, steps 6 through 20										

TC-3 matrix (mxs)										
MASS=	1.733 mg									
J =	3.46E-03	±	7.57E-06	(2 Sigma)				0.219 Percent		
STEP	POWER	40Ar/39Ar	37Ar/39Ar	36Ar/39Ar	Mol 39ArK	Ca/K	% 40ArA	Cum 39ArK	Age [Ma]	2 Sigma
1	1.25E-01	8.82E+01	1.52E+00	2.76E-01	8.36E-16	2.98E+00	92.2	7.44E-03	4.26E+01	1.83E+01
2	2.00E-01	4.46E+01	1.91E+00	1.22E-01	1.10E-15	3.74E+00	80.3	1.72E-02	5.41E+01	1.93E+01
3	3.00E-01	2.04E+01	2.48E+00	6.17E-02	1.60E-15	4.87E+00	87.7	3.15E-02	1.56E+01	7.10E+00
4	4.00E-01	1.27E+01	2.37E+00	4.16E-02	2.62E-15	4.65E+00	94.3	5.48E-02	4.57E+00	2.74E+00
5	5.00E-01	6.82E+00	1.94E+00	2.11E-02	4.25E-15	3.80E+00	87.7	9.26E-02	5.25E+00	1.21E+00
6	**6.00E-01**	**2.26E+00**	**1.42E+00**	**6.37E-03**	**6.14E-15**	**2.79E+00**	**75.3**	**1.47E-01**	**3.47E+00**	**1.07E+00**
7	**7.00E-01**	**1.70E+00**	**1.11E+00**	**3.90E-03**	**7.62E-15**	**2.17E+00**	**59.7**	**2.15E-01**	**4.26E+00**	**7.82E-01**
8	**8.00E-01**	**1.45E+00**	**9.14E-01**	**3.12E-03**	**8.38E-15**	**1.79E+00**	**55.3**	**2.90E-01**	**4.04E+00**	**7.73E-01**
9	**9.00E-01**	**1.32E+00**	**8.61E-01**	**2.74E-03**	**8.20E-15**	**1.69E+00**	**53.0**	**3.63E-01**	**3.85E+00**	**8.51E-01**
10	**1.00E+00**	**1.34E+00**	**8.88E-01**	**2.49E-03**	**8.01E-15**	**1.74E+00**	**46.5**	**4.34E-01**	**4.44E+00**	**7.56E-01**
11	**1.10E+00**	**1.47E+00**	**9.06E-01**	**3.01E-03**	**7.27E-15**	**1.78E+00**	**52.8**	**4.99E-01**	**4.30E+00**	**5.90E-01**
12	**1.20E+00**	**1.43E+00**	**1.25E+00**	**3.38E-03**	**6.03E-15**	**2.46E+00**	**58.5**	**5.52E-01**	**3.70E+00**	**8.27E-01**
13	**1.35E+00**	**1.42E+00**	**1.46E+00**	**3.03E-03**	**5.94E-15**	**2.86E+00**	**49.7**	**6.05E-01**	**4.46E+00**	**1.16E+00**
14	**1.50E+00**	**1.48E+00**	**1.92E+00**	**3.37E-03**	**4.77E-15**	**3.78E+00**	**50.6**	**6.48E-01**	**4.54E+00**	**1.11E+00**
15	**2.00E+00**	**1.62E+00**	**2.81E+00**	**4.35E-03**	**6.26E-15**	**5.52E+00**	**57.1**	**7.03E-01**	**4.33E+00**	**7.24E-01**
16	**3.00E+00**	**2.10E+00**	**2.92E+00**	**6.35E-03**	**1.16E-14**	**5.73E+00**	**71.6**	**8.06E-01**	**3.72E+00**	**5.03E-01**
17	**5.00E+00**	**2.02E+00**	**2.76E+00**	**6.08E-03**	**1.47E-14**	**5.42E+00**	**71.5**	**9.38E-01**	**3.59E+00**	**5.00E-01**
18	**1.00E+01**	**1.81E+00**	**2.93E+00**	**5.36E-03**	**6.59E-15**	**5.76E+00**	**66.5**	**9.96E-01**	**3.79E+00**	**8.68E-01**
19	**1.50E+01**	**2.63E+00**	**2.70E+00**	**5.29E-03**	**3.33E-16**	**5.30E+00**	**46.2**	**9.99E-01**	**8.80E+00**	**1.56E+01**
20	**2.00E+01**	**3.68E+00**	**4.10E+00**	**3.81E-02**	**8.33E-17**	**8.07E+00**	**291.8**	**1.00E+00**	**-4.47E+01**	**6.55E+01**
Total Gas Age =	4.97E+00	±	1.99E-01	Ma (2Sigma)						
Plateau Age = 3.98±0.20 Ma										
(2s, including J-error of .219%)										
MSWD = 0.97, probability = 0.48										
90.7% of the 39Ar, steps 6 through 20										

Table 5 Continued

TC-5 matrix (mxs)										
MASS=	1.418 mg									
J =	3.46E-03	±	7.57E-06	(2 Sigma)				0.219 Percent		
STEP	POWER	40Ar/39Ar	37Ar/39Ar	36Ar/39Ar	Mol 39ArK	Ca/K	% 40ArA	Cum 39ArK	Age [Ma]	2 Sigma
1	1.25E-01	1.32E+03	2.81E+00	4.40E+00	1.15E-16	5.53E+00	98.5	1.67E-03	1.16E+02	1.15E+02
2	2.00E-01	3.26E+02	1.49E+00	1.06E+00	5.25E-16	2.92E+00	96.1	9.31E-03	7.78E+01	2.18E+01
3	3.00E-01	1.23E+02	1.24E+00	4.04E-01	7.67E-16	2.44E+00	96.8	2.05E-02	2.43E+01	1.57E+01
4	4.00E-01	9.25E+01	8.20E-01	3.06E-01	1.20E-15	1.61E+00	97.5	3.79E-02	1.42E+01	1.01E+01
5	5.00E-01	1.79E+02	7.01E-01	5.98E-01	2.39E-15	1.38E+00	98.7	7.27E-02	1.45E+01	6.06E+00
6	6.00E-01	1.43E+02	6.35E-01	4.75E-01	3.56E-15	1.25E+00	98.1	1.25E-01	1.65E+01	3.43E+00
7	7.00E-01	4.66E+01	5.33E-01	1.54E-01	3.95E-15	1.05E+00	97.8	1.82E-01	6.49E+00	1.24E+00
8	**8.00E-01**	**3.48E+01**	**5.72E-01**	**1.15E-01**	**3.43E-15**	**1.12E+00**	**97.7**	**2.32E-01**	**4.97E+00**	**3.05E+00**
9	**9.00E-01**	**6.44E+01**	**1.15E+00**	**2.16E-01**	**3.50E-15**	**2.26E+00**	**99.1**	**2.83E-01**	**3.76E+00**	**4.03E+00**
10	**1.00E+00**	**5.63E+01**	**1.51E+00**	**1.89E-01**	**3.77E-15**	**2.96E+00**	**98.9**	**3.38E-01**	**3.73E+00**	**2.48E+00**
11	**1.10E+00**	**4.87E+01**	**1.85E+00**	**1.63E-01**	**3.45E-15**	**3.63E+00**	**98.3**	**3.88E-01**	**5.18E+00**	**2.44E+00**
12	**1.20E+00**	**5.79E+01**	**1.91E+00**	**1.94E-01**	**5.62E-15**	**3.76E+00**	**98.6**	**4.70E-01**	**5.18E+00**	**1.62E+00**
13	**1.35E+00**	**4.86E+01**	**2.78E+00**	**1.62E-01**	**6.38E-15**	**5.47E+00**	**97.9**	**5.63E-01**	**6.50E+00**	**2.71E+00**
14	**1.50E+00**	**3.93E+01**	**3.27E+00**	**1.32E-01**	**4.15E-15**	**6.43E+00**	**98.3**	**6.23E-01**	**4.29E+00**	**2.90E+00**
15	**2.00E+00**	**3.87E+01**	**6.47E+00**	**1.30E-01**	**4.14E-15**	**1.27E+01**	**97.1**	**6.83E-01**	**7.02E+00**	**3.35E+00**
16	**3.00E+00**	**1.83E+01**	**4.63E+00**	**6.19E-02**	**8.93E-15**	**9.11E+00**	**96.6**	**8.13E-01**	**3.92E+00**	**1.64E+00**
17	**5.00E+00**	**1.46E+01**	**3.29E+00**	**4.88E-02**	**1.04E-14**	**6.47E+00**	**96.1**	**9.65E-01**	**3.60E+00**	**1.19E+00**
18	**8.00E+00**	**1.28E+01**	**2.72E+00**	**4.09E-02**	**2.38E-15**	**5.34E+00**	**92.0**	**1.00E+00**	**6.37E+00**	**2.99E+00**
19	**1.00E+01**	**1.72E+01**	**4.49E+00**	**7.86E-03**	**3.23E-17**	**8.83E+00**	**10.1**	**1.00E+00**	**9.46E+01**	**1.16E+02**
20	**1.50E+01**	**5.24E+02**	**-4.97E+00**	**-6.93E-01**	**9.47E-19**	**-9.70E+00**	**-39.0**	**1.00E+00**	**2.26E+03**	**5.92E+03**
Total Gas Age =	7.00E+00	±	5.59E-01	Ma (2Sigma)						

Plateau Age = 4.54±0.64 Ma
(2s, including J-error of .219%)
MSWD = 1.12, probability = 0.34
81.8% of the 39Ar, steps 8 through 20

TC-8 biotite (bt2)										
MASS=	1.069 mg									
J =	3.46E-03	±	7.57E-06	(2 Sigma)				0.219 Percent		
STEP	POWER	40Ar/39Ar	37Ar/39Ar	36Ar/39Ar	Mol 39ArK	Ca/K	% 40ArA	Cum 39ArK	Age [Ma]	2 Sigma
1	5.00E-02	2.83E+02	-8.51E+00	9.34E-01	7.04E-17	-1.65E+01	98.0	2.17E-04	3.49E+01	4.99E+01
2	1.00E-01	3.62E+02	-2.19E+00	1.20E+00	3.91E-16	-4.28E+00	98.1	1.42E-03	4.22E+01	2.99E+01
3	1.50E-01	2.23E+02	-2.32E+00	7.44E-01	4.40E-16	-4.53E+00	98.6	2.78E-03	1.98E+01	1.37E+01
4	2.00E-01	1.33E+02	-1.10E+00	4.46E-01	7.89E-16	-2.15E+00	99.1	5.21E-03	7.15E+00	1.12E+01
5	2.50E-01	3.38E+01	-1.14E-01	1.09E-01	1.37E-15	-2.24E-01	95.6	9.45E-03	9.36E+00	4.28E+00
6	3.00E-01	1.96E+01	5.89E-01	6.42E-02	2.23E-15	1.15E+00	96.3	1.63E-02	4.49E+00	3.24E+00
7	4.00E-01	7.90E+00	3.80E-01	2.46E-02	6.05E-15	7.45E-01	91.3	3.50E-02	4.27E+00	1.31E+00
8	5.00E-01	3.00E+00	2.13E-01	7.92E-03	1.07E-14	4.19E-01	77.2	6.81E-02	4.27E+00	3.23E-01
9	**6.00E-01**	**1.56E+00**	**1.40E-01**	**3.28E-03**	**1.62E-14**	**2.74E-01**	**61.4**	**1.18E-01**	**3.74E+00**	**2.83E-01**
10	**7.00E-01**	**1.23E+00**	**1.60E-01**	**2.25E-03**	**2.29E-14**	**3.13E-01**	**52.5**	**1.89E-01**	**3.63E+00**	**1.85E-01**
11	**8.00E-01**	**1.03E+00**	**7.90E-02**	**1.51E-03**	**2.92E-14**	**1.55E-01**	**42.4**	**2.78E-01**	**3.69E+00**	**1.74E-01**
12	**9.00E-01**	**9.00E-01**	**6.77E-02**	**1.14E-03**	**3.27E-14**	**1.33E-01**	**36.6**	**3.80E-01**	**3.54E+00**	**1.59E-01**
13	**1.00E+00**	**8.05E-01**	**3.85E-02**	**7.91E-04**	**2.73E-14**	**7.55E-02**	**28.6**	**4.64E-01**	**3.56E+00**	**1.50E-01**
14	**1.10E+00**	**7.78E-01**	**6.20E-02**	**6.75E-04**	**2.63E-14**	**1.21E-01**	**24.8**	**5.45E-01**	**3.63E+00**	**1.37E-01**
15	**1.20E+00**	**7.81E-01**	**3.32E-02**	**6.93E-04**	**2.37E-14**	**6.50E-02**	**25.9**	**6.18E-01**	**3.59E+00**	**2.36E-01**
16	**1.50E+00**	**7.87E-01**	**1.78E-01**	**8.49E-04**	**3.30E-14**	**3.50E-01**	**29.2**	**7.20E-01**	**3.45E+00**	**1.06E-01**
17	**3.00E+00**	**7.13E-01**	**1.02E-01**	**5.18E-04**	**7.18E-14**	**1.99E-01**	**19.8**	**9.41E-01**	**3.54E+00**	**6.67E-02**
18	**5.00E+00**	**7.73E-01**	**2.07E-01**	**7.39E-04**	**1.52E-14**	**4.06E-01**	**24.9**	**9.88E-01**	**3.60E+00**	**2.27E-01**
19	**1.00E+01**	**9.86E-01**	**3.78E-01**	**1.45E-03**	**3.59E-15**	**7.41E-01**	**38.7**	**9.99E-01**	**3.75E+00**	**8.61E-01**
20	**1.50E+01**	**1.29E+00**	**-7.36E-01**	**9.67E-04**	**3.06E-16**	**-1.44E+00**	**29.7**	**1.00E+00**	**5.64E+00**	**7.54E+00**
Total Gas Age =	3.73E+00	±	4.17E-02	Ma (2Sigma)						

Plateau Age = 3.558±0.043 Ma
(2s, including J-error of .219%)
MSWD = 0.94, probability = 0.50
93.2% of the 39Ar, steps 9 through 20

Table 5 Continued

M64C KH hornblende

MASS=	6.163 mg									
J =	3.97E-03	±	1.00E-05	(2 Sigma)				0.252 Percent		
STEP	POWER	40Ar/39Ar	37Ar/39Ar	36Ar/39Ar	Mol 39ArK	Ca/K	% 40ArA	Cum 39ArK	Age [Ma]	2 Sigma
1	1.00E-01	4.55E+02	3.17E+00	1.77E+00	3.48E-18	6.24E+00	115.2	3.02E-05	-5.80E+02	4.19E+03
2	1.50E-01	3.17E+01	2.69E+01	1.65E+00	1.03E-18	5.42E+01	1530.6	3.92E-05	-3.52E+04	1.77E+04
3	2.00E-01	2.70E+02	3.44E+00	9.10E-01	2.10E-17	6.77E+00	99.2	2.22E-04	1.49E+01	2.93E+02
4	2.50E-01	9.84E+01	7.10E+00	4.25E-01	1.68E-17	1.40E+01	126.7	3.68E-04	-2.00E+02	4.35E+02
5	3.00E-01	6.05E+01	4.94E+00	2.07E-01	2.93E-17	9.73E+00	100.3	6.23E-04	-1.17E+00	2.60E+02
6	4.00E-01	1.77E+01	4.26E+00	4.14E-02	8.23E-17	8.38E+00	66.0	1.34E-03	4.29E+01	7.31E+01
7	5.00E-01	4.26E+00	3.91E+00	5.71E-03	2.28E-16	7.69E+00	27.7	3.32E-03	2.20E+01	2.11E+01
8	6.00E-01	2.53E+00	4.19E+00	4.53E-03	6.68E-16	8.25E+00	31.2	9.12E-03	1.25E+01	1.13E+01
9	7.00E-01	1.92E+00	4.32E+00	5.83E-03	1.94E-15	8.50E+00	60.5	2.59E-02	5.43E+00	2.60E+00
10	8.00E-01	1.63E+00	4.57E+00	6.75E-03	4.45E-15	9.00E+00	86.1	6.46E-02	1.63E+00	1.61E+00
11	9.00E-01	1.01E+00	4.49E+00	4.94E-03	6.99E-15	8.83E+00	86.8	1.25E-01	9.59E-01	9.78E-01
12	1.00E+00	7.72E-01	4.45E+00	4.01E-03	8.89E-15	8.76E+00	78.7	2.02E-01	1.17E+00	7.84E-01
13	1.10E+00	1.08E+00	4.45E+00	4.75E-03	8.96E-15	8.76E+00	76.8	2.80E-01	1.79E+00	1.62E+00
14	1.20E+00	7.93E-01	4.50E+00	4.53E-03	8.90E-15	8.86E+00	95.5	3.58E-01	2.53E-01	1.25E+00
15	1.35E+00	1.11E+00	4.45E+00	5.11E-03	1.25E-14	8.77E+00	84.2	4.66E-01	1.25E+00	1.84E+00
16	1.50E+00	7.35E-01	4.49E+00	3.87E-03	9.62E-15	8.84E+00	76.7	5.49E-01	1.22E+00	1.46E+00
17	2.00E+00	6.37E-01	4.52E+00	3.60E-03	1.70E-14	8.89E+00	74.9	6.97E-01	1.14E+00	1.41E+00
18	3.00E+00	7.20E-01	4.80E+00	4.53E-03	1.37E-14	9.46E+00	99.6	8.15E-01	1.87E-02	1.16E+00
19	5.00E+00	2.99E-01	4.98E+00	3.29E-03	1.23E-14	9.81E+00	109.7	9.23E-01	-2.04E-01	8.90E-01
20	1.00E+01	1.83E-01	5.18E+00	3.71E-03	6.85E-15	1.02E+01	238.2	9.82E-01	-1.75E+00	1.42E+00
21	2.00E+01	2.24E-01	5.49E+00	2.05E-03	1.85E-15	1.08E+01	-51.5	9.98E-01	2.37E+00	3.79E+00
22	2.50E+01	-3.60E-01	5.72E+00	-1.36E-02	2.28E-16	1.13E+01	1300.8	1.00E+00	3.15E+01	3.77E+01
Total Gas Age =	6.32E-01	±	3.52E-01	Ma (2Sigma)						

Plateau Age = 0.77±0.37 Ma
(2s, including J-error of .252%)
MSWD = 1.3, probability = 0.21
89.7% of the 39Ar, steps 10 through 19

M65A KH matrix (mxss)

MASS=	8.451 mg									
J =	3.97E-03	±	1.00E-05	(2 Sigma)				0.252 Percent		
STEP	POWER	40Ar/39Ar	37Ar/39Ar	36Ar/39Ar	Mol 39ArK	Ca/K	% 40ArA	Cum 39ArK	Age [Ma]	2 Sigma
1	1.50E-01	4.30E+01	7.20E-02	1.42E-01	3.36E-16	1.41E-01	97.5	7.02E-04	7.76E+00	2.97E+01
2	2.50E-01	1.41E+01	4.52E-01	4.60E-02	3.19E-15	8.86E-01	95.9	7.37E-03	4.15E+00	3.02E+00
3	4.00E-01	4.07E+00	4.47E-01	1.34E-02	1.26E-14	8.77E-01	95.8	3.38E-02	1.23E+00	7.94E-01
4	5.00E-01	1.54E+00	4.96E-01	5.12E-03	1.73E-14	9.73E-01	94.7	6.98E-02	5.84E-01	4.48E-01
5	6.00E-01	9.24E-01	5.81E-01	3.36E-03	2.11E-14	1.14E+00	100.0	1.14E-01	-2.68E-03	4.03E-01
6	7.00E-01	8.38E-01	7.14E-01	3.12E-03	2.06E-14	1.40E+00	99.6	1.57E-01	2.18E-02	3.95E-01
7	8.00E-01	1.11E+00	7.86E-01	3.94E-03	1.76E-14	1.54E+00	96.6	1.94E-01	2.69E-01	4.36E-01
8	9.00E-01	1.76E+00	8.74E-01	6.10E-03	1.41E-14	1.71E+00	96.5	2.23E-01	4.45E-01	4.92E-01
9	1.00E+00	2.66E+00	8.78E-01	9.49E-03	1.30E-14	1.72E+00	101.4	2.50E-01	-2.69E-01	5.69E-01
10	1.10E+00	3.44E+00	6.85E-01	1.18E-02	1.60E-14	1.34E+00	99.1	2.84E-01	2.18E-01	5.03E-01
11	1.20E+00	3.97E+00	5.06E-01	1.37E-02	2.58E-14	9.92E-01	100.1	3.37E-01	-3.48E-02	6.18E-01
12	1.35E+00	4.17E+00	5.17E-01	1.42E-02	4.20E-14	1.01E+00	99.0	4.25E-01	3.10E-01	3.92E-01
13	1.50E+00	4.51E+00	6.28E-01	1.52E-02	3.86E-14	1.23E+00	97.8	5.06E-01	7.21E-01	7.71E-01
14	2.00E+00	4.71E+00	8.70E-01	1.61E-02	6.66E-14	1.71E+00	98.9	6.45E-01	3.86E-01	1.50E-01
15	3.00E+00	4.66E+00	9.37E-01	1.61E-02	7.14E-14	1.84E+00	99.6	7.94E-01	1.36E-01	1.24E-01
16	5.00E+00	5.19E+00	1.05E+00	1.76E-02	4.27E-14	2.07E+00	97.5	8.83E-01	9.42E-01	4.93E-01
17	1.00E+01	5.13E+00	1.14E+00	1.75E-02	4.27E-14	2.23E+00	98.1	9.72E-01	7.14E-01	6.40E-01
18	2.00E+01	5.05E+00	1.34E+00	1.71E-02	1.16E-14	2.63E+00	96.5	9.96E-01	1.28E+00	1.28E+00
19	2.50E+01	5.07E+00	1.24E+00	1.50E-02	1.43E-15	2.44E+00	84.1	9.99E-01	5.76E+00	4.89E+00
20	2.75E+01	4.62E+00	8.09E-01	9.40E-03	3.16E-16	1.59E+00	57.9	1.00E+00	1.39E+01	1.14E+01
Total Gas Age =	4.73E-01	±	7.84E-02	Ma (2Sigma)						

Plateau Age = 0.230±0.081 Ma
(2s, including J-error of .252%)
MSWD = 1.6, probability = 0.083
76% of the 39Ar, steps 4 through 15

Table 5 Continued

SO96-1 matrix										
MASS=	5.543 mg									
J =	3.74E-03	±	1.17E-05	(2 Sigma)				0.313 Percent		
STEP	POWER	40Ar/39Ar	37Ar/39Ar	36Ar/39Ar	Mol 39ArK	Ca/K	% 40ArA	Cum 39ArK	Age [Ma]	2 Sigma
2	1.00E-01	7.12E+03	3.28E+00	2.38E+01	4.06E-18	6.45E+00	98.9	5.91E-05	4.63E+02	6.30E+02
3	1.50E-01	2.44E+03	1.36E+00	8.17E+00	2.67E-17	2.66E+00	99.2	4.46E-04	1.28E+02	1.75E+02
4	2.00E-01	9.21E+02	9.39E-01	3.09E+00	1.01E-16	1.84E+00	99.1	1.91E-03	5.55E+01	5.25E+01
5	2.50E-01	3.58E+02	9.75E-01	1.21E+00	1.93E-16	1.91E+00	99.6	4.71E-03	1.02E+01	2.94E+01
6	3.00E-01	1.46E+02	1.02E+00	4.86E-01	3.12E-16	1.99E+00	98.5	9.25E-03	1.46E+01	9.99E+00
7	3.50E-01	6.23E+01	1.12E+00	2.07E-01	4.44E-16	2.21E+00	98.0	1.57E-02	8.42E+00	5.84E+00
8	4.00E-01	3.34E+01	1.07E+00	1.10E-01	7.30E-16	2.11E+00	97.0	2.63E-02	6.82E+00	3.15E+00
9	**4.50E-01**	**1.69E+01**	**9.94E-01**	**5.55E-02**	**1.12E-15**	**1.95E+00**	**96.6**	**4.26E-02**	**3.86E+00**	**1.42E+00**
10	**5.00E-01**	**9.84E+00**	**9.03E-01**	**3.29E-02**	**1.52E-15**	**1.77E+00**	**97.9**	**6.46E-02**	**1.37E+00**	**1.22E+00**
11	**5.50E-01**	**7.17E+00**	**8.70E-01**	**2.31E-02**	**2.07E-15**	**1.71E+00**	**94.0**	**9.47E-02**	**2.90E+00**	**1.75E+00**
12	**6.00E-01**	**4.88E+00**	**8.22E-01**	**1.58E-02**	**2.42E-15**	**1.61E+00**	**94.2**	**1.30E-01**	**1.91E+00**	**1.05E+00**
13	**7.00E-01**	**4.66E+00**	**8.59E-01**	**1.53E-02**	**4.45E-15**	**1.68E+00**	**94.9**	**1.95E-01**	**1.61E+00**	**5.24E-01**
14	**8.00E-01**	**3.38E+00**	**9.16E-01**	**1.09E-02**	**5.61E-15**	**1.80E+00**	**92.5**	**2.76E-01**	**1.71E+00**	**4.78E-01**
15	**9.00E-01**	**3.21E+00**	**1.06E+00**	**1.05E-02**	**5.98E-15**	**2.08E+00**	**93.2**	**3.63E-01**	**1.46E+00**	**5.09E-01**
16	**1.00E+00**	**3.43E+00**	**1.29E+00**	**1.16E-02**	**5.51E-15**	**2.52E+00**	**96.1**	**4.43E-01**	**9.00E-01**	**3.82E-01**
17	**1.10E+00**	**3.61E+00**	**1.61E+00**	**1.24E-02**	**4.21E-15**	**3.15E+00**	**96.3**	**5.04E-01**	**9.02E-01**	**4.49E-01**
18	**1.20E+00**	**4.27E+00**	**2.15E+00**	**1.46E-02**	**3.96E-15**	**4.22E+00**	**95.6**	**5.62E-01**	**1.27E+00**	**7.15E-01**
19	**1.35E+00**	**5.09E+00**	**3.25E+00**	**1.77E-02**	**4.52E-15**	**6.38E+00**	**95.8**	**6.28E-01**	**1.46E+00**	**4.79E-01**
20	**1.50E+00**	**6.06E+00**	**4.23E+00**	**2.13E-02**	**3.81E-15**	**8.32E+00**	**96.3**	**6.83E-01**	**1.50E+00**	**5.60E-01**
21	**1.75E+00**	**6.57E+00**	**5.68E+00**	**2.40E-02**	**3.88E-15**	**1.12E+01**	**98.4**	**7.39E-01**	**7.30E-01**	**6.50E-01**
22	**2.00E+00**	**7.59E+00**	**6.70E+00**	**2.73E-02**	**3.15E-15**	**1.32E+01**	**96.5**	**7.85E-01**	**1.81E+00**	**1.07E+00**
23	**3.00E+00**	**7.68E+00**	**7.21E+00**	**2.77E-02**	**4.06E-15**	**1.42E+01**	**96.3**	**8.44E-01**	**1.92E+00**	**8.99E-01**
24	**4.00E+00**	**7.77E+00**	**7.20E+00**	**2.82E-02**	**2.91E-15**	**1.42E+01**	**97.3**	**8.86E-01**	**1.40E+00**	**9.48E-01**
25	**6.00E+00**	**7.55E+00**	**6.88E+00**	**2.76E-02**	**2.49E-15**	**1.36E+01**	**98.3**	**9.23E-01**	**8.94E-01**	**6.73E-01**
26	**8.00E+00**	**8.39E+00**	**8.14E+00**	**3.09E-02**	**1.95E-15**	**1.61E+01**	**98.5**	**9.51E-01**	**8.84E-01**	**1.40E+00**
27	**1.00E+01**	**8.48E+00**	**7.48E+00**	**3.09E-02**	**2.38E-15**	**1.48E+01**	**98.0**	**9.86E-01**	**1.17E+00**	**1.00E+00**
28	**1.50E+01**	**9.02E+00**	**8.26E+00**	**3.25E-02**	**8.98E-16**	**1.63E+01**	**96.6**	**9.99E-01**	**2.06E+00**	**2.37E+00**
29	**2.00E+01**	**1.27E+01**	**7.53E+00**	**4.47E-02**	**8.10E-17**	**1.49E+01**	**97.9**	**1.00E+00**	**1.79E+00**	**2.00E+01**
30	2.50E+01	1.77E+01	1.13E+01	4.98E-02	1.75E-17	2.25E+01	76.2	1.00E+00	2.85E+01	9.39E+01
Total Gas Age =	1.81E+00	±	1.49E-01	Ma (2Sigma)						

Plateau Age = 1.30±0.15 Ma
(2s, including J-error of .313%)
MSWD = 1.3, probability = 0.15
95.7% of the 39Ar, steps 9 through 29

CP97-1 matrix (mxst)										
MASS=	-0.000 mg									
J =	3.69E-03	±	5.67E-06	(2 Sigma)				0.154 Percent		
STEP	POWER	40Ar/39Ar	37Ar/39Ar	36Ar/39Ar	Mol 39ArK	Ca/K	% 40ArA	Cum 39ArK	Age [Ma]	2 Sigma
1	7.00E-02	1.76E+02	1.49E+01	6.69E-01	4.47E-17	2.95E+01	111.6	6.19E-04	-1.43E+02	1.13E+02
2	1.00E-01	6.07E+01	-3.82E+00	2.02E-01	3.37E-16	-7.47E+00	98.8	**5.28E-03**	**4.88E+00**	**1.75E+01**
3	1.25E-01	3.01E+01	3.23E+00	9.67E-02	4.67E-16	6.35E+00	93.7	**1.18E-02**	**1.27E+01**	**1.18E+01**
4	1.50E-01	2.18E+01	-1.43E-02	7.43E-02	8.70E-16	-2.81E-02	100.6	**2.38E-02**	**-9.19E-01**	**9.82E+00**
5	1.75E-01	1.39E+01	1.32E+00	4.57E-02	1.37E-15	2.58E+00	96.1	**4.28E-02**	**3.64E+00**	**4.64E+00**
6	2.00E-01	9.14E+00	3.78E-01	3.09E-02	1.89E-15	7.41E-01	99.5	**6.90E-02**	**2.91E-01**	**2.78E+00**
7	2.25E-01	6.39E+00	7.71E-01	2.15E-02	2.42E-15	1.51E+00	97.8	**1.02E-01**	**9.29E-01**	**2.26E+00**
8	2.50E-01	4.80E+00	3.93E-01	1.62E-02	2.92E-15	7.71E-01	99.0	**1.43E-01**	**3.22E-01**	**1.58E+00**
9	2.75E-01	3.95E+00	1.36E+00	1.29E-02	3.08E-15	2.67E+00	92.3	**1.85E-01**	**2.02E+00**	**1.83E+00**
10	3.00E-01	3.44E+00	6.50E-01	1.15E-02	3.43E-15	1.28E+00	96.8	**2.33E-01**	**7.29E-01**	**1.38E+00**
11	3.50E-01	3.06E+00	7.34E-01	9.99E-03	5.17E-15	1.44E+00	93.8	**3.05E-01**	**1.27E+00**	**5.79E-01**
12	4.00E-01	2.84E+00	1.29E+00	9.59E-03	6.23E-15	2.54E+00	94.5	**3.91E-01**	**1.03E+00**	**7.40E-01**
13	4.50E-01	2.80E+00	1.39E+00	8.87E-03	6.67E-15	2.73E+00	87.9	**4.83E-01**	**2.25E+00**	**5.04E-01**
14	5.00E-01	2.73E+00	1.24E+00	9.58E-03	6.09E-15	2.43E+00	98.4	**5.67E-01**	**2.92E-01**	**1.21E+00**
15	5.50E-01	2.82E+00	1.15E+00	9.51E-03	5.26E-15	2.25E+00	94.9	**6.40E-01**	**9.54E-01**	**1.32E+00**
16	6.00E-01	2.98E+00	2.03E+00	9.98E-03	4.08E-15	3.99E+00	90.9	**6.97E-01**	**1.81E+00**	**1.21E+00**
17	7.00E-01	3.60E+00	2.05E+00	1.21E-02	4.16E-15	4.02E+00	92.3	**7.54E-01**	**1.84E+00**	**1.39E+00**
18	8.00E-01	4.10E+00	2.48E+00	1.37E-02	3.39E-15	4.86E+00	91.8	**8.01E-01**	**2.23E+00**	**1.84E+00**
19	9.00E-01	4.51E+00	4.52E+00	1.68E-02	2.95E-15	8.89E+00	98.6	8.42E-01	4.34E-01	1.02E+00
20	1.00E+00	4.56E+00	6.21E+00	1.66E-02	2.54E-15	1.22E+01	91.8	8.77E-01	2.48E+00	1.66E+00
21	1.10E+00	4.64E+00	8.37E+00	1.98E-02	1.76E-15	1.65E+01	105.0	9.01E-01	-1.56E+00	2.15E+00
22	1.20E+00	4.69E+00	1.43E+01	2.29E-02	1.22E-15	2.84E+01	108.0	9.18E-01	-2.54E+00	4.14E+00
23	1.35E+00	4.82E+00	1.87E+01	2.55E-02	1.04E-15	3.72E+01	110.6	9.33E-01	-3.46E+00	6.42E+00
24	1.50E+00	4.84E+00	2.81E+01	3.00E-02	7.32E-16	5.66E+01	114.6	9.43E-01	-4.82E+00	9.28E+00
25	1.75E+00	5.11E+00	3.67E+01	3.47E-02	5.50E-16	7.45E+01	116.0	9.50E-01	-5.64E+00	8.17E+00
26	2.00E+00	5.57E+00	4.33E+01	3.54E-02	4.22E-16	8.84E+01	96.0	9.56E-01	1.55E+00	1.33E+01
27	2.50E+00	6.14E+00	5.08E+01	4.04E-02	4.74E-16	1.04E+02	96.9	9.63E-01	1.33E+00	1.06E+01
28	3.00E+00	6.52E+00	5.36E+01	4.27E-02	4.47E-16	1.10E+02	96.3	9.69E-01	1.67E+00	9.35E+00
29	4.00E+00	7.16E+00	5.30E+01	4.31E-02	5.55E-16	1.09E+02	90.5	9.77E-01	4.77E+00	9.13E+00
30	6.00E+00	8.26E+00	5.13E+01	4.65E-02	8.67E-16	1.05E+02	93.0	9.89E-01	4.00E+00	7.33E+00
31	8.00E+00	1.24E+01	5.17E+01	6.36E-02	7.10E-16	1.06E+02	102.3	9.99E-01	-1.99E+00	7.21E+00
32	1.00E+01	1.71E+01	6.29E+01	8.41E-02	7.24E-17	1.31E+02	101.7	1.00E+00	-2.03E+00	3.74E+01
33	1.50E+01	6.26E+01	2.11E+01	5.78E-02	6.49E-18	4.22E+01	23.3	1.00E+00	2.99E+02	4.83E+02
34	2.00E+01	1.70E+02	4.99E+01	5.49E-01	2.89E-17	1.03E+02	92.3	1.00E+00	8.93E+01	1.25E+02
Total Gas Age =	1.08E+00	±	2.60E-01	Ma (2Sigma)						

Plateau Age = 1.50±0.28 Ma
(2s, including J-error of .154%)
MSWD = 1.7, probability = 0.047
80% of the 39Ar, steps 2 through 18

Table 5 Continued

M105 KH matrix										
MASS=	4.957 mg									
J =	4.01E-03	±	8.15E-06	(2 Sigma)				0.203 Percent		
STEP	POWER	40Ar/39Ar	37Ar/39Ar	36Ar/39Ar	Mol 39ArK	Ca/K	% 40ArA	Cum 39ArK	Age [Ma]	2 Sigma
1	**1.50E-01**	**1.27E+02**	**1.18E+00**	**4.23E-01**	**3.27E-16**	**2.31E+00**	**97.9**	**2.47E-03**	**1.89E+01**	**3.14E+01**
2	**2.50E-01**	**2.52E+01**	**9.72E-01**	**8.52E-02**	**1.63E-15**	**1.91E+00**	**99.3**	**1.48E-02**	**1.19E+00**	**6.37E+00**
3	**4.00E-01**	**5.56E+00**	**7.28E-01**	**1.86E-02**	**7.11E-15**	**1.43E+00**	**97.2**	**6.86E-02**	**1.13E+00**	**1.46E+00**
4	**5.00E-01**	**2.42E+00**	**5.91E-01**	**7.71E-03**	**1.00E-14**	**1.16E+00**	**91.3**	**1.44E-01**	**1.53E+00**	**7.60E-01**
5	**6.00E-01**	**2.02E+00**	**5.93E-01**	**6.78E-03**	**1.20E-14**	**1.16E+00**	**95.6**	**2.35E-01**	**6.39E-01**	**8.31E-01**
6	**7.00E-01**	**2.04E+00**	**7.25E-01**	**6.69E-03**	**1.10E-14**	**1.42E+00**	**92.6**	**3.18E-01**	**1.09E+00**	**5.92E-01**
7	**8.00E-01**	**2.49E+00**	**9.96E-01**	**8.12E-03**	**9.24E-15**	**1.95E+00**	**91.6**	**3.88E-01**	**1.51E+00**	**6.57E-01**
8	**9.00E-01**	**3.42E+00**	**1.40E+00**	**1.18E-02**	**8.62E-15**	**2.75E+00**	**96.7**	**4.53E-01**	**8.06E-01**	**1.04E+00**
9	**1.00E+00**	**4.49E+00**	**1.74E+00**	**1.50E-02**	**9.65E-15**	**3.42E+00**	**93.8**	**5.26E-01**	**2.00E+00**	**1.14E+00**
10	**1.10E+00**	**4.30E+00**	**2.29E+00**	**1.48E-02**	**8.14E-15**	**4.50E+00**	**94.6**	**5.88E-01**	**1.67E+00**	**8.19E-01**
11	**1.20E+00**	**4.52E+00**	**2.82E+00**	**1.58E-02**	**7.15E-15**	**5.53E+00**	**95.3**	**6.42E-01**	**1.54E+00**	**1.50E+00**
12	**1.35E+00**	**4.53E+00**	**3.55E+00**	**1.62E-02**	**7.20E-15**	**6.98E+00**	**95.7**	**6.96E-01**	**1.43E+00**	**1.33E+00**
13	**1.50E+00**	**4.61E+00**	**4.00E+00**	**1.64E-02**	**5.40E-15**	**7.87E+00**	**93.5**	**7.37E-01**	**2.16E+00**	**1.53E+00**
14	**2.00E+00**	**3.96E+00**	**5.50E+00**	**1.48E-02**	**6.43E-15**	**1.08E+01**	**92.3**	**7.86E-01**	**2.20E+00**	**1.34E+00**
15	**3.00E+00**	**3.73E+00**	**6.13E+00**	**1.43E-02**	**6.44E-15**	**1.21E+01**	**91.8**	**8.35E-01**	**2.23E+00**	**1.39E+00**
16	**5.00E+00**	**3.55E+00**	**6.36E+00**	**1.42E-02**	**1.15E-14**	**1.25E+01**	**95.1**	**9.22E-01**	**1.27E+00**	**8.44E-01**
17	**1.00E+01**	**3.43E+00**	**7.21E+00**	**1.41E-02**	**9.22E-15**	**1.42E+01**	**93.8**	**9.92E-01**	**1.53E+00**	**1.02E+00**
18	**2.00E+01**	**3.40E+00**	**8.01E+00**	**1.28E-02**	**1.02E-15**	**1.58E+01**	**80.9**	**9.99E-01**	**4.72E+00**	**7.30E+00**
19	**2.50E+01**	**6.22E+00**	**6.60E+00**	**-2.41E-04**	**5.61E-17**	**1.30E+01**	**-15.0**	**1.00E+00**	**5.13E+01**	**9.71E+01**
20	**2.75E+01**	**1.01E+01**	**6.33E+00**	**-4.54E-02**	**2.92E-17**	**1.25E+01**	**-141.1**	**1.00E+00**	**1.69E+02**	**2.02E+02**
Total Gas Age =	1.57E+00	±	2.43E-01	Ma (2Sigma)						
Plateau Age = 1.40±0.24 Ma										
(2s, including J-error of .203%)										
MSWD = 0.92, probability = 0.55										
100% of the 39Ar, steps 1 through 20										

M118a KH matrix										
MASS=	4.901 mg									
J =	4.20E-03	±	8.62E-06	(2 Sigma)				0.205 Percent		
STEP	POWER	40Ar/39Ar	37Ar/39Ar	36Ar/39Ar	Mol 39ArK	Ca/K	% 40ArA	Cum 39ArK	Age [Ma]	2 Sigma
1	1.50E-01	1.20E+02	8.77E-01	4.12E-01	3.61E-16	1.72E+00	101.3	2.28E-03	-1.16E+01	3.48E+01
2	2.50E-01	2.36E+01	6.99E-01	7.92E-02	1.76E-15	1.37E+00	98.7	1.34E-02	2.40E+00	5.18E+00
3	4.00E-01	6.36E+00	5.11E-01	2.14E-02	7.14E-15	1.00E+00	98.7	5.85E-02	6.22E-01	9.80E-01
4	5.00E-01	2.27E+00	4.27E-01	7.48E-03	9.41E-15	8.37E-01	95.3	1.18E-01	8.13E-01	6.58E-01
5	**6.00E-01**	**1.88E+00**	**4.31E-01**	**6.05E-03**	**1.04E-14**	**8.44E-01**	**92.2**	**1.83E-01**	**1.11E+00**	**5.82E-01**
6	**7.00E-01**	**2.70E+00**	**5.46E-01**	**8.85E-03**	**1.13E-14**	**1.07E+00**	**94.5**	**2.55E-01**	**1.12E+00**	**8.39E-01**
7	**8.00E-01**	**3.14E+00**	**8.39E-01**	**1.03E-02**	**1.20E-14**	**1.65E+00**	**93.8**	**3.30E-01**	**1.46E+00**	**5.34E-01**
8	**9.00E-01**	**3.74E+00**	**1.17E+00**	**1.29E-02**	**1.17E-14**	**2.29E+00**	**98.0**	**4.04E-01**	**5.76E-01**	**1.10E+00**
9	**1.00E+00**	**4.24E+00**	**1.35E+00**	**1.42E-02**	**1.08E-14**	**2.64E+00**	**94.8**	**4.73E-01**	**1.67E+00**	**8.10E-01**
10	**1.10E+00**	**4.39E+00**	**1.53E+00**	**1.45E-02**	**9.89E-15**	**3.01E+00**	**92.9**	**5.35E-01**	**2.36E+00**	**8.67E-01**
11	**1.20E+00**	**4.43E+00**	**1.75E+00**	**1.56E-02**	**9.12E-15**	**3.44E+00**	**99.0**	**5.93E-01**	**3.51E-01**	**1.26E+00**
12	**1.35E+00**	**4.50E+00**	**2.03E+00**	**1.57E-02**	**8.90E-15**	**3.99E+00**	**97.4**	**6.49E-01**	**8.74E-01**	**1.11E+00**
13	**1.50E+00**	**4.37E+00**	**2.52E+00**	**1.59E-02**	**6.40E-15**	**4.95E+00**	**100.4**	**6.89E-01**	**-1.32E-01**	**1.82E+00**
14	**2.00E+00**	**4.23E+00**	**3.36E+00**	**1.53E-02**	**7.71E-15**	**6.62E+00**	**96.4**	**7.38E-01**	**1.17E+00**	**1.01E+00**
15	**3.00E+00**	**4.37E+00**	**3.74E+00**	**1.55E-02**	**1.19E-14**	**7.36E+00**	**94.0**	**8.13E-01**	**2.00E+00**	**8.15E-01**
16	**5.00E+00**	**4.48E+00**	**4.33E+00**	**1.62E-02**	**1.79E-14**	**8.52E+00**	**94.7**	**9.26E-01**	**1.81E+00**	**5.63E-01**
17	**1.00E+01**	**4.85E+00**	**4.54E+00**	**1.77E-02**	**1.07E-14**	**8.94E+00**	**95.8**	**9.94E-01**	**1.54E+00**	**7.49E-01**
18	**2.00E+01**	**4.96E+00**	**4.78E+00**	**2.01E-02**	**9.27E-16**	**9.41E+00**	**107.4**	**1.00E+00**	**-2.78E+00**	**9.66E+00**
19	**2.50E+01**	**1.65E+01**	**4.12E+00**	**8.65E-02**	**4.84E-17**	**8.11E+00**	**151.8**	**1.00E+00**	**-6.62E+01**	**1.60E+02**
20	**2.75E+01**	**3.22E+01**	**4.16E+00**	**1.99E-01**	**1.52E-17**	**8.18E+00**	**181.0**	**1.00E+00**	**-2.10E+02**	**5.93E+02**
Total Gas Age =	1.17E+00	±	2.03E-01	Ma (2Sigma)						
Plateau Age = 1.43±0.22 Ma										
(2s, including J-error of .205%)										
MSWD = 1.5, probability = 0.10										
88.2% of the 39Ar, steps 5 through 20										

Table 5 Continued

M121a KH matrix										
MASS=	5.045 mg									
J =	4.01E-03	±	8.15E-06	(2 Sigma)				0.203 Percent		
STEP	POWER	40Ar/39Ar	37Ar/39Ar	36Ar/39Ar	Mol 39ArK	Ca/K	% 40ArA	Cum 39ArK	Age [Ma]	2 Sigma
1	1.50E-01	2.07E+02	8.07E-01	7.02E-01	6.02E-16	1.58E+00	100.0	4.41E-03	-1.22E-02	2.74E+01
2	2.50E-01	5.24E+01	6.48E-01	1.76E-01	2.66E-15	1.27E+00	99.0	2.39E-02	3.97E+00	5.92E+00
3	4.00E-01	9.37E+00	5.07E-01	3.04E-02	1.08E-14	9.94E-01	95.4	1.03E-01	3.14E+00	8.10E-01
4	**5.00E-01**	**6.70E+00**	**4.63E-01**	**2.09E-02**	**1.23E-14**	**9.08E-01**	**91.6**	**1.93E-01**	**4.05E+00**	**8.47E-01**
5	**6.00E-01**	**5.60E+00**	**4.96E-01**	**1.68E-02**	**1.28E-14**	**9.73E-01**	**87.4**	**2.86E-01**	**5.12E+00**	**9.12E-01**
6	**7.00E-01**	**4.69E+00**	**7.85E-01**	**1.39E-02**	**1.36E-14**	**1.54E+00**	**85.4**	**3.86E-01**	**4.95E+00**	**9.35E-01**
7	**8.00E-01**	**4.52E+00**	**1.25E+00**	**1.40E-02**	**1.33E-14**	**2.45E+00**	**88.1**	**4.84E-01**	**3.88E+00**	**1.03E+00**
8	**9.00E-01**	**5.05E+00**	**1.63E+00**	**1.58E-02**	**1.31E-14**	**3.20E+00**	**88.1**	**5.79E-01**	**4.34E+00**	**9.64E-01**
9	**1.00E+00**	**4.17E+00**	**2.24E+00**	**1.31E-02**	**1.08E-14**	**4.40E+00**	**86.1**	**6.59E-01**	**4.20E+00**	**9.75E-01**
10	**1.10E+00**	**3.90E+00**	**3.01E+00**	**1.29E-02**	**6.90E-15**	**5.91E+00**	**87.6**	**7.09E-01**	**3.51E+00**	**1.57E+00**
11	**1.20E+00**	**4.35E+00**	**3.34E+00**	**1.41E-02**	**6.64E-15**	**6.56E+00**	**86.1**	**7.58E-01**	**4.36E+00**	**1.57E+00**
12	**1.35E+00**	**3.87E+00**	**4.93E+00**	**1.29E-02**	**5.60E-15**	**9.71E+00**	**82.2**	**7.99E-01**	**5.01E+00**	**1.44E+00**
13	**1.50E+00**	**3.91E+00**	**5.96E+00**	**1.34E-02**	**4.42E-15**	**1.17E+01**	**81.8**	**8.31E-01**	**5.17E+00**	**1.86E+00**
14	2.00E+00	4.43E+00	7.91E+00	1.56E-02	6.84E-15	1.56E+01	80.7	8.81E-01	6.20E+00	1.31E+00
15	3.00E+00	5.55E+00	9.39E+00	1.96E-02	6.86E-15	1.86E+01	82.1	9.31E-01	7.22E+00	9.34E-01
16	5.00E+00	7.12E+00	1.08E+01	2.48E-02	6.20E-15	2.13E+01	83.1	9.77E-01	8.76E+00	1.73E+00
17	1.00E+01	1.10E+01	1.08E+01	3.42E-02	2.43E-15	2.14E+01	79.1	9.94E-01	1.67E+01	4.35E+00
18	2.00E+01	1.61E+01	1.13E+01	5.75E-02	7.54E-16	2.25E+01	96.5	1.00E+00	4.17E+00	1.18E+01
19	2.50E+01	1.32E+02	2.91E+01	8.77E-01	2.35E-18	5.87E+01	193.0	1.00E+00	-1.28E+03	5.34E+03
Total Gas Age =	4.92E+00	±	2.88E-01	Ma (2Sigma)						

Plateau Age = 4.45 ± 0.35 Ma
(2s, including J-error of .203%)
MSWD = 0.93, probability = 0.50
72.8% of the 39Ar, steps 4 through 13

3-12-4-03 matrix										
MASS=	7.188 mg									
J =	2.39E-03	±	8.71E-06	(2 Sigma)				0.364 Percent		
STEP	POWER	40Ar/39Ar	37Ar/39Ar	36Ar/39Ar	Mol 39ArK	Ca/K	% 40ArA	Cum 39ArK	Age [Ma]	2 Sigma
1	1.50E-01	3.68E+02	1.86E+00	7.82E-01	1.99E-16	3.65E+00	62.7	1.17E-03	5.14E+02	9.64E+01
2	2.50E-01	8.08E+01	1.33E+00	2.11E-01	1.57E-15	2.61E+00	77.0	1.04E-02	7.87E+01	1.81E+01
3	4.00E-01	1.23E+01	9.92E-01	2.01E-02	6.32E-15	1.95E+00	47.2	4.76E-02	2.79E+01	4.76E+00
4	5.00E-01	3.41E+00	8.01E-01	9.09E-03	9.04E-15	1.57E+00	75.9	1.01E-01	3.54E+00	1.58E+00
5	6.00E-01	1.85E+00	6.90E-01	6.51E-03	1.33E-14	1.35E+00	99.6	1.79E-01	3.06E-02	6.40E-01
6	**7.00E-01**	**1.34E+00**	**6.19E-01**	**3.76E-03**	**1.63E-14**	**1.21E+00**	**77.5**	**2.74E-01**	**1.29E+00**	**4.76E-01**
7	**8.00E-01**	**1.17E+00**	**6.36E-01**	**2.98E-03**	**1.65E-14**	**1.25E+00**	**68.7**	**3.72E-01**	**1.57E+00**	**4.74E-01**
8	**9.00E-01**	**1.13E+00**	**7.28E-01**	**3.09E-03**	**1.45E-14**	**1.43E+00**	**73.0**	**4.57E-01**	**1.30E+00**	**4.34E-01**
9	**1.00E+00**	**1.26E+00**	**9.64E-01**	**3.27E-03**	**1.21E-14**	**1.89E+00**	**67.1**	**5.28E-01**	**1.78E+00**	**5.35E-01**
10	**1.10E+00**	**1.53E+00**	**1.42E+00**	**4.36E-03**	**9.12E-15**	**2.79E+00**	**72.5**	**5.82E-01**	**1.81E+00**	**7.00E-01**
11	**1.20E+00**	**2.05E+00**	**2.04E+00**	**5.71E-03**	**7.68E-15**	**4.00E+00**	**69.4**	**6.27E-01**	**2.71E+00**	**8.63E-01**
12	**1.35E+00**	**2.67E+00**	**4.08E+00**	**9.45E-03**	**8.83E-15**	**8.02E+00**	**84.8**	**6.79E-01**	**1.76E+00**	**8.83E-01**
13	**1.50E+00**	**4.57E+00**	**6.27E+00**	**1.69E-02**	**9.85E-15**	**1.24E+01**	**91.3**	**7.37E-01**	**1.72E+00**	**9.41E-01**
14	2.00E+00	4.03E+00	1.12E+01	1.51E-02	1.48E-14	2.22E+01	74.4	8.24E-01	4.48E+00	1.89E+00
15	3.00E+00	4.63E+00	1.28E+01	1.11E-02	9.77E-15	2.55E+01	35.1	8.81E-01	1.31E+01	4.18E+00
16	5.00E+00	6.10E+00	1.18E+01	1.76E-02	1.18E-14	2.34E+01	60.3	9.51E-01	1.05E+01	2.44E+00
17	1.00E+01	9.57E+00	1.43E+01	2.34E-02	7.67E-15	2.84E+01	52.7	9.96E-01	1.97E+01	2.06E+00
18	2.00E+01	6.07E+01	1.74E+01	1.73E-01	5.70E-16	3.47E+01	80.2	9.99E-01	5.20E+01	2.07E+01
19	2.50E+01	7.46E+01	2.24E+01	2.92E-01	5.52E-17	4.49E+01	112.0	1.00E+00	-3.98E+01	1.15E+02
20	2.75E+01	2.56E+01	1.40E+01	1.45E-02	5.61E-17	2.77E+01	9.6	1.00E+00	9.84E+01	1.06E+02
Total Gas Age =	6.43E+00	±	1.92E-01	Ma (2Sigma)						

Plateau Age = 1.59 ± 0.21 Ma
(2s, including J-error of .364%)
MSWD = 1.6, probability = 0.13
55.8% of the 39Ar, steps 6 through 13

Table 6

Primary Magma	Unit	Country	SiO2	TiO2	Al2O3	Cr2O3	Fe2O3	FeO	MnO	MgO	CaO	Na2O	K2O	NiO	P2O5
3-12-4-03	Panama Alkaline	Panama	46.004	1.354	12.662	0.000	1.352	8.644	0.174	13.603	11.642	2.645	0.930	0.000	0.989
P21-2	Guayacan Fm.	Costa Rica	45.602	2.232	12.964	0.051	2.228	8.375	0.164	13.174	10.824	2.101	1.342	0.047	0.895
P21-14	Guayacan Fm.	Costa Rica	46.212	1.725	13.365	0.057	1.722	8.133	0.161	12.746	11.562	2.111	1.145	0.047	1.016
P24-4	Guayacan Fm.	Costa Rica	46.216	1.698	13.051	0.050	1.695	8.268	0.157	12.911	11.610	2.124	1.238	0.045	0.937
P24-9	Guayacan Fm.	Costa Rica	46.512	1.757	14.202	0.047	1.754	7.865	0.156	12.592	10.724	2.098	1.251	0.037	1.005
BO-062306-4	Guayacan Fm.	Costa Rica	46.452	1.138	14.967	0.099	1.137	8.347	0.175	13.038	11.086	2.828	0.252	0.000	0.483
CO-070206-2	C. Coronel	Costa Rica	45.147	2.247	13.542	0.061	2.245	8.337	0.185	13.106	10.621	3.115	0.603	0.000	0.791
CO-070206-4	C. Coronel	Costa Rica	46.617	2.436	12.543	0.000	2.435	8.275	0.164	13.370	10.434	2.588	0.609	0.000	0.528
TO-070106-2	L. Colorado	Costa Rica	45.841	2.018	13.488	0.067	2.014	8.478	0.165	13.769	10.799	1.994	0.782	0.000	0.586
TO-072106-1	C. Tortuguero	Costa Rica	46.888	1.560	13.552	0.094	1.559	8.235	0.163	13.281	10.819	2.532	0.780	0.000	0.537
TO-072106-3	C. Tortuguero	Costa Rica	46.856	1.573	13.611	0.000	1.572	8.251	0.164	13.353	10.873	2.388	0.816	0.000	0.544
TO-072106-4	C. Tortuguero	Costa Rica	46.650	1.605	13.486	0.000	1.604	8.259	0.164	13.168	10.872	2.336	1.213	0.000	0.641
P-132B	C. Tortugero	Costa Rica	47.226	1.569	13.482	0.000	1.566	8.221	0.155	13.588	10.526	2.088	1.004	0.051	0.522
P-133	C. Tortugero	Costa Rica	46.834	1.540	13.495	0.000	1.538	8.422	0.151	13.775	10.477	2.460	0.702	0.049	0.557

Sample	Unit	Country	T Ol	TP	Ol Mg#	Fe2O3/ TiO2	Fe2O3/ FeO	F (AFM)	Pi (GPa)	Pf (GPa)	Di (km)	Df (km)	MC (km)
3-12-4-03	Panama Alkaline	Panama	1315	1421	0.907	0.999	0.156	0.0052	2.97	2.53	98.92	84.42	14.50
P21-2	Guayacan Fm.	Costa Rica	1305	1409	0.907	0.998	0.266	0.0150	2.85	2.30	95.11	76.81	18.30
P21-14	Guayacan Fm.	Costa Rica	1295	1396	0.906	0.998	0.212	0.0180	2.70	2.13	90.05	71.08	18.96
P24-4	Guayacan Fm.	Costa Rica	1299	1401	0.905	0.998	0.205	0.0090	2.77	2.25	92.18	74.89	17.28
P24-9	Guayacan Fm.	Costa Rica	1292	1391	0.907	0.998	0.223	0.0610	2.64	1.76	87.83	58.81	29.02
BO-062306-4	Guayacan Fm.	Costa Rica	1302	1405	0.905	0.999	0.136	0.0020	2.81	2.30	93.66	76.83	16.83
CO-070206-2	C. Coronel	Costa Rica	1304	1407	0.908	0.999	0.269	0.0150	2.83	2.28	94.40	75.85	18.55
CO-070206-4	C. Coronel	Costa Rica	1310	1415	0.908	1.000	0.294	0.0600	2.91	2.07	96.98	69.03	27.96
TO-070106-2	L. Colorado	Costa Rica	1319	1426	0.908	0.998	0.238	0.0600	3.00	2.25	100.14	75.02	25.12
TO-072106-1	C. Tortuguero	Costa Rica	1308	1412	0.908	0.999	0.189	0.0580	2.88	2.04	96.16	68.10	28.06
TO-072106-3	C. Tortuguero	Costa Rica	1310	1414	0.908	0.999	0.191	0.0640	2.90	2.03	96.83	67.81	29.02
TO-072106-4	C. Tortuguero	Costa Rica	1305	1409	0.907	0.999	0.194	0.0380	2.85	2.14	95.05	71.34	23.70
P-132B	C. Tortugero	Costa Rica	1315	1421	0.909	0.998	0.190	0.1060	2.96	1.82	98.80	60.75	38.06
P-133	C. Tortugero	Costa Rica	1319	1426	0.908	0.999	0.183	0.0750	3.01	2.14	100.18	71.41	28.77

Unit Mean	Country	Initial Melting Depth	Standard Error of the Mean	Final Melting Depth	Standard Error of the Mean	Lat	Lon	Distance Along the Arc (km)	Distance from the Trench (km)
Panama	Panama	-98.92	-	-84.42	-	7.47	-82.24	1361	30
Guayacan Fm.	Costa Rica	-91.76	1.29	-71.68	3.38	10.07	-83.51	1093	132
C. Coronel/Lomas Colorado	Costa Rica	-97.17	1.66	-73.30	2.15	10.28	-83.56	1077	149
C. Tortuguero	Costa Rica	-97.40	0.92	-67.88	1.94	10.58	-83.53	1062	179

CURRICULUM VITA
ESTEBAN GAZEL

EDUCATION

2005-2009 Department of Earth and Planetary Sciences, *Rutgers University*, PhD in Geological Sciences (Petrology and Geochemistry)
Committee: M.J Carr, C. Herzberg, M. Feigenson and Kaj Hoernle

2001- 2004 Central American School of Geology, *University of Costa Rica*, Bachelor in Geology. Undergraduate thesis: Volcanology of the Sabana Redonda Cinder Cones, Poás Volcano, Costa Rica.

PROFESSIONAL AND ACADEMIC EXPERIENCE

2005-2007 *Department of Earth and Planetary Sciences, Rutgers University*
Teaching Assistant, Introductory Geology, Mineralogy, Petrology

2001-2005 *Central American School of Geology, University of Costa Rica.*
Geochemistry and petrology of southern Central America oceanic complexes and Miocene arc.
Lecturer of Introductory Geology, Volcanology, Petrography and Economic Geology and responsible for the university collection of rocks and minerals

2001-2004 *Research Center in Atomic, Nuclear and Molecular Sciences*
(CICANUM), University of Costa Rica: Dynamics of natural radioactive isotopes in active volcanic systems.

SELECTED PUBLICATIONS

Herzberg, C. & **Gazel. E.**, Petrological evidence for secular cooling in mantle plumes. ***Nature***,458, 618-622.

Gazel, E., Carr, M.J., Hoernle, K., Feigenson, M.D., Hauff, F., Szymanski, D., & van den Bogaard, P, 2009. The Galapagos-OIB signature in southern Central America: Mantle re-fertilization by arc-hotspot interaction. ***Geochemistry, Geophysics, Geosystems (G^3)***, Q02S11, doi:10.1029/2008GC002246.

Gazel, E. & Denyer, P. Jurassic to Miocene Costa Rican oceanic complexes: Description, structures and relationships. ***Journal of South American Earth Science***, *in press.*

Saginor, I., **Gazel, E.**, Carr, M.J., Swisher III, C., Turrin, B. Miocene to Recent volcanic history of Western Nicaragua: Insights from geochemistry and geochronology. ***Geochemistry, Geophysics, Geosystems (G^3),*** *in revision.*

Gazel, E., Denyer, P. & Baumgartner, P.O., 2006. Magmatic and geotectonic significance of Santa Elena Peninsula, Costa Rica. ***Geologica Acta*** 4(1-2), 193-202.

Denyer, P., Baumgartner, P.O. & **Gazel, E**., 2006. Characterization and tectonic implications of Mesozoic-Cenozoic oceanic assemblages of Costa Rica and Western Panama. ***Geologica Acta*** 4(1-2), 219-235.